UNIVERSIDAD DE LAS PALMAS
DE GRAN CANARIA

MÁSTER EN TECNOLOGÍAS DE TELECOMUNICACIÓN

MASTER THESIS

ANALYZING CANARIAN ARCHAEOLOGY HERITAGE THROUGH HYPERSPECTRAL IMAGE ANALYSIS

Author: D. Josua Mateo Hernández Rodríguez
Tutors: Dr. Gustavo Marrero Callicó
D. Himar Fabelo Gómez
D. Samuel Ortega Sarmiento
Date: January - 2019

MÁSTER EN TECNOLOGÍAS DE TELECOMUNICACIÓN

MASTER THESIS

ANALYZING CANARIAN ARCHAEOLOGY HERITAGE THROUGH HYPERSPECTRAL IMAGE ANALYSIS

SIGNATURE PAPER

Author: Josua Mateo Hernández Rodríguez Fdo: Josua Mateo Hernández Rodríguez - 42231703T Firmado digitalmente por Josua Mateo Hernández Rodríguez - 42231703T Fecha: 2019.01.15 00:28:27 +01'00'

Tutor: Dr. Gustavo Marrero Callicó Fdo: MARRERO CALLICO GUSTAVO - 42875067P Firmado digitalmente por MARRERO CALLICO GUSTAVO - 42875067P Nombre de reconocimiento (DN): c=ES, serialNumber=42875067P, sn=MARRERO CALLICO, givenName=GUSTAVO, cn=MARRERO CALLICO GUSTAVO - 42875067P Fecha: 2019.01.14 19:52:58 Z

Cotutor: D. Himar Fabelo Gómez Fdo: FABELO GOMEZ HIMAR ANTONIO - 78528094E Firmado digitalmente por FABELO GOMEZ HIMAR ANTONIO - 78528094E Nombre de reconocimiento (DN): c=ES, serialNumber=IDCES-78528094E, givenName=HIMAR ANTONIO, sn=FABELO GOMEZ, cn=FABELO GOMEZ HIMAR ANTONIO - 78528094E Fecha: 2019.01.14 20:05:08 Z

Cotutor: D. Samuel Ortega Sarmiento Fdo: SAMUEL ORTEGA SARMIENTO Firmado digitalmente por SAMUEL ORTEGA SARMIENTO Nombre de reconocimiento (DN): 2.5.4.13=Qualified Certificate: RACER-PF-SW-KPSC, l=TEROR, st=LAS PALMAS, serialNumber=78524517X, 1.3.6.1.4.1.17326.30.4=DNI, sn=ORTEGA SARMIENTO, givenName=SAMUEL, cn=SAMUEL ORTEGA SARMIENTO, c=ES Fecha: 2019.01.14 20:49:47 Z

Date: January - 2019

MÁSTER EN TECNOLOGÍAS DE TELECOMUNICACIÓN

FINAL MASTER WORK

ANALYZING CANARIAN ARCHAEOLOGY HERITAGE THROUGH HYPERSPECTRAL IMAGE ANALYSIS

EVALUATION PAPER

CALIFICATION:

President: Fdo:

Secretary: Fdo:

Vocal: Fdo:

Date: January - 2019

ACKNOWLEGEDMENT

First, I would like to thank my family for giving me the possibility of my achieving university studies, especially my parents and sister, for the love and moral support shown during my stay in this master.

Secondly, I want to thank my friends and colleagues of the master for the support and the help that they give me throughout this master.

Finally, I wanted to thank the IUMA department for providing and giving me the necessary resources for the realization and execution of this research work. In particular, I want to thank Dr. Gustavo Marrero Callicó, D. Himar Fabelo Gómez and D. Samuel Ortega Sarmiento for giving me the opportunity and supervising me in this Master Thesis.

TABLE OF CONTEXT

FIGURES

TABLES

SUMMARY

Hyperspectral imaging is an emerging technology suitable to be used in archaeological diagnosis. Some previous studies have employed this technology for detecting lost remains in pictures and art rocks, like pigments or carved on the stones. In this research work, a multidisciplinary team formed by archaeologists and engineers presents a proof of concept on the use of hyperspectral imaging analysis to determine the origin of different obsidian rocks. The samples were acquired from the Canarian Museum archaeologists. The hyperspectral acquisition system consists on two hyperspectral cameras coupled to a scanning platform to move them linearly. One of the cameras works in the visual and near infrared (VNIR) spectral range (from 400 to 1000 nm) with a spectral resolution of 3 nm. The other camera works in the short-wave infrared (SWIR) spectral range (1000 to 2800 nm) with a spectral resolution of 12 nm. After the hyperspectral images acquisition process, the images were processed to remove the effect caused by both the acquisition system and the environmental conditions. Later, and based on the archaeologist's criteria, a spectra dataset containing only labeled spectra from obsidian rocks belonging to different places of Gran Canaria and Tenerife was created. The labels indicate the precedence of each obsidian rock.

The data were processed using three different supervised learning algorithms: Support Vector Machines (SVMs) with two different kernel types (Linear and Gaussian) and Random Forest (RF). The capabilities of discriminating between Gran Canaria and Tenerife obsidians were evaluated in different phases (4 phases). Each phase consisted on the combination of supervised classification (including parameter optimization) and different pre-processing approaches to find the best results in the classification process. The results achieved in this research study are highly promising, showing that it is not possible to distinguish the origin of obsidian rock between Gran Canaria and Tenerife at different classification levels (island level, municipality level and deposit level) obsidian exclusively attending to the spectral signature of the obsidian rocks.

1. INTRODUCTION

1.1 Context

"They had no tools, neither iron nor any other metal, they took advantage of cutting stones as black as flint, which, giving one stone with another, they made rajas, and with these rajas they cut and cut and flayed. These cutting tools were called Tabona"

With these words, Fr. Abreu Galindo describes a work process related to the obsidians exploitation with raw material for the manufacturing of lithic instruments in *"Historia de la Conquista de las siete islas de Canarias"* (1590-1602)[1].

An obsidian is a rock formed by the fusion of natural volcanic mass from the rapid cooling of magma composed of basalt and other stones present in the crust of Earth as Andesite and Rhyolite. This solidification originates a compound of silicon dioxide or silica with vitreous characteristics called glass, volcanic rock or simply, obsidian. In addition, this rock presents irregular shapes, being opaque due to its characteristic of formation and it barely passes the light inwards and it has no crystalline structure.

The main motivation to carry out this research work is to advance in the research world on archaeological heritage such us obsidians. This work has the main goal of applying hyperspectral imaging techniques for the precise identification of different obsidians with different origin. Also, this work aims to find the optimal configuration of the hyperspectral acquisition system, available in the hyperspectral laboratory of the institute for Applied Microelectronics (IUMA), to be used as instrumentation for this particular application. Unlike other destructive analysis techniques, hyperspectral imaging is non-invasive and has no effect on the materials under study.

On the other hand, to understand the context of this project it is necessary to know that the Integrated System Design Division, DSI, from IUMA is specialized in the treatment of hyperspectral images. DSI team has already undergoing projects such as:

- **HELICOID: Hyperspectral Imaging Cancer Detection (FP7-618080).** The main goal of the HELICoiD project is to apply hyperspectral imaging techniques for the precise localization of malignant tumors during surgical procedures. The HELICoiD project has developed an experimental intraoperative setup based on non-invasive hyperspectral cameras connected to a platform running a set of algorithms capable of discriminating between healthy or pathological tissues. The University of Las Palmas de Gran Canaria/IUMA has coordinated this European project.
- **CCSDS Lossless Compression IP-core Space Applications (ITT-No. AO/1-8032/14/NL/AK).** The main objective of this ITT (invitation to Tender) is to implement two separate IP-cores corresponding to the CCSDS 123 and CCSDS 121 standards respectively. The former corresponds to a Lossless Multispectral

and Hyperspectral Image Compression architecture, while latter is a Lossless Data Compressor. Both IP-cores will be mapped for space qualified FPGAs (from Microsemi and Xilinx) and also for radiation hardened standard cells (180 nm ATMEL ATC18RHA).

- **REBECCA: Resilient Embedded Electronic Systems for Controlling Cities under Atypical Situations (TEC2014-58036-C4-4-R).** REBECCA is oriented to the Smart City paradigm. This topic brings up important challenges in different areas related with the sustainable development of the city and the provision of services to citizens. Among these areas, REBECCA focuses on urban security for large public spaces and/or celebration of major events. In this context, REBECCA works on the design of a platform for sensing and distributed computing of visible and multi-hyper-spectral image processing.
- **ENABLE-S3: European initiative to Enable Validation for Highly Automated Safe and Secure Systems.** ENABLE-S3 is a strongly industry-driven project. It will pave the way for accelerated application of highly automated and autonomous systems in the mobility domains automotive, aerospace, rail, maritime and health, through provision of highly effective test and validation methodology and platforms. ENBALE-S3 will help the European industry to gain leadership in the strategic field of autonomous systems due to faster development and test of new products.
- **HYLOC: Multispectral and Hyperspectral Image Compression System.** The objective of this industrial project is the implementation of a prototype suitable for its implementation on a space-qualified FPGA for the compression of multispectral and hyperspectral images based on the standard CCSDS-123. The effect of the several configuration parameters on the compression efficiency and hardware complexity is taken into consideration to provide flexibility in such a way that the implementation can be adapted to different applications scenarios.

1.2 Objectives

Global objectives

The main objective of this Master's Thesis is to propose and validate several classification models using data mining techniques in order to obtain an automatic identification tool for archaeological HSI. These HSI are captures from obsidian samples from Gran Canaria and Tenerife, previously identified by the archaeologists of Canarian Museum in the VNIR (400 to 1000 nm) and SWIR (1000 to 2800 nm) spectral ranges.

Specific objectives

1. To understand the hyperspectral concept and its characteristics.

2. To understand the operation of hyperspectral cameras and their properties for the capturing process. In this process the hyperspectral data are obtained.
3. To understand the nature of the hyperspectral data in order to exploit correctly the main features of the available dataset. To know the main techniques for processing hyperspectral imaging, their applications and study the most suitable data mining techniques for processing this type of data.
4. To propose different frameworks for processing and classifying hyperspectral data, using different classification schemes and processing techniques.
5. To evaluate the performance of the proposed frameworks and decide which of them are most suitable for distinguishing between Gran Canaria and Tenerife obsidian rocks.

1.3 Methodology

The methodology followed in this research work is related with the previously described objectives. This methodology can be summarized as follows. Firstly, the documentation regarding HS images was analyzed, paying special attention to the use of this technology in the archaeological field. Then, a specific protocol for the capturing process of the HS images of the obsidian rocks was proposed. Next, the process to capture the data with both HS cameras for further processing is established in this process, the spectral signatures of all obsidians were extracted and labelled. In addition, a supervised classification framework was proposed in order to automatically distinguish between Gran Canaria and Tenerife obsidians by using the obsidian spectral signatures. The two last phases were proposed to evaluate the performance of different models that were generated using different classifiers. Finally, the classification results obtained by each classifier were evaluated.

1.4 Document Overview

This document is organized as follows:

Chapter 1: The first chapter of this document consists on a brief introduction to the research work that will be described in this document. This chapter covers the context where this research work is developed, the principal and operative objectives and a brief description of the methodology followed in order to achieve the objectives.

Chapter 2: In this chapter, a state of the art of HIS, especially in the archaeological field, is presented. This state of art covers the basic concepts of this technology, the most relevant processing techniques that usually are applied to this kind of data and the main applications where the HS images are useful. Finally, the progress and the current use of this technique in the archaeological field are exposed.

Chapter 3: This chapter presents the materials employed in this research work, where the acquisition systems and database employed in this research work is described. Also, this chapter describes the capturing process for the next further processing and foundations of the proposed processing techniques employed to extract knowledge from hyperspectral data.

Chapter 4: In this chapter, the results obtained after processing the hyperspectral images are presented.

Chapter 5: The last chapter describes the conclusions achieved during the development of this research work. Additionally, some future works are described.

2. STATE OF ART

In this section, the reader we will be introduced to the context in which this project is developed, explaining and summarizing the principal terms that will be used in the rest of the document. In the first place, the hyperspectral imaging (HSI) concept and their main characteristics are described. Next, the different types of HS sensors that currently exist in the literature are presented. Finally, the current relation between HSI and mineralogy-archeology are exposed, due to this project is related with the study of HS images obtained from Canarian archeological heritage, such us obsidian rocks.

2.1 HYPERSPECTRAL IMAGING

2.1.1 Electromagnetic Spectrum

The electromagnetic spectrum (ES) is referred to the range of all types of electromagnetic radiation that emits or absorbs a certain substance.

Due to the interaction of physic mechanisms of the electromagnetic radiation with the materials are different along the electromagnetic spectrum, the remote observation of this spectrum offers additional information about the state of the observed material [2].

The human eye uses the visible light, which covers the spectral range from 400 to 700 nm, emitted or reflected by the objects existing in nature to provide us information about the elements that are around us. However, our perception of this phenomenon is limited because we are only sensitive to a few wavelengths in the complete ES. Figure 1 shows the different parts that compose the complete ES, where it is possible to see that the visible light is a small part of the entire ES.

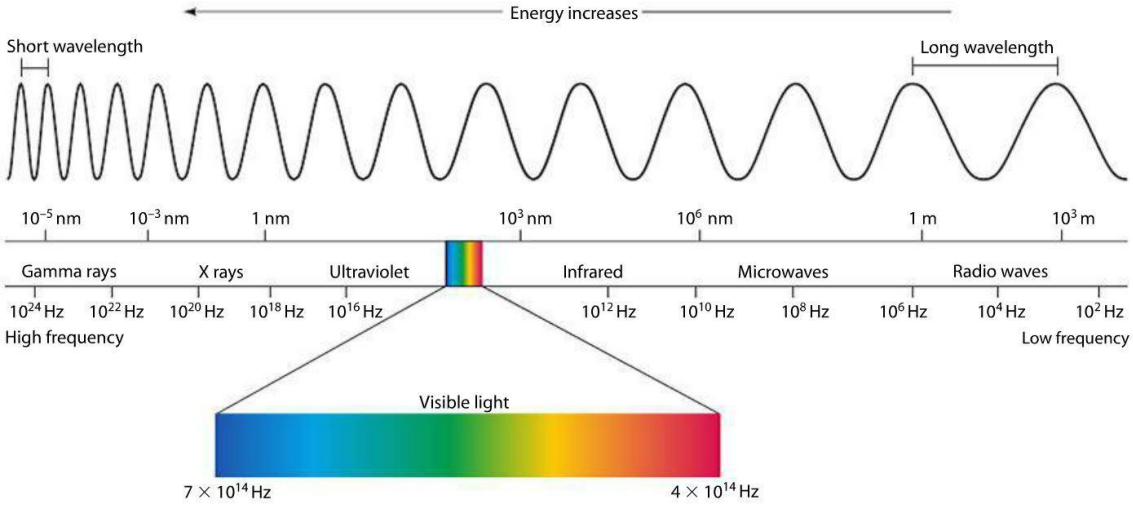

Figure 1. Electromagnetic spectrum [3].

The most common wavelengths range employed in HSI are the visible, ultraviolet and infrared spectral regions. These spectral ranges are the most practical in the HSI

formation, because it is possible to obtain information about the state of the observed object beyond what it is possible to perceive with the naked eye.

The ultraviolet radiation is a portion of the spectrum below the visible range, between 15 and 400 nm.

The infrared region is a portion of spectrum above the visible light between 0.7 and 100 µm. This region can be divided into two categories based in its radiation properties: reflected infrared region and emitted infrared region. Normally, this radiation is associated with the temperature emitted by the object.

The fundamentals of spectral imaging are based primarily on the interaction of light with matter. Light and other electromagnetic radiations are commonly described in terms of their wavelengths, but the designation of spectral ranges varies often with the application, especially for the infrared. Normally, the nomenclature used to indicate the spectral range is as follows: ultraviolet (UV): 0.2-0.4 µm; visible (VIS): 0.38–0.8 µm; near-infrared (NIR): 0.9–1.7 µm; short-wave infrared (SWIR): 0.97–2.5 µm; and mid-infrared (MWIR): 3–5 µm. The near-infrared range is sometimes grouped with the visible and referred to as visible-near-infrared (VNIR). In Table 1 show a resume about this nomenclature:

Table 1. Spectral ranges.

Range	Wavelength (nm)
UV = Ultraviolet	200-400
VIS = Visible	380-800
VNIR =Visible Near Infrared	400-1000
NIR = Near Infrared	900-1700
SWIR = Short-wave Infrared	970-2500
MWIR = Middle Infrared	3000-5000
LWIR = Long-wave Infrared	8000-12000

2.1.2 Irradiance

The irradiance is the light energy per time unit (power) that hits a surface, normalized by the surface area (W/m^2) [4]. When the irradiance ($L_I(\lambda)$) hits on the matter, this absorbs ($L_a(\lambda)$), transmits ($L_T(\lambda)$) and reflects ($L_y(\lambda)$) the light in a peculiar way. All components are in function of wavelength (Eq. 1), where the $L_a(\lambda), L_T(\lambda), L_y(\lambda)$ proportions oscillate with the spectral actions of different matters.

$$\mathbf{L_I = L_a(\lambda) + L_T(\lambda) + L_y(\lambda)} \quad (1)$$

In spectroscopy of reflected light, the fundamental property that we obtain is the spectral reflectance p_λ that is the relation between reflected energy and incident energy as function of wavelength [5]. In the next chapter, the spectroscopy concept will be explained.

$$p_\lambda = L_y(\lambda)/L_I(\lambda) \quad (2)$$

Also, we can obtain the spectral transmittance (σ_λ) that is the relation between transmitted energy on incident energy as function of wavelength:

$$\sigma_\lambda = L_T(\lambda)/L_I(\lambda) \quad (3)$$

Both reflectance and transmittance oscillate with the wavelength in different ways due to the energy in some wavelengths is absorbed in greater or lesser extent. The pronounced deviations downward from the spectral curves indicate the ranges of wavelengths in which material selectively absorbs the incident energy. Generally, these characteristic peaks in the ES are called absorption bands.

2.1.3 Hyperspectral Imaging Concept

HSI is an imaging modality in where each pixel is not described by a single value (as occurs in a monochromatic image) or by three components of color (as occur in an RGB image). In an HS image, each pixel offers detailed spectral information that can be used to extract spectral features from the materials that appear in the image.

Historically, the HSI concept has been associated with one of the first NASA instrument for exploration on Earth [6], the AVIRIS system (Jet Propulsion Laboratory's Airborne Visible-Infrared Imaging Spectrometer) [7], [8]. The progress of the HS technology in the remote sensing applications resulted in the development of measure instruments of high resolution in spatial and spectral domains. HS sensors obtain digital image in a high quantity of spectral channels, obtaining for every pixel a spectral signature that is characteristic of each material in the nature[9]. The spectral signature is the function that describes the quantity of reflected or absorbed radiation in each wavelength of the spectra.

The result of the data collected by a HS sensor on a certain scene can be represented as a data cube (HS cube), with two dimensions to representing the spatial location of a pixel and a third dimension to represent the spectral information of each pixel in the different wavelengths. Figure 2 shows the structure of an HS cube where the X axis is the indicator of lines, the Y axis is the indicator of samples and the Z axis is the band number, i.e., the wavelength of that band. The utilization of HS cube visualization as an analytic tool is the first step in analysis and exploitation of data. The data size necessary to storage a cube of HS data increases as spectral and spatial dimensions increases.

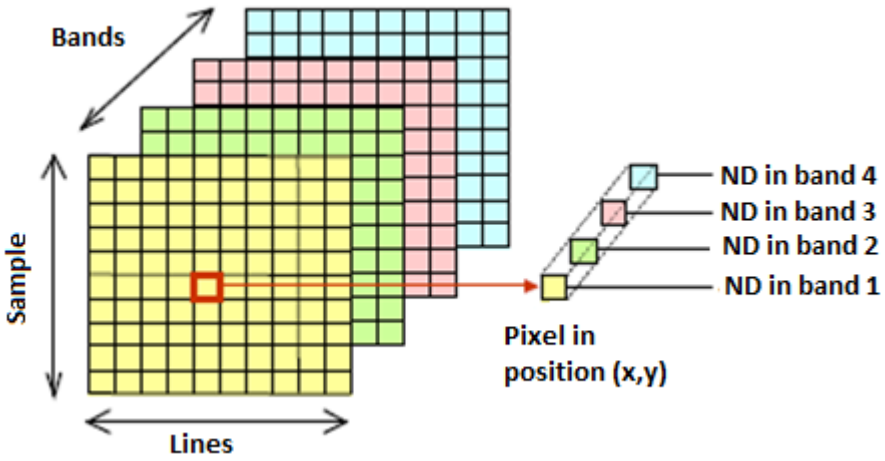

Figure 2. Hyperspectral cube structure.

The nature of HS sensors allows obtaining a detailed spectral signature for each pixel of the image due to the reflectance values acquired by the sensor in the different wavelengths. These spectral signatures allow a very precise characterization of the captured surface. As an illustrative example, Figure 3 shows a simple HS cube analysis method by means of a simple diagram, in where AVIRIS sensor has been considered. In this example, one satellite is capturing a HS image and there are different surface types and each surface has its characteristic spectral signature.

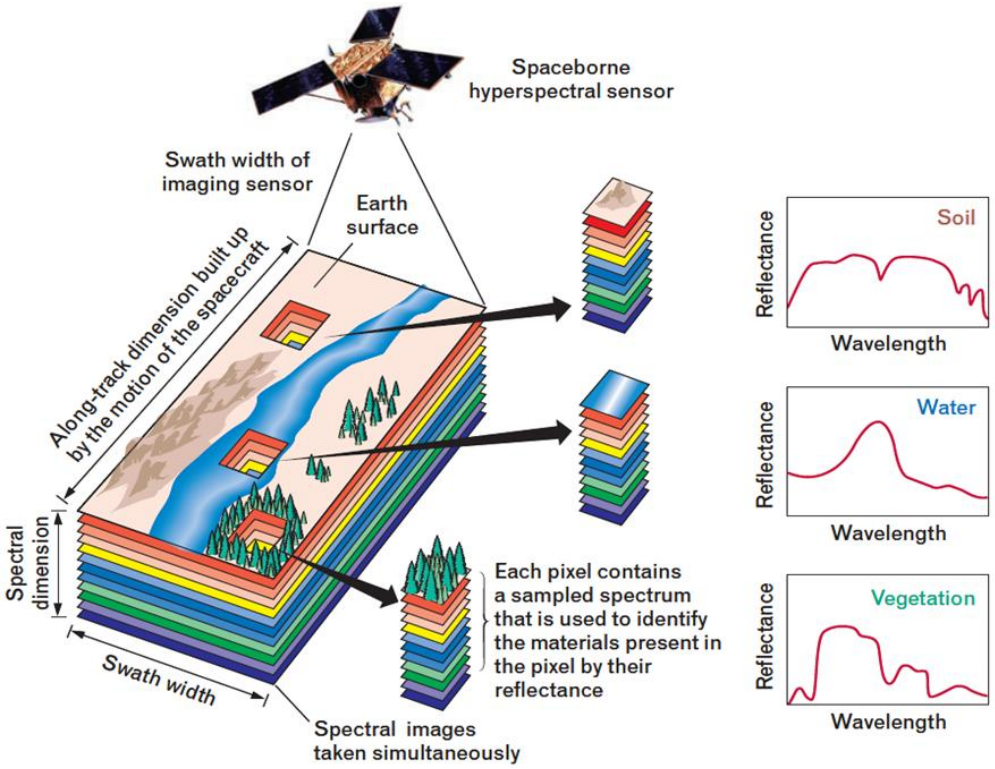

Figure 3. Hyperspectral analyses method with AVIRIS sensor [10].

In this type of image modality is usual the presence of mixtures at sub-pixel level, so it is possible to find two different types of pixel: pure pixel and mixed pixel.

A pure pixel refers to a pixel that is composed of only one distinct material and a mixed pixel is a pixel where it is possible to find different materials. Mixed pixels

constitutes the most part of HSI because of this phenomenon is independent of the considerate scale. Figure 4 shows an example of pure pixel acquisition process and mixing in HIS, where one HS image have different types of pixel with their spectral signature.

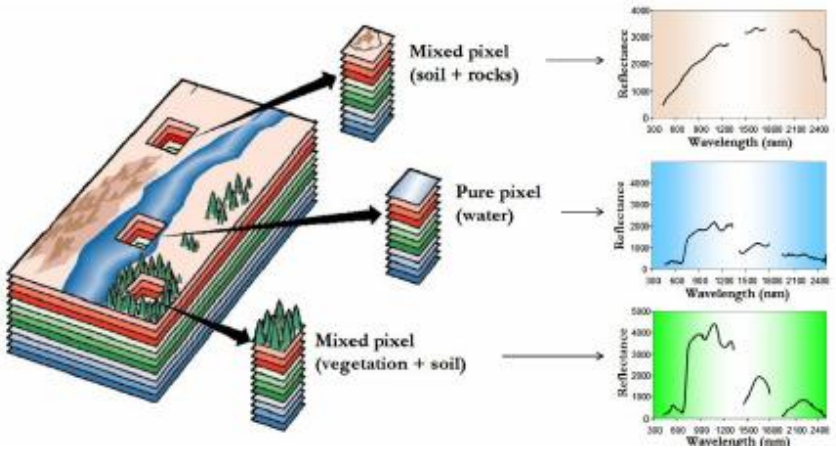

Figure 4. Process of acquisition of pure pixels and mixing in hyperspectral imaging [11]**.**

2.1.3.1. The Imaging Spectrometer

HSI is based on the development of the so-called imaging spectrometers. The development of the HS sensors has involved the convergence of two related but distinct technologies: spectroscopy and remote imaging of Earth and planetary surfaces.

Spectroscopy is the study of light that is emitted by or reflected from materials and its variation in energy with wavelength. As applied to the field of optical remote sensing, spectroscopy deals with the spectrum of sunlight that is diffusely reflected (scattered) by materials at the Earth's surface. Instruments called spectrometers are used to make ground-based or laboratory measurements of the light reflected from a test material. An optical dispersing element such as a grating or prism in the spectrometer splits this light into many narrow, adjacent wavelength bands and the energy in each band is measured by separate detector. By using hundreds or even thousands of detectors, spectrometers can make spectral measurements of bands as narrow 0.01 µm over a wide wavelength range, typically at least 0.4 to 2.4 µm (VIS to SWIR ranges)

Remote imagers are designed to focus and measure the light reflected from many adjacent areas on the Earth's surface. In many digital images, sequential measurements of small areas are made in a consistent geometric pattern as the sensor platform moves and subsequent processing is required to assemble them into an entire image. Until recently, imagers were restricted to one or a few relatively broad wavelength bands by limitations of detector designs and the requirements of data storage, transmission, and processing. Recent advances in these areas have allowed the design of imagers that have spectral ranges and resolutions comparable to ground-

based spectrometers. Some sensors use multiple detector arrays to measure hundreds of narrow wavelength bands. Figure 5 shows a schematic diagram of the basic elements of an imaging spectrometer.

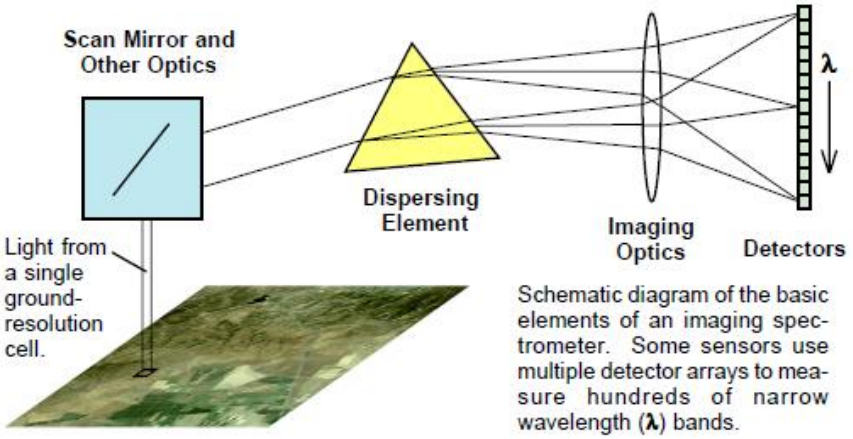

Figure 5. Schematic diagram of the basic elements of imaging spectrometers [2].

2.1.4 Hyperspectral Acquisition Systems

HS acquisition systems are the combination of spectroscopy and digital photography. A HS camera is formed by the combination of a spectroscope and monochromatic sensor. When a detector is placed on a spectroscope at its output, it is called spectrograph. The spectroscope is an instrument designed to decompose the radiation of light in the wavelengths that form it. The monochromatic sensor is in charge of register the decomposed light in their fundamental components. Figure 6 presents a diagram of HS camera. For a dispersive imaging spectrometer some means of dispersing the input radiation such as a grating or prism is used. By coupling the dispersing grating or prism with a two-dimensional array of detector, a spectral image is formed such the spatial information is along one axis and spectral information is along the other [12], [13].

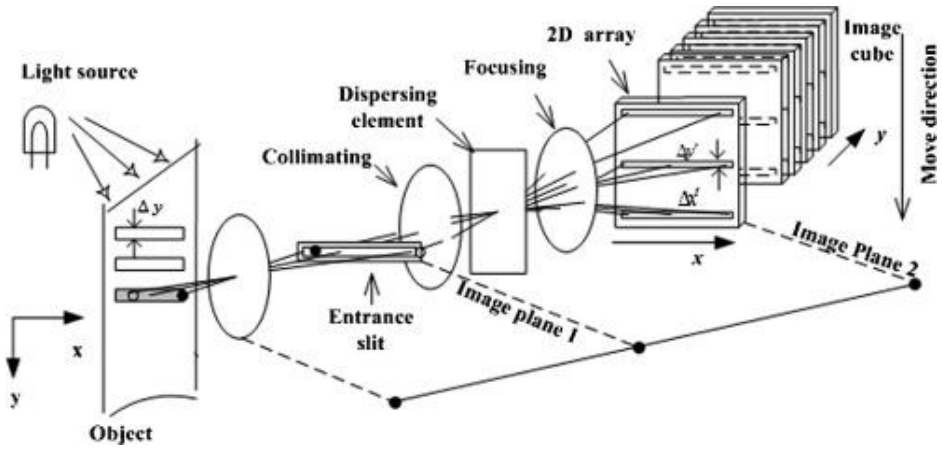

Figure 6. Block diagram of hyperspectral camera [13].

There are two fundamental optical principles that allow scattering light, the differential refraction and the interference. The differential refraction gives rise to

prism spectroscopes and the interference gives rise to the based in diffraction gratings. In Figure 7 shows an example of these two types of light dispersion in a spectrograph.

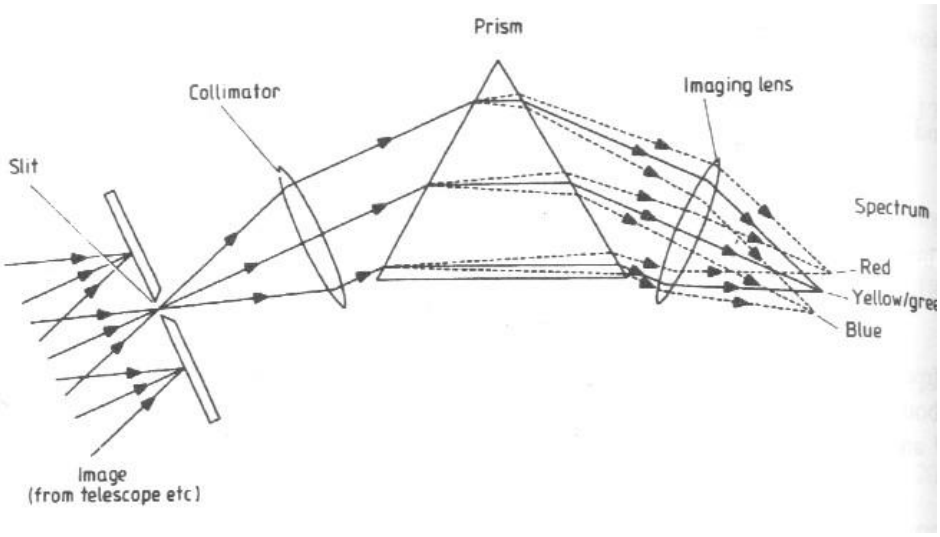

(a)

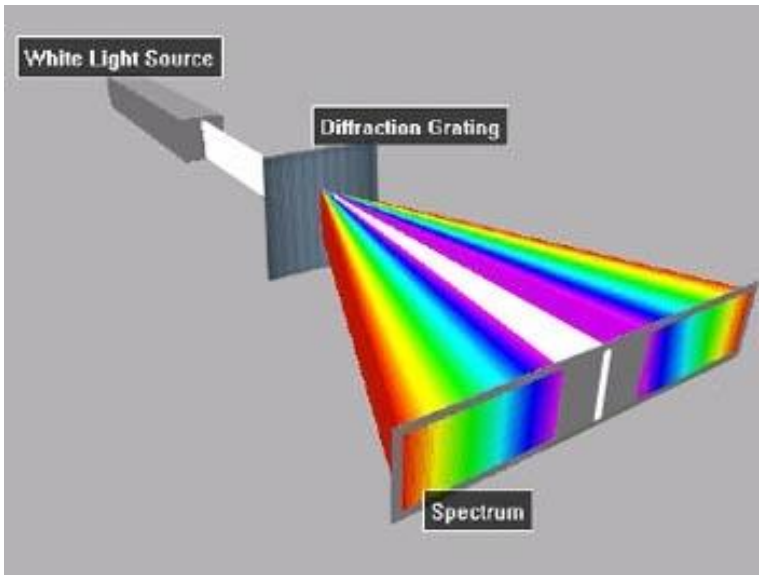

(b)

Figure 7. Light dispersion in spectrograph. (a) Prism (b) Diffraction gratings

Independently of the spectroscope design and its disperser element, its fundamental characteristic is the spectral resolution (R). This parameter shows the spectroscope capacity to separate two close spectral components:

$$R = \lambda / \delta\lambda \quad (4)$$

In Eq. 4, λ is the wavelength on which we are working and δλ is the spectral purity (Full Width at Half Maximum, FWHM), which corresponds with the wide to medium height that would have a monochromatic line when observed with spectroscope. Figure 8 shows an example of the FWHM.

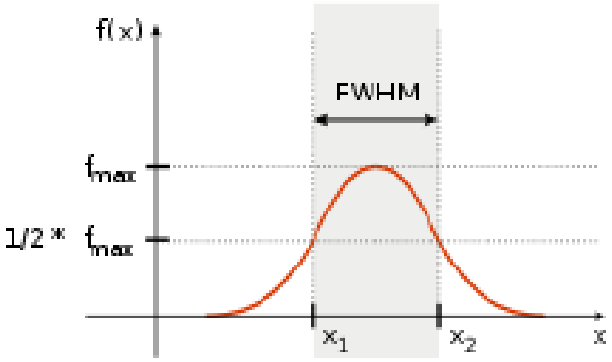

Figure 8. Representation of the FWHM [14].

To decide if two lines are separated it must be established a criterion. A criterion very famous is the Rayleigh criterion($\Delta\lambda$), where we can suppose that spectroscope separates two lines when the difference of wavelength of maximums is greater or equal to the spectral purity (Eq. 5). Figure 9 shows an example of Rayleigh criterion. The spectral purity will depend on the optical system which is being used besides of quality of disperser element [10].

$$\Delta\lambda \geq \delta\lambda \tag{5}$$

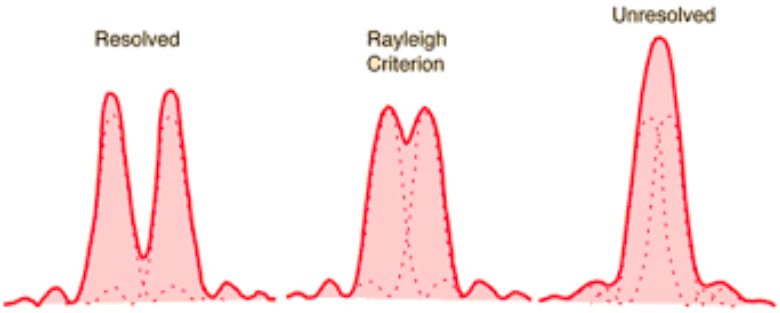

Figure 9. Rayleigh criterion [14].

2.1.4.1. Hyperspectral Cameras

HS sensors have some several parameters that must be taking into account, such as spatial resolution, spectral resolution, radiometric resolution and temporary resolution [15], [16].

The spatial resolution is given by the pixel size of the image and refers to the size of the smallest characteristic that can be detected. To determinate the spatial resolution, the Instantaneous Field of Vision (IFOV) is used. The IFOV is defined as the angular section observed in a determined time. The basic components of a sensor define the parameter that describes intern geometry of the sensor, as the Field of View (FOV) and IFOV. Also, it is important to have a good lens in the camera to capture with greater clarity the image you want to take. Figure 10 shows a representation of the IFOV and

the FOV parameters and Figure 11 shows an intuitive description of the spatial resolution.

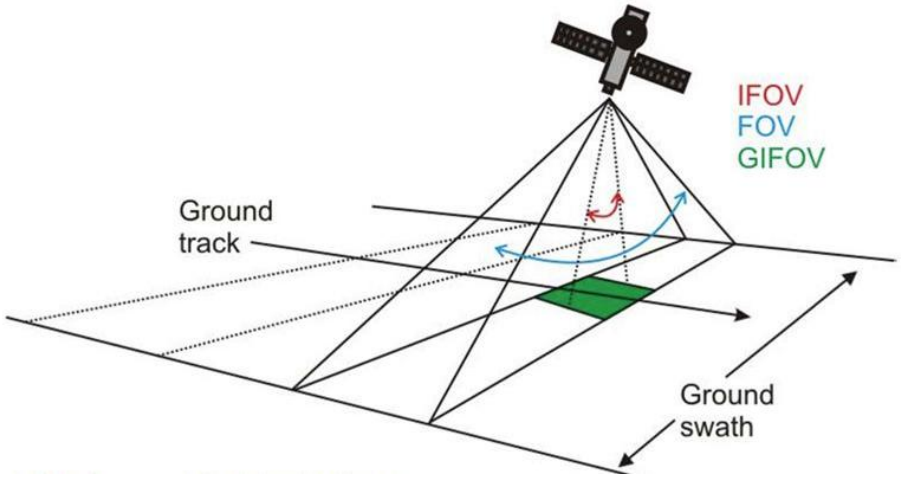

Figure 10. Example of FOV and IFOV [16]**.**

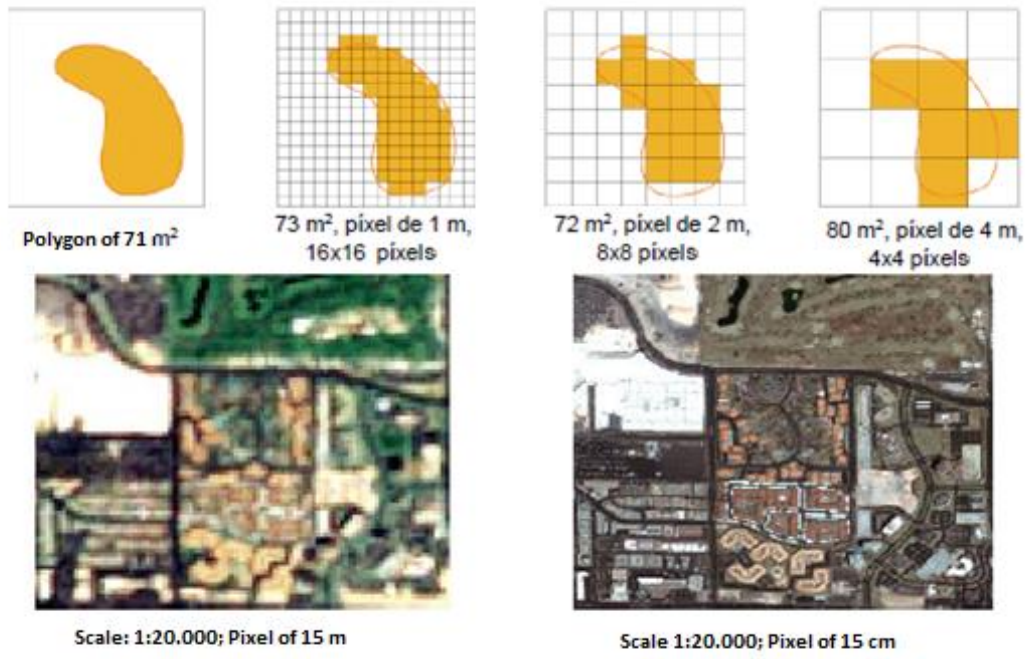

Figure 11. Spatial resolution [17].

The spectral resolution is a parameter that keeps being the principal discrimination factor between multispectral and HS systems. This indicates the number and the width of spectrum region for which the sensor captures data. Figure 12 shows the main difference between multispectral image and HS image, the number of band and the distance between the bands. Figure 13 shows different spectra for the same HS cube captured with different spectral resolutions, at a higher resolution, higher spectral information quantity is captured.

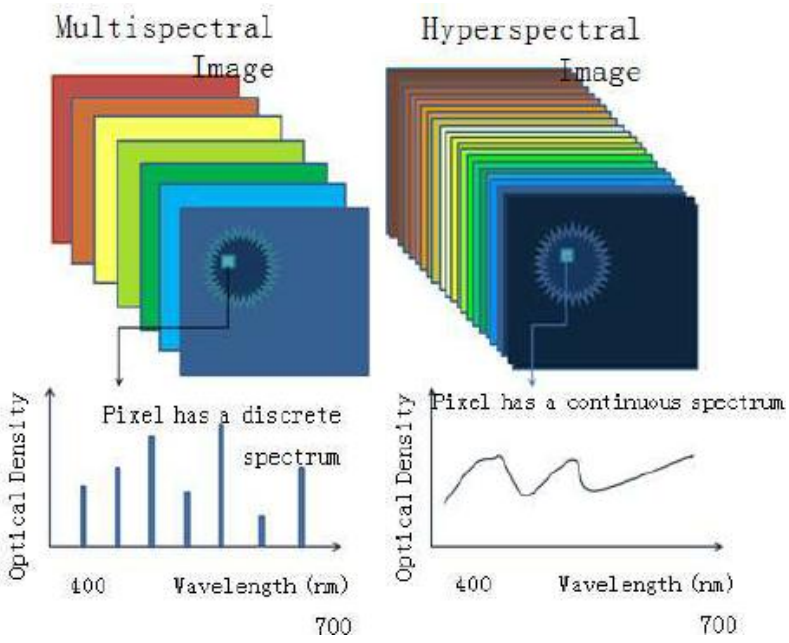

Figure 12. Comparative between spectral resolution of a multispectral imaging and hyperspectral imaging [18].

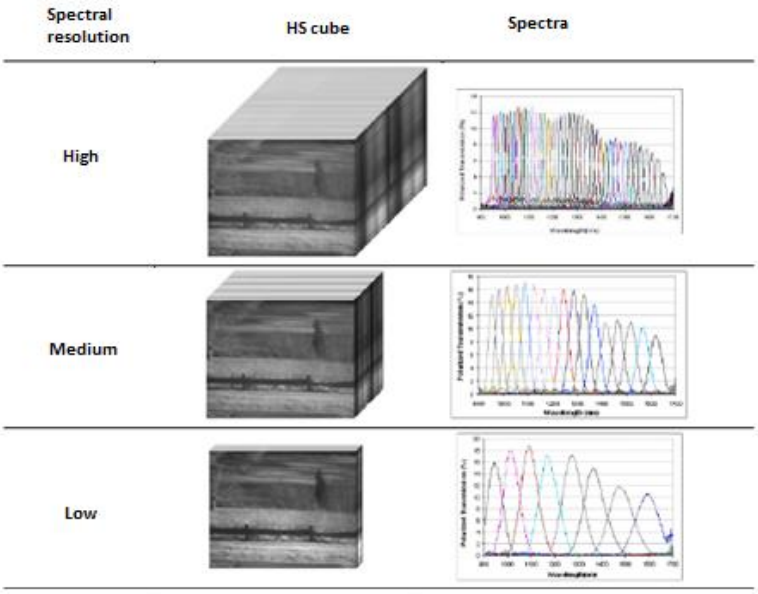

Figure 13. Different spectra for the same HS cube captured with different spectral resolutions

The temporary resolution represents the periodicity with which the sensor acquires information of a same sector of observed surface.

The radiometric resolution is the parameter that indicates the sensor sensitivity, i.e. the sensor capacity to discriminate between spectral radiance for a determined wavelength range.

In general, at higher spatial resolution, lower temporary and spectral resolution due to every increase of resolution multiplies the data volumes which the sensor must process.

There are two types of HS depending on their way to operate: active sensors and passive sensors.

- **Active sensors:** These sensors generate their own energy to later store the response which an object provides emitted electromagnetic energy. Figure 14 shows an example of an active sensor. Active sensors emit a signal, typically a burst of waves (light, microwaves or sound) which is reflected by the surroundings elements. Then, the reflected signal is received by the sensor and takes necessary action. When something moves within the area of an active motion sensor, the change in the signal that is reflected to the sensor activates the system.

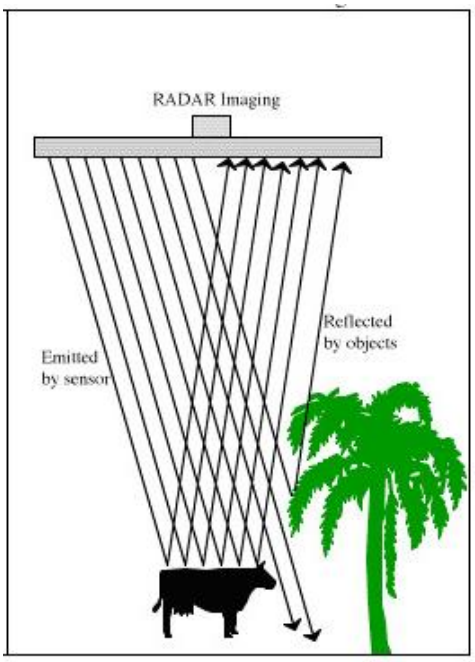

Figure 14. Active sensor example [16]**.**

- **Passive sensors:** These sensors do not emit energy and they need a field of extern energy like the photography cameras installed in aerial platforms. Figure 15 shows an example of a passive sensor. As this sensor detects temperature differences, it is well suited to detecting the motion of people, animals or plants or the temperature emitted by the fire or sun.

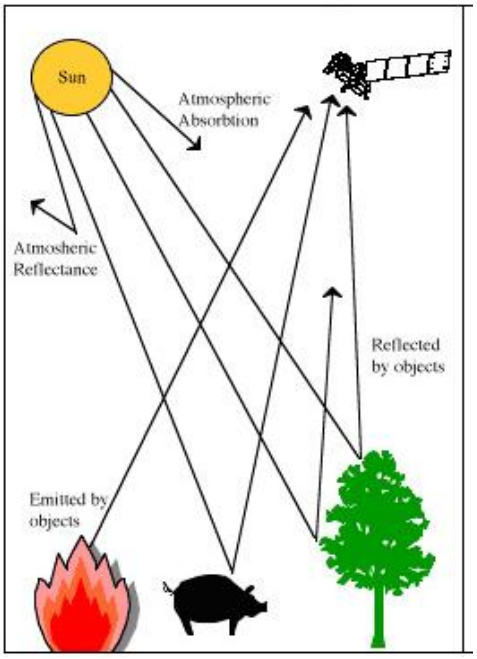

Figure 15. Passive sensor example [16].

There are different technologies able to capture a HS cube. In this sense, there are four different types according to the way of capturing the radiation capture whisk-broom scanning, push-broom scanning, staring scanning and snapshot scanning[19], [20].

Whisk-broom scanning

In this type of cameras, a single point is scanned at one pixel to provide the spectrum of this point. To obtain the rest of point it is necessary to move the detector or the sample along two spatial dimensions. Its obtained HS cube is stored in the band-interleave-by-pixel (BIP) format. In a BIP format, the first pixel for all band is in sequential order, followed by the second pixel for all bands and so on. One problem of this type of camera is very time-consuming for positioning the sample and need advanced repositioning hardware to ensure repeatability. Figure 16(a) shows how this type of cameras capture the sample.

Push-broom scanning

These systems record a whole line of an image as well as spectral information at the same time corresponding to each spatial pixel in the line. A complete HS cube can be obtained as the line is scanned along of one dimension and the obtained cube is stored in the format of band-interleaved-by-line (BIL). This format is a scheme for storing the pixel values of an image in a file band by band for each line or row of the image. These cameras are the most popular methods of acquiring HSI. One problem of these cameras is the exposure time. Such exposure time must be short enough to avoid saturation of spectrum at any wavelength, resulting in underexposure of other spectral bands and low accuracy of their spectral measurement. Figure 16(b) presents the capture process of this type of camera.

Staring scanning

These devices use elements which allow the passage of some wavelengths. To obtain a HS cube is necessary to oscillate the wavelength of a band-pass filter for each capture. Various types of filters exist for this function, like the AOTF (Acoustic-Optic Tunable Filters) or the LCTF (Liquid Crystal Tunable Filter).

- AOTF: these filters are based in piezoelectric material properties and they are built by joining piezoelectric transconductors to a crystalline material. The transconductors are excited with a radiofrequency producing a perturbation in the material[21].
- LCTF: these filters are based on liquid crystal elements electronically controlled, to transmit a specific wavelength and exclude the others. Their structure consist in one liquid crystal sheet and one quartz sheets placed between two lineal polarizer to obtain the range and the selectivity in frequency [22], [23]. Figure 16(c) shows how this camera type captures one sample.

Such scanning repeats over the whole wavelength range, results in a stack of single band images stored in the band sequential (BSQ) format. It is a simple format, where BSQ encodes each lines of the image at the first band is followed immediately by the next line in the same spectral band, followed by the second band for all lines and so on, interleaved up to the number of bands. This format provides an easy access of spatial access of at a single spectral band.

Snapshot

This method is registers spatial and spectral information in a detector surface with a single exposure. Unlike the whiskbroom, pushbroom and staring scanning methods, where it is required to perform a scan in the spatial or spectral dimension limiting its temporal resolution, the snapshot cameras do not require the scanning. This method can acquire a full HS cube in one shot. However, its spatial and spectral resolution are limited due to the total number of voxel (cubic unit that conforms a tridimensional object) cannot exceed the total number of pixels in the sensor. Figure 16(d) presents the functionating of these cameras.

In Figure 16 and Table 2 it can be seen a comparative among the different HSI acquisition methods that have been exposed previously. Since the whiskbroom and pushbroom modes use a dispersion element (prism, diffraction gratings, PGP, etc.) to divide the light. They have advantage of high efficiency, low dispersion and low-cost respect to other methods[24].

On the other hand, the most important advantages of staring mode are the short time of recollection of the HS cube and the facility of coupling with other optical instruments due to it does not require performing a spatial movement between the detector and the sample. Another advantage is the flexibility of selecting the optimum spectral range depending on the application.

In the case of snapshot cameras, the principal advantage is the lower time of captured and the disadvantages are the limitation due to the total number of voxel (cubic unit that forms a tridimensional object) cannot exceed the total number of pixels in the sensor.

In summary, each HS camera type has advantages and disadvantages to be used in archaeology or mineralogy analyses. For example, the whiskbroom and pushbroom systems can obtain high spectral and spatial resolution with a low cost but their hardware mounting is more complex than the other camera types. Staring mode can be mounted in a compact way and can be easily coupled to other optical instruments. Finally, snapshot cameras can capture quickly the HS cube, but its spectral and spatial resolution is limited.

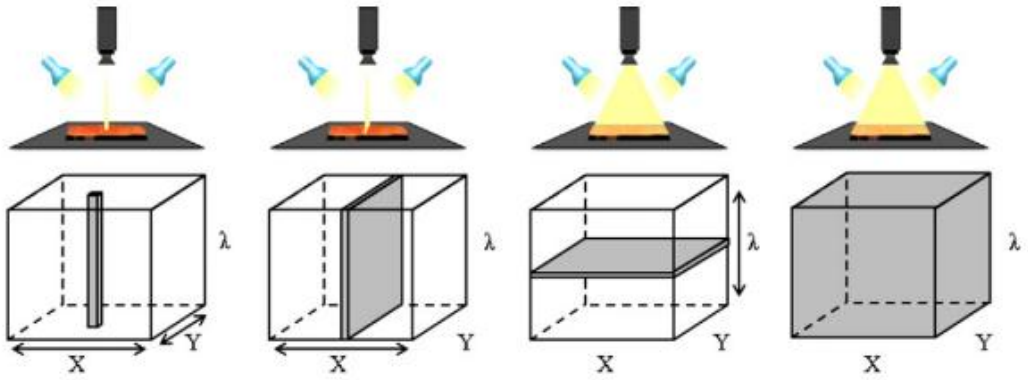

(a) (b) (c) (d)

Figure 16. Comparative among hyperspectral sensors. (a) Whiskbroom (b) Pushbroom (c) Staring (d) Snapshot [20].

Table 2. Comparative among hyperspectral sensors.

	Whiskbroom	Pushbroom	Staring	Snapshot
Scanning	Spatial (axis X and Y)	Spatial (lineal)	Spectral	No
Element dispersion	Prism, diffraction gratings, PGP	Prism, diffraction gratings, PGP	AOTF, LCTF, lineal and circular tunable filters, interferometer	Prism, diffraction gratings, digital hologram
Spectral range (nº bands)	Large	Large	Medium	Large
Spectral resolution	High	High	Medium	Low
Throughput	High	High	Low	High
Time of cube capture	Large	Large	Medium	Short or instantaneous
Complexity	High	High	Simple	Medium

2.2 Hyperspectral Imaging Applications

The discrimination capacity among different materials provided by HSI makes this technology is much highly useful in several fields. In this section, some applications of HSI will be presented and later, the archaeological applications found in the literature will be addressed.

The HSI impact in scientific community is reflected in many numbers of investigations [25]–[27] that involve improvements in its technology and applications in diverse scientific disciplines, like biology, agronomy, ecology, geology, geography, mineralogy, among others [28]–[30].

2.2.1 Remote Sensing

Historically, the first application of HSI was remote sensing. This technique allows acquire spatial, temporal and spectral information of an object or scene without physically coming into contact [31]. For example, remote sensing provides information about species of plants that are nonnative invasions. The species of invasive plant involve a significant threat to global biodiversity and the ecosystem performance. An example of this application can be found in a study performed in the central coast of California (USA) [32], where six types of vegetation were discriminated using HSI. Three of these types were dominated by three invasive species: ice plant (Carpobrotus edulis), jubata (Cortaderiajubata) and eucalyptus (Eucalyptus globulus). Figure 17 shows the species involved in the study and a comparative of their respective spectral signatures. Thanks to this spectral analysis is possible to detect and identify the species from a satellite (Figure 18), in order to eradicate them.

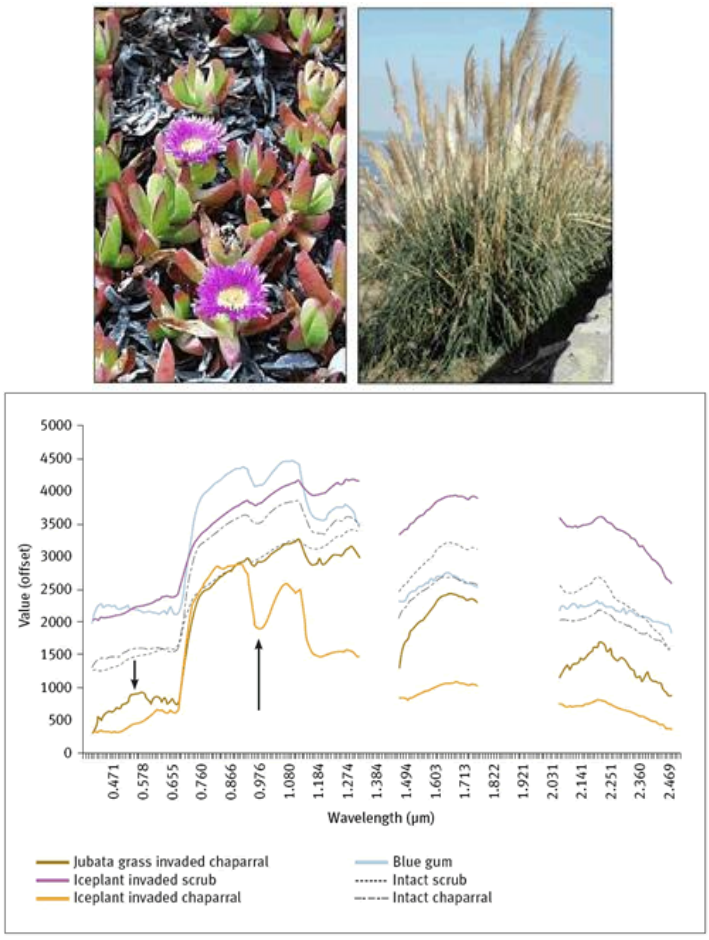

Figure 17. Species of non-native plants invasions and spectral signature of invasive species [32].

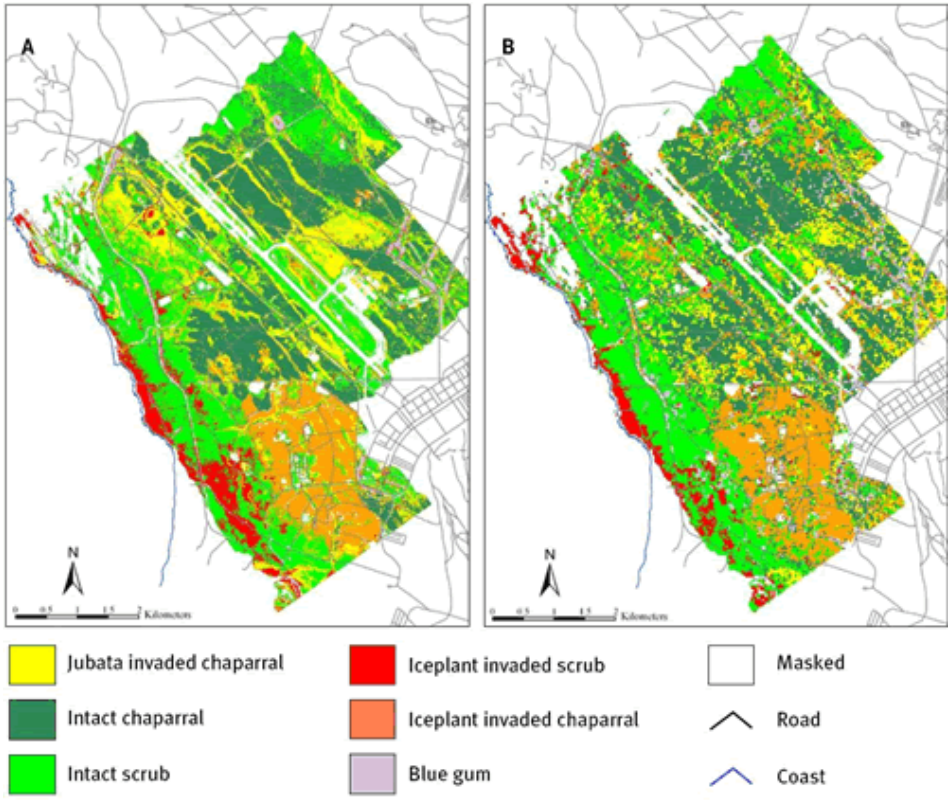

Figure 18. Identification of invasive plants using: (A) hyperspectral AVIRIS image (B) hyperspectral LANDSAT ETM image [32].

2.2.2 Food Inspection

On the other hand, HSI systems are used also to evaluate the quality of aliments. There are many ways of evaluating the quality of aliments, like sensorial evaluation in meats or chemical methods but, in general, these analytic methods time-consuming and cause the destruction of the aliments. For this reason, these methods are not appropriate to make aliment analyses in a large scale. In this context, HSI has earned importance in the recent years, demonstrating to be an effective technology for the analysis and evaluation of food products in a quick, non-invasive and non-destructive way. An example of this application of HSI can be found in [20], where a study of fishes imperfections using HSI was done.

Nowadays, the automatic classification systems are not precise enough in the detection of food imperfections, so the manual classification is still in use. In the case of fish inspection, the imperfection is defined as the damage of the fish skin due to some external forces cause physical changes or chemical changes of color, smell and flavor of fish. Figure 19 shows the result of imperfections identification of a fish for the VNIR range, where using HSI is possible to identify the imperfections [33].

Figure 19. Fish defect detection in VNIR range for each wavelength layer (500 to 800 nm) [33].

2.2.3 Defense and Security

This technology is used in defense and security applications too. For example, HSI allows the detection, identification and quantification of chemical vapors presented in the atmosphere. After the capture of HS cube of one scene where there are a background landscape and one gaseous cloud in front of the image, a processing algorithm is applied to make the detection, identification and quantification of gas the[34].

The algorithms evaluate the chemical clouds characteristics thought recognition of spectral intrinsic signatures of the chemical species in the measured data. Figure 20 shows different chemical products detected with different colors.

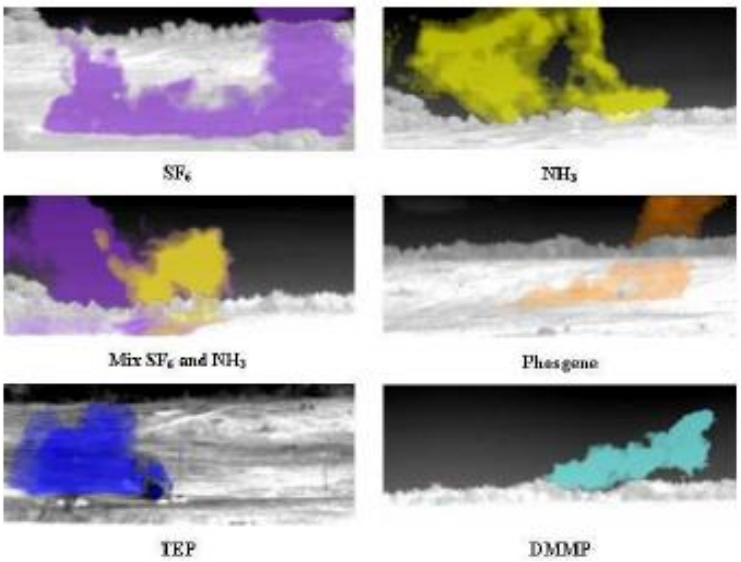

Figure 20. Chemical gases liberation [34].

2.2.4 Drug Identification

Also, the pharmaceutical sector has used HSI with the objective of improving the quality control, identification and detection of false medicaments. HSI has proved advantages in comparison with traditional techniques of medicaments analyses, generally based on chemical analyses. For example, the falsified medicaments do not expire with standards of quality and security provided by the laboratories, so that the active ingredients can differ of optimum doses causing unpredictable reactions in patients [35]. Figure 21 shows an example of this application, where the different false medicament is detected using HSI.

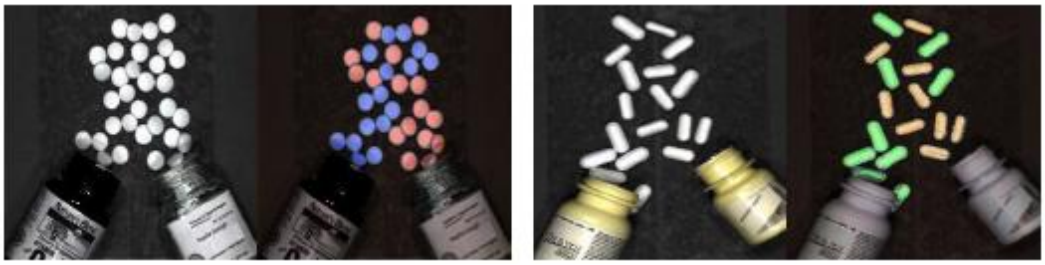

Figure 21. Falsified pharmaceutics products identification using HIS [35].

2.3 Mineralogy and Archeology

Due to its non-invasive and non-destructive nature, HSI is an image modality extremely useful in art works studies and analyses. Since many years there has been a high demand in the use of HSI for art conservation process, art history and mineralogy-archeology [36].

Over the last two decades, different types of detectors and filtering/dispersing technologies have been integrated in custom-made or commercial HSI systems for these applications. Although it is still in an early stage, its potential has been witnessed through different studies in which paintings have been attributed and interpreted,

pigments and inks differentiated and identified, and important illegible scripts revealed, enhanced and studied. HSI has revolutionized the non-invasive techniques such as infrared reflectography (IRR)[37], ultraviolet reflectance and ultraviolet induced visible fluorescence[38], commonly employed in the study and conservation of artifacts. Some example are the study of materials of archeological, samples with an historic value, monitoring and evaluation of conservation treatments or digital imaging for documentation and achieving [39].

In the case of the visualization of under drawings and pentimenti in paintings, IRR has been the most widely used to perform the imaging analyses and study of the under drawings.

In the beginning of this application, the cameras did not have a great resolution because of the technology was limited, since the maximum penetration of most paints can be achieved at wavelengths of around 2 µm. After the appearance of new sensor types, such as CMOS or CCD, the problem with the optimal spectral range and image resolution has disappeared.

Two of the most important parameters that conservators have sought in IRR devices is the high image resolution and the image penetration. However, not all under drawing are visible in the infrared, so and multispectral and HS imaging could assist in finding the right wavelengths to image under drawing, as we can see in Figure 22(a) and Figure 22(b). Moreover, in the study of paintings it is important to image not only the under drawings but also the under modeling and colored grounds that could be significant for the attribution of painting

(a) (b)

Figure 22. Monochromatic spectral images at 640 nm and 1000 nm of a Byzantine icon showing an increase in the reflectivity of the paint layer at 1000 nm. At this wavelength, the painterly pentimenti of the hand beneath become visible [36]**.**

There are some experiments about the application of HS camera in painting or drawing, like the Russian Icon. Some companies of different institutions around Europe, among them Spain, worked in the performance of different systems for spectral digitization of artworks, in this case, using the Russian Icon [40]. The objective was getting a quantitative estimate of accuracy and characterizes the colorants icon by means of results obtained with HS cameras used by observers of different companies.

Figure 23 shows the HS camera used in Italy to experiment with the Russian Icon and the RGB image. Figure 24 shows the reflectance spectra from different locations of the images.

(a) (b)

Figure 23. (a) HS camera capturing the HS image of the Russian Icon. (b) RGB image of the Russian Icon [40]**.**

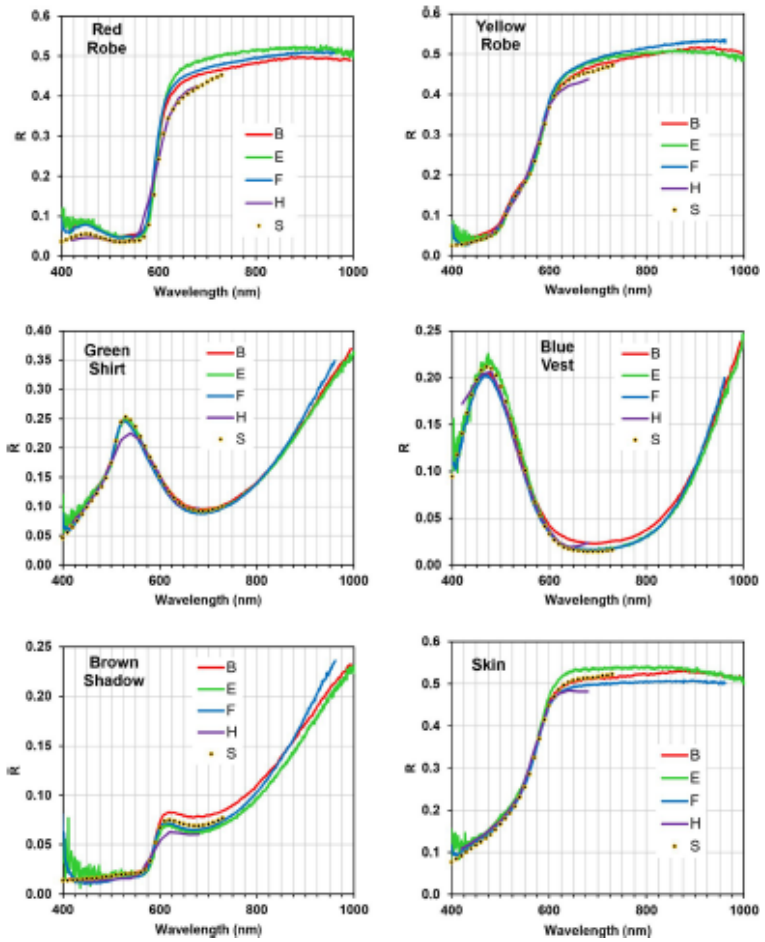

Figure 24. Reflectance spectra from six different locations of the Russian Icon image [40]**.**

Other application of HSI is the characterization and mapping of pigments and inks in painted artifacts and drawings. The non-invasive characterization of pigments and other pictorial materials has been done primarily using fiber optics reflectance spectroscopy (FORS) in the UV-VIS and NIR spectral range and more recently in the MWIR range [36]. The development of multispectral and HS systems capable of providing imaging spectroscopy has opened new perspective for this application, for example, such systems capture images at a large number of spectral bands and can identify materials with unique spectral signatures. Moreover, with adequate data-processing methods, these materials can be mapped based on their spectral characteristics, which is a significant advantage compared with spectroscopy point analysis.

VNIR spectral imaging has found innovative applications for study of mural paintings and rock arts[41], [42]. Despite the constraints imposed by outdoor measurements on large-scale paintings and inscriptions, spectral differences in pigments with similar coloration but different chemical composition were recorded in the Mayan hieroglyphs found at the Naj Tunich cave in Guatemala. The data obtained were further analyzed by clustering analysis, which led to differentiation between original pigments and later repainting and revealed interrelationships between the inscriptions. However, some identification of pigments cannot be achieved because the limitations in the spectral range, like the identification of a red pigment as vermilion from an illuminated manuscript was also achieved with multispectral imaging but the blue pigment could not be identified. Comparing Figure 25(a) and their corresponding spectra, it can be observed that variations in reflectance as a function of the wavelength for each individual red pigment is correlated with the tonal intensity (transparency) of the images at the specific wavelength. For example, the reflectance of cadmium red clearly increases with the shift from 620 to 680 nm as shown in both the image and the reflectance spectrum (Figure 25). In contrast, red ochre remains non-reflective at the same wavelengths.

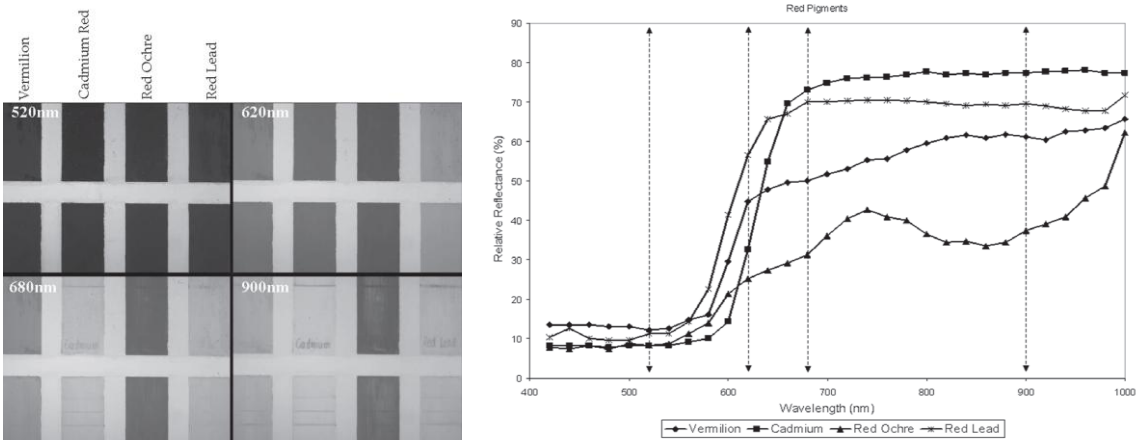

(a) (b)

Figure 25. Spectral images at narrow spectral bands (520, 620, 680 and 900 nm) of a custom-made reference pigment chart illustrating four different red pigments and reflectance spectra of the pigments illustrated in (a) [36].

Multispectral imaging (MSI) in the SWIR spectral range with a limited number of broadband filters has evolved over time and has opened new possibilities for the characterization of pigments with similar reflectance in the VNIR. Results on test panels show a good correlation with the reflectance spectra obtained by high resolution VNIR-SWIR spectroscopy. The respective images collected as image spectral cubes were also used as a visual criterion to differentiate the pigments, as they showed clear differences at varying wavelengths. A parameter that seems to affect the intensity of the spectra is the light-absorbing white ground often found as a preparatory layer beneath thin paint that alters the reflectance spectra of the paint layer. The same methodology for MSI in the SWIR range was also applied in the examination of blue pigments in two works by Van Gogh: La Mousmé (1888) and the Van Gogh Self-Portrait (1899). The results indicate that data collected in the SWIR spectral range were adequate to differentiate, characterize and map the distribution of the different blue pigments on the paintings[36].

The results obtained by different companies for the identification of pigments and their admixtures show clearly the current limitations of spectral imaging for this application. This can be attributed primarily to the restricted spectral range and to the non-availability of an exhaustive database of the reflectance spectra of pigments. The current lack of a pigment spectrum database indicates that it is a challenge to resolve the spectra of pigment mixtures into their single components. Although enhanced discriminating capabilities are expected with future technological developments, complementary and often invasive techniques requiring micro-sampling will still be needed to assist in the characterization of individual materials and pictorial layers.

On the other hand, the study and differentiation of organic binding media is other applications into the archeological sector. Multispectral and HS imaging using UV-induced and VIS-fluorescence imaging have been employed for the differentiation of

organic binding media as certain materials show different intensities and colors of fluorescence that can be useful for their identification. Other non-invasive techniques have been used for the characterization of organic binding media with varying degrees of success, including fluorescence lifetime imaging, FORS and Fourier transform infrared spectroscopy (FTIR)[36].

Also, the study of minerals and gems is a great application to archaeological monuments or caves. Multispectral and HS imaging have been used for the analysis of semi-precious and precious stones. HSI have been used to detect injures due to maintain process through laser techniques in marbles, paper and scrolls, where have been used assisted methods by computer to compare the state of art work before of realize the maintenance tasks and after of that[36].

The Faculty of Geodesy (Croatia) made an experiment of this application [43]. They used a HS camera with the objective to find the correlation among different fragments of archaeological artifacts. To obtain this goal, they used a spectrograph, a matrix detector and a CCD sensor (see Table 3 reference [43]). Figure 26 and Figure 27 shows the results of this experiment, where they concluded that the use of HS scanning technology has a big and real potential in the classification of fragments of archaeological artifacts, like rocks, gems or other precious stones.

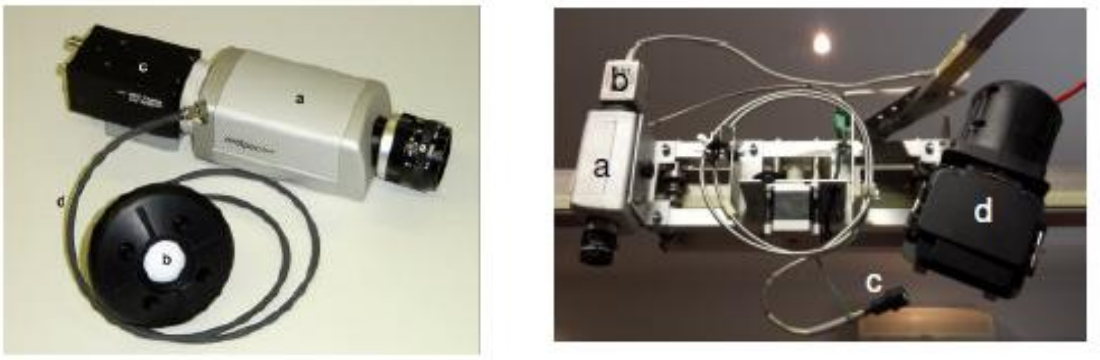

(a) (b)

Figure 26. (a) Imaging Spectrograph ImSpector V9. (b) Hyperspectral camera assembly [43].

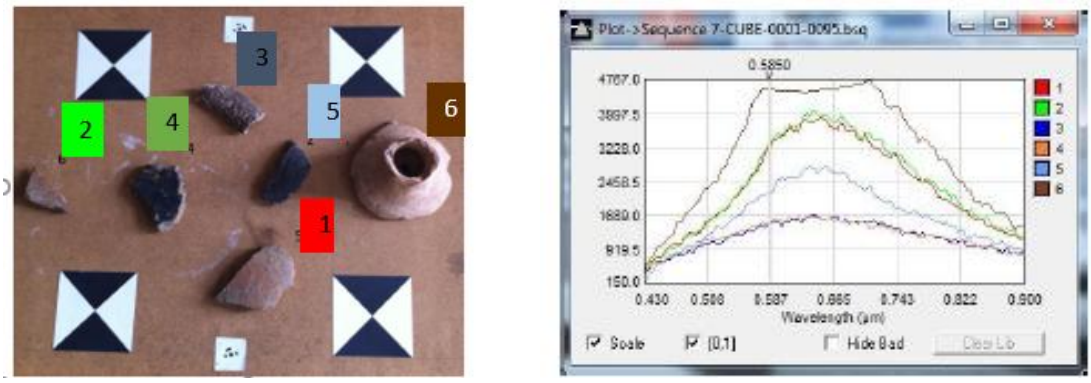

(a) (b)

Figure 27. (a) Archaeological artifacts. (b) Spectral plot of sample taken from different fragments [43].

Other application of HSI in the mineralogy filed is the soil characterization. A natural field is a heterogenic structure compound of rocks, liquids, vegetation and

other materials. HSI techniques have been used to evaluate the soil perturbation in comparison with others land sections [44]. Using advanced techniques of data processing is possible calculate that a land section has been altered in comparison with other part of the same land. Figure 28 shows an example of soil characterization application, where different rocks samples, such as norite, obsidian, soapstone, alabaster and jasper are differentiated thanks to HSI. Also, this picture presents the false-color composite of three bands.

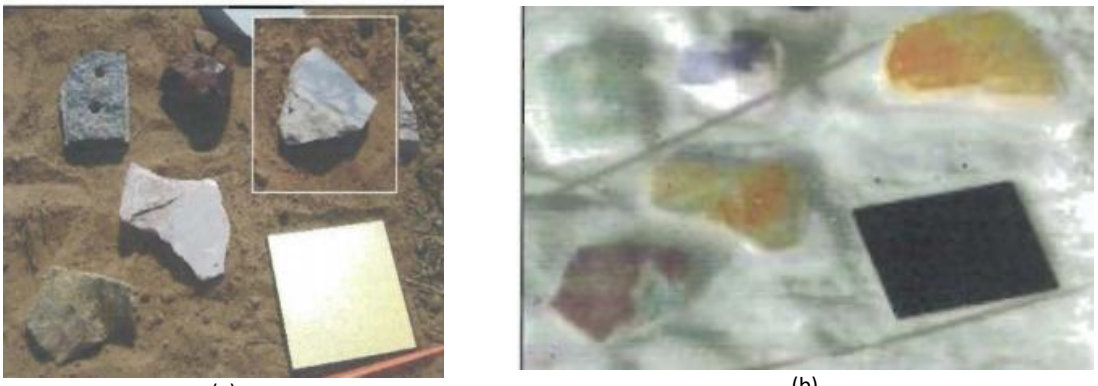

(a) (b)

Figure 28. (a) Photograph of the sample rock. Norite is in the upper left, obsidian in the upper center, soapstone in the insert, alabaster near the center, jasper in the lower left and the white reference panel in the lower right. (b) False-color composite of tape [44].

2.4 Summary

The main characteristics of the systems used in the field of conservation are summarized in Table 3 together with the applications for which they have been used. Most of them, however, offer enough flexibility to be used successfully for other applications as well.

Table 3. Characteristics of MSI and HSI imaging systems used in conservation.

Ref	Detectors / Camera	Spectral Range (nm)	Disper. Device / Filters	Algorithm / SW	Bands	App.
[45]	CCD	650-1100 (NIR)	LCTF	PCA/ENVI	40	Pigments, paintings, drawings
[40]	Monochrome CCD	400-1000	Pushbroom	ENVI 4.7 IIP-Image	61	Pictures, Paintings
[40]	Monochorme CCD	400-720	LCTF	ENVI 4.7 IIP-Image	33	Pictures, Paintings
[46]	Firelly IR Imager (OPO Technology) Red Eye 1.7 (NIR)	900-1850 (NIR) 2500-3750 (MIR) 900-1700	Whiskbroom Pushbroom	PCA	61 209 61	Paintings, pigments artwork
[47]	-	383-893	-	SAM SCM PPI Sparse unmixing	240	Pigments, paintings
[48]	VNIR-E series	380-1000	Quartz Tungsten Halogen QTH +Protection of UV radiation	MNF PCA ICA	-	Paintings, rock arts, pictographic
[49]	CCD/Chroma C4	450-1100	Bandpass Interferential filters (±25 nm pass bands → central band)	Orthogonalization(OMP)	4	Paintings, rocks art
[43]	ImSpector V9 and matrix CCD sensor PIXELFLY	430-900	Optical and PGP Pushbroom	HS cube	67	Rock arts, ceramics, archeological artefacts
[50]	Temperature-stabilized mercury-cadmium-telluride (MCT)/SWIR XEVA CL 2.5 350 TE4 + ImSpector N25E	1100-2400	Pushbroom	PCA PLS-DA (MATLAB)	209	Taphonomic analyses, assemblage integrity, rock arts, gems
[51]	CCD + V10EimSpectror (VNIR)	400-1000 380-1700	Pushbroom Whiskbroom/ broadband	SAM Raman Spectroscopy and X-RAY EDXRF (IDAQ) (ENVI15.1 + IDL) →DA	4	Paintings, pigments, artworks, colours, historic documents
[41]	LabRam-IR HR-800 + Olympus BX41	5882-10000	LWD	SNR		Cave art, pigments, rock arts
[52]	CCD InGaAs/(SWIR)	300-1000 900-1700	LCTF AOTF	-	-	Paintings, pigments, colours
[53]	CCD/InGaAs	400-1700	Pushbroom PGP	PCA PPI	30	Paintings, pictures, pigments
[54]	BWTEK BWS415 i-Raman spectometer	4000-10000	-	ED-XRF (BWSpec 3.26)	21551	Rock arts, paintings, pigments

3. MATERIALS AND METHODS

3.1 Obsidians samples descriptions

In this research study all obsidians were provided by the Canarian Museum and the Department of Historical Science of the la ULPGC. In total, there are 69 obsidians with different deposit origin.

Before to start capturing HS images from these samples, it is necessary to prepare a database with all the information provided by the archaeologists, such us their physical features (size, weight, etc.), references, the different classification levels (deposit level, municipality level and island level) of each obsidian sample. The classification levels are different scales where the different samples are classified. Within the classification levels we find two islands at the island classification level, where on each island there are different municipalities at the municipality classification level, and within each municipality we find one or more deposits at the deposit classification level. Annex I present all the characteristics of each obsidian.

Once all the information was gathered, it is important to know how many samples are available, how is possible to group them and how is possible to effectively process them. For that reason, an organization scheme was done to classify each sample. In this scheme (Figure 29), the 69 obsidian samples were grouped into three different levels: deposit (orange), municipality (green) and island (blue).

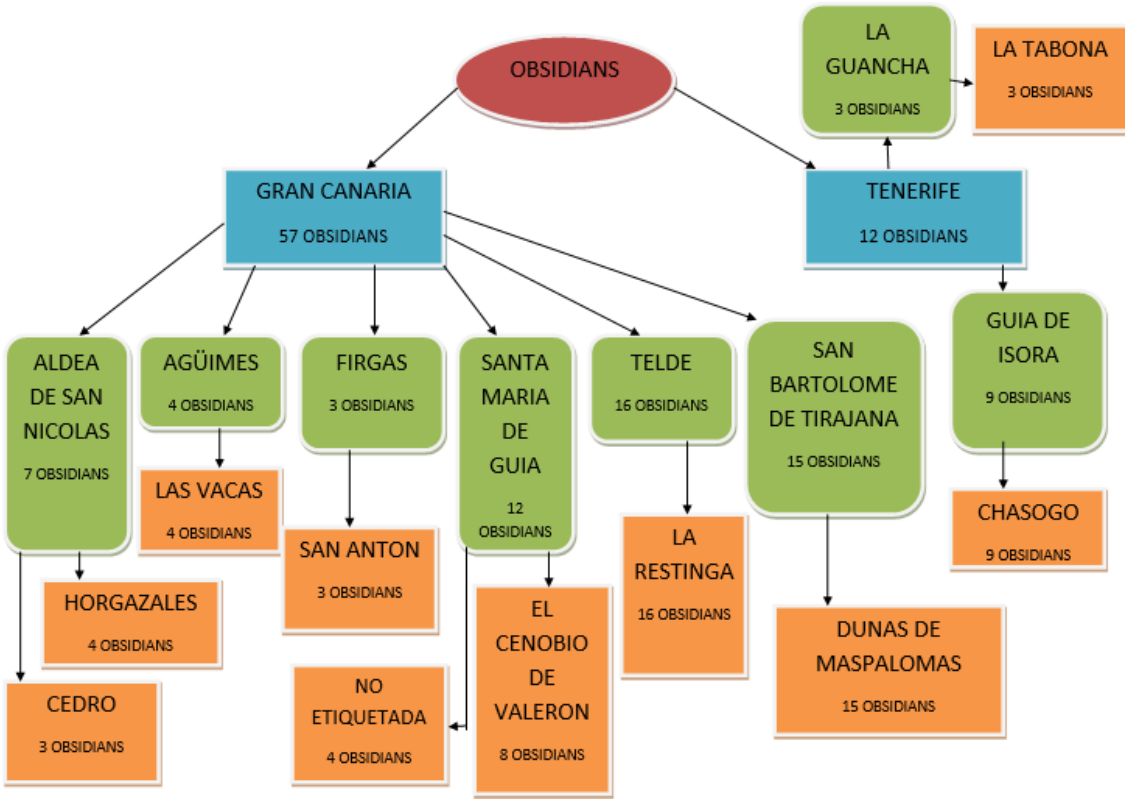

Figure 29. Organization scheme of the obsidian sample database.

In this scheme, the labeling provided by the archaeologist was changed (maintaining a correlation with the original labeling) by a new labeling based on different levels to facilitate the processing of the images. In Table 4 this labeling based on by levels is shown.

Table 4. Labeled by deposit, municipality and island.

Class ID			Class Name			Nº of obsidians		
LEVEL 1	LEVEL 2	LEVEL 3				LEVEL 1	LEVEL 2	LEVEL 3
100	110	111	Gran Canaria	Telde	La Restinga	57	16	16
	120	121		Aldea de San Nicolás	Cedro		7	3
		122			Horgazales			4
	130	131		Firgas	San Antón		3	3
	140	141		Agüimes	Las Vacas		4	4
	150	151		Santa María de Guía	El Cenobio		12	8
		152			No Etiqueta			4
	160	161		San Bartolomé de Tirajana	Dunas de Maspalomas		15	15
200	210	211	Tenerife	Guía de Isora	Chasobo	12	9	9
	220	221		La Guancha	La Tabona		3	3

The next step is making a template for image acquisition. This template helps us to place the obsidians in an organized way and to facilitate the information extraction process that will be explained later. In Figure 30 it can be seen a page of this template where the obsidians are placed inside the drawn square with its respective reference. S1, S2, S3, etc, is the labeling format appointed to facilitate the processing of the images.

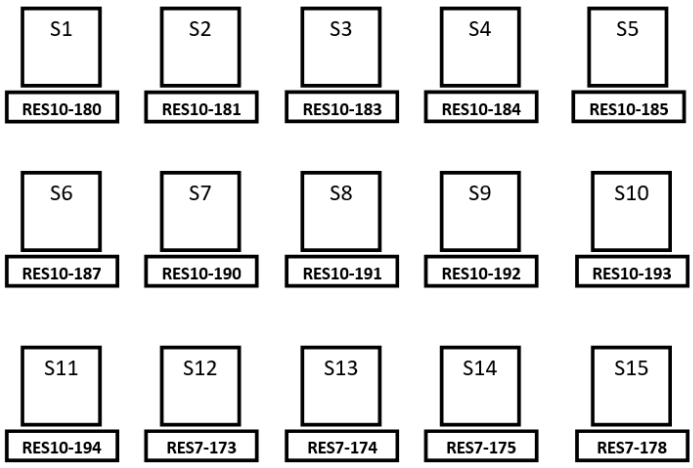

Figure 30. Template for HSI capture process.

3.2 Acquisition systems

To capture the HS images from the obsidian rocks, an acquisition system was used. This system consists in two cameras; on the one hand, the SWIR camera and on the other hand, the VNIR camera. These two cameras are coupled to a scanning platform and a light system to illuminate the samples. Figure 31 presents this acquisition system. This acquisition system consists in one illumination source (1), one SWIR

camera (2), one VNIR camera (3) and one linear displacement (4), where the cameras move along the line. The hyperspectral cameras used in this work are the Headwall Hyperspec® SWIR and Headwall Hyperspec® VNIR E-Series. The principal characteristics of these two cameras are shown in Table 5.

Table 5. Cameras characteristics.

Characteristic	Headwall Hyperspec® SWIR	Headwall Hyperspec® VNIR E-Series.
Spectral range (nm)	900 – 2500	380 – 1000
Spectral resolution (nm)	12	3
Spectral bands	267	923
Spatial bands	384	1600
Dispersion/Pixel (nm/pixel)	6	0.65
Capture type	Pushbroom	Pushbroom
Pixel Pitch (µm)	24	6.5

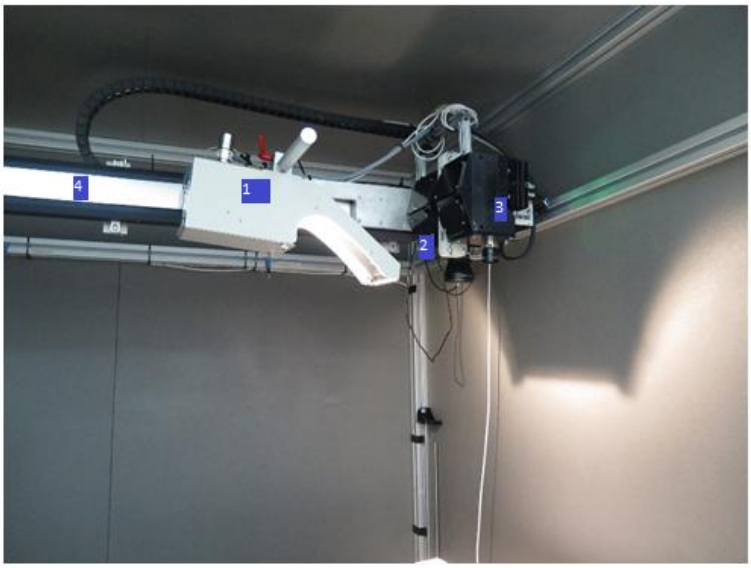

Figure 31. The acquisition system compound of the illumination source (1), the SWIR camera (2), the VNIR camera (3) and the linear displacement (4).

These cameras are pushbroom cameras, so to capture a whole HS cube, either the camera or the sample must be moved synchronously with the shoot of the camera. In this case, the linear movement is done by the camera using a linear actuator drove by a stepper motor along a line.

The illumination system consists of a halogen light and a light power supply with intensity regulator. This system permits us to regulate the light intensity in function of the sample characteristics, such us color, size or other parameters dependent on light. This light has been tested to emit in all the spectral range.

Before starting the capturing process, the cameras must be focused and calibrated with a dark reference and a white reference. There are many white references in the market with different reflectance value. It is necessary to choose an adequate white reference to capture the samples properly.

To obtain the dark reference image, we made a capture with the light off and with the lens tap on. To obtain the white reference image, we must to choose which reflectance percentage is the most suitable for this application for the white reference tile. In this process, a white reference tile with 99.9% of reflectance was chosen for the white reference as starting point. If the spectral signature does not show relevant information, such as characteristic peaks, the white reference tile with a reflectance of 50% and 10% will be tested for the same process. When the white reference reflectance percentage is changed, it is necessary to calibrate each camera again. Figure 32(a) shows the white reference tile being used to obtain the white reference image, while Figure 32(b) shows the chessboard pattern employed to focus the HS cameras.

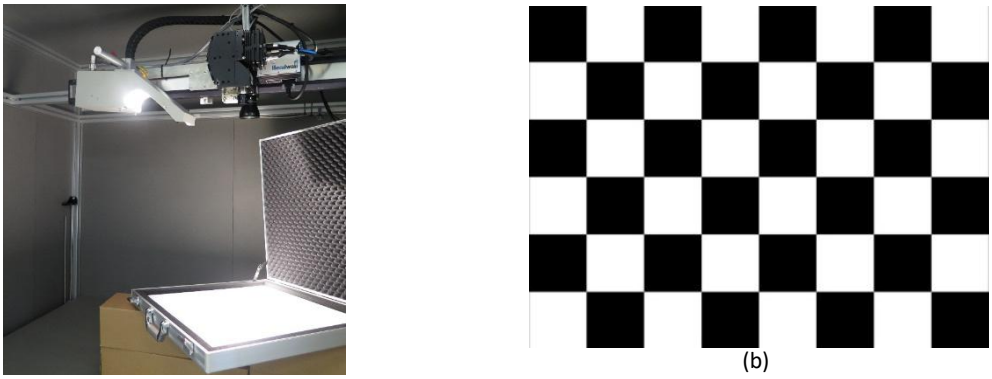
(b)

Figure 32. (a) White reference (b) Chessboard pattern for the HS camera focusing procedure.

When the calibration and focusing procedure is finished, it is necessary to calculate the FOV of the camera. Exactly, the obsidians are located in a distance of 620 mm from the camera lens, because using this distance, the obsidian captures are taken clearly and visibly. If the obsidians were bigger, the height between camera and obsidians sample would be bigger. The main objective is to take the captures quickly and with a good quality for the later processing. Furthermore, we must to define the camera movement speed for obtaining an optimal capture. It is evident that the parameters for two cameras are different because they have different spatial resolution and frame rate of the cameras. If pixel size is larger, the camera should adjust with a higher speed or a lower frame-rate (fps). If the pixel size is smaller, the speed will be lower, or the frame-rate will be higher. Figure 33 shows the distribution of the obsidians and the work area. The equation 6 was applied to calculate FOV:

$$\boldsymbol{FOV} = \frac{\boldsymbol{SSxWD}}{\boldsymbol{FL}} = \frac{\boldsymbol{NPxPPxWD}}{\boldsymbol{FL}} \quad (6)$$

Where:

- SS: sensor size → SS = NP x PP
- NP: number of pixel = 1600 to VNIR and 384 to SWIR
- PP: pixel pitch = $6.5 \cdot 10^{-3}$ mm to VNIR and $24 \cdot 10^{-3}$ mm to SWIR
- FL: focal length = 16.4 mm to VNIR and 16 mm to SWIR

- WD: work distance = 630 mm

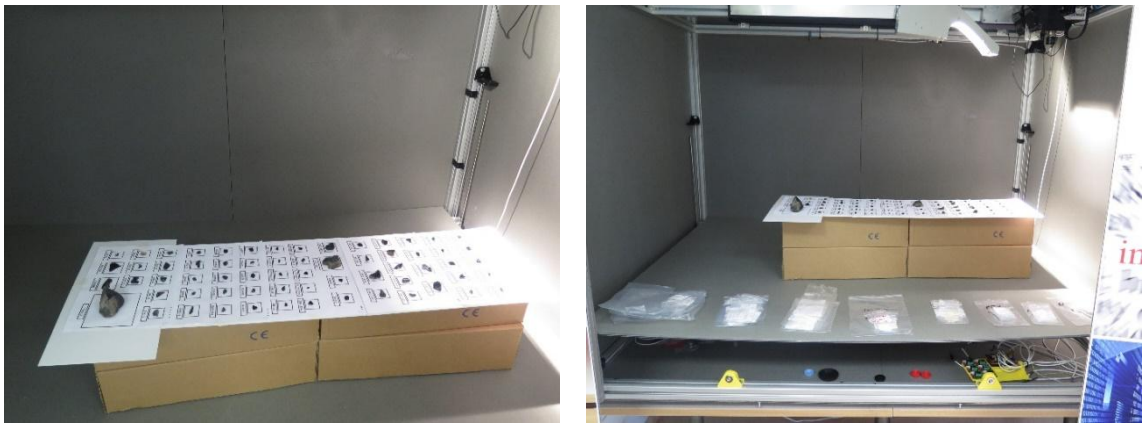

(a) (b)

Figure 33. (a) Obsidian distribution. (b) Work area.

Using Eq.6 we generate graphs, such us Figure 34, that help us to have an idea of the value that the FOV should have in relation to the working distance without having to apply the equation 5. This picture represents a lineal behavior between these two parameters. As the working distance increases, the FOV also increases.

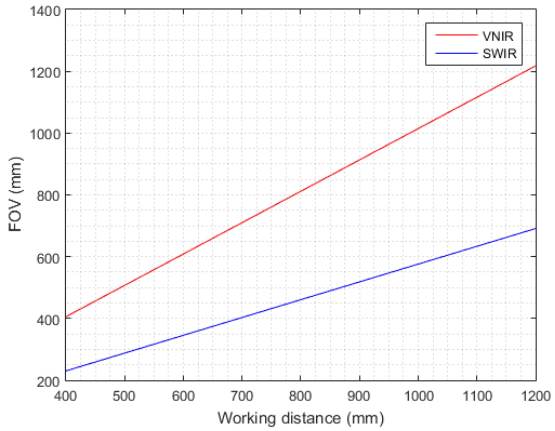

Figure 34. FOV vs working distance graph.

Before starting the capturing process, it is necessary to know how many captures must be made. The number of captures for this research work is 4 per template.

- One capture per camera with the obsidians placed in the “formal” (initial position).
- One capture per camera with the obsidians placed “inversely” to the initial position.

It is necessary to capture the obsidian by both positions due to the external impurities. This factor can affect in the classification process. Further, in this way you can get more spectral information about the obsidian.

Finally, the capturing process can start. When all parameters to capture the image were defined and the HSI was captured, the software gives you the possibility to save the image RAW, the calibrated image and the dark and white reference image

selected. Figure 35 shows obsidians capture with the SWIR camera and another with the VNIR camera.

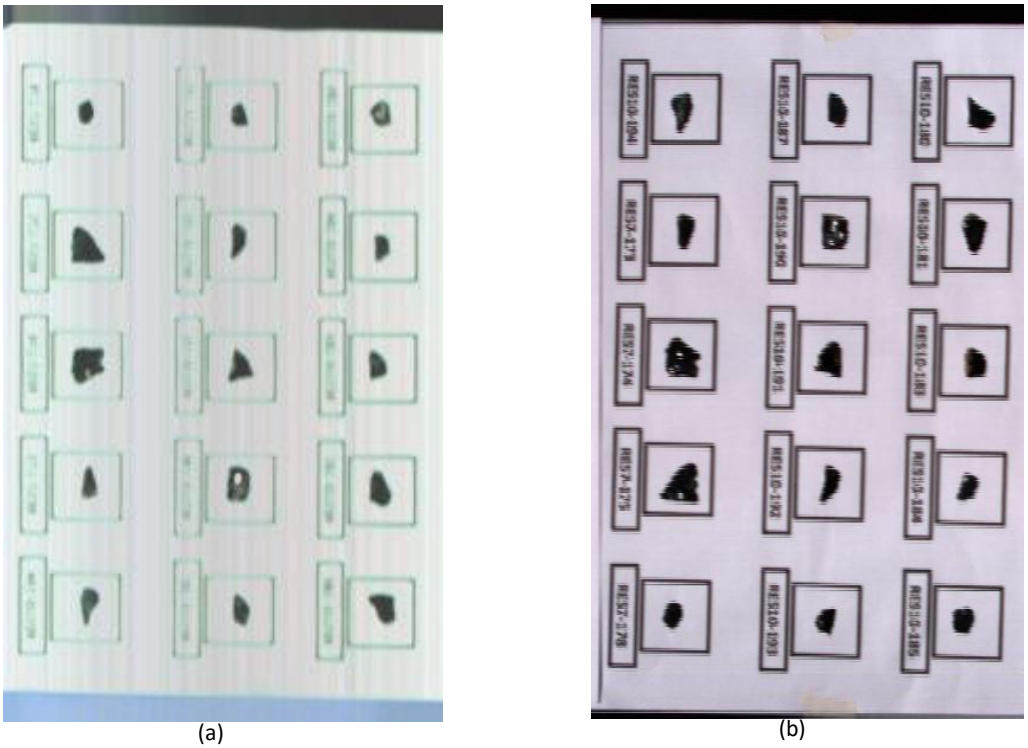

(a) (b)

Figure 35. (a) Obsidian capture with SWIR camera. (b) Obsidian capture with VNIR camera.

3.3 Data labeling procedure

After the capture process, it is necessary to apply a pre-processing of HS images to obtain the best possible results. This process is done in a mathematical tool called MATLAB. The objective of this process is to obtain the spectral signatures of the obsidians and the labeling of the data for the classification process.

First, is necessary to organize the step to make the program. For this, some steps were elaborated to make the program. These steps will give us clear results and in an orderly manner. These steps were:

1. Calibrate the image.
2. Crop each obsidian separately from the original image.
3. Obtain the mask and the number of pixel of each obsidian.
4. Obtain the spectral signatures and labels of each obsidian.

1) Calibrate the image.

Before to start the processing of the data, it is necessary to calibrate the image. When the obsidians were captured in the laboratory, the dark and white reference image were also obtained for this calibration process. The calibration is obtained through equation 7, where C is the calibrated image and RAW is the raw image.

$$C = \frac{RAW - DARK\_REFERENCE}{WHITE\_REFERENCE - DARK\_REFERENCE} \quad (7)$$

Figure 36 presents the raw data acquired by the HS camera, the reference spectral signature and the calibrated spectral signature.

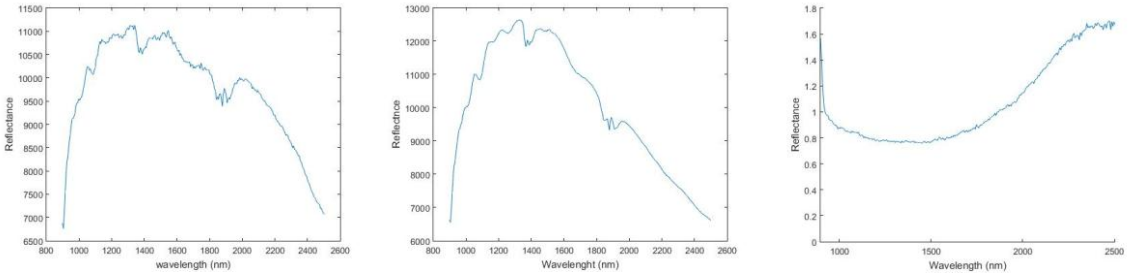

(a) (b) (c)

Figure 36. (a) Obsidian spectral signature without calibration (RAW image) with SWIR camera. (b) White reference spectral signature. (c) Calibrate spectral signature.

There is white a reference selection process that works with the raw image. This process consists in comparing all white reference spectral signatures to choose the best white reference for the processing. This procedure was realized to select the white reference (with a reflectance of 99%, 50%, or 10%). The reason for using other white references with a lower percentage of reflection is because of the low reflectance that the obsidian present in both spectral ranges.

2) Crop each obsidian separately from the original image.

As the template has not the same number of obsidians in each sheet, it is necessary to introduce the number of obsidians that we can find in the imaged to perform the same number of crops. The trimming process is realized in a semi-automatic way due to the user is who marks where he wants to cut the image and the software is who save the cropped image. So, the time of execution of the program created by the user is reduced compared to doing the trim one by one without asking about the number of obsidians in the image. Figure 37 presents an example of one entire image and the cropped image corresponding to a single obsidian rock.

(a) (b)

Figure 37. (a) Example of the entire sheet image with the SWIR camera. (b) Example of a cropped image with one obsidian rock.

Regarding the VNIR camera, before starting to crop the obsidian images, it is necessary to do an additional crop because the VNIR image size is too big to process in the MATLAB code using a standard desktop computer (Figure 38(a)). This action consists of cropping the VNIR image in three samples (Figure 38(b)) and work with

each one of these cropped images independently. The final step is the cropped image of each obsidian rock (Figure 38(c)).

(a) (b) (c)

Figure 38. (a) Synthetic RGB image of the entire sheet obtained with the VNIR camera. (b) First row cropping to reduce the image size for the processing. (c) Final cropping example to obtain the obsidian sample.

3) Obtain the mask and number of pixels of each obsidian.

The mask is a golden standard map where we can differentiate the obsidian from the background. In this map, the obsidian pixels have a value equal to 1 (white pixels) and the background pixels a value equal to 0 (black pixels). In addition, the total number of pixels is obtained by simply counting the 1s in the image. This is done by counting the number of pixel with value equal to 1. This process is automatic; the mask is generated and saved by the software. Figure 39 shows three example of obsidian rock mask.

(a) (b) (c)

Figure 39. Obsidian mask examples. (a) Obsidian of the municipality of La Restinga. (b) Obsidian of the municipality of San Bartolomé de Tirajana. (c) Obsidian of the municipality of La Tabona.

4) Obtain the spectral signatures and labels of each obsidian.

The objective in this part of the process is to generate the spectral signatures dataset that will be used in the experiments. The HS cube generated after cropping process has three dimensions [x,y,lambda] and the label matrix has two dimensions [x,y]. To be able to represent the spectral signatures, it is necessary to reshape the HS cube matrix to a two dimensions matrix [N, lambda], where N is the product of the dimensions x and y (N=x*y), i.e., the total number of pixels. On the other hand, the label matrix is transformed to a vector of dimension N. After that, the background pixels are eliminated in the dataset because they do not have relevant information, obtaining the final obsidian spectral signature dataset with its respective labels. Figure 40 presents an example the average signature of one obsidian image obtained with both cameras.

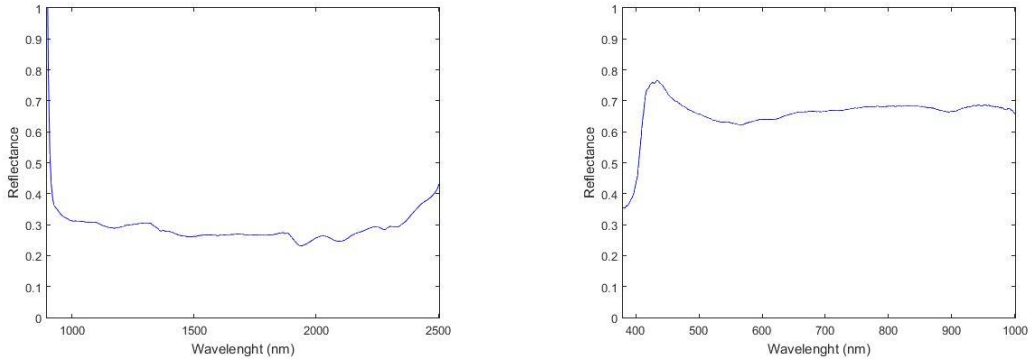

(a) (b)

Figure 40. (a) Spectral signature to SWIR camera. (b) Spectral signature to VNIR camera.

As a result, several datasets were obtained, classifying them by island, municipality and deposit. For each origin there is the same number of datasets. In total, there are 2 datasets per obsidian position, where each obsidian has its appropriate label by level, which is its island label, its municipality label and its deposit label. Table 6 presents the number of spectral signatures for each case (island, municipality or deposit) and the obsidian position when it was captured.

Table 6. Specification of the datasets.

Number of spectral signatures				**Number of spectra**					
Position	Island	Municipality	Deposit	Island		Municipality		Deposit	
FRONTAL	69	69	69	Gran Canaria	9554	Telde	1627	La Restinga	1627
						Aldea de San Nicolás	2001	Cedro	783
								Horgazales	1218
						San Bartolomé de Tirajana	1609	Dunas de Maspalomas	1609
						Firgas	436	San Antón	436
						Agüimes	3087	Las Vacas	3087
						Santa María de Guía	794	El Cenobio	623
								No Etiqueta	171
				Tenerife	5968	Guía de Isora	1570	Chasobo	1570
						La Guancha	4398	La Tabona	4398
				TOTAL = 15522					
REVERSE	69	69	69	Gran Canaria	8896	Telde	1477	La Restinga	1477
						Aldea de San Nicolás	1875	Cedro	824
								Horgazales	1051
						San Bartolomé de Tirajana	1609	Dunas de Maspalomas	1609
						Firgas	407	San Antón	407
						Agüimes	2740	Las vacas	2740
						Santa María de Guía	788	El Cenobio	655
								No Etiqueta	133
				Tenerife	5916	Guía de Isora	1484	Chasogo	1484
						La Guancha	4432	La Tabona	4432
				TOTAL = 14812					
TOTAL	**138**			**30334**					

3.4 Processing framework

The proposed processing framework is based on a typical supervised classification scheme. This way, the inputs of the classifier are the measured spectral signature from all obsidian samples. The first step consists on a pre-processing chain that aims to compensate the effects produced by both the environmental conditions and the system response of the capturing system during the acquisition of the HS cubes. Then, a supervised classification is performed using three different classification methods. Finally, the performance of the classifiers is evaluated using standard metrics for assessing a classifier performance. Figure 41 shows this workflow. This section explains the details of each step of this workflow.

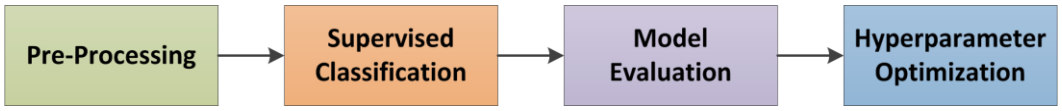

Figure 41. Workflow of the processing framework.

The next section explained the details of each step of this workflow:

3.4.1 Pre-processing

Three different pre-processing chains were proposed and employed to prepare the data before using it in the classification process. With this selection process, it is possible to improve the quality of the data and obtain better results in the classification process. Next, each one of these pre-processing chains is explained in detail.

1) Pre-Processing 0 (P0)

This pre-processing chain is composed by three steps: Calibration, Region of interest (ROI) Selection, and Band Reduction (Figure 42).

Figure 42. Pre-processing 0 chain.

First, due to the high dimensionality of the HS cubes, that slow down the processing of data, calibration process and a manual Region of Interest (ROI) selection is applied, as explained in the previous section “Data labeling procedure” (Section 3.3).

The next stage of this pre-processing chain performs a band reduction of the spectral signatures. There are bands that does not offer relevant information due to the low efficiency of the sensor in the extreme bands [55]. For this reason, these bands can be removed of the spectral signature. Figure 43 shows this elimination of bands with low information and the final obsidian spectral signature after applying the pre-processing 0.

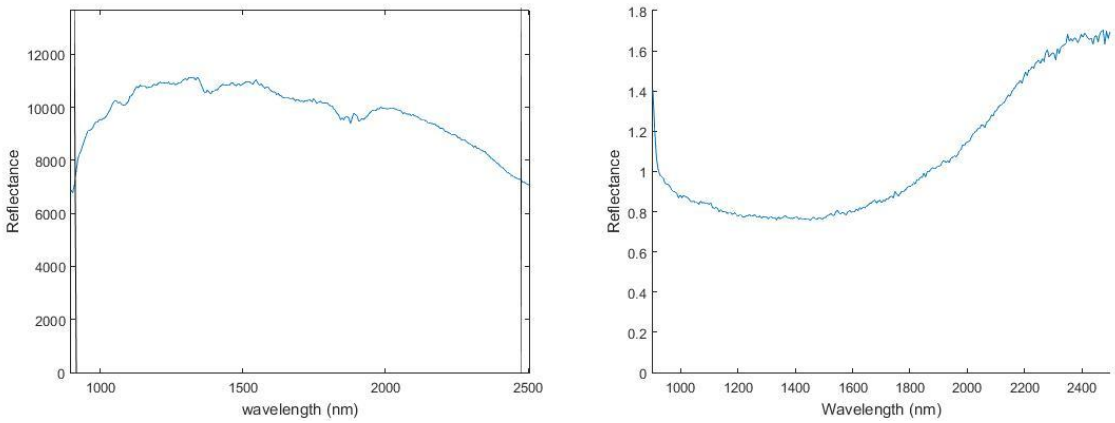

(a) (b)

Figure 43. (a) Raw spectral signature of the SWIR camera with the operating bandwidth. (b) Final spectral signature obtained in pre-processing 0.

2) Pre-processing 1 (P1)

This pre-processing chain composed by five steps: Calibration, ROI Selection, Band reduction, Smooth filtering and Data normalization (Figure 44).

Figure 44. Pre-processing 1 chain.

In this pre-processing chain, the first three steps are the same as in the pre-processing 0. The differences are the new steps 4 and 5.

In the fourth step, a noise filtering based on a smoothing technique is applied to the data in order to reduce the noise present in the spectral signatures. This algorithm filters the data by replacing each data point with the average of neighboring data points defined within the range, that is, the spectral signature does not have protruding peaks along the wavelength but a smoother spectral signature. As an example, Figure 45 presents a part of spectral signature with the smooth filter applied.

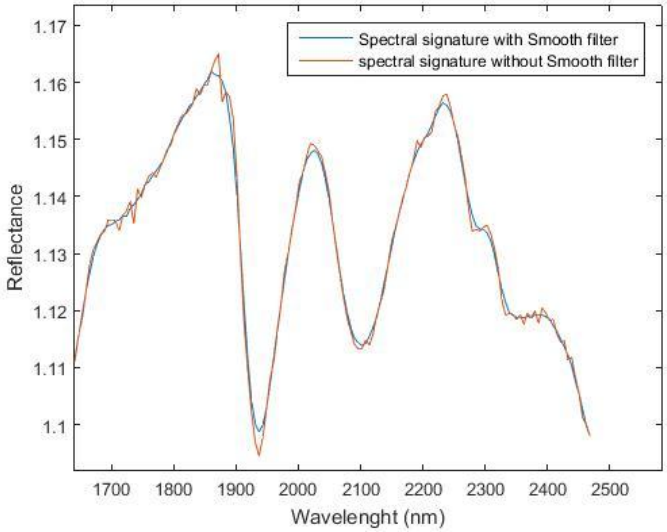

Figure 45. Smooth filter effect.

In the final stage the normalization of the data is performed. The objective of this step is to obtain all the reflectance values of spectral signatures comprised between 0 and 1. The maximum value of this new vector must be 1 and the minimum 0. The equation 9 was applied to achieve this normalization.

$$Y_N = \frac{Y_i}{max(Y)} \quad (9)$$

Where Y_N is the normalized spectral signature, Y_i is the pixel to be corrected and max(Y) is the maximum value of vector to apply the normalization. Figure 46 shows the spectral signature after applying the normalization of the data.

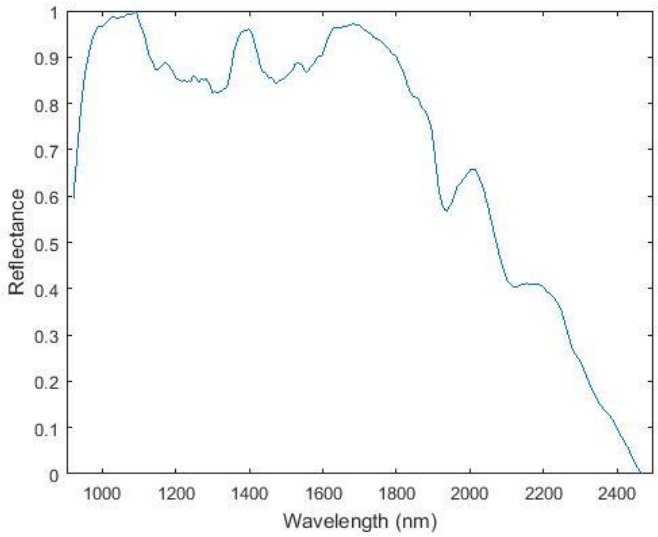

Figure 46. Spectral signature with normalized data.

3) Pre-Processing 2 (P2).

This pre-processing chain is composed by five steps: Calibration, AOI Selection, Band reduction, Smooth filtering and Data brightness normalization (Figure 47).

Figure 47. Pre-processing 2 chain.

This preprocessing stage is equivalent to pre-processing 1, except that here a data bright correction is employed instead of the 0 to 1 data normalization. This last stage process calculates the brightness of each pixel of the HS image and divides each pixel by its brightness[55], as shown in equation 10.

$$Y_{BC} = \frac{Y}{\sqrt{\sum_{i=1}^{n} y_i^2}} \quad (10)$$

Where Y_{BC} the pixel with the bright correction, Y is is the pixel to be corrected and y_i is the i-th component of thispixeland n is the number of bands of spectral signature. Using this pre-processing, the brightness of each pixel is homogenized without

modifying its spectral signature. Figure 48 shows the final spectral signature with this full pre-processing chain applied.

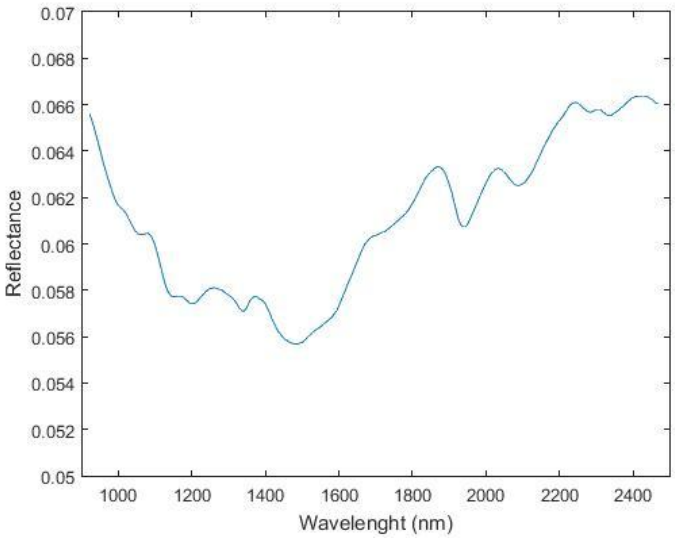

Figure 48. Spectral signature with data bright correction.

3.4.2 Selected classification algorithms

An extensive literature is available on pixel-wise classification of HS images, where each pixel is assigned to one of the classes based on its spectral signature. For this purpose, methods based on decision trees, neural networks and kernel-based methods has been widely used. These algorithms must face with two main problems: the high dimensionality of data and a limited size of sample data. The selected algorithms for this research work are Support Vector Machine (SVM) with two different kernels (Linear and Gaussian) and Random Forest (RF).

SVM is a kernel-based supervised algorithm that has been extensively used in the classification of HS images. Some references said that it has been proved that SVM provides a good performance for classifying HS data when a limited number of training sample are available[56]. Due to its strong theoretical foundation, good generalization capabilities, low sensitivity to the curse of dimensionality, and ability to find global classification solutions, SVM is usually preferred by many researches over other classification paradigms for classifying HS images. In this research work LIBSVM[57], integrated software for Support Vector classification, has been employed.

The other algorithm used in this supervised classification approach is Random Forest. This classifier an ensemble classification algorithm, which constructs a set of classifiers and then classify new data by taking a vote of their predictions[58]. Some studies have shown that these ensemble methods can provide a classification result as accurate as other traditional classifier. In this research work the MATLAB Machine Learning Toolbox has been employed.

3.4.3 Evaluation metrics

The metric chosen for estimating the classifier performance in this study is the overall accuracy. This metric summarizes the information supplied by a confusion matrix, but due to the large number of simulations that are being performed (there are several simulations from each obsidian, and each obsidian is performed using different classification algorithm), these parameters are not provided[59]. The evaluation metrics employed in this work is overall accuracy. Is necessary to define some terms:

- **True Positive (TP):** Correctly detected conditions, that is, the result of the test positive and the actual value of the classification is positive
- **True Negative (TN):** Correctly rejected conditions, that is, the result of the test negative and the actual value of the classification is negative
- **False Positive (FP):** Incorrectly detected conditions, that is, the result of the test negative and the actual value of the classification is positive
- **False Negative (FN):** Incorrectly detected conditions, that is, the result of the test positive and the actual value of the classification is negative

Where overall accuracy refers to the ability of the model to correctly predict the class label of new or previously unseen data and the equation to apply is:

$$Overallaccuracy = \frac{TP + TN}{TP + TN + FP + FN} \quad (11)$$

3.4.4 Model evaluation

For classification problems, the performance is usually measured as the error rate of the classifier. The classifier predicts the class for each instance in the dataset: if the class of the instance is correctly predicted it is counted as a success. However, if the predicted label is not the same as the label of the instance that have been classified it is a classification error. The error rate is just the proportion of errors made over a whole set of instances, and it measure the overall performance of a classifier.

The error rate measured over the training set is not likely to be a good indicator of future performance, because the classifier has been trained using the same training data, so the error estimation based on the training data will be optimistic. To predict the performance of a classifier over new data, it is necessary to assess its error rate on a dataset that played no part in the formation of the classifier. This independent dataset consisting in previously unseen data is called the test set.

The number of instances in the dataset is not a problem because it is possible to split the dataset into two parts with a larger number of instances where one subsets can be used to train the classifier and the other subsets can be used to measure its performance[60].

The disadvantages in the model evaluation appears when the available data is limited, a common problem of machine learning scene. In such situation, the amounts

of data that can be used for train and evaluate the performance of classifier are limited. Generally, the larger training sample give the better classifier, and the larger test samples give the more accurate the error estimate. So, a premise: to find a good classifier it is advisable to use as much data for training, and to obtain a good error estimate it is necessary to use as much of it as possible for testing.

However, is possible handle this problem through several techniques. For this reason, in this project we use both the hold out and the cross-validation methods will be employed.

- **Hold out**

This method to evaluate the classifier performance consist on selecting a certain amount of data for measuring the model performance (test set) and reversing the rest of instances on the data set for building the classifier (train set). Normally, one-third of the data is used for testing and the remaining two-thirds for training.

This method presents a weakness: it is possible that neither the sample used for training or testing nor even both might be not representative. At least, the hold out procedure must guarantee that all classes are represented both in the training set and in the test set. This process is called stratification. A more general way to mitigate any bias caused by the specific sample chosen for holding out is to repeat the whole process, training and testing, several times with different random samples. The error rates of the different iterations are average to yield an overall error rate. This method is called repeated hold out error rate estimation [61].

In this research study, hold-out will be used to optimize the different parameters for different classifier like cost value in SVM-linear, number of tree in Random Forest or cost-gamma values in SVM RBF (Real Basis Function).

- **Cross-validation**

In the k-fold cross validation method the whole dataset is partitioned into k disjoint folds. As occurs in the hold out method, it is advisable that each fold has the same class proportion. The basis of this method consists in using k-1 folds for training a classifier and the remaining for assessing its performance. This process is repeated k times varying the test set in each iteration until all folds have been used to evaluate the model performance. Finally, the model performance is calculated as the average performance of the k iterations. Figure 49 shows a graphical representation of this method.

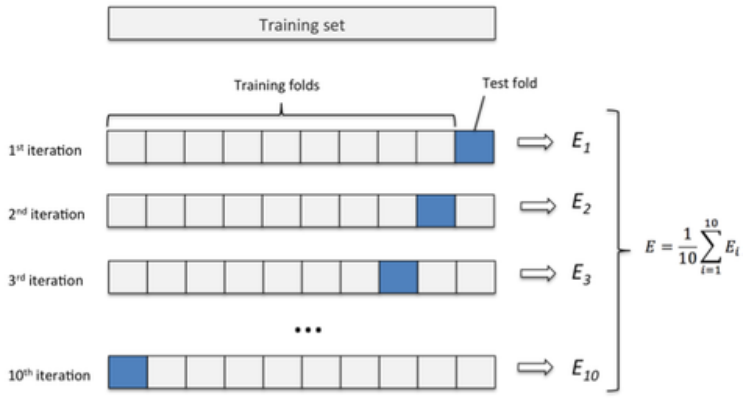

Figure 49. K-fold cross-validation example [62].

First of all, we have k determined, which is the number of fold adequate to apply cross-validation. Extensive test on numerous different datasets, with different learning techniques have shown that k=10 fold is the right number of fold to get the best estimate of error, and ten-fold cross-validation has become the standard method in practical terms. Nevertheless, a single ten-fold cross-validation might not be enough to get a reliable error estimate. When seeking an accurate error estimation, it is a standard procedure to repeat the ten-fold cross-validation several times and average the results [61].

In this research study, 10-fold cross-validation will be used as model validation scheme in all case of studies.

3.4.5 Parameter Optimization of the Classifier

The process to optimize the parameters of the classifier consists of finding the parameters that obtain the best classification results. This is an iterative process that consists in four steps:

1. First, a vector with the parameter to be optimized is created with different values to find the best. This vector is within a considerable and premeditated range, considering that the best value of that parameter is inside the parameter's vector. Otherwise, it will be necessary to expand the search range to obtain the best value
2. Then, a loop is created to obtain different results with different values of the parameter to be optimized. This loop consists in a combination between the Hold-Out and the 10-fold cross validation, where in each iteration the dataset is partitioned in 70% for training, to which the 10 fold cross validation is applied to vary the values of the parameters (train and validation set) that are in the vector created previously, and 30% to test the final results once the classifier parameter has been tuned. When each iteration ends, the classification results is obtained and stored in a file.
3. When the optimal parameter search is finished, it is necessary to generate graphs to visually represent the results obtained in each iteration for each

classifier parameter value. Normally two graphs are needed; a graph showing the results of the 10 observations of the loop for each value of the vector and another graph of the average results for each value of the vector.

4. Finally, the best value of the classifier parameter is selected for the final classification process. The choice of the value of the parameter to be optimized is established by the average of the 10 observations, choosing the value with the highest accuracy percentage.

3.5 Description of the experimental phases

To validate the supervised classification algorithms for discriminating between obsidians of different provenances, four different phases have been proposed. These phases are accomplished using different pre-processing stages and different classification algorithms. The proposed phases are described below.

- **Phase 1: Selection of the white reference and the obsidian position.**

The goal of this phase is to test and compare the different results after applying SVM classifier with the linear kernel without parameter optimization employing the P0 pre-processing chain. In this case, the obsidians will be characterized by three different spectral signature dataset, depending on the position of the sample (Frontal, Reverse or Frontal + Reverse). The aim of this phase is to select the dataset that offers the best results for the classification of the obsidian rocks and the best white reference tile to calibrate the HS images (10%, 50% and 99%).

All the available labeled data are merged in a unified dataset. It means that a unique database is created by joining all single obsidian dataset for each obsidian position. The position of the obsidian that obtains good results and presents more spectral information about the obsidians is chosen for the rest of the classification process.

- **Phase 2: Selection of the pre-processing chain.**

Once the white reference and the optimal dataset have been chosen, the next step is to select the best pre-processing chain for this type of samples. In this phase, the three previously described pre-processing chains are evaluated.

The best dataset chosen in the phase 1 is subject to a classification process to find the best pre-processing for this research work.

- **Phase 3: Selection of optimal classifier parameters in experiment 1.**

Before evaluating both the accuracy and computational cost performance of the three different classifiers, it is necessary to optimize the parameters. Each classifier has different parameters to optimize. In case of SVM with linear kernel, only it is necessary

to optimize the cost value (C), in Random Forest the number of trees, and for the SVM RBF it is necessary to optimize two parameters; the cost value and gamma value.

In this case, once the best pre-processing has been chosen, the unique database with all information about the obsidians is subjected to a classification process with the three different classifiers to obtain and compare the results among them. This process is called experiment 1.

- **Phase 4: Classifiers evaluation in experiment 2.**

In this phase, the leave-one-out method is employed to evaluate the results. In this process, the data of single obsidian is used as test set of a classification algorithm and the classifier model is built using the information from the rest of HS labeled data (belonging to the other obsidians). This phase represents the real case of new obsidian rock arriving to the Canarian Museum laboratory or other archaeology museum, where the classification must be performed with a classifier trained with data from previous obsidians. This process is called experiment 2.

In this research work, three classifiers have been chosen for the classification process: SVM classifier with linear kernel, Random Forest classifier and SVM classifier with Gaussian (Radial Basis Function, RBF) kernel.

3.6 Summary

In this chapter, the obsidian samples employed in this study have been presented, including the information provided by the archaeologist and describing how the samples have been captured using HS acquisition system. On the one hand, the pre-processing framework was presented, where the procedure to perform the parameter optimization of the classifier, the pre-processing chains, the supervised classifier and the different model evaluation techniques were described. On the other hand, four phases have been proposed to obtain the experimental results.

4. RESULTS

This chapter presents the results achieved when applying the supervised classification framework to the obsidian rocks described on Chapter 3. These results present the performance estimation of each classifier at each different phase. In addition, the computational cost of each classifier is calculated as a measured of the time required to train and evaluate the performance of each classifier for each experiment. This computational cost was calculated with one standard laptop Lenovo Ideapad 110-15ISK with a CPU Intel i3-6006U 2.0G.

In this chapter, only the SWIR data was used due to the high computational cost of the algorithm with VNIR data. For this reason, the images obtained with the VNIR camera will be studied in future works.

4.1 Phase 1: Selection of the white reference and the obsidian position.

As named in Chapter 3, this phase consists in classifying data in order to choose the white reference and the best obsidian position to achieve the best accuracy results. No parameters were optimized in the classifiers employed in this phase.

First, the results of the obsidian spectral signatures of the SWIR camera were realized performing the calibration of the data using the white reference tile of 99% of reflectance. The results were not relevant because the obsidians spectral signatures did not present differences possible to be identified by visual inspection. The spectral signatures were similar among the different obsidian types, respect to of the obsidian position (Frontal or Reverse). Figure 50 presents the spectral signatures obtained with the SWIR camera and calibrated using the 99% white reference tile.

After this preliminary analysis, it is necessary to compare the obsidian spectral signatures obtained with each white reference in order to choose the best white reference for the calibration procedure, in our case the white references employed are 99%, 50% and 10% of reflectance. Figure 50(a) shows that employing the white reference with 99% of reflectance the obtained spectral signatures do not contain remarkable information. Figure 50(b) and (c) presents the results obtained with the other references, 50% and 10% respectively, where it is possible to see that calibrating the images with the white reference of 99% of reflectance produce the worst results. On the other hand, the white reference with 50% and 10% of reflectance presents characteristic peaks, where it is possible to observe some differences between the obsidian spectral signatures.

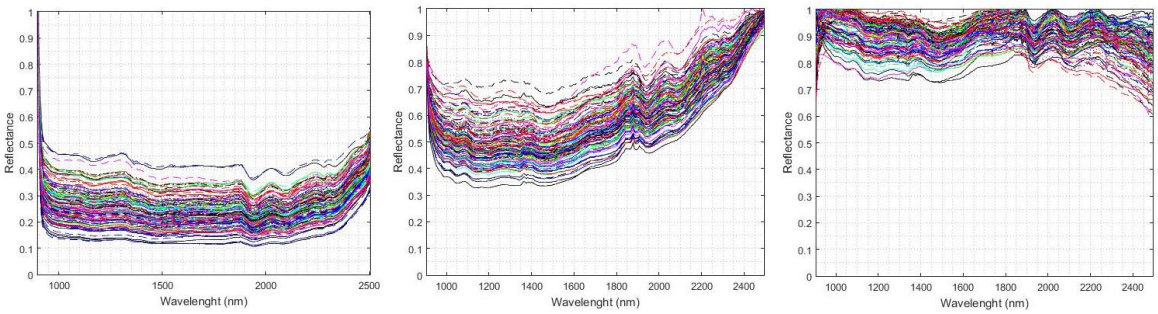

Figure 50. Obsidian spectral signatures with SWIR camera calibrated with the white reference of 99& of reflectance (a) the white reference of 50% of reflectance (b) and with the white reference of 10% of reflectance (c) in the two positions (frontal and reverse).

Finally, to choose the best obsidian position, the two databases (the database of the frontal and the reverse position) created were classified to obtain the accuracy metrics. In addition, in order to quantitatively evaluate the performance of the classifier using the different calibration methods, several classifications were performed to obtain the best configuration (white reference and database selection). The three selected classifiers were employed to achieve the results of this phase and the models were evaluated through a 10-fold cross-validation.

4.1.1 SVM Linear Kernel

In the evaluation of the SVM with linear kernel, two different libraries were employed to prove which is the most advantageous in terms of results and computational cost; LIBLINEAR[63] and LIBSVM. Table 7 and Table 8 present the results of the classification process in experiment 1 for each different level (island, municipality and deposit) for the SVM Linear classifier employing the LIBSVM and LIBLINEAR libraries, respectively. In addition, the white reference with 99% of reflectance was included in this process to demonstrate that the classification of the samples using this white reference is not useful. These tables also present the results obtained when both datasets are unified (Frontal + Inverse), where it is possible to observe that the accuracy is not increased when both datasets are merged.

As it can be seen in the tables, the best results were obtained using the LIBSVM library. Although LIBLINEAR provides lower computational times, this library does not work well when solving certain problems. In this case, the accuracy results obtained with LIBLINEAR are quite poor.

Using LIBSVM, the best results are obtained at island level in comparison with the rest of the levels. In addition, the best results are achieved when using the frontal dataset; however they are quite similar to the results obtained with the other two obsidian positions. Concerning to the computational cost in this phase, in the experiment 1, the worst classification results are obtained with the white reference with 99% of reflection, but also using this white reference it is required a higher computational cost than using the other references. For both reason, it is not a good option choose this

reference for this work. As see in Figure 51(a) and (b), the other two white references are very similar, but the white reference with 10% of reflection is better than the 50% white reference.

Table 7. Classification results obtained in experiment 1 using SVM lineal classifier employing different calibration white references and LIBSVM.

Obsidian Position	Level	Accuracy Ref 10%	Simulation time (h)	Accuracy Ref 50%	Simulation time (h)	Accuracy Ref 99%	Simulation time (h)
Frontal	Island	90.97%	0.20	89.69%	0.22	65.50%	0.51
	Municipality	63.19%	0.49	54.66%	0.49	33.41%	0.78
	Deposit	63.48%	0.51	54.64%	0.41	33.44%	0.94
Reverse	Island	89.21%	0.16	88.11%	0.16	69.25%	0.42
	Municipality	66.53%	0.31	58.28%	0.33	33.29%	0.71
	Deposit	65.62%	0.32	57.35%	0.43	33.23%	0.79
Frontal + Reverse	Island	90.21%	0.65	89.05%	0.66	66.93%	1.70
	Municipality	67.35%	1.33	58.71%	1.43	33.21%	2.99
	Deposit	67.78%	1.31	57.87%	1.49	33.46%	3.54

Table 8. Classification results obtained in experiment 1 using SVM linear employing different calibration white references and LIBLINEAR.

Obsidian Position	Level	Accuracy Ref 10%	Simulation time (h)	Accuracy Ref 50%	Simulation time (h)	Accuracy Ref 99%	Simulation time (h)
Frontal	Island	77.97%	0.26	66.13%	0.25	66.00%	0.03
	Municipality	55.71%	1.62	51.53%	0.41	43.90%	0.27
	Deposit	56.62%	1.70	52.00%	0.45	43.56%	0.30
Reverse	Island	80.43%	0.25	75.58%	0.25	67.52%	0.03
	Municipality	59.01%	1.50	50.58%	0.39	42.56%	0.26
	Deposit	58.34%	1.72	51.00%	0.43	43.16%	0.30
Frontal + Reverse	Island	79.16%	0.56	68.28%	0.25	69.21%	0.06
	Municipality	56.84%	3.00	50.74%	0.80	41.60%	0.56
	Deposit	56.59%	3.27	50.52%	0.86	41.88%	0.65

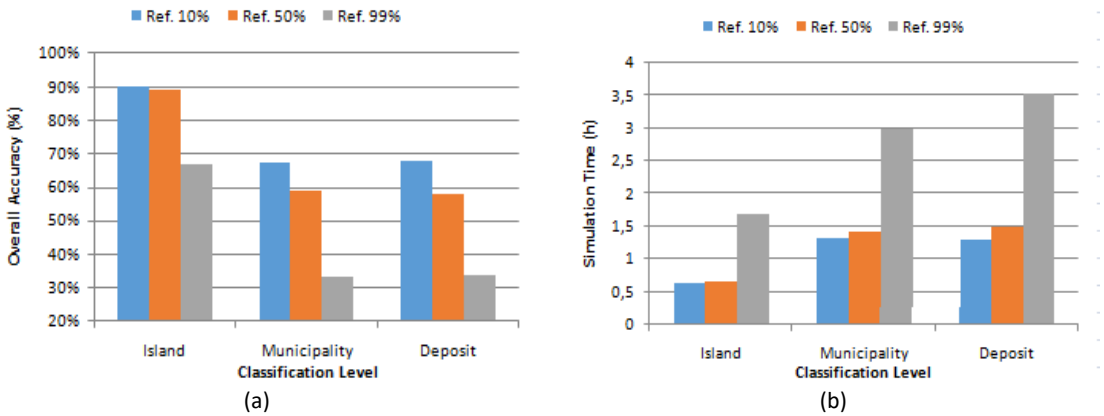

Figure 51. Results comparison between the three different white references using the SVM linear (with LIBSVM) in terms of accuracy (a) and computational cost (b).

Table 9 presents the results of the classification process using SVM with linear kernel in the experiment 2 employing the LIBSVM library and the white reference of 10% of reflectance. Although the best results were obtained with the frontal database in the previous experiments, for this work the database chosen was the unified (Frontal + Inverse) due to it has more information about the obsidian rocks and the classification results achieved were quite similar.

Table 9. Results of average overall accuracy in the experiment 2 using SVM linear and the white reference of 10%.

Obsidian Position	Obsidian sample	Classification level	Results
Frontal + Reverse	Mean (%)	Island	62.33%
		Municipality	20.49 %
		Deposit	20.38 %
Frontal + Reverse	STD (%)	Island	16.63 %
		Municipality	22.87 %
		Deposit	22.26 %
Frontal + Reverse	Total Time (h)	Island	23.45 h
		Municipality	47.12 h
		Deposit	46.56 h

4.1.2 Random Forest

In the evaluation of the Random Forest classifier, the white reference with 99% of reflectance was included in this process, as in the SVM with linear kernel. Table 10 present the results of the classification process in experiment 1 for each different level (island, municipality and deposit) for Random Forest classifier. This table also present the results obtained with frontal dataset, reverse dataset and frontal + reverse, where it is possible to observe that the accuracy is not increased when both datasets are merged.

The best results are obtained at island level in comparison with the rest of the levels. In addition, the best results are achieved when using the frontal dataset; however they are quite similar to the results obtained with the other two obsidian positions. As in the classification with SVM linear, the worst computational cost and accuracy results were obtained with the white reference with 99% of reflection. On the other hand, the other two references are very similar accuracy results, but the white reference with 50% of reflection has the best computational cost. Figure 52 presents the accuracy and computational cost results of the three white references.

Table 10. Classification results obtained in experiment 1 using Random Forest, with 50 trees by default, employing different calibration white references.

Obsidian Position	Level	Accuracy Ref 10%	Simulation time (h)	Accuracy Ref 50%	Simulation time (h)	Accuracy Ref 99%	Simulation time (h)
Frontal	Island	91.24%	0.08	91.01%	0.11	84.02%	0.13
	Municipality	67.70%	0.21	67.21%	0.22	50.28%	0.24
	Deposit	67.43%	0.19	67.34%	0.17	50.08%	0.26
Reverse	Island	90.21%	0.08	90.20%	0.07	82.36%	0.13
	Municipality	69.15%	0.16	68.94%	0.15	48.75%	0.24
	Deposit	68.66%	0.17	68.71%	0.15	48.43%	0.24
Frontal + Reverse	Island	90.80%	0.16	90.58%	0.16	82.92%	0.31
	Municipality	67.82%	0.35	67.72;%	0.34	48.34%	0.54
	Deposit	67.61%	0.36	67.43%	0.34	48.00%	0.54

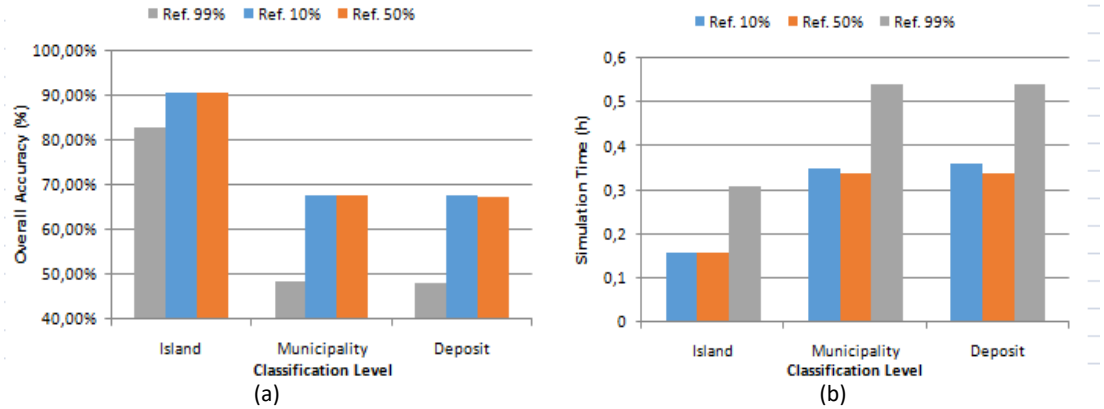

Figure 52. Results comparison between the three different white references using Random Forest in terms of accuracy (a) and computational cost (b).

Table 11 presents the results of the classification process using Random Forest classifier in the experiment 2 and the white reference of 10% of reflectance. As in the classification process with SVM linear, the best results were obtained with the frontal database in the previous experiments. To this work the database chosen was the unified (Frontal + Inverse) due to it has more information about the obsidian rocks and the classification results achieved were quite similar.

Table 11. Average overall accuracy results obtained in the experiment 2 using Random Forest and the white reference of 10%.

Obsidian Position	Obsidian sample	Classification level	Results (%)
Frontal + Reverse	Mean (%)	Island	83.94 %
		Municipality	31.87 %
		Deposit	31.23 %
Frontal + Reverse	STD (%)	Island	24.47 %
		Municipality	20.08 %
		Deposit	22.68 %
Frontal + Reverse	Total Time	Island	5.22 hours
		Municipality	11.15 hours
		Deposit	10.92 hours

4.1.3 SVM RBF Kernel

In the evaluation of the SVM RBF, the LIBSVM library was employed to the classification process. Table 12 present the results of the classification process in experiment 1 for each different level (island, municipality and deposit) for the SVM RBF employing the LIBSVM library.

The best results are obtained at island level in comparison with the rest of the levels. In addition, the best results are achieved when using the frontal + reverse dataset; however they are quite similar to the results obtained with the other two obsidian positions. Concerning to the computational cost in this phase, in the experiment 1, the worst classification results are obtained with the white reference with 99% of reflection, but also using this white reference it is required a higher computational cost than using the other references. For both reason, it is not a good option choosing this reference for this work. As see in Figure 53(a) and (b), the other two white references are very similar, but the white reference with 10% of reflection is better than the other reference in terms of computational cost and accuracy.

Table 12. Classification results obtained in experiment 1 using SVM RBF employing different calibration white references.

Obsidian Position	Level	Accuracy Ref 10%	Simulation time (h)	Accuracy Ref 50%	Simulation time (h)	Accuracy Ref 99%	Simulation time (h)
Frontal	Island	83.72%	0.26	82.89%	0.30	65.49%	0.45
	Municipality	43.51%	0.45	34.24%	0.46	29.79%	0.73
	Deposit	43.62%	0.46	34.29%	0.48	29.83%	0.72
Reverse	Island	82.71%	0.22	78.30%	0.25	66.80%	0.39
	Municipality	43.98%	0.38	36.86%	0.40	29.78%	0.68
	Deposit	43.04%	0.38	36.78%	0.52	29.87%	0.68
Frontal + Reverse	Island	84.80%	1.00	83.17%	1.07	66.13%	1.65
	Municipality	46.09%	1.70	38.33%	2.21	29.78%	3.03
	Deposit	46.24%	1.70	38.62%	1.81	29.90%	3.00

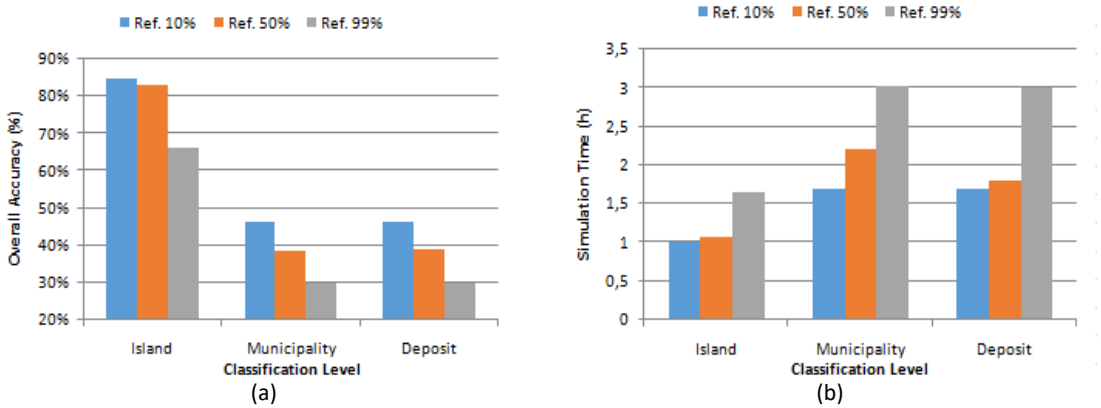

Figure 53. Results comparison between the three different white references using SVM RBF in terms of accuracy (a) and computational cost (b).

Table 13 presents the results of the classification process using SVM RBF classifier in the experiment 2 and the white reference of 10% of reflectance. Unlike the other two classifiers, the best results were obtained with the frontal + reverse database in the previous experiments. To this work, the database chosen was the unified (Frontal + Inverse) due to it has more information about the obsidian rocks.

Table 13. Results of average overall accuracy in the experiment 2 using SVM RBF.

Obsidian Position	Obsidian sample	Classification level	Results
Frontal + Reverse	Mean (%)	Island	82.54 %
		Municipality	11.33 %
		Deposit	11.66 %
Frontal + Reverse	STD (%)	Island	31.03 %
		Municipality	16.98 %
		Deposit	17.56 %
Frontal + Reverse	Total Time	Island	33.88 hours
		Municipality	61.65 hours
		Deposit	61.52 hours

4.1.4 Classifiers comparison

Comparing the results obtained in the previous experiments, the best accuracy results are achieved with the Random Forest classifier in experiment 1 and 2. Also, the Random Forest classifier has the lowest computational cost. On the other hand, the worst classifier is the SVM RBF due to it has the highest computational cost and the lowest accuracy results. Figure 54 presents two graphics where the accuracy and computational cost results versus the classification level obtained for each classifier in the experiment 1 are shown. Furthermore, Figure 55 presents the boxplots obtained for experiment 2 with each classifier for each classification level using the frontal + reverse dataset, where is possible to compare the mean accuracy results and their quartiles as well as their outliers. As it can be seen in these plots, the Random Forest classifier is the one that achieves the best results in this phase.

In summary, in this phase, the white reference of 10% of reflectance, the database with obsidian information in frontal and reverse position, and the three level of classification (island, municipality and deposit) have been chosen for the rest of phases of this research work. The LIBSVM library has been chosen for the classification process with the SVM linear kernel, due to it provides better accuracy results and also lowers computational cost, in this particular problem, than the LIBLINEAR library. In addition, the best classifier in this phase is the Random Forest and the worst is the SVM RBF. Thus, the Random Forest with the white reference with 10% of reflection and the database with obsidian information in frontal and reverse position is used in the next phase with the objective of selecting the best pre-processing chain.

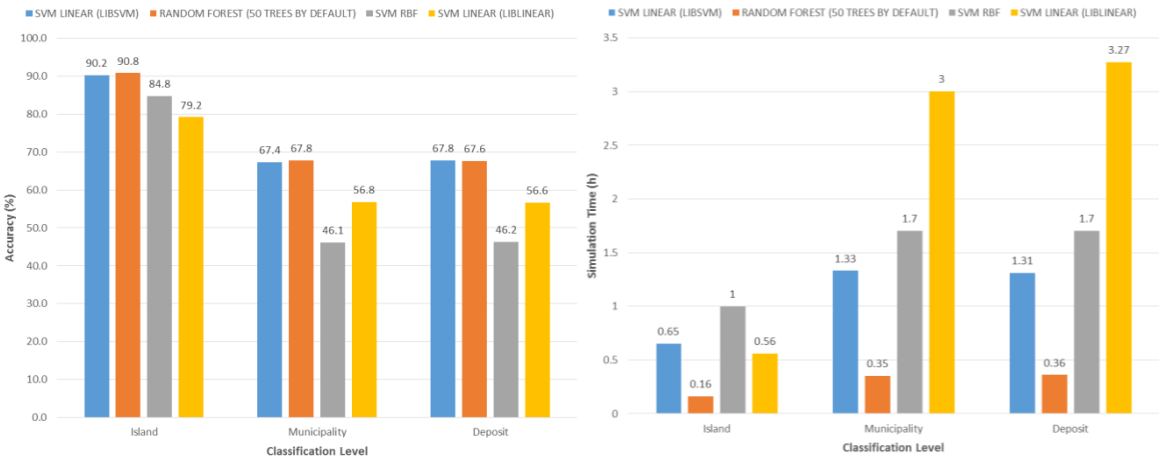

(a) (b)

Figure 54. Results obtained in experiment 1 of overall accuracy (a) and computational cost (b).

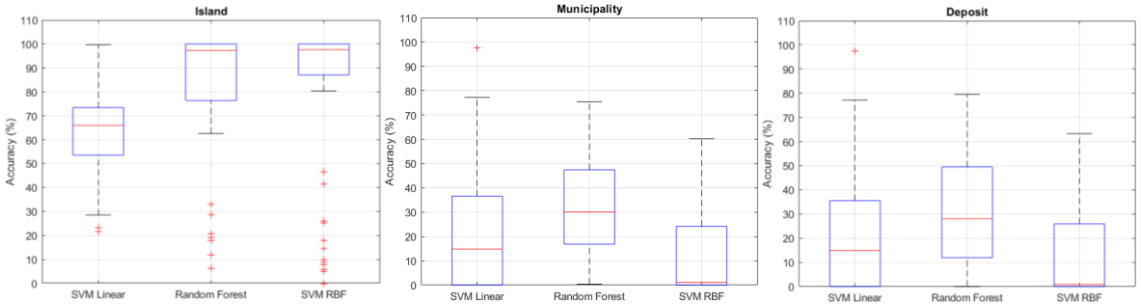

(a) (b) (c)

Figure 55. Boxplots to observe the results obtained in experiment 2 with the three classifiers: (a) Island level (b) Municipality level (c) Deposit level.

4.3 Phase 2: Selection of the pre-processing chain

The objective in this phase is to evaluate three different pre-processing chain results for the database. Three type of pre-processing chain is proposed in this phases, explained in section 3.4.1. The Random Forest classifier was chosen for this process and the model evaluation was accomplished through a 10-fold cross-validation, without to optimize the parameters.

Table 14 presents the results of the three pre-processing chains using the Random Forest classifier. In this phase, the standard deviation (STD) is also presented in the results. This parameter helps to visualize the dispersion of the database to the different classification levels respect to the 10-fold cross-validation.

Table 14. Average accuracy and standard deviation (STD) results obtained using the datasets generated with each pre-processing chain for each classification level.

Pre-processing Type	Accuracy (%) ± STD			Simulation Time (h)		
	Island	Municipality	Deposit	Island	Municipality	Deposit
P0	90.80% ± 0.0045	67.82% ± 0.0080	67.61% ± 0.0100	0.16	0.35	0.36
P1	84.13% ± 0.0066	60.08% ± 0.0100	59.82% ± 0.0068	0.30	0.46	0.47
P2	83.81% ± 0.0064	57.81% ± 0.0110	57.50% ± 0.0045	0.29	0.47	0.48

Taking into account the results obtained in Table 14, the pre-processing chain 0 should be selected due to it provides the better accuracy results. However, a visual

evaluation of the spectral signatures generated with each pre-processing chain has been performed. Figure 56, Figure 57 and Figure 58 show the mean and the variances of the spectral signatures for each pre-processing chain and classification level. The Figure 56(a), (b) and (c) only presents the mean of spectral signatures to facilitate the visualization at the island level, the Figure 57(a), (b) and (c) at the municipality level and the Figure 58 (a), (b) and (c) at the deposit level

In Figure 29, an organization scheme of the provenances of the obsidians employed in this study was presented at different levels, where there are 57 Gran Canaria (GC) obsidians and 12 Tenerife (TF) obsidians at island level. The number of samples of Gran Canaria is much bigger than the samples of Tenerife, where the samples of Gran Canaria present less external impurities than the Tenerife samples. This detail may suggest that Gran Canaria obsidians reflect more light than the Tenerife obsidians. This fact can be clearly seen in Figure 56(a), where the shape of the mean spectral signatures of GC and TF obsidians are practically the same but having the GC obsidians more amplitude than TF obsidians. Due to this, it is possible that the Random Forest classifier is differentiating the data according to the amplitude of the signature and not according to their shape. Thus, in this particular case, where all obsidians are taken into account (both the obsidian clean part and the obsidian impurities external part), the classifier is differentiating the samples depending on the impurities of the samples that reflect more or less light. That is why the P0 obtain the best results.

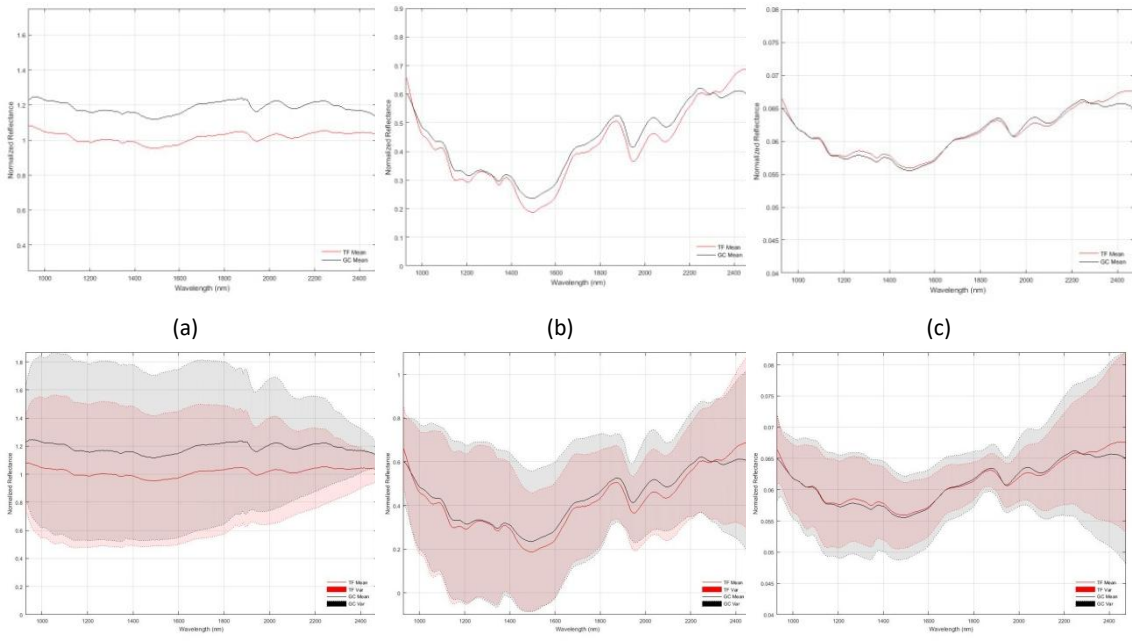

Figure 56. Mean of the spectral signatures of the P0 (a), P1 (b), P2 (c) and variances of the P0 (d), P1 (e) and P2 (f) at Island level.

However, if we want to avoid this differentiation that depends on the obsidians surface impurities, we should use a preprocessing chain where the spectral signatures

are normalized, in order to perform a classification depending on the shape of the spectral signatures. For this reason, this pre-processing is discarded to the next phases.

The other two pre-processing chains are very similar in the results, both the accuracy and the computational cost. So, it would be necessary to perform different tests to select the best pre-processing chain. However, due to the high computational cost and the lack of time to finish the research experiment, we have selected the pre-processing chain P1 to continue with the next phases of this work, since it provides slightly better results than P2.

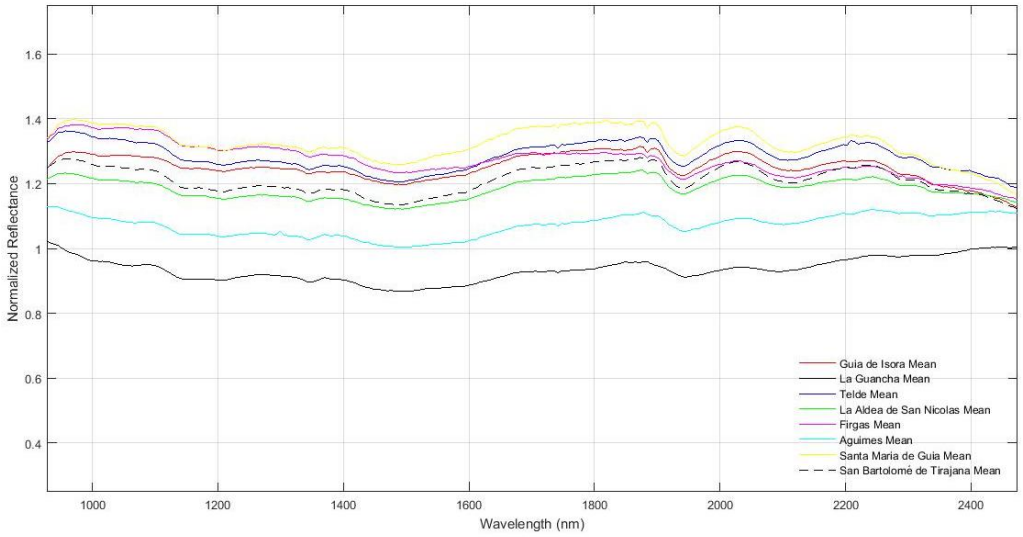

(a)

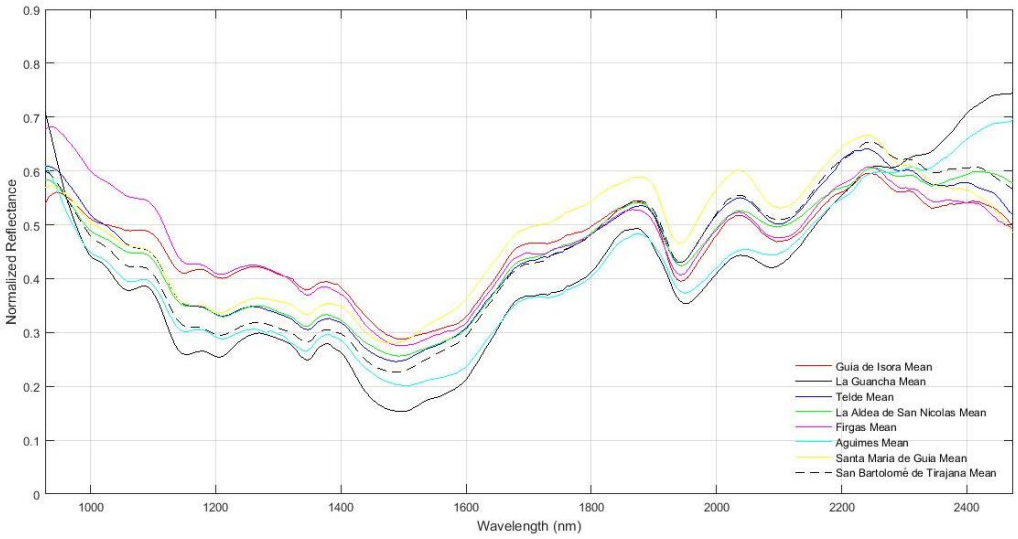

(b)

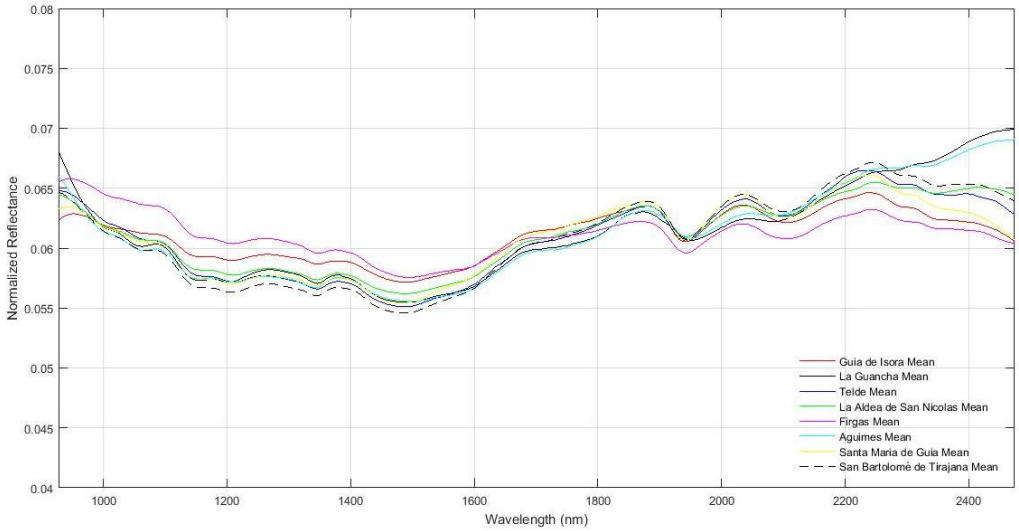
Normalized Reflectance
Wavelength (nm)
Guia de Isora Mean
La Guancha Mean
Telde Mean
La Aldea de San Nicolas Mean
Firgas Mean
Aguimes Mean
Santa Maria de Guia Mean
San Bartolomé de Tirajana Mean

(c)

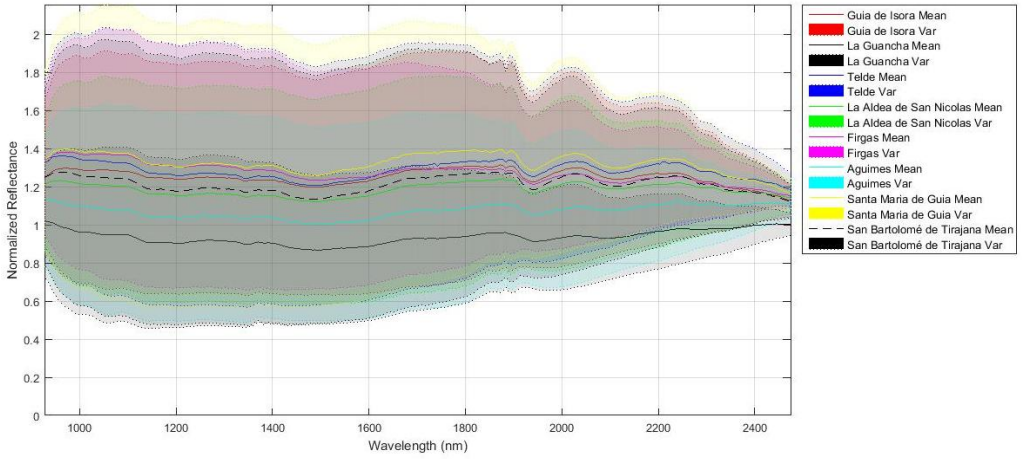
Normalized Reflectance
Wavelength (nm)
Guia de Isora Mean
Guia de Isora Var
La Guancha Mean
La Guancha Var
Telde Mean
Telde Var
La Aldea de San Nicolas Mean
La Aldea de San Nicolas Var
Firgas Mean
Firgas Var
Aguimes Mean
Aguimes Var
Santa Maria de Guia Mean
Santa Maria de Guia Var
San Bartolomé de Tirajana Mean
San Bartolomé de Tirajana Var

(d)

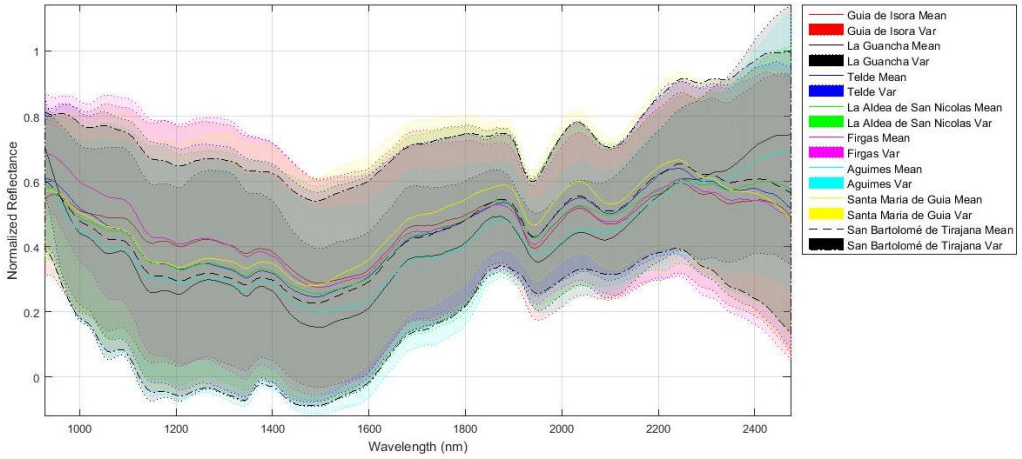
Normalized Reflectance
Wavelength (nm)
Guia de Isora Mean
Guia de Isora Var
La Guancha Mean
La Guancha Var
Telde Mean
Telde Var
La Aldea de San Nicolas Mean
La Aldea de San Nicolas Var
Firgas Mean
Firgas Var
Aguimes Mean
Aguimes Var
Santa Maria de Guia Mean
Santa Maria de Guia Var
San Bartolomé de Tirajana Mean
San Bartolomé de Tirajana Var

(e)

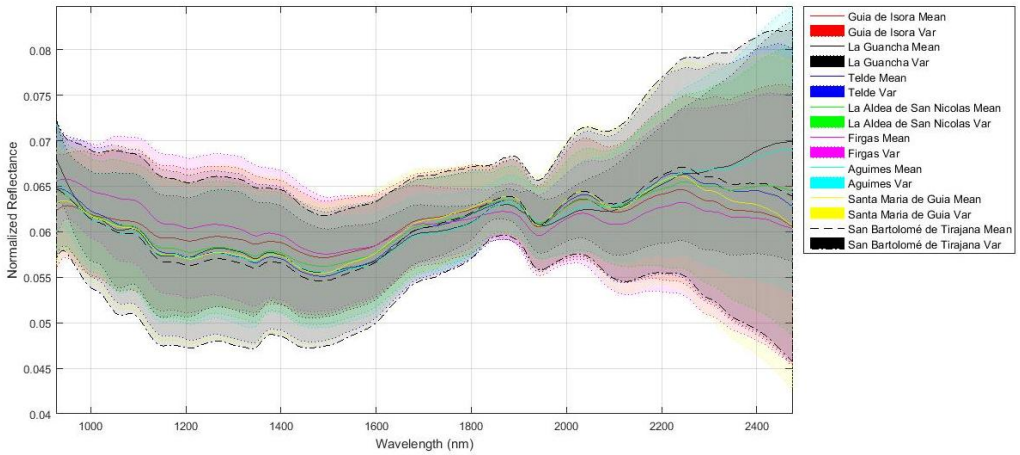

(f)

Figure 57. Mean of the spectral signatures of the P0 (a), P1 (b), P2 (c) and variances of the P0 (d), P1 (e) and P2 (f) at municipality level.

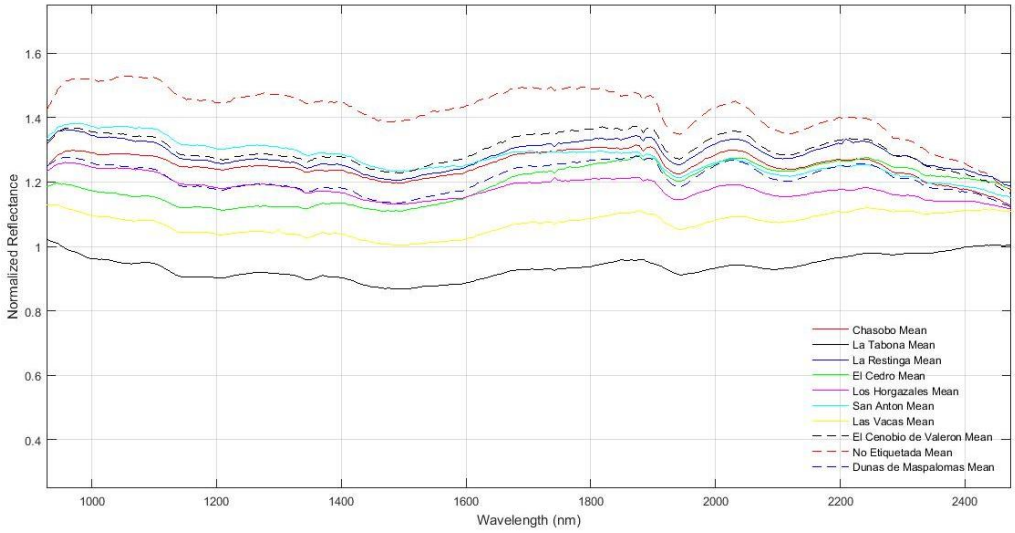

(a)

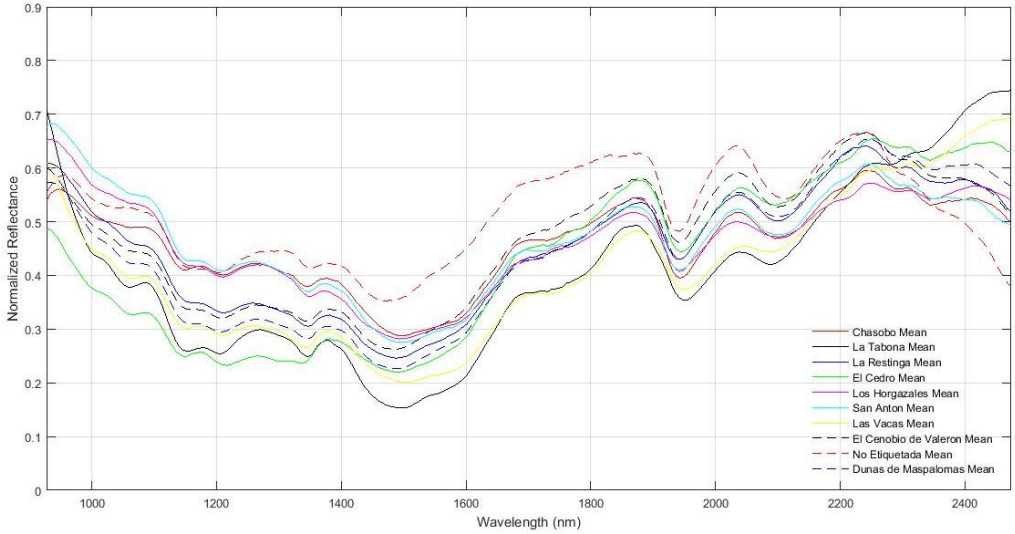

(b)

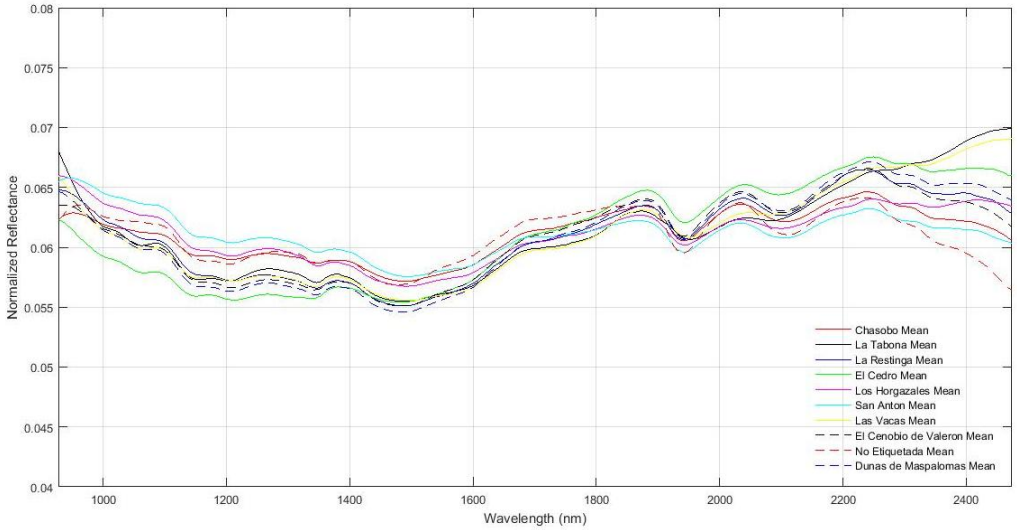
Normalized Reflectance
Wavelength (nm)
Chasobo Mean
La Tabona Mean
La Restinga Mean
El Cedro Mean
Los Horgazales Mean
San Anton Mean
Las Vacas Mean
El Cenobio de Valeron Mean
No Etiquetada Mean
Dunas de Maspalomas Mean

(c)

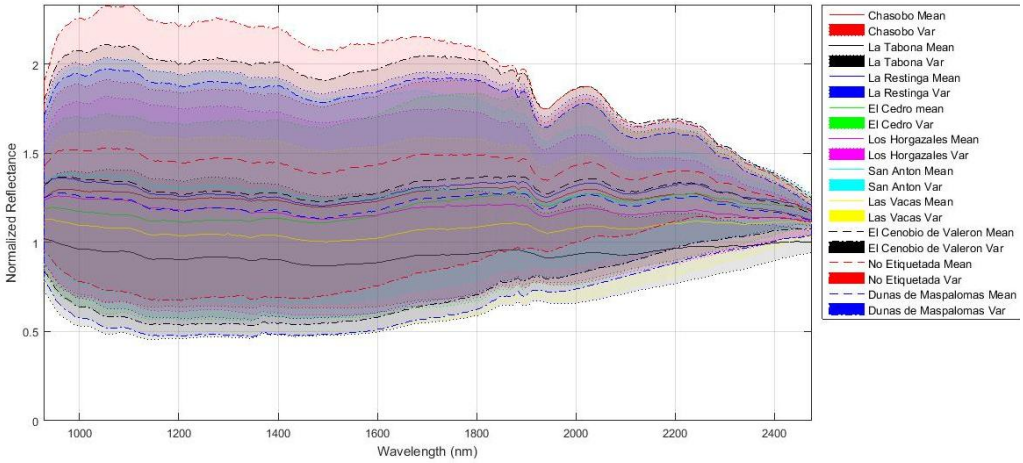
Normalized Reflectance
Wavelength (nm)
Chasobo Mean
Chasobo Var
La Tabona Mean
La Tabona Var
La Restinga Mean
La Restinga Var
El Cedro mean
El Cedro Var
Los Horgazales Mean
Los Horgazales Var
San Anton Mean
San Anton Var
Las Vacas Mean
Las Vacas Var
El Cenobio de Valeron Mean
El Cenobio de Valeron Var
No Etiquetada Mean
No Etiquetada Var
Dunas de Maspalomas Mean
Dunas de Maspalomas Var

(d)

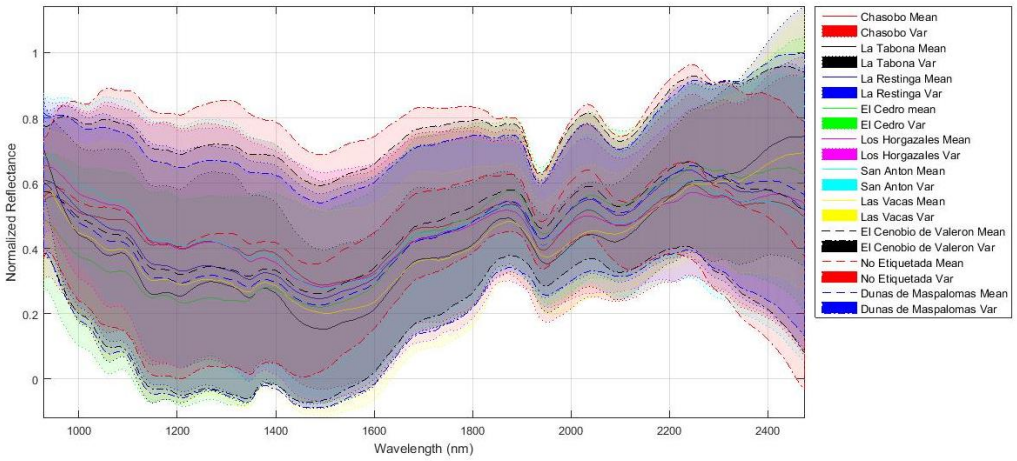
Normalized Reflectance
Wavelength (nm)
Chasobo Mean
Chasobo Var
La Tabona Mean
La Tabona Var
La Restinga Mean
La Restinga Var
El Cedro mean
El Cedro Var
Los Horgazales Mean
Los Horgazales Var
San Anton Mean
San Anton Var
Las Vacas Mean
Las Vacas Var
El Cenobio de Valeron Mean
El Cenobio de Valeron Var
No Etiquetada Mean
No Etiquetada Var
Dunas de Maspalomas Mean
Dunas de Maspalomas Var

(e)

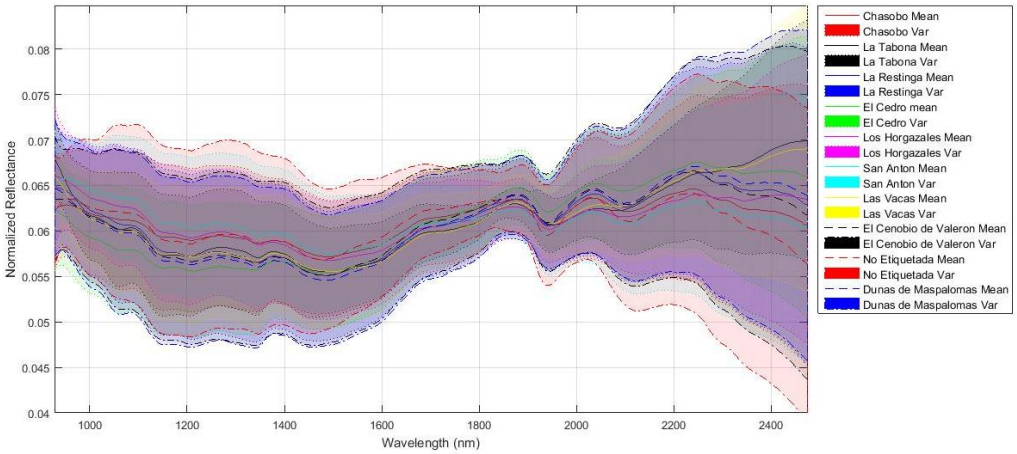

(f)

Figure 58. Mean of the spectral signatures of the P0 (a), P1 (b), P2 (c) and variances of the P0 (d), P1 (e) and P2 (f) at deposit level.

4.4 Phase 3: the optimal classifier parameters and classification process with different classifiers to experiment 1

Although in Phase 1 a comparison was made between different classifiers, in that comparison the pre-processing chain and the different configurations of the classifier were not taken into account.

This phase consists of evaluating the results obtained using different supervised classifiers. Before this, it is necessary to optimize the parameters in each classifier, such as the cost value in the SVM classifier with linear kernel, the number of trees in the Random Forest algorithm and the cost and gamma values in the SVM classifier with RBF kernel.

4.4.1 SVM Linear optimization

For the SVM with linear kernel, the parameter to optimize is the cost (C). The cost is the weight that is given to each observation at the time of classifying. A higher cost would imply a greater weight of an observation and the SVM would be stricter. This process is automatic, and consists of find the best value of cost for each classification level to apply the classification process. In this case, the parameter sweep was done from 2^{-10} to 2^{20} in steps of 2^2 and evaluating the results using the accuracy metric. This process was realized with the experiment 1 only with the unified dataset (Frontal + Inverse) that was selected in phase 1. Figure 59 presents the parameter sweep results obtained for each classification level.

The choice of the cost value is established by the average of the 10 observations, choosing the parameter value with the highest accuracy percentage [64], [65]. For this reason, the optimal cost value to all classification levels is 2^{10}, where the accuracy to the island level reaches 82%, to the municipality level reaches 66% and to the deposit level reaches 68%.

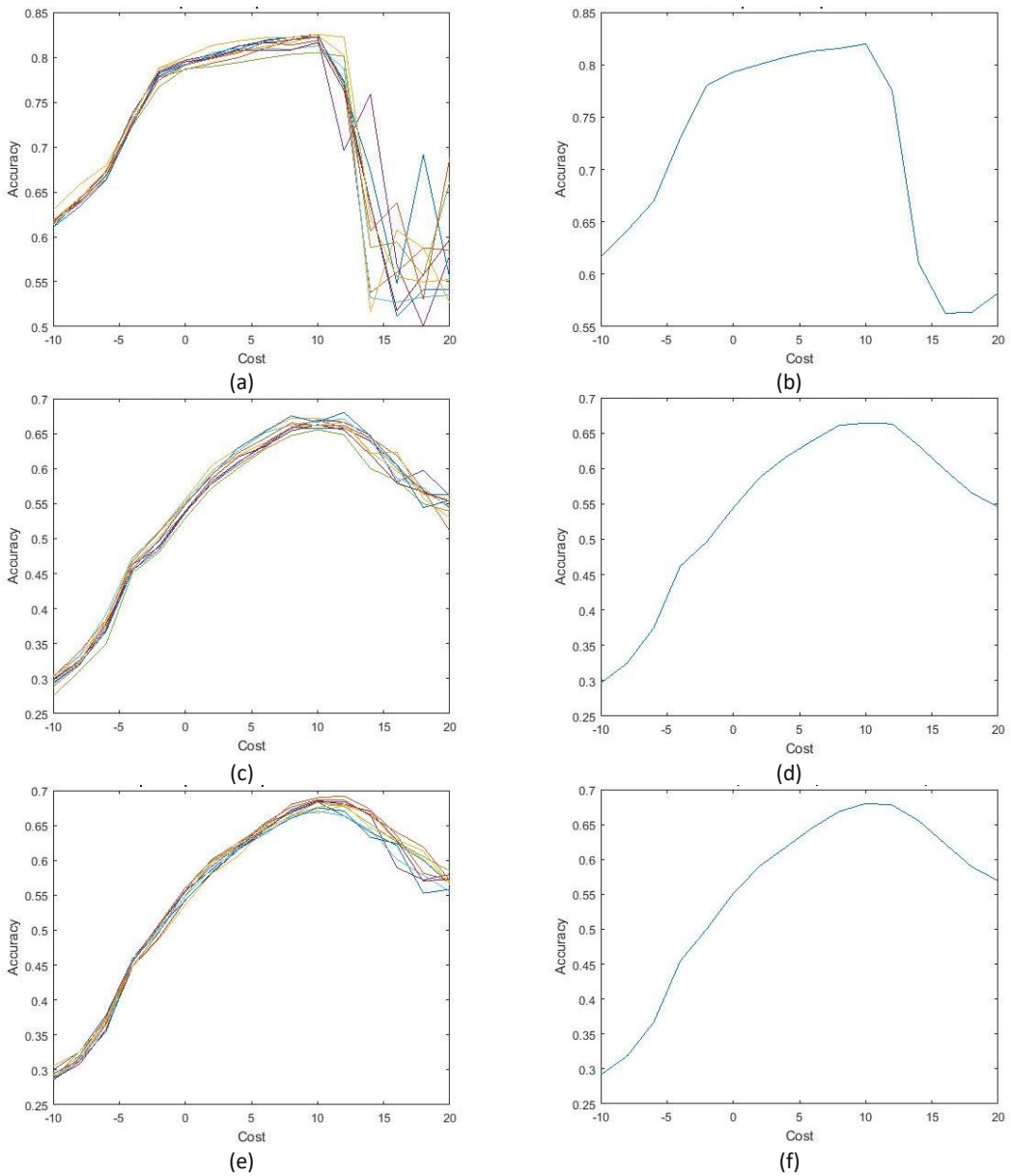

Figure 59. Representation of the parameter sweep results for the 10-fold cross-validation and its mean for the SVM with linear kernel: (a) Island parameter optimization (10-fold cross-validation) (b) Mean of island parameter optimization (c) Municipality parameter optimization (10-fold cross-validation) (d) Mean of municipality parameter optimization (e) Deposit parameter optimization (10-fold cross-validation) (f) Mean of deposit parameter optimization.

4.4.2 Random Forest optimization

For Random Forest algorithm, the parameter to be optimized is the number of trees. The procedure to obtain the optimal parameter in this case is equivalent as the SVM linear kernel parameter optimization process.

A decision tree is a collection of hierarchically organized nodes and edges. The nodes can be internal or terminal nodes. A sample enters above the tree and is subjected to a series of binary tests on each node until it reaches a page, where the answer lies [66]. In these experiments, the parameter sweep for Random Forest was performed from 10 to 500 trees in steps of 20 and evaluating the results using also the

accuracy metric. Figure 60 presents the parameter sweep results obtained for each classification level.

The decision to choose the optimal parameter is the same as in the case of SVM with linear kernel. Thus, the optimal number of trees value to the island levels is 310, where the accuracy reaches 84.5%, to the municipality level is 410, where the accuracy reaches 61.8% and to the deposit level is 390, where the accuracy reaches 61.3%.

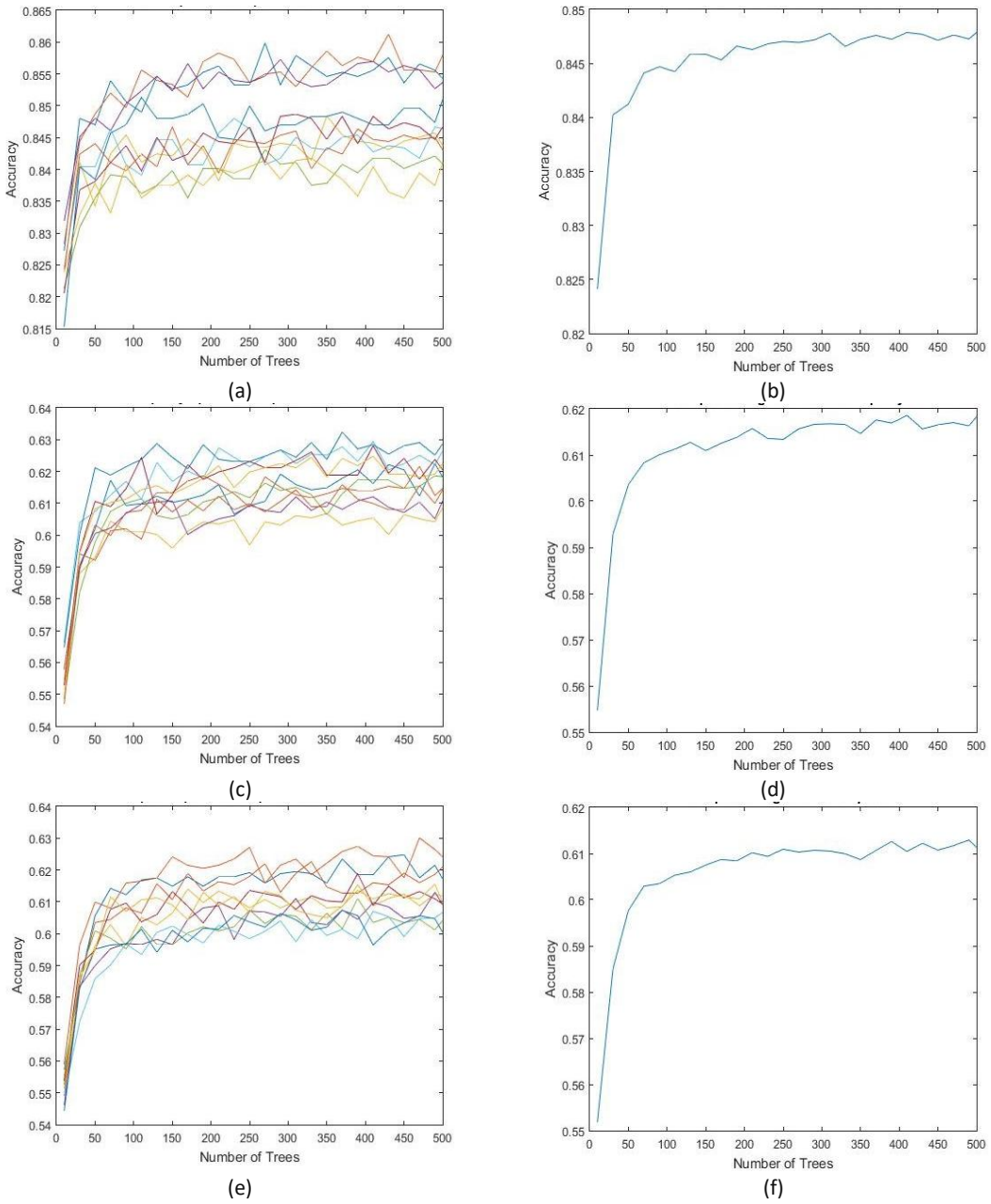

Figure 60. Representation of the parameter sweep results for the 10-fold cross-validation and its mean for the Random Forest classifier: (a) Island parameter optimization (10-fold cross-validation) (b) Mean of island parameter optimization (c) Municipality parameter optimization (10-fold cross-validation) (d) Mean of municipality parameter optimization (e) Deposit parameter optimization (10-fold cross-validation) (f) Mean of deposit parameter optimization.

4.4.3 SVM RBF optimization

In case of the SVM classifier with RBF kernel, the parameters to be optimized are two: the cost (C) and gamma (G) value. Gamma can be considered as the spread of the kernel, therefore, the decision region. When gamma is low, the curve of the decision limit is very low and, therefore, the decision region is very broad. When gamma is high, the curve of the decision boundary is high[67]. All optimization process is computed automatically in MATLAB®, as SVM with linear kernel and Random Forest process. In the SVM RBF case, the two parameters sweep were done performing a grid search of both parameters from 2^{-10} to 2^{20} in steps of 2^{5} and evaluating the results using the accuracy metric. Figure 61 presents the parameter sweep results obtained for each classification levels.

In this case, the choice of the best cost-gamma values is the point where this pair obtains the best accuracy result. Thus, the optimal cost/gamma values to all classification levels is $2^{15}/2^{-5}$, where the accuracy to the island level reaches 90.14%, to the municipality level reaches 80.05% and to the deposit level reaches 80.42%.

It is possible that these good results are at a local maximum. In case it is a local maximum, the values of the border must be expanded to obtain the new accuracy results in this new region. Due to the lack of time and the simulation time so high that this procedure presents, it has not been included in this research work.

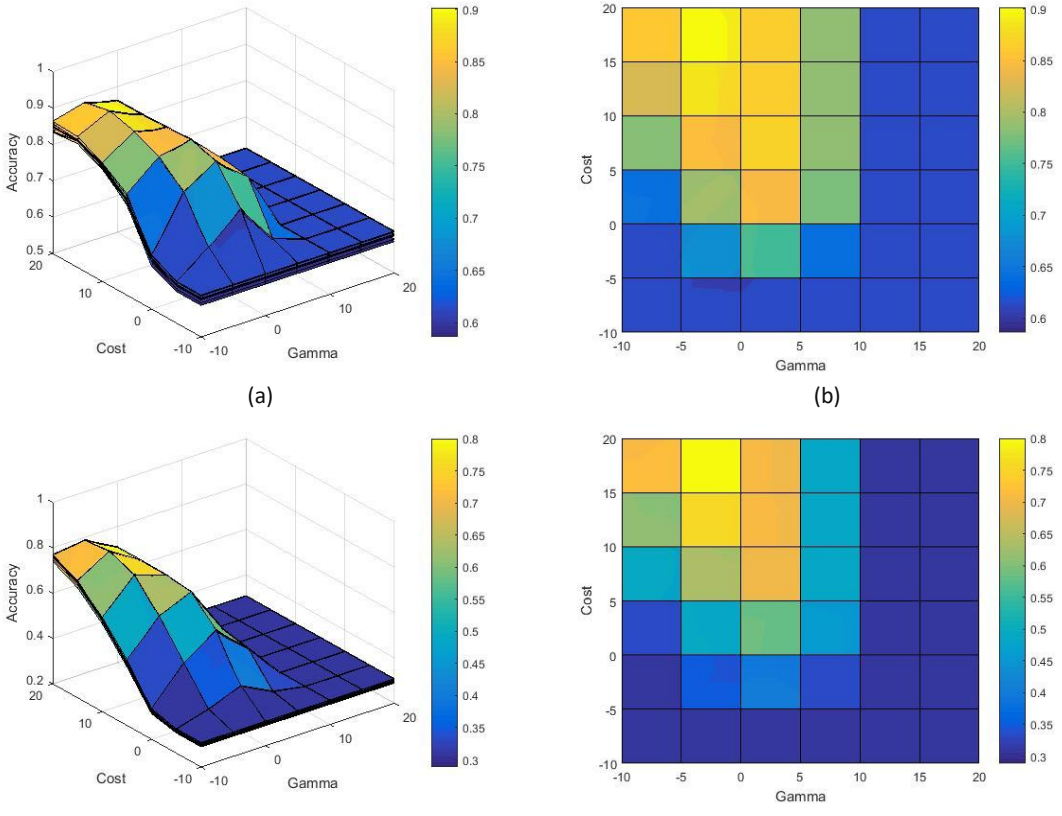

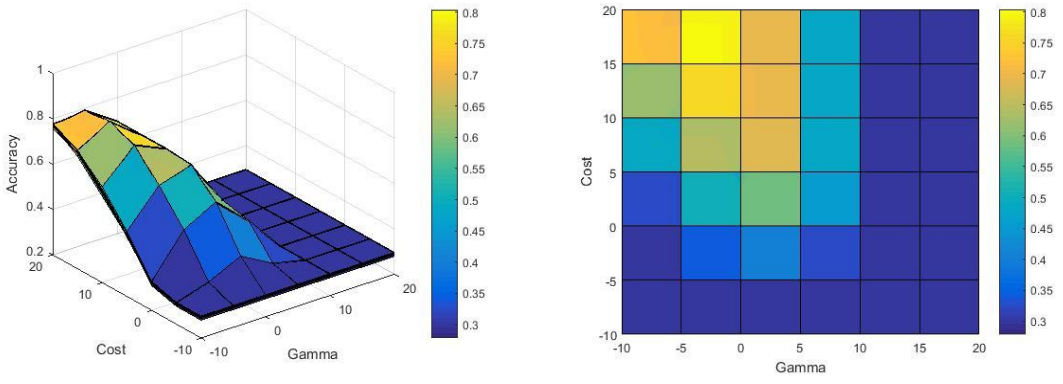

(e) (f)

Figure 61. Representation of the grid search results for the 10-fold cross-validation and its mean for the SVM with RBF kernel: (a) Island parameter optimization (10-fold cross-validation) (b) Mean of island parameter optimization (c) Municipality parameter optimization (10-fold cross-validation) (d) Mean of municipality parameter optimization (e) Deposit parameter optimization (10-fold cross-validation) (f) Mean of deposit parameter optimization.

4.4.4 Experiment 1 optimized classifiers comparison

As the parameters for each classifier have been optimized, the classification process has also been carried out through experiment 1. The results achieved with all classifiers for this phase are shown in Table 15.

Comparing the results obtained in the parameter optimization with the experiment 1, the best accuracy results are achieved with the SVM RBF classifier with a 90.14% at island level, 80.05% at municipality level and 80.41% at deposit level. In comparison with the phase 1, where SVM RBF was the worst classifier, the accuracy results have improved a lot. However, the computational cost has increased to the pre-processing of the data. In terms of computational cost, the Random Forest classifier still has a lower computational cost but the accuracy results has not varied significantly respect to phase 1, where Random Forest obtained the best accuracy results. Figure 62 present two graphics where the accuracy and computational cost results versus the classification levels obtained for each classifier in the experiment 1 are shown. As it can be seen in these graphics, the SVM RBF classifier achieved the best accuracy results and the Random Forest obtained the lowest computational cost in this phase.

If these results are compared with the phase 1, the only classifier that has improved the accuracy result has been the SVM RBF, where the accuracy result has improved by 7% at island level and 34% at municipality and deposit level. In the Random Forest and SVM with linear kernel classifiers, the accuracy results has worsened in comparison with the phase 1 due to pre-processing, that is, for these classifiers another type of pre-processing would be necessary to improve the results of the classification process. In Random Forest the accuracy results have dropped by 6% in all the classification levels, while in SVM with lineal kernel the accuracy results have dropped by 8% at island level only.

Table 15. Comparison of the results obtained using optimized three different classifiers in the experiment 1.

Classifier	Classification level	Pre-processing	Obsidian Position	**Optimized parameter**	**Ref 10%** Accuracy (%)	**Simulation Time (h)**
SVM linear kernel	Island	P1	Frontal + Reverse	Cost = 2^{10}	82.00	693.24
	Municipality			Cost = 2^{10}	66.84	113.92
	Deposit			Cost = 2^{10}	68.00	105.37
Random Forest	Island	P1	Frontal + Reverse	Number of trees = 310	84.55	28.42
	Municipality			Number of trees = 410	61.84	54.41
	Deposit			Number of trees = 390	61.35	63.52
SVM RBF kernel	Island	P1	Frontal + Reverse	Cost/Gamma = $2^{15}/2^{-5}$	90.14	344.86
	Municipality			Cost/Gamma = $2^{15}/2^{-5}$	80.05	251.12
	Deposit			Cost/Gamma = $2^{15}/2^{-5}$	80.41	212.59

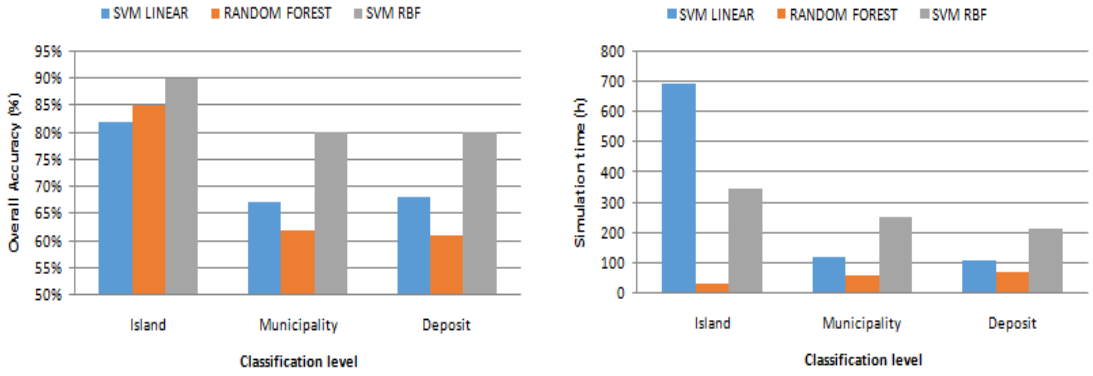

Figure 62. Results comparison between the three different optimized classifiers in terms of accuracy (a) and computational cost (b).

4.5 Phase 4: Classifier evaluation in experiment 2

This experiment setup reproduces a practical situation where a new obsidian is going to be classified employing a classification model generated based on the information from the previous obsidians. In this scenario, the model evaluation is performed following a leave-one-out classification method, where the samples from previous obsidians are used as training set and data from the new obsidian (Frontal+Reverse) is used to evaluate the model performance.

Table 16 shows the results obtained using the three classifiers in the experiment 2. Comparing the results obtained in the previous experiments, the best accuracy results are achieved with the SVM linear kernel and SVM RBF classifiers in experiment 2. Both classifiers obtained similar results but the difference is in the computational cost, where the SVM RBF classifier has the lowest computational cost. In general terms of computational cost, the Random Forest classifier has the lowest computational cost as the phase 1 but this classifier has the worst accuracy result. The Figure 63 presents the

boxplots obtained for the experiment 2 with each classifier for each classification level, where is possible to compare the mean accuracy results and their quartiles as well as their outliers. As it can be seen in these plots, the SVM linear kernel and SVM RBF classifiers achieved the best accuracy results while Random Forest obtained the worst accuracy results.

Table 16. Comparison of the classification results generated using the three classifiers in the experiment 2.

Classifier	Classification level	Pre-processing	Obsidian Position	**Optimized parameter**	**Ref 10%** Mean Accuracy (%)	**Standard deviation (%)**	**Simulation Time (h)**
SVM linear kernel	Island	P1	Frontal + Reverse	Cost = 10	79.36	31.89	475.47
	Municipality			Cost = 10	38.60	26.08	30.47
	Deposit			Cost = 10	35.49	27.08	29.91
Random Forest	Island	P1	Frontal + Reverse	Number of trees = 310	78.08	29.45	10.00
	Municipality			Number of trees = 410	20.00	13.75	24.08
	Deposit			Number of trees = 390	18.57	15.46	27.26
SVM RBF kernel	Island	P1	Frontal + Reverse	Cost/Gamma = $2^{15}/2^{-5}$	76.82	24.63	326.92
	Municipality			Cost/Gamma = $2^{15}/2^{-5}$	39.86	25.24	16.66
	Deposit			Cost/Gamma = $2^{15}/2^{-5}$	35.29	24.25	13.71

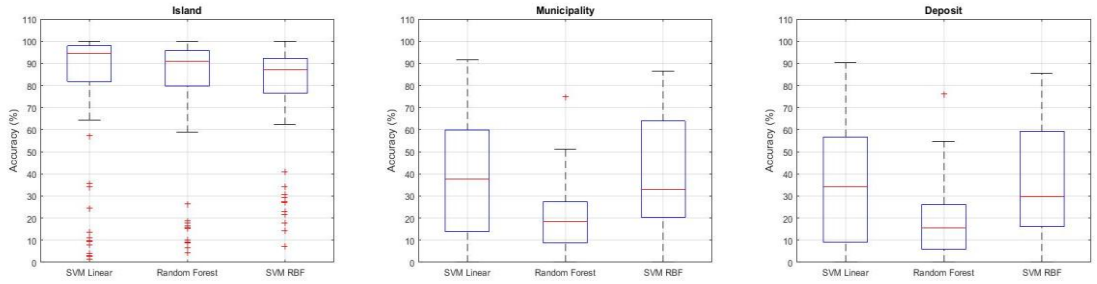

(a) (b) (c)

Figure 63. Boxplots to observe the results obtained in experiment 2, after the pre-processing P1, with the three classifiers: (a) Island level (b) Municipality level (c) Deposit level.

4.6 Summary

In this chapter, we have presented the results achieved when applying the supervised classification framework to the obsidian rocks.

Firstly, in the phase 1, the white reference of 10% of reflectance, the database with obsidian information in frontal and reverse position, and the three level of classification (island, municipality and deposit) have been chosen for the rest of phases of this research work. In addition, there was a classifier that obtained quite better accuracy results and lower computational cost than the other two classifiers, the Random Forest, where it obtained 83% at the island level with a simulation time of

5.22 hours, 31.87% at the municipality level with a simulation time of 11.15 hours and 31.23% at the deposit level with a simulation time of 10.92 hours. Thus, this classifier is used in the phase 2 to select the best pre-processing chain.

Secondly, in the phase 2, the best pre-processing chain obtained was the P0 but this pre-processing chain presented one problem, i.e. the obsidian surface impurities. This factor affected the results of the classification because it classified all the obsidian, both the surface impurity and the clean part. For these reason, we should use a preprocessing chain where the spectral signatures are normalized. Thus, the pre-preprocessing chain P0 was discarded. The other two pre-processing chains are very similar in the results, both the accuracy and the computational cost. So, it would be necessary to realize different tests to select the best pre-processing chain. However, due to the high computational cost and the lack of time to finish the research experiment, we have selected the pre-processing chain P1 to continue with the phase 3.

Thirdly, in the phase 3, it is necessary to optimize the principal parameters of each classifier: as the cost value in SVM with linear kernel, the number of tree in Random Forest and the cost/gamma value in SVM RBF. After this process, the best accuracy results are achieved with the SVM RBF classifier, where at island level obtained 90.14%, at municipality level obtained 80.05% and deposit level obtained 80.41%. In terms of computational cost, the Random Forest classifier still has a lower computational cost but the accuracy results have not varied significantly respect to phase 1, where Random Forest obtained the best accuracy results.

In the last phase, the best accuracy results are achieved with the SVM linear kernel and SVM RBF classifiers in experiment 2. Both classifiers obtained similar results but the difference is in the computational cost, where the SVM RBF classifier has the lowest computational cost. In comparison with the phase 1, the SVM with linear kernel has improved the accuracy results in all the classification levels, while the SVM RBF has improved the accuracy results in municipality and deposit level. In the Random Forest case, in all the classification levels the accuracy results has worsened. In terms of computational cost, the Random Forest classifier has the lowest computational cost.

In all the phases, the classification at the island level has been better in all cases. This factor indicates that the classifiers can make a good classification when we want to classify an obsidian at the island level, but not at the other levels (municipality and deposit), where the accuracy results have a very lower percentages and the computational cost is very high in any classifier. Therefore, it is not advisable to realize a classification of the obsidians at levels lower than the island level with these classifiers.

5. CONCLUSIONS AND FUTURE WORKS

The main goal of this Master's Thesis was to propose and validate several supervised classification models and to use data mining techniques in order to obtain an automatic mathematical tool for archaeological samples using HSI, have been successfully achieved. Also, an exhaustive documentation about archaeological HS images has been acquired, finding new ways to treat the same problem from different points of view (for example, following a strategy similar to the one followed by the Czech research group analyzed in Chapter 2).

As far as classification results is concerned, it has been shown in Chapter 4 that competitive results in the discrimination between Gran Canaria and Tenerife obsidian are obtained in experiment 1 whatever classifier is employed. This trend is not kept in experiment 2, where the SVM classifier with linear kernel obtained bad results at island level compared with Random Forest and the SVM RBF classifier. At the other classification levels (municipality and deposit), the Random Forest obtained the best accuracy results and the lowest computational cost. This success in the experiment 2 is due to the high quantity of information from 69 obsidians. For these reason, it is possible that the classifier has enough information to build a model with high generalization.

Regarding the supervised classifier used in this research work, in experiment 1 the best classification results are obtained using the SVM RBF. This classifier achieved better accuracy results at any level of classification. However, in terms of computational cost, this classifier is the worst at municipality and deposit level, being the Random forest the one that has lower computational cost. Conversely, in experiment 2 the better classification results are obtained using SVM with linear kernel, although the SVM RBF classifier obtained similar results in all classification levels. The Random Forest is still the worst classifier in terms of accuracy results. However, the opposite occurs in term of computational cost, where the Random Forest achieved the lowest computational cost while the SVM with lineal kernel achieved the highest computational cost.

In all classification process, one level of classification has always obtained better accuracy results than the other two, the classification at island level. If we compare the results, in 90% of the cases, the accuracy results at the island level usually obtain a difference of 40% with respect to the other two levels. This indicates that the classification results at the island level is very good using these three classifiers but does not have good results at the municipality and deposit levels, where it is not advisable to apply these classifiers in this classification process.

Summing up, although more efforts must be put in developing an automatic diagnostic tool for archaeological samples, HSI has been presented as a suitable tool for handling this problem. While a more exhaustive study must be carried out, HS

images with higher spectral and more sophisticated classification schemes, this study presents promising results in discriminating between Gran Canaria and Tenerife obsidian rocks. This kind of tools can help archaeologists to analyze the archaeological samples, such us obsidians or pictures, without spending a long time in the examination of each sample.

Any research work developed contributes to clearing some unknowns about the treated topic but, simultaneously, it generates new questions, new ideas and opens new lines of work. In this section there are some lines of research that can be the subject of interest, based on the work presented in this research work.

In relation with the HS images capture and data acquisition process, the methodology described in this research work can be directly applied to VNIR camera. Thus, the results can be compared to decide which camera offer the best information about obsidian rocks.

Regarding the analysis of the obsidian with the camera, it would be interesting to invest more work in the area of pre-processing and classification processes. An example would be to eliminate the external impurities of the obsidians or perform the classification process with other classifiers, e.g. neural networks. Consequently, we can expand information on the subject under study.

On the other hand, it can be interesting to apply this methodology to other canarian archaeology heritage samples, such us mummy skins, ceramics or other rocks type. Currently, the archaeologists need very expensive and destructive processes to obtain information on some historical material. With this camera type and this methodology, this information can be obtained non-invasively, that is, without making contact with the material to be studied, which would help to improve research and development in the world of archeology.

6. BIBLIOGRAFY

[1] J. de Abreu Galindo, *Historia de la conquista de las siete islas de Canarias*. Santa Cruz de Tenerife, 1848.

[2] A. F. H. Goetz, G. Vane, J. E. Solomon, and B. N. Rock, "Imaging Spectrometry for Earth Remote Sensing," *Science (80-.).*, vol. 228, no. 4704, pp. 1147–1153, 1985.

[3] Mini Physics, "The Electromagnetic Spectrum." [Online]. Available: https://www.miniphysics.com/electromagnetic-spectrum_25.html.

[4] G. Shaw and H. Burke, "Spectral Imaging for Remote sensing," *Lincoln Lab. J.*, vol. 14, no. 1, pp. 3–28, 2003.

[5] R. Smith, "Introduction to hyperspectral imaging," *Microimages. Retrieved June*, pp. 1–24, 2006.

[6] P. Colarusso, L. H. Kidder, I. W. Levin, J. C. Fraser, J. F. Arens, and E. N. Lewis, "Infrared spectroscopic imaging: From planetary to cellular systems," *Appl. Spectrosc.*, vol. 52, no. 3, 1998.

[7] M. J. Giardino, "A history of NASA remote sensing contributions to archaeology," *J. Archaeol. Sci.*, vol. 38, no. 9, pp. 2003–2009, 2011.

[8] F. D. van der Meer *et al.*, "Multi- and hyperspectral geologic remote sensing: A review," *International Journal of Applied Earth Observation and Geoinformation*, vol. 14, no. 1. pp. 112–128, 2012.

[9] A. Camacho-Velasco, C. A. Vargas-García, F. A. Rojas-Morales, S. F. Castillo-Castelblanco, and H. Arguello-Fuentes, "Aplicaciones y retos del sensado remoto hiperespectral en la geología colombiana," *Rev. Fac. Ing. (Fac. Ing.)*, vol. 24, no. 40, pp. 17–29, 2015.

[10] J. M. Lerner and a. Thevenon, "Optics of Spectroscopy Tutorial - HORIBA," *1996-2013 HORIBA, Ltd*, 2013.

[11] G. Martín and A. Plaza, "Spatial-spectral preprocessing prior to endmember identification and unmixing of remotely sensed hyperspectral data," *IEEE J. Sel. Top. Appl. Earth Obs. Remote Sens.*, vol. 5, no. 2, pp. 380–395, 2012.

[12] Niraj Kumar Soni, "Optical design of hyperspectral imager and evaluation of unwanted diffraction order," India, 2015.

[13] Z. Liu, J. Yan, D. Zhang, and Q.-L. Li, "Automated tongue segmentation in hyperspectral images for medicine.," *Appl. Opt.*, 2007.

[14] H. L. and Vision, "The Rayleigh Criterion." [Online]. Available: http://hyperphysics.phy-astr.gsu.edu/hbase/phyopt/Raylei.html#c2.

[15] F. Ayuso Márquez and V. M. Ochoa Sánchez, "Aplicación de la tecnología grid al tratamiento de imágenes hiperespectrales," Universidad de Extremadura, 2008.

[16] E. Sánchez Bernabé, "Procesado de imágenes hiperespectrales," Universidad Politécnica de Madrid, 2016.

[17] ArcMap, "Cell size of raster data." [Online]. Available: http://desktop.arcgis.com/en/arcmap/10.3/manage-data/raster-and-images/cell-size-of-raster-data.htm.

[18] M. Aboras, H. Amasha, and I. Ibraheem, "Early detection of melanoma using multispectral imaging and artificial intelligence techniques," *Http://Www.Sciencepublishinggroup.Com*, 2015.

[19] N. Afonso Rivero, "Desarrollo de un sistema de adquisición de imágenes hiperespectrales para muestras de anatomía patológica," Universidad de Las Palmas de Gran Canaria, 2017.

[20] D. Wu and D.-W. Sun, "Advanced applications of hyperspectral imaging technology for food quality and safety analysis and assessment: A review — Part I: Fundamentals," *Innov. Food Sci. Emerg. Technol.*, vol. 19, pp. 1–14, 2013.

[21] L. Bei, G. I. Dennis, H. M. Miller, T. W. Spaine, and J. W. Carnahan, "Acousto-optic tunable filters: Fundamentals and applications as applied to chemical analysis techniques," *Progress in Quantum Electronics*, vol. 28, no. 2. pp. 67–87, 2004.

[22] J. Beeckman, "Liquid-crystal photonic applications," *Opt. Eng.*, vol. 50, no. 8, p. 081202, 2011.

[23] E. Hecht, "Optics 4th edition," *Optics 4th edition by Eugene Hecht Reading MA AddisonWesley Publishing Company 2001*, vol. 1. p. 122, 2001.

[24] N. Mehta, S. Shaik, R. Devireddy, and M. R. Gartia, "Single-Cell Analysis Using Hyperspectral Imaging Modalities," *J. Biomech. Eng. ASME*, 2018.

[25] L. Homolová, Z. Malenovský, J. G. P. W. Clevers, G. García-Santos, and M. E. Schaepman, "Review of optical-based remote sensing for plant trait mapping," *Ecological Complexity*, vol. 15. pp. 1–16, 2013.

[26] D. Manolakis, D. Marden, and G. a Shaw, "Hyperspectral Image Processing for Automatic Target Detection Applications," *Lincoln Lab. J.*, vol. 14, no. 1, pp. 79–116, 2003.

[27] N. M. Nasrabadi, "Hyperspectral Target Detection : An Overview of Current and Future Challenges," *Signal Process. Mag. IEEE*, vol. 31, no. 1, pp. 34–44, 2014.

[28] S. M. Arafat, M. A. Aboelghar, and E. F. Ahmed, "Crop Discrimination Using Field Hyper Spectral Remotely Sensed Data," *Adv. Remote Sens.*, vol. 02, no. 02, pp. 63–70, 2013.

[29] E. Bastidas-Obando and J. A. Carbonell, "Caracterización espectral y mineralógica de los suelos del valle del río Cauca por espectroscopía visible e infrarroja (400 - 2,500 nm)," *Agron. Colomb.*, vol. 28, no. 2, pp. 291–301, 2010.

[30] M. Zhang, Z. Qin, X. Liu, and S. L. Ustin, "Detection of stress in tomatoes induced by late blight disease in California, USA, using hyperspectral remote sensing," *Int. J. Appl. Earth Obs. Geoinf.*, vol. 4, no. 4, pp. 295–310, 2003.

[31] J. a Richards and X. Jia, *Remote sensing digital image analysis: an introduction*. 2006.

[32] E. Underwood, S. Ustin, and D. DiPietro, "Mapping nonnative plants using hyperspectral imagery," *Remote Sens. Environ.*, vol. 86, no. 2, pp. 150–161, 2003.

[33] P. Menesatti, C. Costa, and J. Aguzzi, "Quality Evaluation of Fish by Hyperspectral Imaging," in *Hyperspectral Imaging for Food Quality Analysis and Control*, 2010, pp. 273–294.

[34] Y. Montembeault, P. Lagueux, V. Farley, A. Villemaire, and K. C. Gross, "Hyper-Cam: Hyperspectral IR imaging applications in defence innovative research," in *2nd Workshop on Hyperspectral Image and Signal Processing: Evolution in Remote Sensing, WHISPERS 2010 - Workshop Program*, 2010.

[35] E. W. Ciurczak, "Uses of near-infrared spectroscopy in pharmaceutical analysis," *Appl. Spectrosc. Rev.*, vol. 23, no. 1–2, pp. 147–163, 1987.

[36] C. Fischer and I. Kakoulli, "Multispectral and hyperspectral imaging technologies in conservation : current research and potential applications," *Rev. Conserv.*, no. 7, pp. 3–16, 2007.

[37] C. Daffara, E. Pampaloni, L. Pezzati, M. Barucci, and R. Fontana, "Scanning multispectral IR reflectography SMIRR: An advanced tool for art diagnostics," *Acc. Chem. Res.*, 2010.
[38] R. Nakamura, Y. Tanaka, A. Ogata, and M. Naruse, "Dye analysis of Shosoin textiles using excitation-emission matrix fluorescence and ultraviolet-visible reflectance spectroscopic techniques," *Anal. Chem.*, 2009.
[39] R. Padoan, T. Steemers, M. Klein, and B. Aalderink, "Quantitative Hyperspectral Imaging of Historical Documents: Technique and Application," *ART Proc.*, no. May, pp. 25–30, 2008.
[40] L. W. MacDonald *et al.*, "Assessment of multispectral and hyperspectral imaging systems for digitisation of a Russian icon," *Herit. Sci.*, vol. 5, no. 1, 2017.
[41] A. Hernanz *et al.*, "Spectroscopy of Palaeolithic rock paintings from the Tito Bustillo and El Buxu Caves, Asturias, Spain," in *Journal of Raman Spectroscopy*, 2012, vol. 43, no. 11, pp. 1644–1650.
[42] P. Bourke, "Enhancing rock art recordings through hyperspectral photography," Australia, 2014.
[43] V. Miljković and D. Gajski, "Adaptation of industrial hyperspectral line scanner for archaeological applications," in *International Archives of the Photogrammetry, Remote Sensing and Spatial Information Sciences - ISPRS Archives*, 2016, vol. 41, pp. 343–345.
[44] L. Balick, A. Gillespie, A. French, I. Danilina, J. P. Allard, and A. Mushkin, "Longwave thermal infrared spectral variability in individual rocks," *IEEE Geosci. Remote Sens. Lett.*, vol. 6, no. 1, pp. 52–56, 2009.
[45] M. Attas *et al.*, "Near-infrared spectroscopic imaging in art conservation: Investigation of drawing constituents," *J. Cult. Herit.*, vol. 4, no. 2, pp. 127–136, 2003.
[46] A. Polak *et al.*, "Hyperspectral imaging combined with data classification techniques as an aid for artwork authentication," *J. Cult. Herit.*, vol. 26, pp. 1–11, 2017.
[47] N. Rohani, J. Salvant, S. Bahaadini, O. Cossairt, M. Walton, and A. Katsaggelos, "Automatic pigment identification on Roman Egyptian paintings by using sparse modeling of hyperspectral images," in *European Signal Processing Conference*, 2016, vol. 2016–Novem, pp. 2111–2115.
[48] L. Snijders, T. Zaman, and D. Howell, "Using hyperspectral imaging to reveal a hidden precolonial Mesoamerican codex," *J. Archaeol. Sci. Reports*, vol. 9, pp. 143–149, 2016.
[49] S. Legnaioli *et al.*, "Recovery of archaeological wall paintings using novel multispectral imaging approaches," *Herit. Sci.*, vol. 1, no. 1, 2013.
[50] D. Vincke *et al.*, "Analysis of collagen preservation in bones recovered in archaeological contexts using NIR Hyperspectral Imaging," *Talanta*, vol. 125, pp. 181–188, 2014.
[51] F. Daniel *et al.*, "Hyperspectral imaging applied to the analysis of Goya paintings in the Museum of Zaragoza (Spain)," *Microchem. J.*, vol. 126, pp. 113–120, 2016.
[52] H. Liang, "Advances in multispectral and hyperspectral imaging for archaeology and art conservation," *Appl. Phys. A Mater. Sci. Process.*, vol. 106, no. 2, pp. 309–323, 2012.
[53] C. Cucci, J. K. Delaney, and M. Picollo, "Reflectance Hyperspectral Imaging for

Investigation of Works of Art: Old Master Paintings and Illuminated Manuscripts," *Acc. Chem. Res.*, vol. 49, no. 10, pp. 2070–2079, 2016.

[54] M. Maguregui, Ulla Knuutinen, I. Martínez-Arkarazo, K. C. Anastasia Giakoumaki, and J. M. Madariaga, "Field Raman analysis to diagnose the conservation state of excavated walls and wall paintings in the archaeological site of Pompeii (Italy)†."

[55] H. Fabelo *et al.*, "A novel use of hyperspectral images for human brain cancer detection using in-vivo samples," in *BIOSIGNALS 2016 - 9th International Conference on Bio-Inspired Systems and Signal Processing, Proceedings; Part of 9th International Joint Conference on Biomedical Engineering Systems and Technologies, BIOSTEC 2016*, 2016.

[56] G. Camps-valls, L. Bruzzone, E. Electr, T. Escola, and U. De Val, "Regularized methods for hyperspectral image classification," *IEEE Trans. Geosci. Remote Sens.*, 2005.

[57] C.-C. Chang and C.-J. Lin, "LIBSVM : a library for support vector machines," *ACM Trans. Intell. Syst. Technol.*, 2011.

[58] T. G. Dietterich, "Ensemble methods in machine learning," in *International workshop on multiple classifier systems. Springer Berlin Heidelberg*, 2000.

[59] S. Ortega, H. Fabelo, R. Camacho, M. de la Luz Plaza, G. M. Callicó, and R. Sarmiento, "Detecting brain tumor in pathological slides using hyperspectral imaging," *Biomed. Opt. Express*, vol. 9, no. 2, pp. 818–831, Feb. 2018.

[60] S. Ortega, "Técnicas de reconocimiento automático de patrones aplicadas a imágenes hiperespectrales médicas," Universidad de Las Palmas de Gran Canaria, 2016.

[61] I. H. Witten, E. Frank, and M. A. Hall, *Data mining Practical Machine Learning Tools and Techniques*. 2011.

[62] K. Dhindsa, "Generalized Methods for User-Centered Brain-Computer Interfacing."

[63] C.-J. Fan, R.-E., Chang, K.-W., Hsieh, C.-J., Wang, X.-R., & Lin, "LIBLINEAR: A library for large linear classification," *J. Mach. Learn. Res.*, 2008.

[64] J. Zhou, X. Shi, and X. Li, "Utilizing gradient boosted machine for the prediction of damage to residential structures owing to blasting vibrations of open pit mining," *JVC/Journal Vib. Control*, 2016.

[65] Tom Tracy, "Demos: Automata-Based Random Forest." [Online]. Available: http://www.cs.virginia.edu/~tjt7a/demos/demos.html.

[66] J. M. Sandín, "Técnicas de regresión para la estimación de la localización de la mirada," 2012.

[67] C. Albon, "SVC parameters when using RBF kernel," 2017. [Online]. Available: https://chrisalbon.com/machine_learning/support_vector_machines/svc_parameters_using_rbf_kernel/.

ANEXX I

The all obsidian spectral signatures

This Annex I present the obsidian spectral signatures, with their references labeling, the group they belong to, their deposit and their measures.

Table A1. Information about the S1 obsidian.

Original label	Virtual label	Sigla	Group	Weight (g)	Measurement (cm) (Width/Large/Thickness)	Deposit	Municipality	Island
RES10-180	S1	544	HOG		1/1.5/0.5	La Restinga	Telde	Gran Canaria

(a)

(b)

(c)

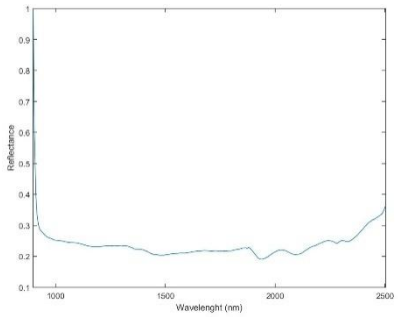

(d)

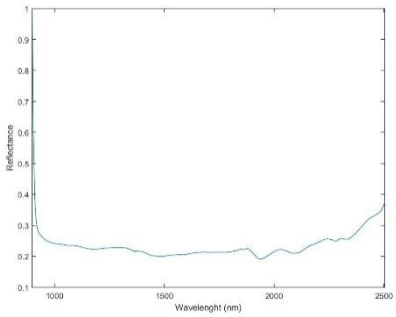

(e)

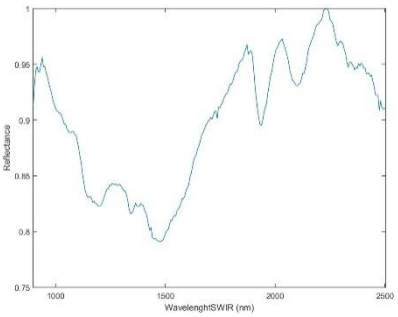

(f)

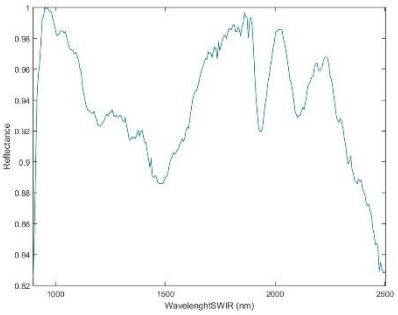

(g)

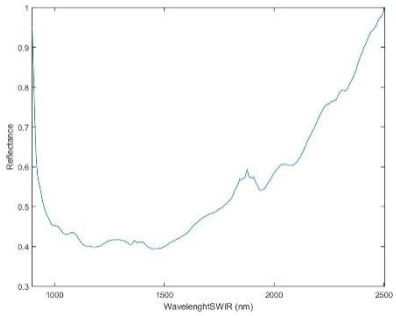

(h)

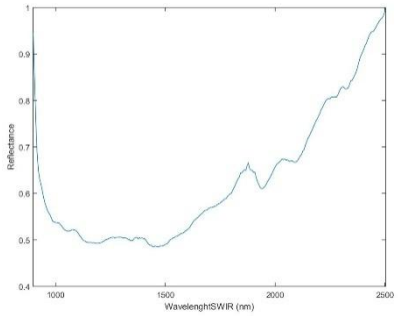

(i)

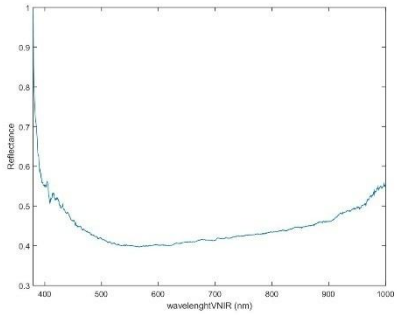

(j)

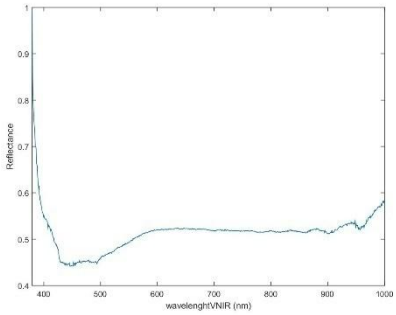

(k)

Figure A1. (a) Obsidian in frontal position. (b) Obsidian in reverse position. (c) Obsidian thickness. (d) Spectral signature calibrated and normalized (Frontal-SWIR-Ref. 99%). (e) Spectral signature calibrated and normalized (Reverse-SWIR-Ref. 99%). (f) Spectral signature calibrated and normalized (Frontal-SWIR-Ref. 10%). (g) Spectral signature calibrated and normalized (Reverse-SWIR-Ref. 10%). (h) Spectral signature calibrated and normalized (Frontal-SWIR-Ref. 50%). (i) Spectral signature calibrated and normalized (Reverse-SWIR-Ref. 50%). (j) Spectral signature calibrated and normalized (Frontal-VNIR-Ref.99%). (k) Spectral signature calibrated and normalized (Reverse-VNIR-Ref.99%).

Table A2. Information about the S2 obsidian.

Original label	Virtual label	Sigla	Group	Weight (g)	Measurement (cm) (Width/Large/Thickness)	Deposit	Municipality	Island
RES10-181	S2	543	HOG		1,1/1.75/0.4	La Restinga	Telde	Gran Canaria

(a)

(b)

(c)

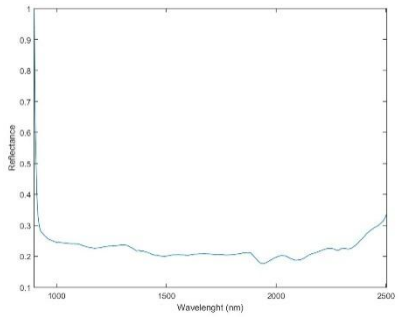

(d)

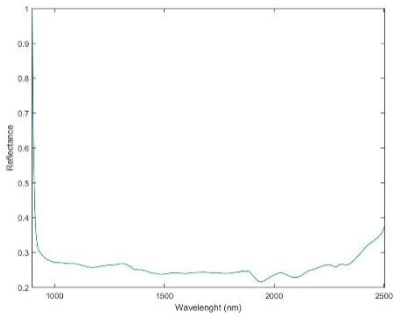

(e)

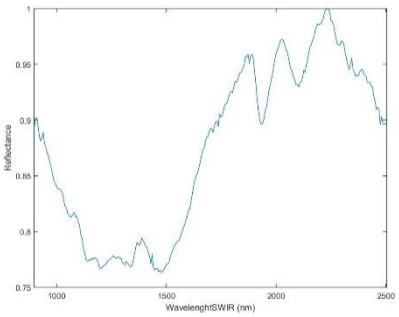

(f)

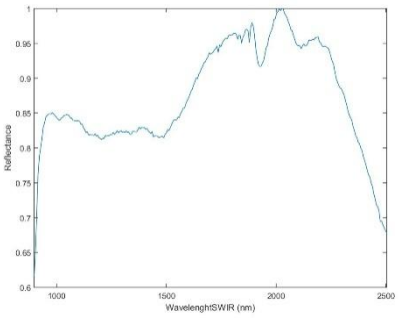

(g)

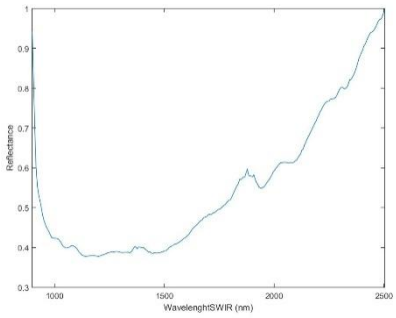

(h)

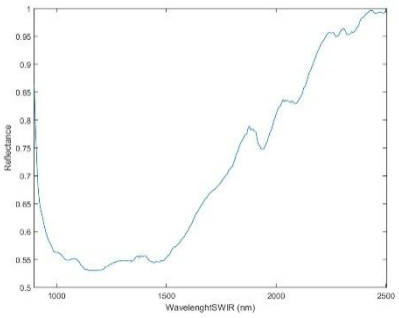

(i)

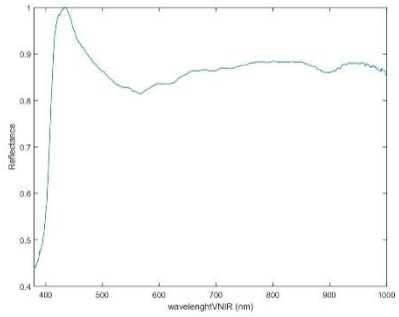

(j)

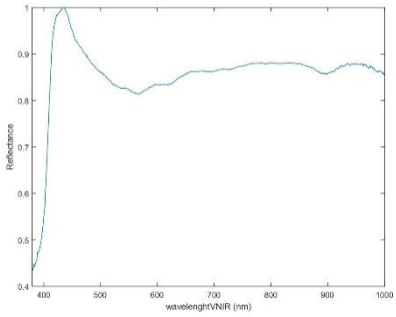

(k)

Figure A2. (a) Obsidian in frontal position. (b) Obsidian in reverse position. (c) Obsidian thickness. (d) Spectral signature calibrated and normalized (Frontal-SWIR-Ref. 99%). (e) Spectral signature calibrated and normalized (Reverse-SWIR-Ref. 99%). (f) Spectral signature calibrated and normalized (Frontal-SWIR-Ref. 10%). (g) Spectral signature calibrated and normalized (Reverse-SWIR-Ref. 10%). (h) Spectral signature calibrated and normalized (Frontal-SWIR-Ref. 50%). (i) Spectral signature calibrated and normalized (Reverse-SWIR-Ref. 50%). (j) Spectral signature calibrated and normalized (Frontal-VNIR-Ref.99%). (k) Spectral signature calibrated and normalized (Reverse-VNIR-Ref.99%).

Table A3. Information about the S3 obsidian.

Original label	Virtual label	Sigla	Group	Weight (g)	Measurement (cm) (Width/Large/Thickness)	Deposit	Municipality	Island
RES10-183	S3	499	HOG		0.95/1.3/0.4	La Restinga	Telde	Gran Canaria

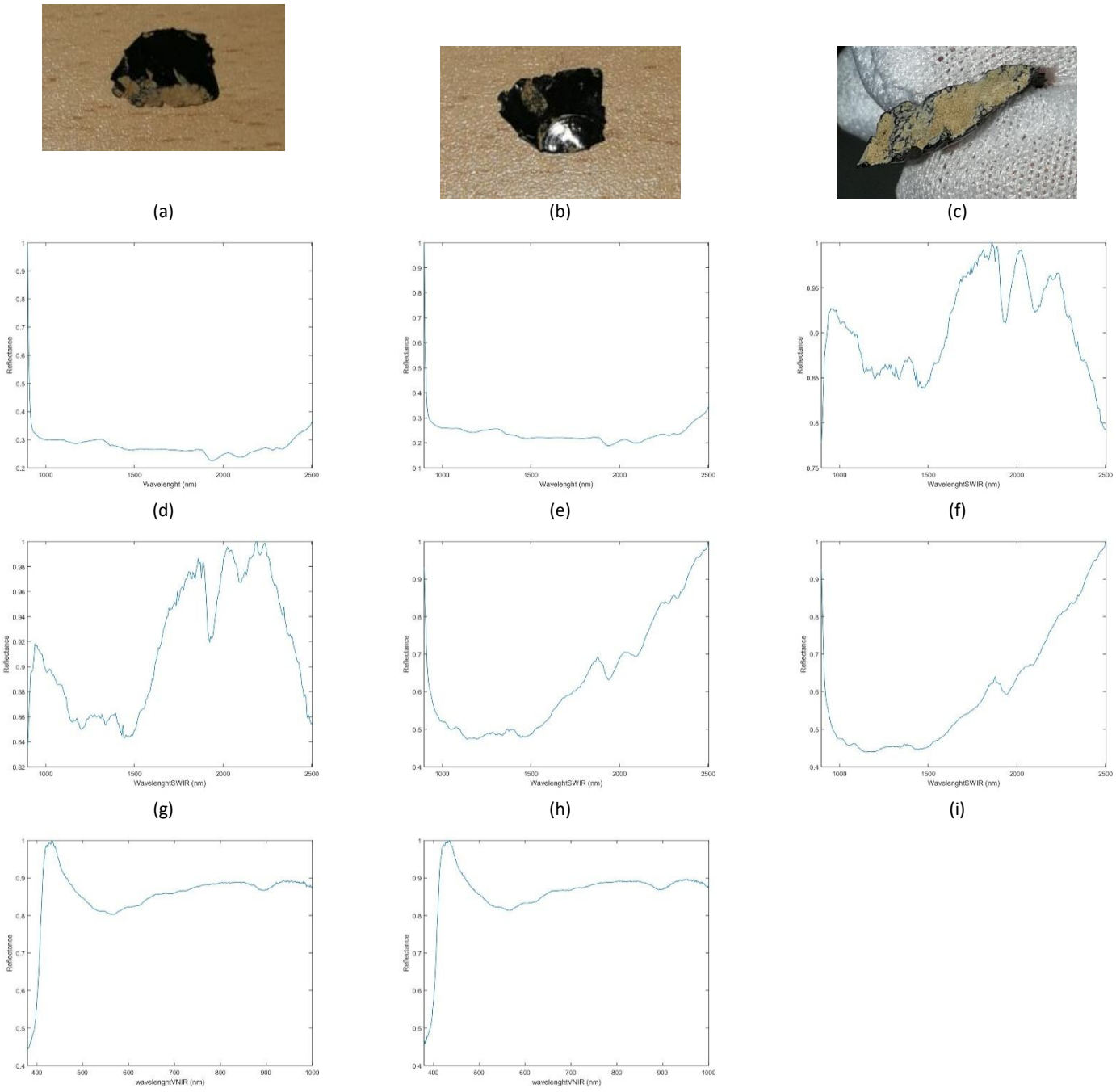

(a) (b) (c)

(d) (e) (f)

(g) (h) (i)

(j) (k)

Figure A3. (a) Obsidian in frontal position. (b) Obsidian in reverse position. (c) Obsidian thickness. (d) Spectral signature calibrated and normalized (Frontal-SWIR-Ref. 99%). (e) Spectral signature calibrated and normalized (Reverse-SWIR-Ref. 99%). (f) Spectral signature calibrated and normalized (Frontal-SWIR-Ref. 10%). (g) Spectral signature calibrated and normalized (Reverse-SWIR-Ref. 10%). (h) Spectral signature calibrated and normalized (Frontal-SWIR-Ref. 50%). (i) Spectral signature calibrated and normalized (Reverse-SWIR-Ref. 50%). (j) Spectral signature calibrated and normalized (Frontal-VNIR-Ref.99%). (k) Spectral signature calibrated and normalized (Reverse-VNIR-Ref.99%).

Table A4. Information about the S4 obsidian.

Original label	Virtual label	Sigla	Group	Weight (g)	Measurement (cm) (Width/Large/Thickness)	Deposit	Municipality	Island
RES10-184	S4	645	HOG		0.75/1.1/0.1	La Restinga	Telde	Gran Canaria

(a)

(b)

(c)

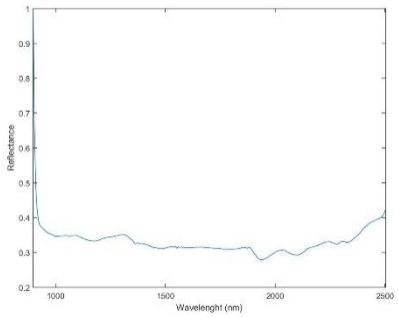

(d)

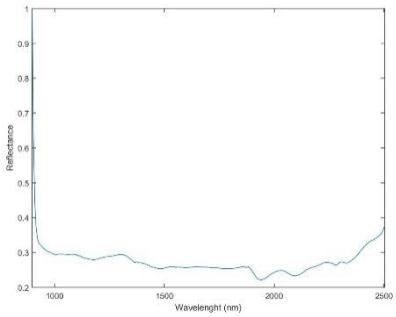

(e)

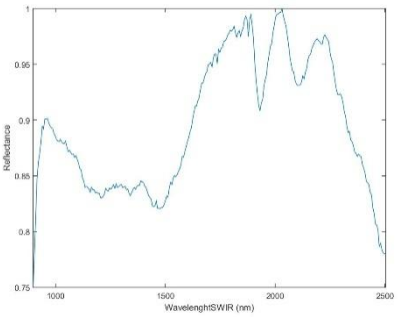

(f)

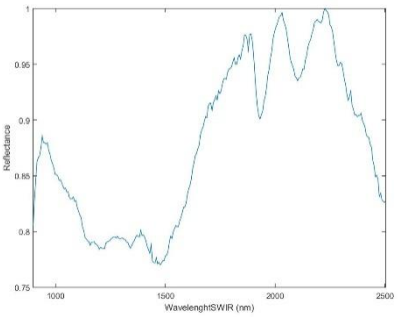

(g)

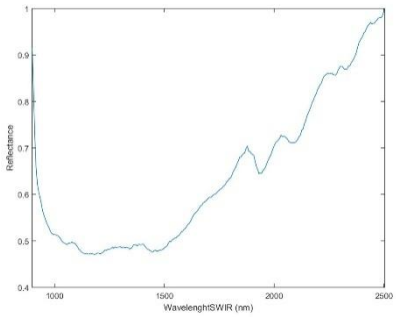

(h)

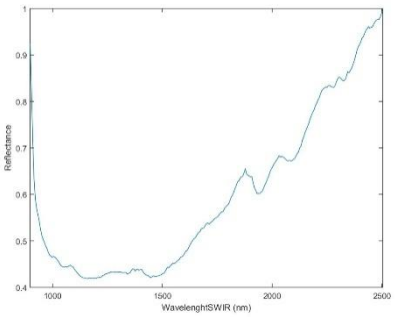

(i)

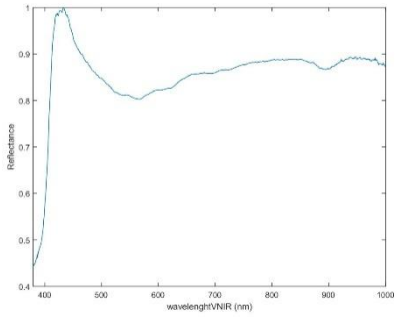

(j)

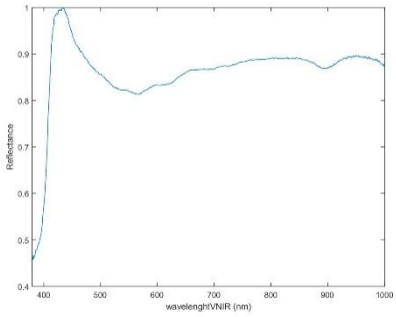

(k)

Figure A4. (a) Obsidian in frontal position. (b) Obsidian in reverse position. (c) Obsidian thickness. (d) Spectral signature calibrated and normalized (Frontal-SWIR-Ref. 99%). (e) Spectral signature calibrated and normalized (Reverse-SWIR-Ref. 99%). (f) Spectral signature calibrated and normalized (Frontal-SWIR-Ref. 10%). (g) Spectral signature calibrated and normalized (Reverse-SWIR-Ref. 10%). (h) Spectral signature calibrated and normalized (Frontal-SWIR-Ref. 50%). (i) Spectral signature calibrated and normalized (Reverse-SWIR-Ref. 50%). (j) Spectral signature calibrated and normalized (Frontal-VNIR-Ref.99%). (k) Spectral signature calibrated and normalized (Reverse-VNIR-Ref.99%).

Table A5. Information about the S5 obsidian.

Original label	Virtual label	Sigla	Group	Weight (g)	Measurement (cm) (Width/Large/Thickness)	Deposit	Municipality	Island
RES10-185	S5	624	HOG		0.95/1.15/0.2	La Restinga	Telde	Gran Canaria

(a)

(b)

(c)

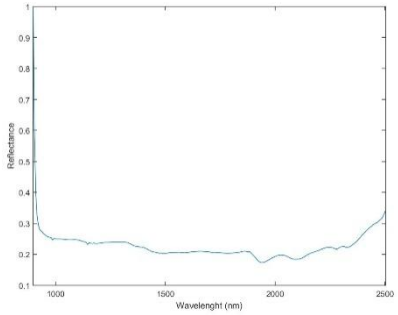

(d)

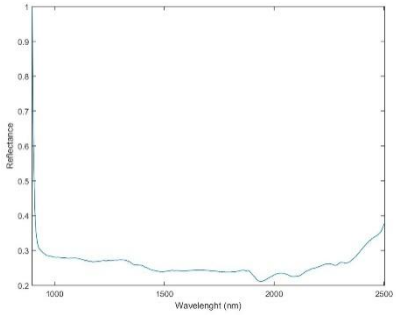

(e)

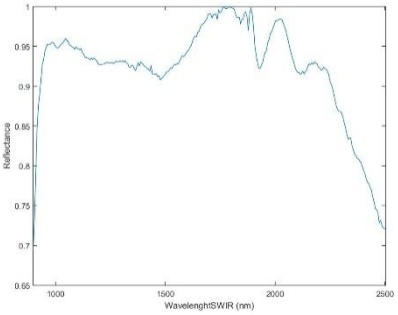

(f)

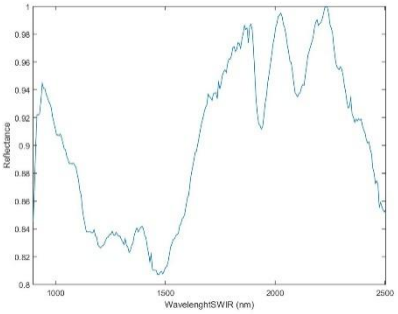

(g)

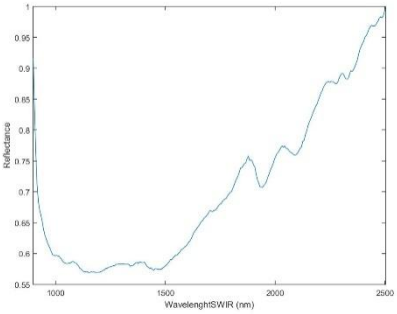

(h)

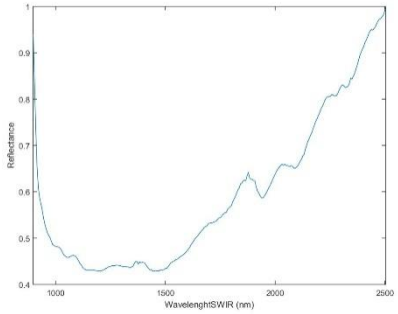

(i)

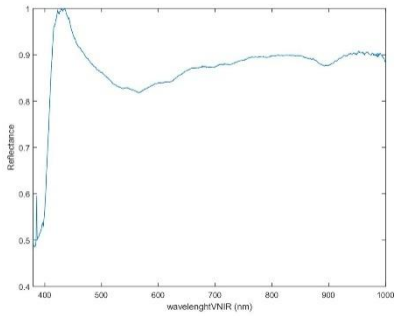

(j)

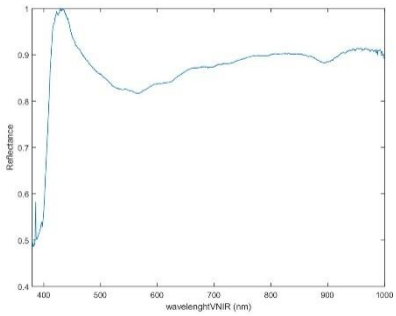

(k)

Figure A5. (a) Obsidian in frontal position. (b) Obsidian in reverse position. (c) Obsidian thickness. (d) Spectral signature calibrated and normalized (Frontal-SWIR-Ref. 99%). (e) Spectral signature calibrated and normalized (Reverse-SWIR-Ref. 99%). (f) Spectral signature calibrated and normalized (Frontal-SWIR-Ref. 10%). (g) Spectral signature calibrated and normalized (Reverse-SWIR-Ref. 10%). (h) Spectral signature calibrated and normalized (Frontal-SWIR-Ref. 50%). (i) Spectral signature calibrated and normalized (Reverse-SWIR-Ref. 50%). (j) Spectral signature calibrated and normalized (Frontal-VNIR-Ref.99%). (k) Spectral signature calibrated and normalized (Reverse-VNIR-Ref.99%).

Table A6. Information about the S6 obsidian.

Original label	Virtual label	Sigla	Group	Weight (g)	Measurement (cm) (Width/Large/Thickness)	Deposit	Municipality	Island
RES10-187	S6	629	HOG		0.8/1.5/0.4	La Restinga	Telde	Gran Canaria

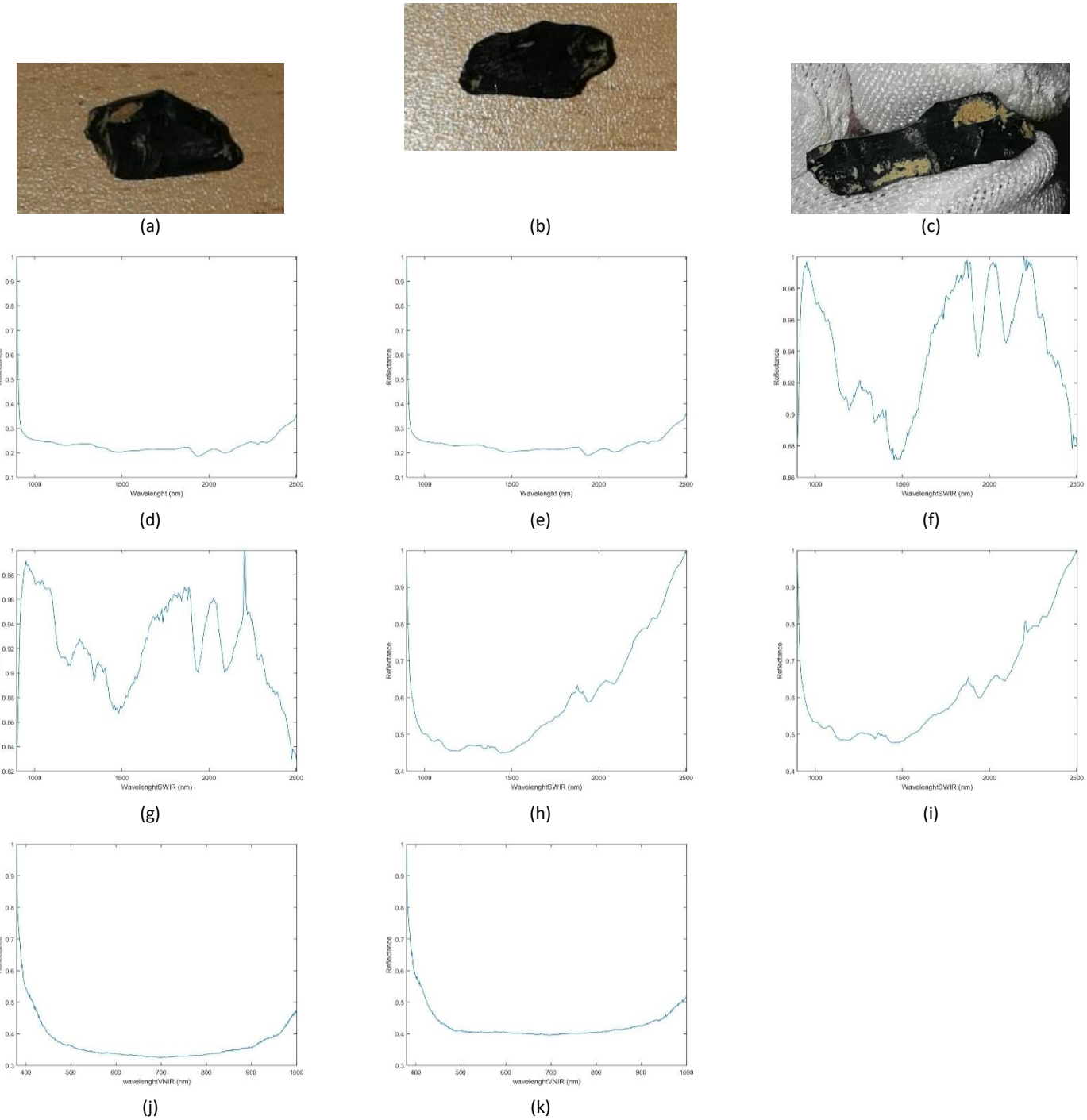

Figure A6. (a) Obsidian in frontal position. (b) Obsidian in reverse position. (c) Obsidian thickness. (d) Spectral signature calibrated and normalized (Frontal-SWIR-Ref. 99%). (e) Spectral signature calibrated and normalized (Reverse-SWIR-Ref. 99%). (f) Spectral signature calibrated and normalized (Frontal-SWIR-Ref. 10%). (g) Spectral signature calibrated and normalized (Reverse-SWIR-Ref. 10%). (h) Spectral signature calibrated and normalized (Frontal-SWIR-Ref. 50%). (i) Spectral signature calibrated and normalized (Reverse-SWIR-Ref. 50%). (j) Spectral signature calibrated and normalized (Frontal-VNIR-Ref.99%). (k) Spectral signature calibrated and normalized (Reverse-VNIR-Ref.99%).

Table A7. Information about the S7 obsidian.

Original label	Virtual label	Sigla	Group	Weight (g)	Measurement (cm) (Width/Large/Thickness)	Deposit	Municipality	Island
RES10-190	S7	461			1.2/1.5/0.4	La Restinga	Telde	Gran Canaria

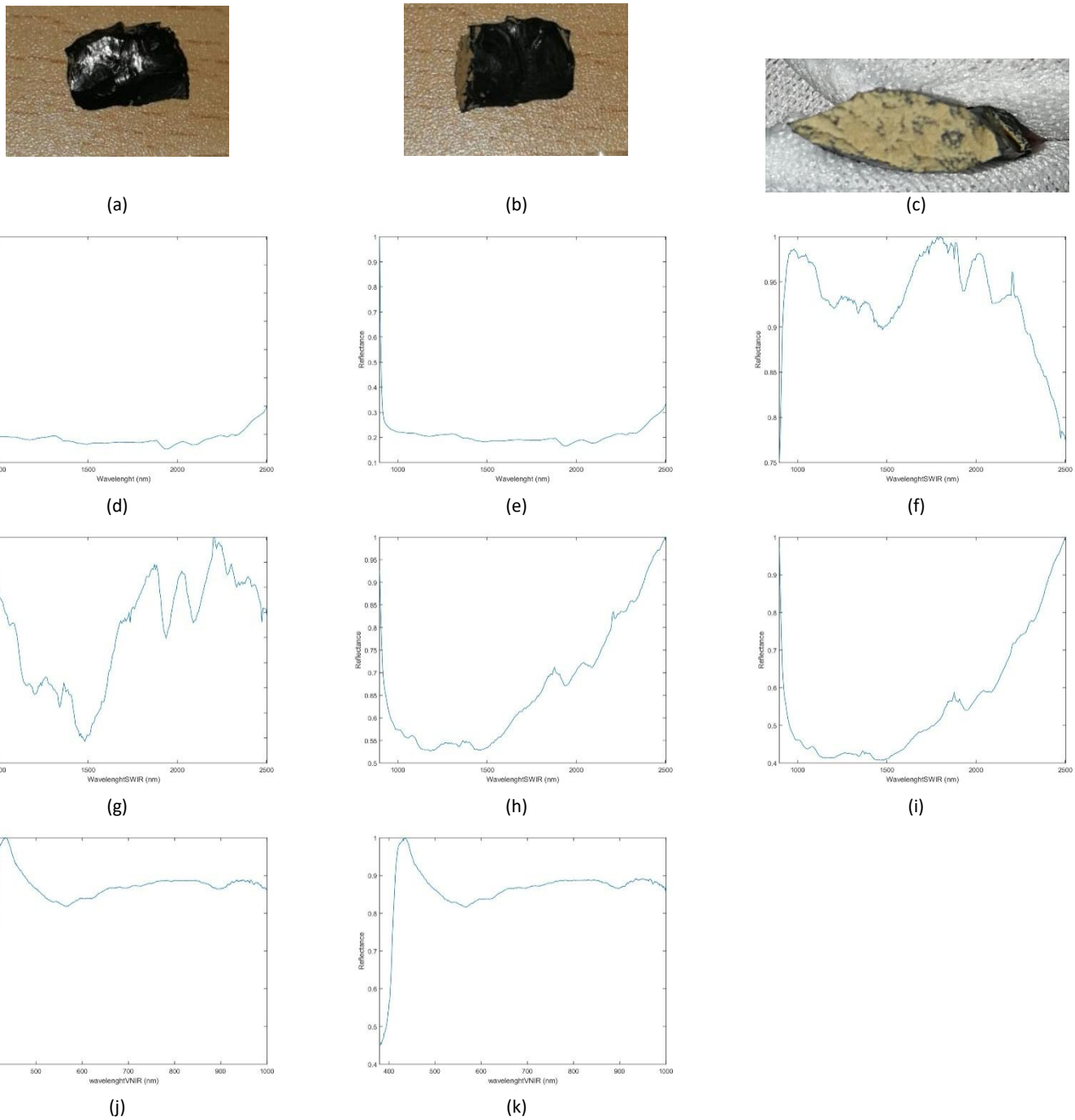

Figure A7. (a) Obsidian in frontal position. (b) Obsidian in reverse position. (c) Obsidian thickness. (d) Spectral signature calibrated and normalized (Frontal-SWIR-Ref. 99%). (e) Spectral signature calibrated and normalized (Reverse-SWIR-Ref. 99%). (f) Spectral signature calibrated and normalized (Frontal-SWIR-Ref. 10%). (g) Spectral signature calibrated and normalized (Reverse-SWIR-Ref. 10%). (h) Spectral signature calibrated and normalized (Frontal-SWIR-Ref. 50%). (i) Spectral signature calibrated and normalized (Reverse-SWIR-Ref. 50%). (j) Spectral signature calibrated and normalized (Frontal-VNIR-Ref.99%). (k) Spectral signature calibrated and normalized (Reverse-VNIR-Ref.99%).

Table A8. Information about the S8 obsidian.

Original label	Virtual label	Sigla	Group	Weight (g)	Measurement (cm) (Width/Large/Thickness)	Deposit	Municipality	Island
RES10-191	S8	496	-		1.15/1.5/0.5	La Restinga	Telde	Gran Canaria

(a)

(b)

(c)

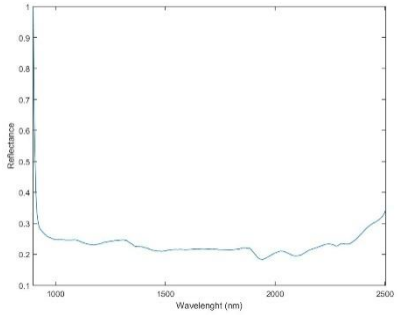

(d)

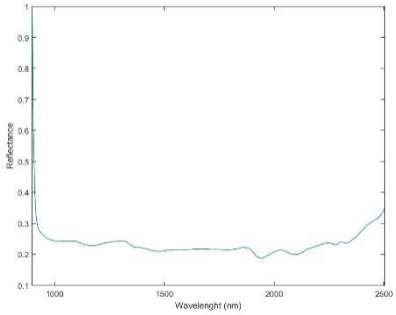

(e)

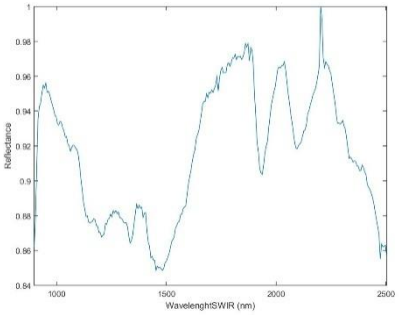

(f)

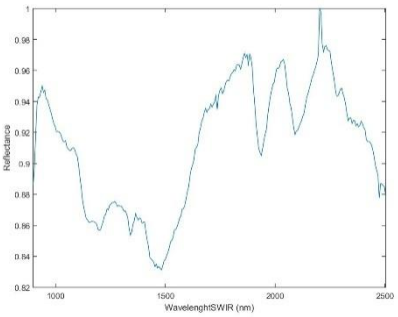

(g)

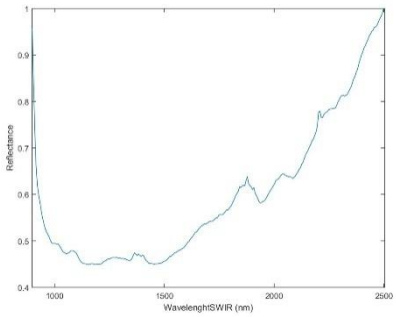

(h)

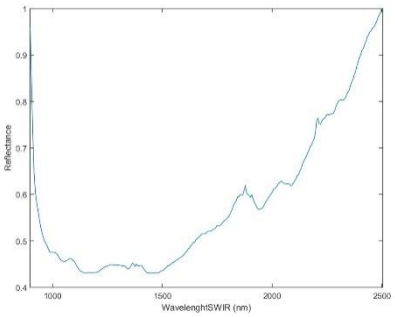

(i)

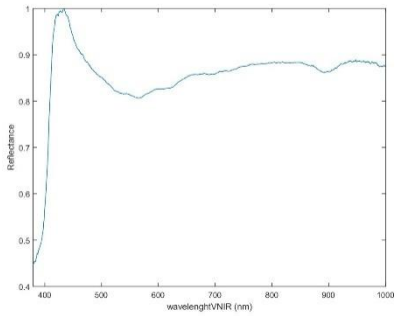

(j)

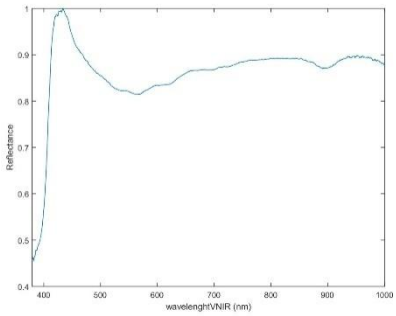

(k)

Figure A8. (a) Obsidian in frontal position. (b) Obsidian in reverse position. (c) Obsidian thickness. (d) Spectral signature calibrated and normalized (Frontal-SWIR-Ref. 99%). (e) Spectral signature calibrated and normalized (Reverse-SWIR-Ref. 99%). (f) Spectral signature calibrated and normalized (Frontal-SWIR-Ref. 10%). (g) Spectral signature calibrated and normalized (Reverse-SWIR-Ref. 10%). (h) Spectral signature calibrated and normalized (Frontal-SWIR-Ref. 50%). (i) Spectral signature calibrated and normalized (Reverse-SWIR-Ref. 50%). (j) Spectral signature calibrated and normalized (Frontal-VNIR-Ref.99%). (k) Spectral signature calibrated and normalized (Reverse-VNIR-Ref.99%).

Table A9. Information about the S9 obsidian.

Original label	Virtual label	Sigla	Group	Weight (g)	Measurement (cm) (Width/Large/Thickness)	Deposit	Municipality	Island
RES10-192	S9	579	HOG		0.7/1.5/0.3	La Restinga	Telde	Gran Canaria

(a)

(b)

(c)

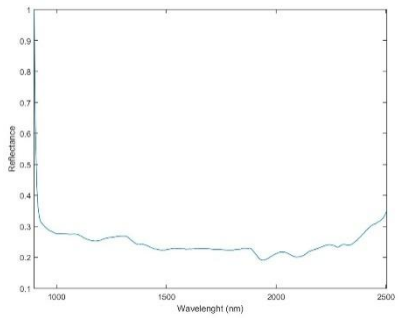

(d)

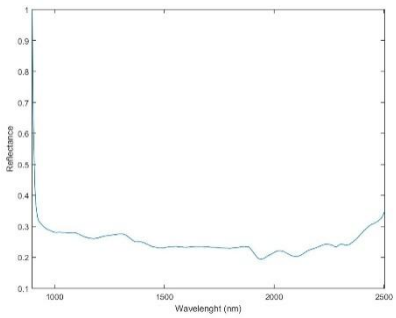

(e)

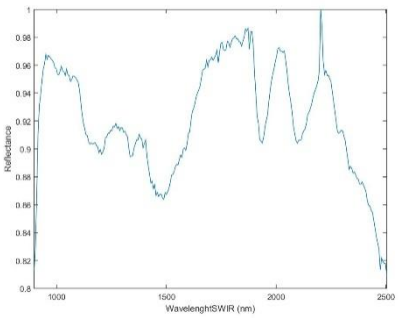

(f)

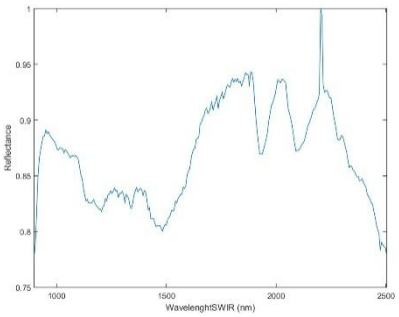

(g)

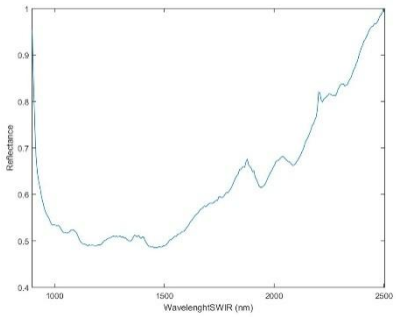

(h)

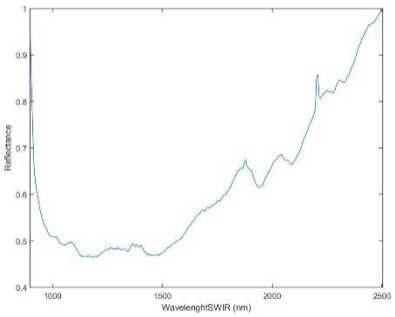

(i)

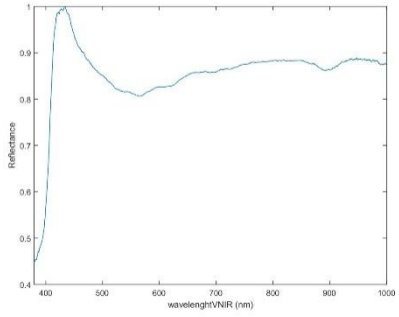

(j)

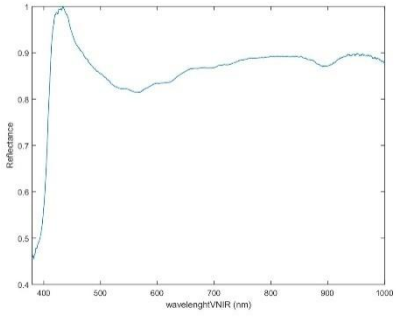

(k)

Figure A9. (a) Obsidian in frontal position. (b) Obsidian in reverse position. (c) Obsidian thickness. (d) Spectral signature calibrated and normalized (Frontal-SWIR-Ref. 99%). (e) Spectral signature calibrated and normalized (Reverse-SWIR-Ref. 99%). (f) Spectral signature calibrated and normalized (Frontal-SWIR-Ref. 10%). (g) Spectral signature calibrated and normalized (Reverse-SWIR-Ref. 10%). (h) Spectral signature calibrated and normalized (Frontal-SWIR-Ref. 50%). (i) Spectral signature calibrated and normalized (Reverse-SWIR-Ref. 50%). (j) Spectral signature calibrated and normalized (Frontal-VNIR-Ref.99%). (k) Spectral signature calibrated and normalized (Reverse-VNIR-Ref.99%).

Table A10. Information about the S10 obsidian.

Original label	Virtual label	Sigla	Group	Weight (g)	Measurement (cm) (Width/Large/Thickness)	Deposit	Municipality	Island
RES10-193	S10	487	HOG		0.8/1.2/0.3	La Restinga	Telde	Gran Canaria

(a)

(b)

(c)

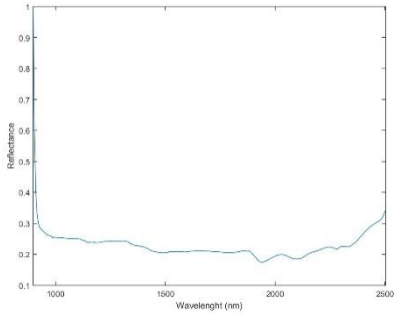

(d)

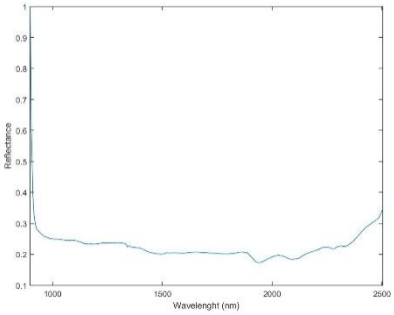

(e)

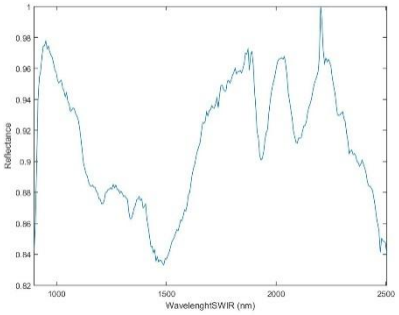

(f)

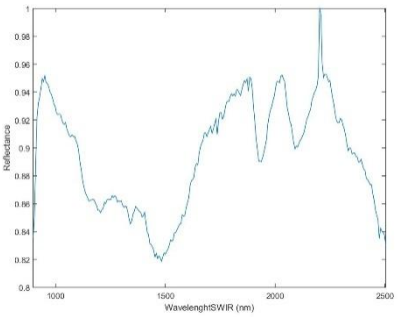

(g)

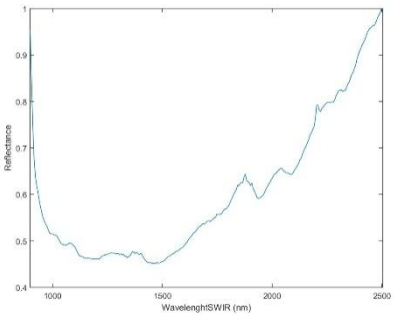

(h)

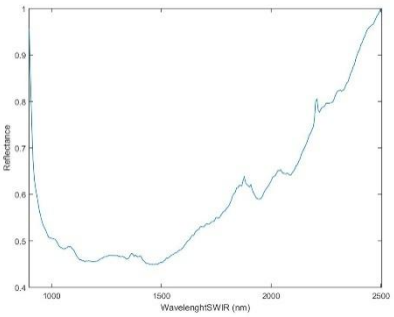

(i)

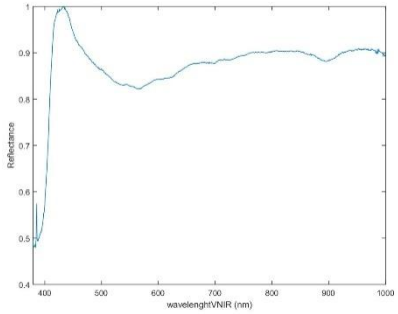

(j)

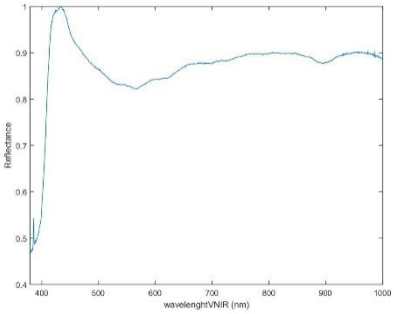

(k)

Figure A10. (a) Obsidian in frontal position. (b) Obsidian in reverse position. (c) Obsidian thickness. (d) Spectral signature calibrated and normalized (Frontal-SWIR-Ref. 99%). (e) Spectral signature calibrated and normalized (Reverse-SWIR-Ref. 99%). (f) Spectral signature calibrated and normalized (Frontal-SWIR-Ref. 10%). (g) Spectral signature calibrated and normalized (Reverse-SWIR-Ref. 10%). (h) Spectral signature calibrated and normalized (Frontal-SWIR-Ref. 50%). (i) Spectral signature calibrated and normalized (Reverse-SWIR-Ref. 50%). (j) Spectral signature calibrated and normalized (Frontal-VNIR-Ref.99%). (k) Spectral signature calibrated and normalized (Reverse-VNIR-Ref.99%).

Table A11. Information about the S11 obsidian.

Original label	Virtual label	Sigla	Group	Weight (g)	Measurement (cm) (Width/Large/Thickness)	Deposit	Municipality	Island
RES10-194	S11	581	HOG		0.85/1.65/0.75	La Restinga	Telde	Gran Canaria

(a)

(b)

(c)

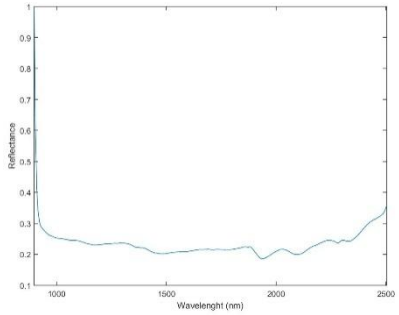

(d)

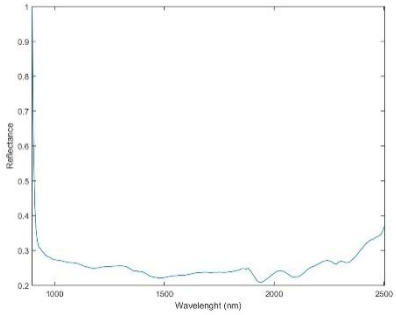

(e)

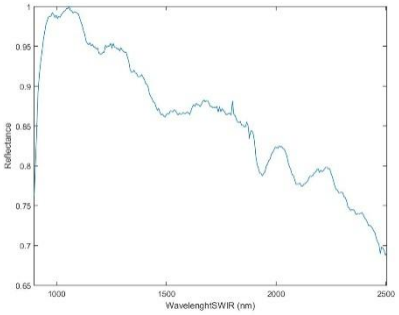

(f)

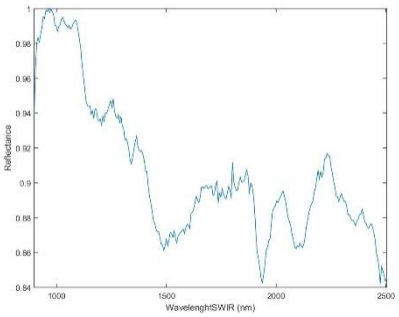

(g)

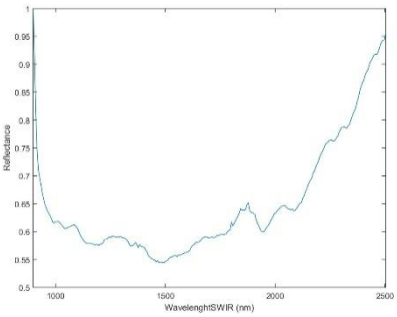

(h)

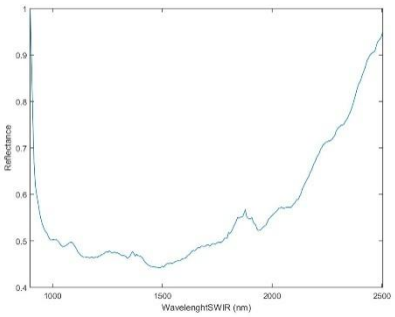

(i)

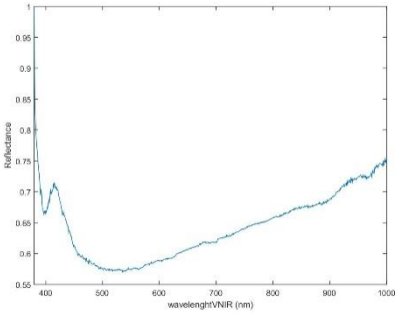

(j)

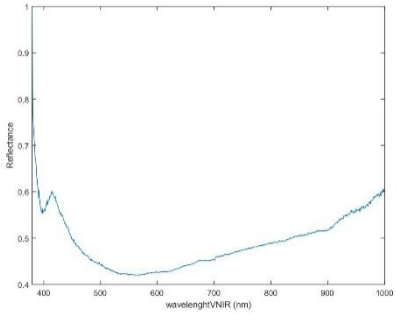

(k)

Figure A11. (a) Obsidian in frontal position. (b) Obsidian in reverse position. (c) Obsidian thickness. (d) Spectral signature calibrated and normalized (Frontal-SWIR-Ref. 99%). (e) Spectral signature calibrated and normalized (Reverse-SWIR-Ref. 99%). (f) Spectral signature calibrated and normalized (Frontal-SWIR-Ref. 10%). (g) Spectral signature calibrated and normalized (Reverse-SWIR-Ref. 10%). (h) Spectral signature calibrated and normalized (Frontal-SWIR-Ref. 50%). (i) Spectral signature calibrated and normalized (Reverse-SWIR-Ref. 50%). (j) Spectral signature calibrated and normalized (Frontal-VNIR-Ref.99%). (k) Spectral signature calibrated and normalized (Reverse-VNIR-Ref.99%).

Table A12. Information about the S12 obsidian.

Original label	Virtual label	Sigla	Group	Weight (g)	Measurement (cm) (Width/Large/Thickness)	Deposit	Municipality	Island
RES7-173	S12	11272	N1		0.8/1.5/0.3	La Restinga	Telde	Gran Canaria

(a)

(b)

(c)

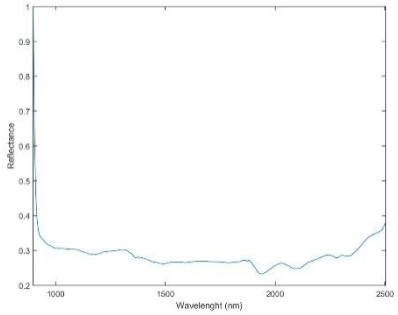

(d)

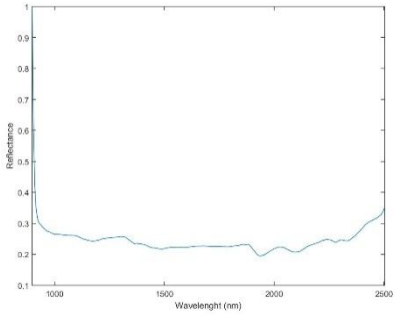

(e)

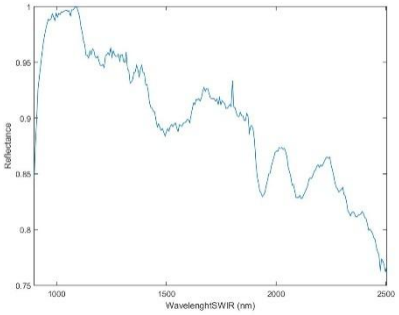

(f)

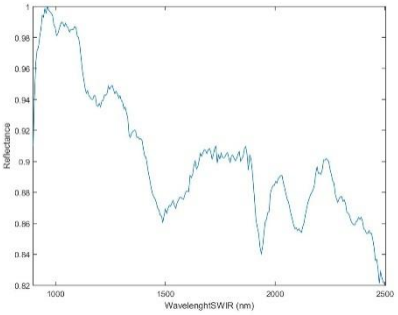

(g)

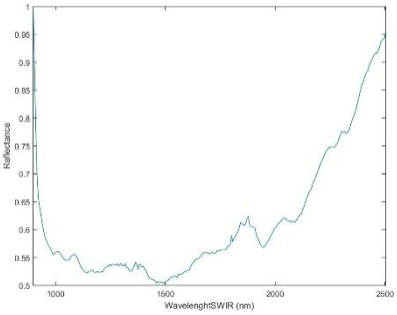

(h)

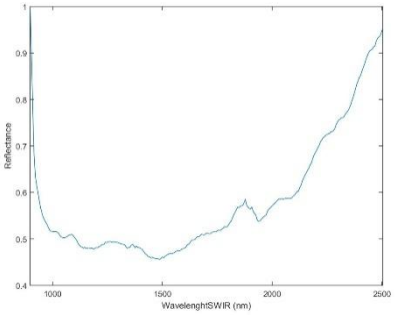

(i)

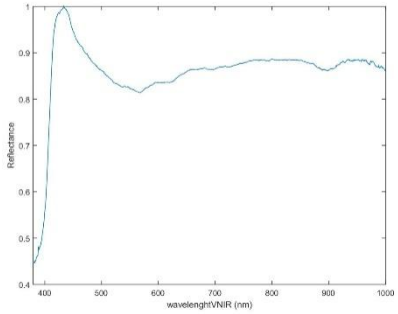

(j)

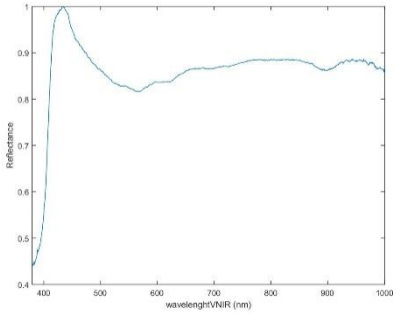

(k)

Figure A12. (a) Obsidian in frontal position. (b) Obsidian in reverse position. (c) Obsidian thickness. (d) Spectral signature calibrated and normalized (Frontal-SWIR-Ref. 99%). (e) Spectral signature calibrated and normalized (Reverse-SWIR-Ref. 99%). (f) Spectral signature calibrated and normalized (Frontal-SWIR-Ref. 10%). (g) Spectral signature calibrated and normalized (Reverse-SWIR-Ref. 10%). (h) Spectral signature calibrated and normalized (Frontal-SWIR-Ref. 50%). (i) Spectral signature calibrated and normalized (Reverse-SWIR-Ref. 50%). (j) Spectral signature calibrated and normalized (Frontal-VNIR-Ref.99%). (k) Spectral signature calibrated and normalized (Reverse-VNIR-Ref.99%).

Table A13. Information about the S13 obsidian.

Original label	Virtual label	Sigla	Group	Weight (g)	Measurement (cm) (Width/Large/Thickness)	Deposit	Municipality	Island
RES7-174	S13	11377	HOG		1.5/1.7/0.3	La Restinga	Telde	Gran Canaria

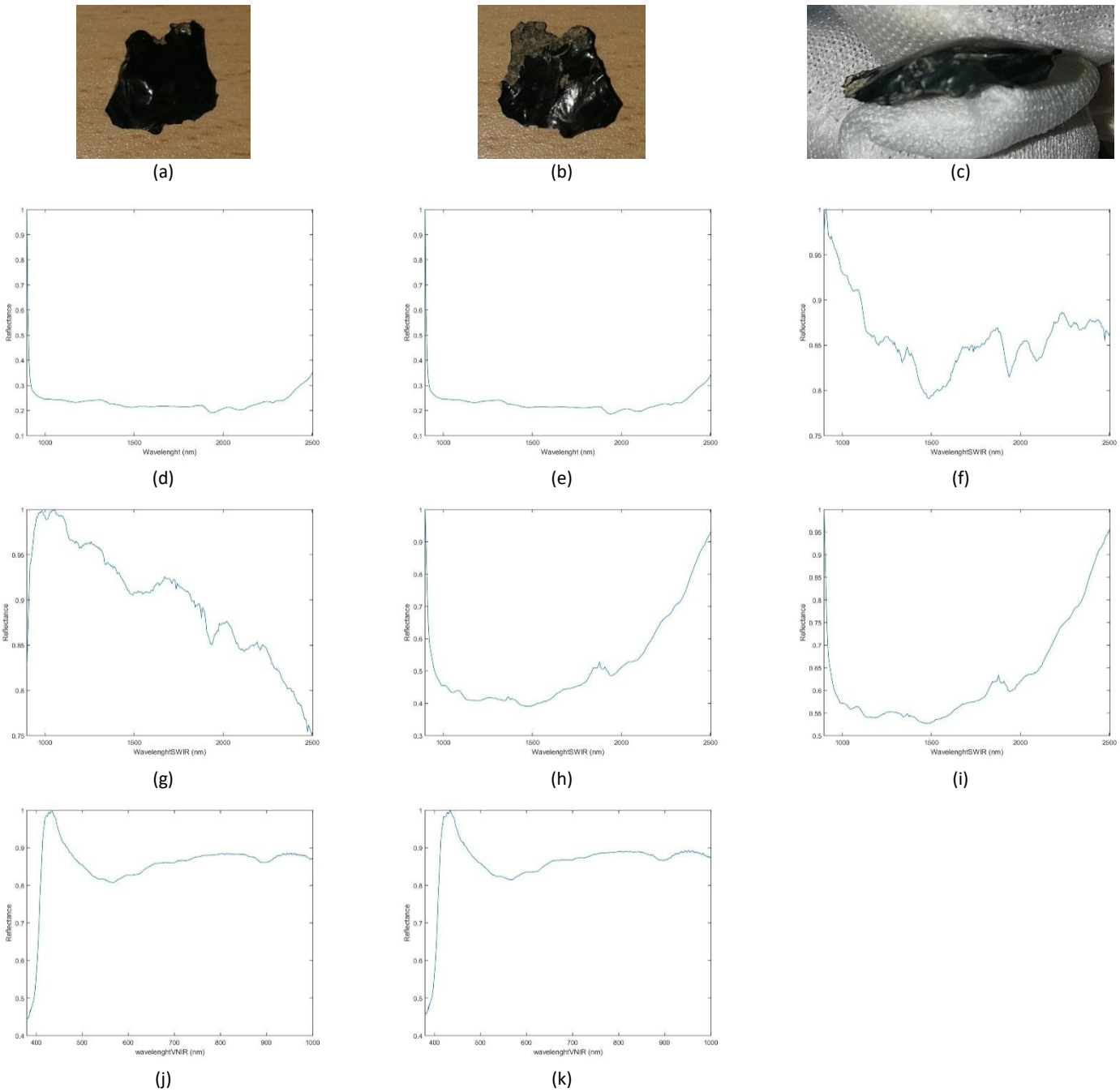

Figure A13. (a) Obsidian in frontal position. (b) Obsidian in reverse position. (c) Obsidian thickness. (d) Spectral signature calibrated and normalized (Frontal-SWIR-Ref. 99%). (e) Spectral signature calibrated and normalized (Reverse-SWIR-Ref. 99%). (f) Spectral signature calibrated and normalized (Frontal-SWIR-Ref. 10%). (g) Spectral signature calibrated and normalized (Reverse-SWIR-Ref. 10%). (h) Spectral signature calibrated and normalized (Frontal-SWIR-Ref. 50%). (i) Spectral signature calibrated and normalized (Reverse-SWIR-Ref. 50%). (j) Spectral signature calibrated and normalized (Frontal-VNIR-Ref.99%). (k) Spectral signature calibrated and normalized (Reverse-VNIR-Ref.99%).

Table A14. Information about the S14 obsidian.

Original label	Virtual label	Sigla	Group	Weight (g)	Measurement (cm) (Width/Large/Thickness)	Deposit	Municipality	Island
RES7-175	S14	11378	HOG		1.6/1.5/0.5	La Restinga	Telde	Gran Canaria

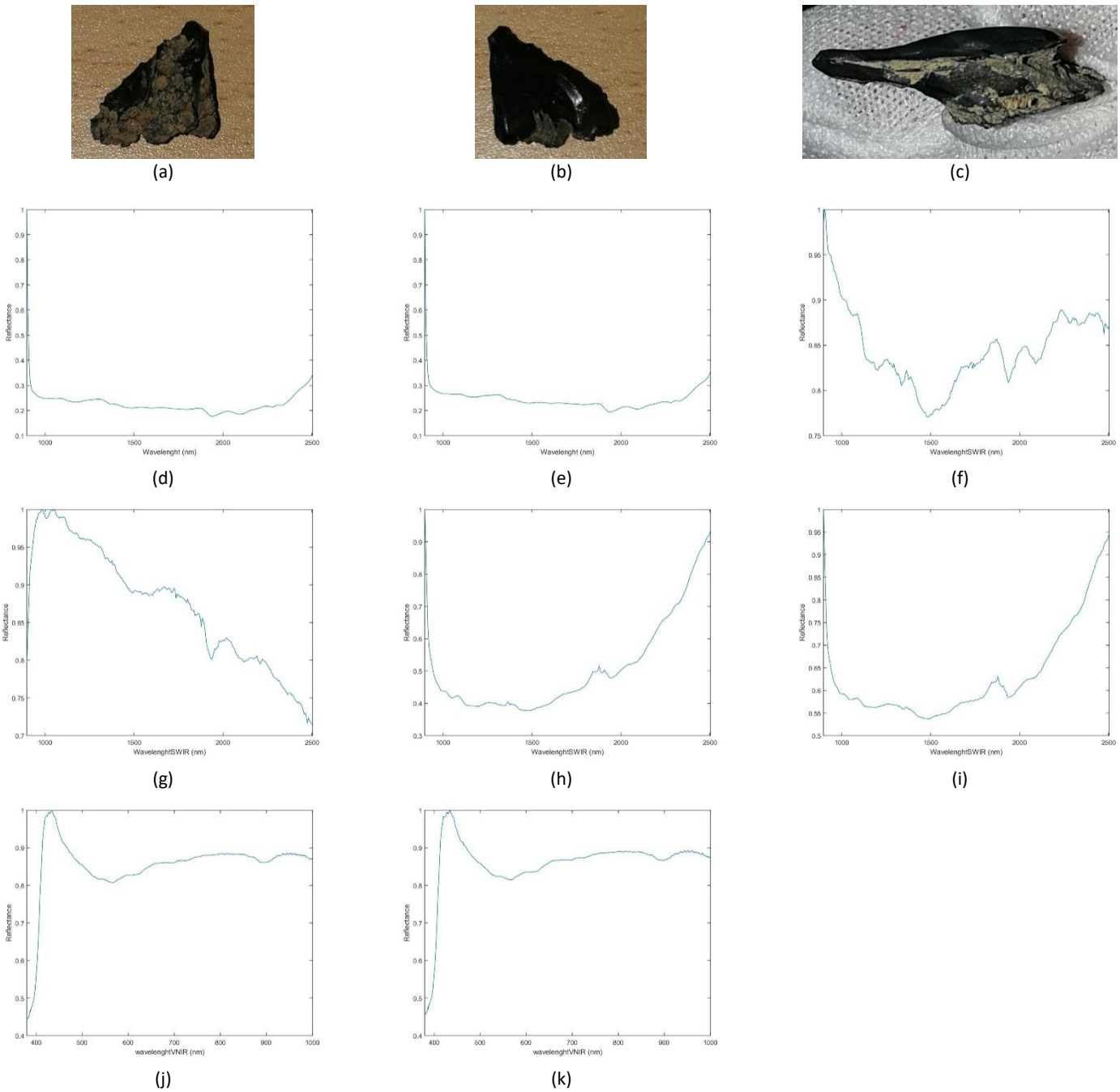

Figure A14. (a) Obsidian in frontal position. (b) Obsidian in reverse position. (c) Obsidian thickness. (d) Spectral signature calibrated and normalized (Frontal-SWIR-Ref. 99%). (e) Spectral signature calibrated and normalized (Reverse-SWIR-Ref. 99%). (f) Spectral signature calibrated and normalized (Frontal-SWIR-Ref. 10%). (g) Spectral signature calibrated and normalized (Reverse-SWIR-Ref. 10%). (h) Spectral signature calibrated and normalized (Frontal-SWIR-Ref. 50%). (i) Spectral signature calibrated and normalized (Reverse-SWIR-Ref. 50%). (j) Spectral signature calibrated and normalized (Frontal-VNIR-Ref.99%). (k) Spectral signature calibrated and normalized (Reverse-VNIR-Ref.99%).

Table A15. Information about the S15 obsidian.

Original label	Virtual label	Sigla	Group	Weight (g)	Measurement (cm) (Width/Large/Thickness)	Deposit	Municipality	Island
RES7-178	S15	7394	N1		0.7/11.5/0.3	La Restinga	Telde	Gran Canaria

(a)

(b)

(c)

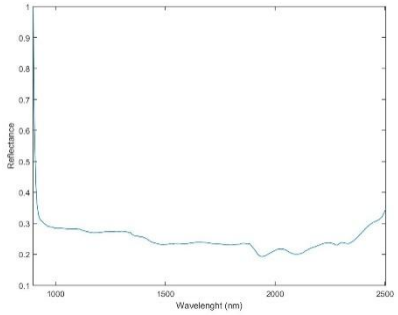

(d)

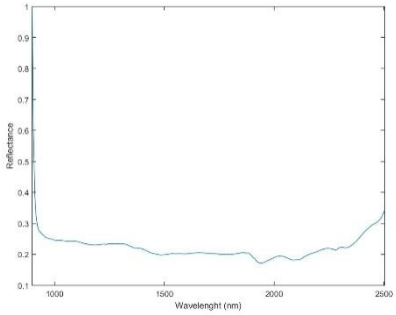

(e)

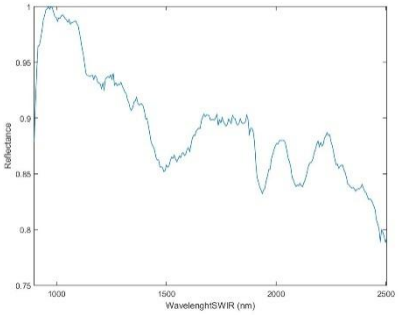

(f)

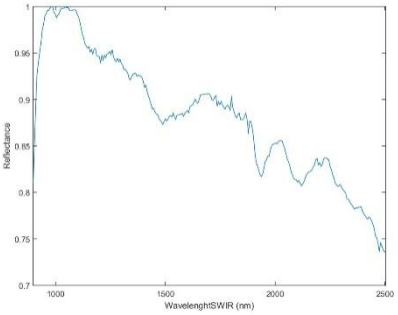

(g)

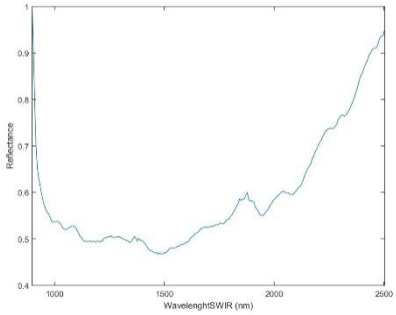

(h)

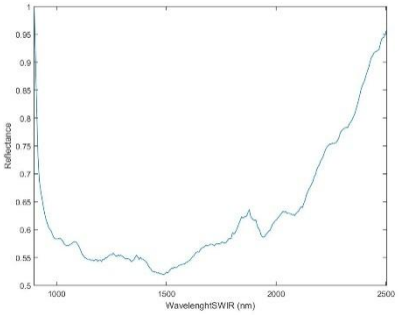

(i)

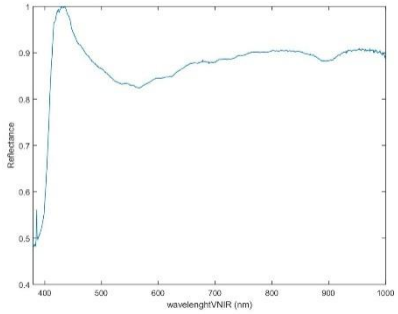

(j)

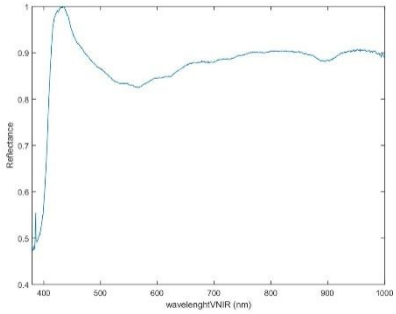

(k)

Figure A15. (a) Obsidian in frontal position. (b) Obsidian in reverse position. (c) Obsidian thickness. (d) Spectral signature calibrated and normalized (Frontal-SWIR-Ref. 99%). (e) Spectral signature calibrated and normalized (Reverse-SWIR-Ref. 99%). (f) Spectral signature calibrated and normalized (Frontal-SWIR-Ref. 10%). (g) Spectral signature calibrated and normalized (Reverse-SWIR-Ref. 10%). (h) Spectral signature calibrated and normalized (Frontal-SWIR-Ref. 50%). (i) Spectral signature calibrated and normalized (Reverse-SWIR-Ref. 50%). (j) Spectral signature calibrated and normalized (Frontal-VNIR-Ref.99%). (k) Spectral signature calibrated and normalized (Reverse-VNIR-Ref.99%).

Table A16. Information about the S16 obsidian.

Original label	Virtual label	Sigla	Group	Weight (g)	Measurement (cm) (Width/Large/Thickness)	Deposit	Municipality	Island
RES7-179	S16	544	OTHERS		1.35/2/0.3	La Restinga	Telde	Gran Canaria

(a)

(b)

(c)

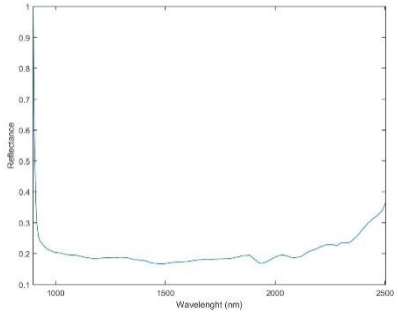

(d)

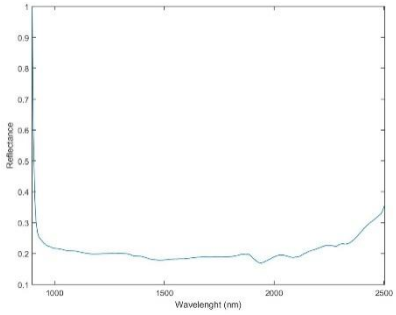

(e)

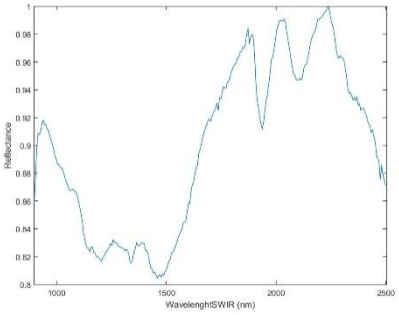

(f)

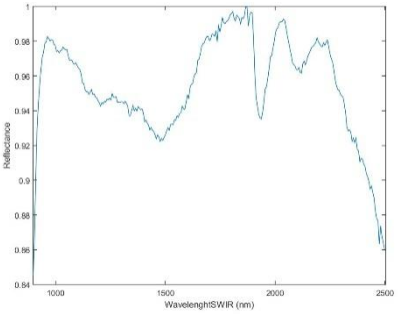

(g)

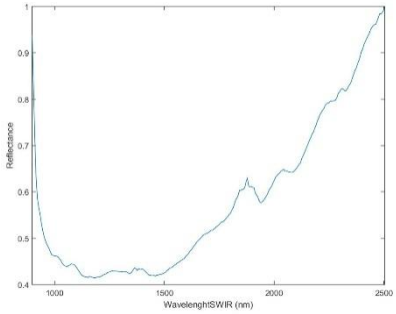

(h)

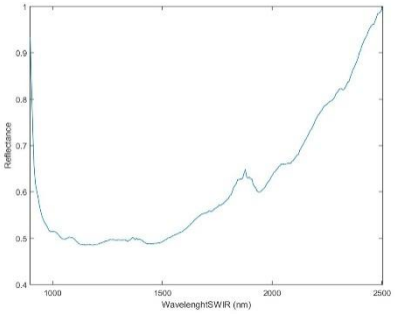

(i)

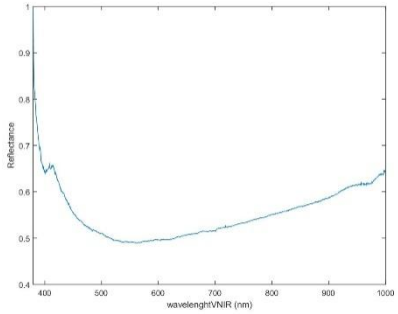

(j)

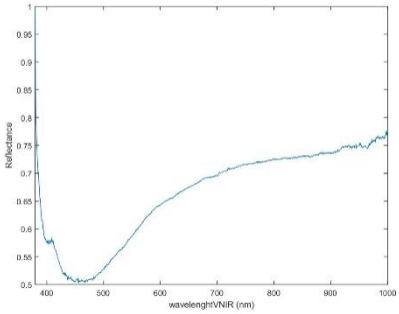

(k)

Figure A16. (a) Obsidian in frontal position. (b) Obsidian in reverse position. (c) Obsidian thickness. (d) Spectral signature calibrated and normalized (Frontal-SWIR-Ref. 99%). (e) Spectral signature calibrated and normalized (Reverse-SWIR-Ref. 99%). (f) Spectral signature calibrated and normalized (Frontal-SWIR-Ref. 10%). (g) Spectral signature calibrated and normalized (Reverse-SWIR-Ref. 10%). (h) Spectral signature calibrated and normalized (Frontal-SWIR-Ref. 50%). (i) Spectral signature calibrated and normalized (Reverse-SWIR-Ref. 50%). (j) Spectral signature calibrated and normalized (Frontal-VNIR-Ref.99%). (k) Spectral signature calibrated and normalized (Reverse-VNIR-Ref.99%).

Table A17. Information about the S17 obsidian.

Original label	Virtual label	Sigla	Group	Weight (g)	Measurement (cm) (Width/Large/Thickness)	Deposit	Municipality	Island
CED-18-114	S17	6	HOG		1/1.7/0.5	El Cedro	Aldea de San Nicolás	Gran Canaria

(a)

(b)

(c)

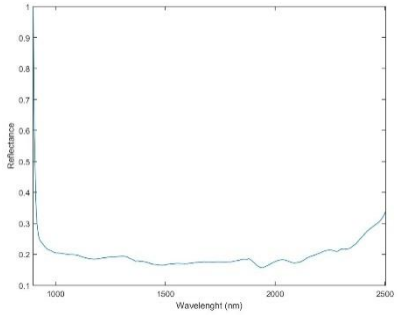

(d)

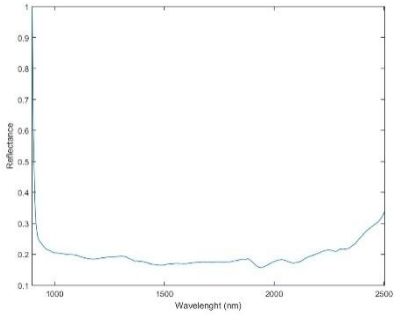

(e)

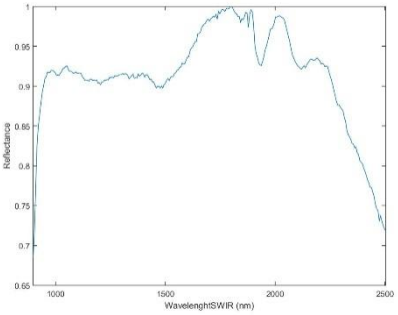

(f)

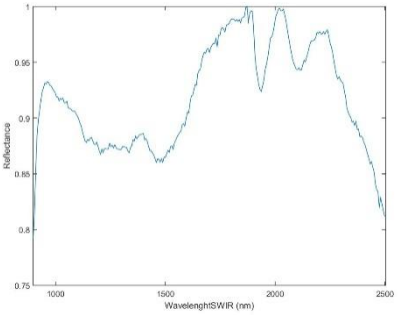

(g)

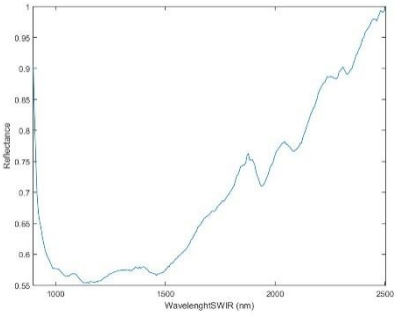

(h)

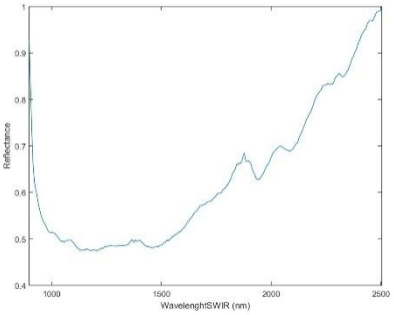

(i)

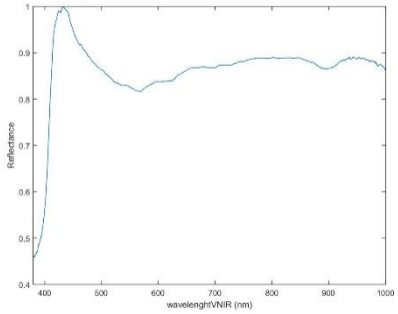

(j)

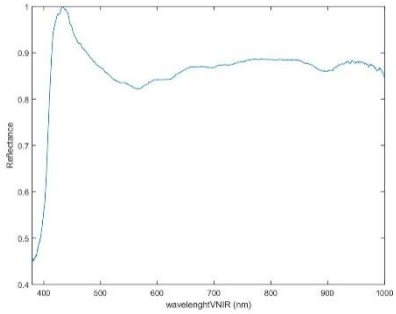

(k)

Figure A17. (a) Obsidian in frontal position. (b) Obsidian in reverse position. (c) Obsidian thickness. (d) Spectral signature calibrated and normalized (Frontal-SWIR-Ref. 99%). (e) Spectral signature calibrated and normalized (Reverse-SWIR-Ref. 99%). (f) Spectral signature calibrated and normalized (Frontal-SWIR-Ref. 10%). (g) Spectral signature calibrated and normalized (Reverse-SWIR-Ref. 10%). (h) Spectral signature calibrated and normalized (Frontal-SWIR-Ref. 50%). (i) Spectral signature calibrated and normalized (Reverse-SWIR-Ref. 50%). (j) Spectral signature calibrated and normalized (Frontal-VNIR-Ref.99%). (k) Spectral signature calibrated and normalized (Reverse-VNIR-Ref.99%).

Table A18. Information about the S18 obsidian.

Original label	Virtual label	Sigla	Group	Weight (g)	Measurement (cm) (Width/Large/Thickness)	Deposit	Municipality	Island
CED-C-115	S18	1	HOG		1.5/2.7/0.75	El Cedro	Aldea de San Nicolás	Gran Canaria

(a)

(b)

(c)

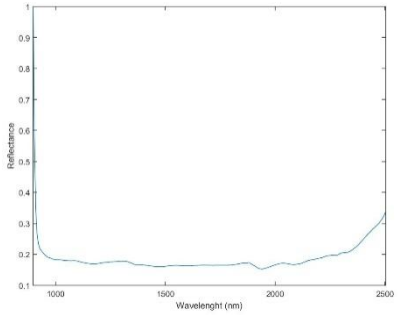

(d)

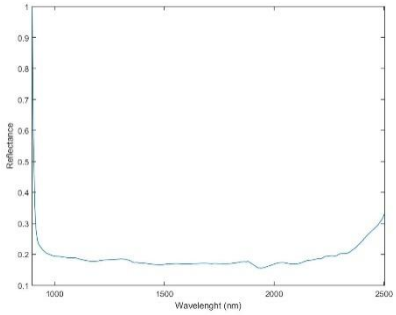

(e)

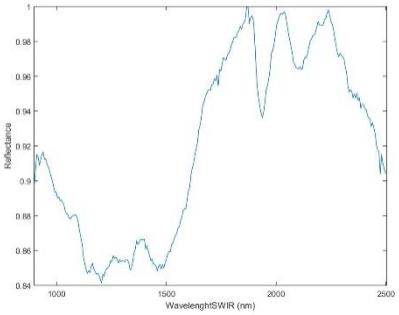

(f)

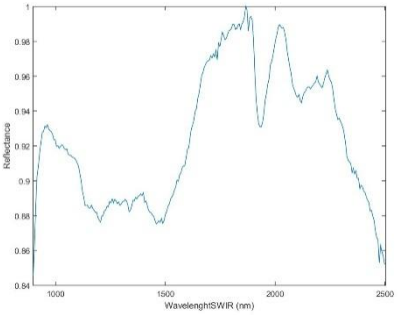

(g)

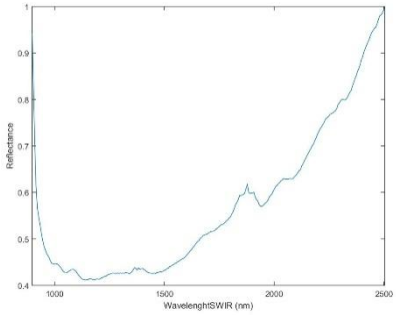

(h)

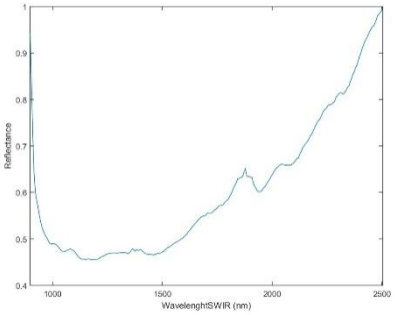

(i)

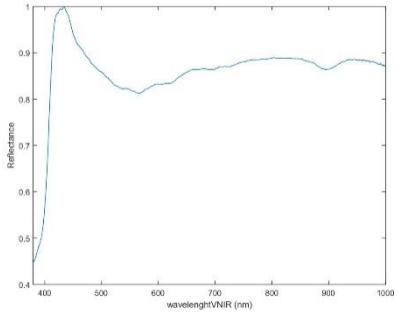

(j)

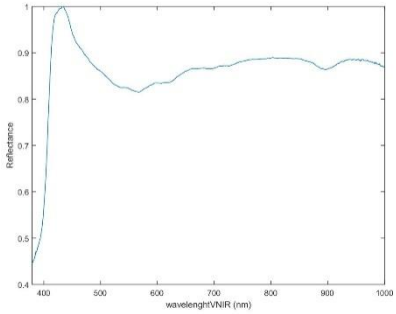

(k)

Figure A18. (a) Obsidian in frontal position. (b) Obsidian in reverse position. (c) Obsidian thickness. (d) Spectral signature calibrated and normalized (Frontal-SWIR-Ref. 99%). (e) Spectral signature calibrated and normalized (Reverse-SWIR-Ref. 99%). (f) Spectral signature calibrated and normalized (Frontal-SWIR-Ref. 10%). (g) Spectral signature calibrated and normalized (Reverse-SWIR-Ref. 10%). (h) Spectral signature calibrated and normalized (Frontal-SWIR-Ref. 50%). (i) Spectral signature calibrated and normalized (Reverse-SWIR-Ref. 50%). (j) Spectral signature calibrated and normalized (Frontal-VNIR-Ref.99%). (k) Spectral signature calibrated and normalized (Reverse-VNIR-Ref.99%).

Table A19. Information about the S19 obsidian.

Original label	Virtual label	Sigla	Group	Weight (g)	Measurement (cm) (Width/Large/Thickness)	Deposit	Municipality	Island
CED-T-113	S19	4	HOG		2/2.9/0.5	El Cedro	Aldea de San Nicolás	Gran Canaria

(a)

(b)

(c)

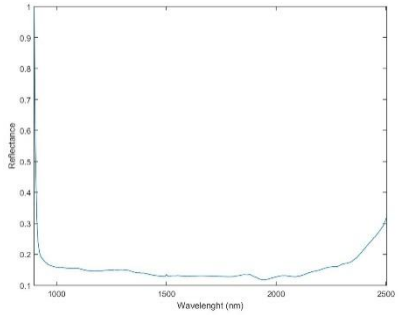

(d)

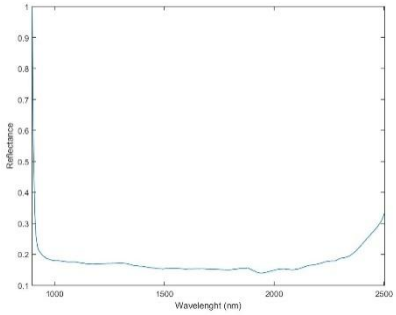

(e)

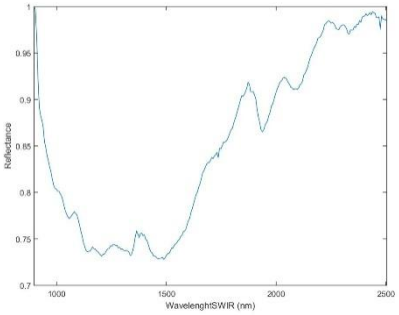

(f)

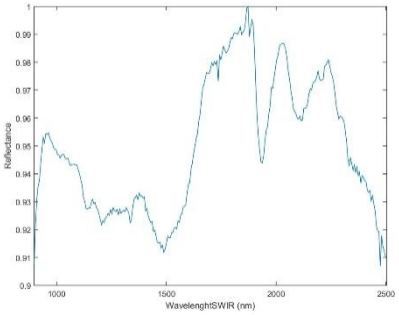

(g)

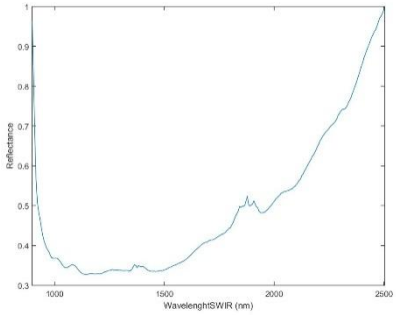

(h)

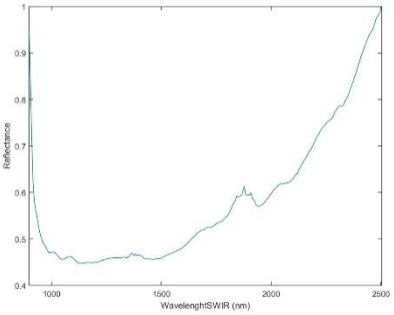

(i)

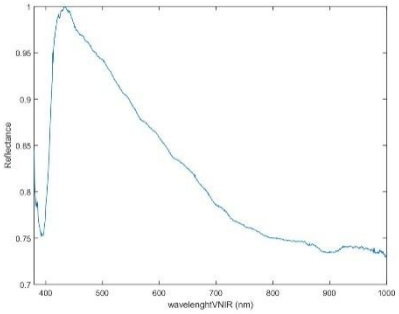

(j)

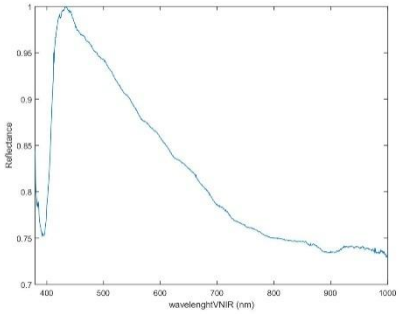

(k)

Figure A19. (a) Obsidian in frontal position. (b) Obsidian in reverse position. (c) Obsidian thickness. (d) Spectral signature calibrated and normalized (Frontal-SWIR-Ref. 99%). (e) Spectral signature calibrated and normalized (Reverse-SWIR-Ref. 99%). (f) Spectral signature calibrated and normalized (Frontal-SWIR-Ref. 10%). (g) Spectral signature calibrated and normalized (Reverse-SWIR-Ref. 10%). (h) Spectral signature calibrated and normalized (Frontal-SWIR-Ref. 50%). (i) Spectral signature calibrated and normalized (Reverse-SWIR-Ref. 50%). (j) Spectral signature calibrated and normalized (Frontal-VNIR-Ref.99%). (k) Spectral signature calibrated and normalized (Reverse-VNIR-Ref.99%).

Table A20. Information about the S20 obsidian.

Original label	Virtual label	Sigla	Group	Weight (g)	Measurement (cm) (Width/Large/Thickness)	Deposit	Municipality	Island
HOG-38-818-65	S20	816-822	HOG		1.65/2.5/0.3	Horgazales	Aldea de San Nicolás	Gran Canaria

(a)

(b)

(c)

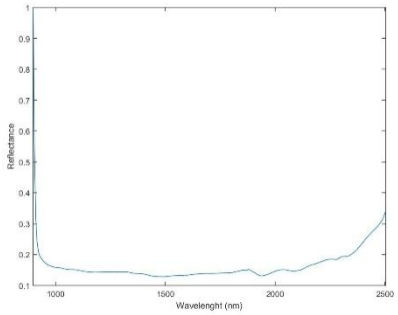

(d)

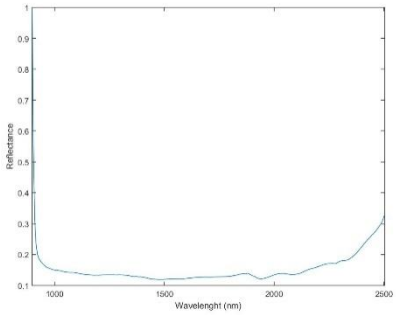

(e)

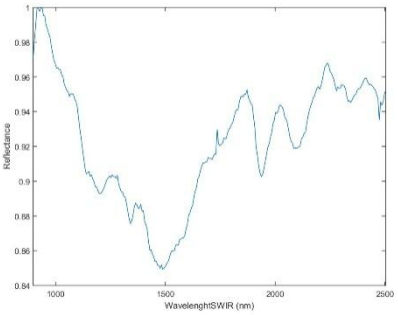

(f)

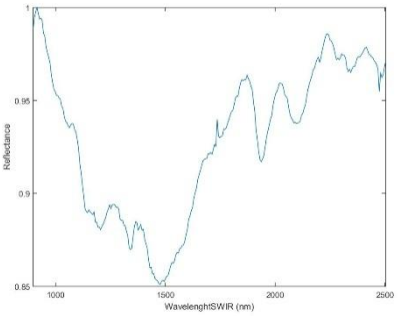

(g)

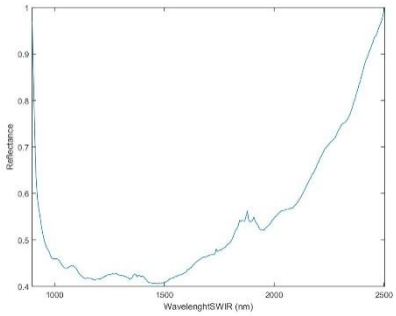

(h)

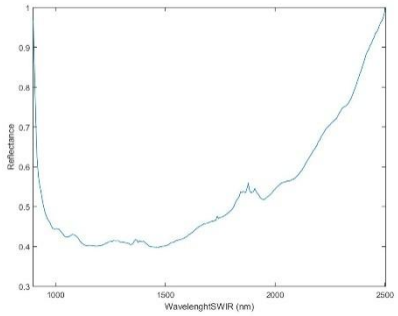

(i)

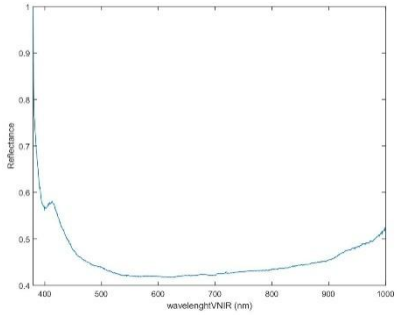

(j)

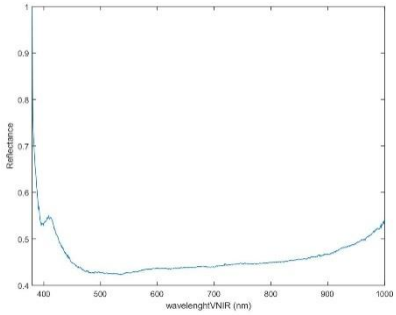

(k)

Figure A20. (a) Obsidian in frontal position. (b) Obsidian in reverse position. (c) Obsidian thickness. (d) Spectral signature calibrated and normalized (Frontal-SWIR-Ref. 99%). (e) Spectral signature calibrated and normalized (Reverse-SWIR-Ref. 99%). (f) Spectral signature calibrated and normalized (Frontal-SWIR-Ref. 10%). (g) Spectral signature calibrated and normalized (Reverse-SWIR-Ref. 10%). (h) Spectral signature calibrated and normalized (Frontal-SWIR-Ref. 50%). (i) Spectral signature calibrated and normalized (Reverse-SWIR-Ref. 50%). (j) Spectral signature calibrated and normalized (Frontal-VNIR-Ref.99%). (k) Spectral signature calibrated and normalized (Reverse-VNIR-Ref.99%).

Table A21. Information about the S21 obsidian.

Original label	Virtual label	Sigla	Group	Weight (g)	Measurement (cm) (Width/Large/Thickness)	Deposit	Municipality	Island
HOG-38-816-65	S21	824-835	HOG		1.7/2.35/1.1	Horgazales	Aldea de San Nicolás	Gran Canaria

(a)

(b)

(c)

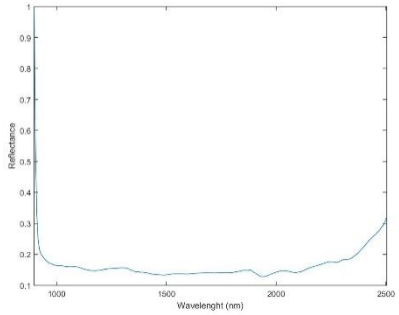

(d)

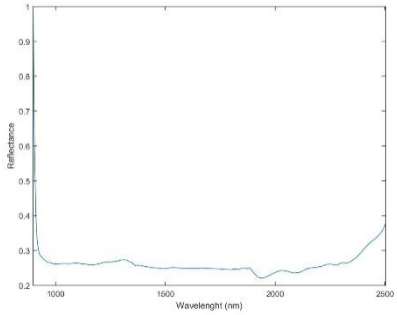

(e)

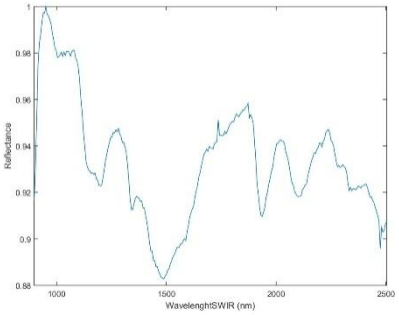

(f)

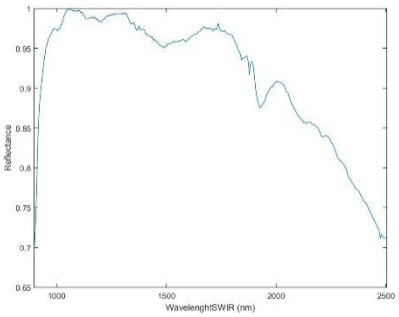

(g)

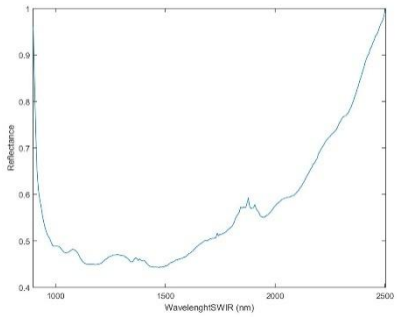

(h)

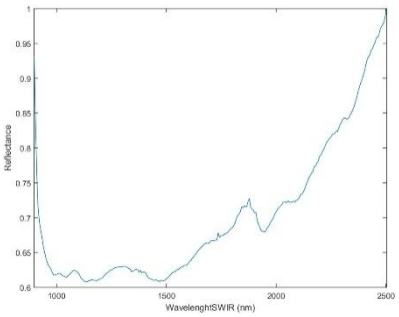

(i)

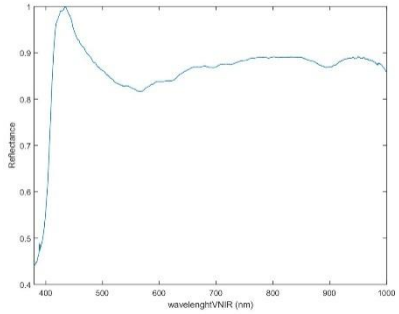

(j)

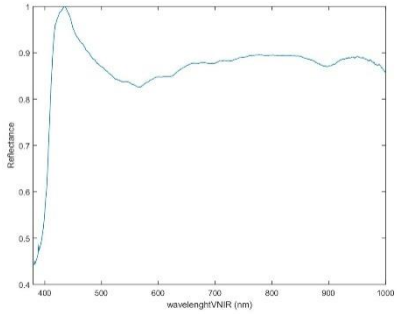

(k)

Figure A21. (a) Obsidian in frontal position. (b) Obsidian in reverse position. (c) Obsidian thickness. (d) Spectral signature calibrated and normalized (Frontal-SWIR-Ref. 99%). (e) Spectral signature calibrated and normalized (Reverse-SWIR-Ref. 99%). (f) Spectral signature calibrated and normalized (Frontal-SWIR-Ref. 10%). (g) Spectral signature calibrated and normalized (Reverse-SWIR-Ref. 10%). (h) Spectral signature calibrated and normalized (Frontal-SWIR-Ref. 50%). (i) Spectral signature calibrated and normalized (Reverse-SWIR-Ref. 50%). (j) Spectral signature calibrated and normalized (Frontal-VNIR-Ref.99%). (k) Spectral signature calibrated and normalized (Reverse-VNIR-Ref.99%).

Table A22. Information about the S22 obsidian.

Original label	Virtual label	Sigla	Group	Weight (g)	Measurement (cm) (Width/Large/Thickness)	Deposit	Municipality	Island
HOG-38-1368-73	S22	1367-1392	HOG		1.3/2.5/0.7	Horgazales	Aldea de San Nicolás	Gran Canaria

(a)

(b)

(c)

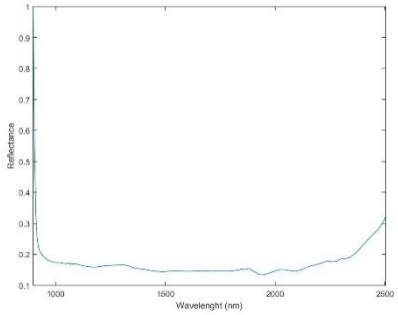

(d)

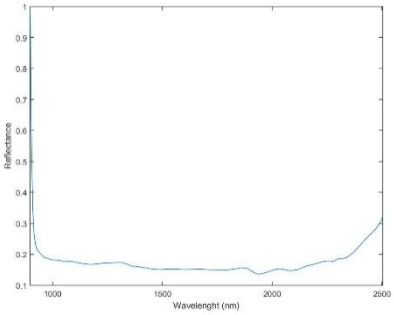

(e)

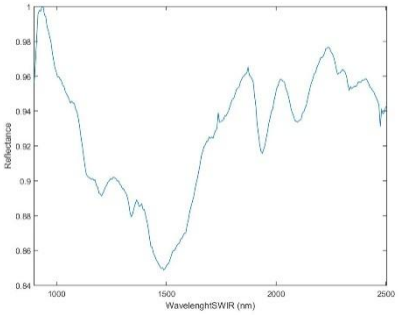

(f)

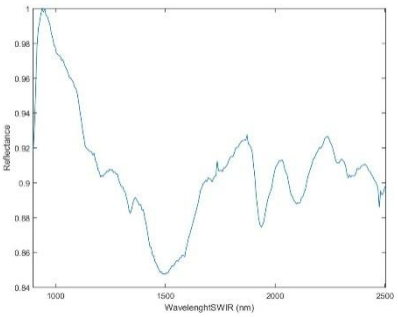

(g)

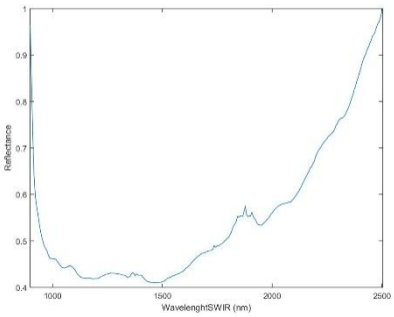

(h)

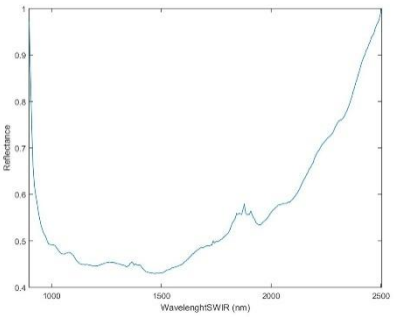

(i)

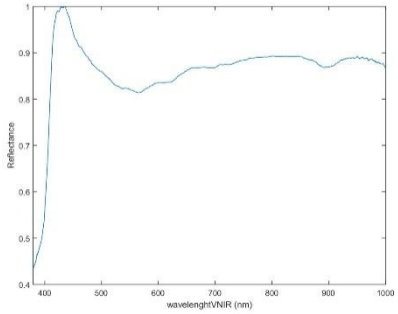

(j)

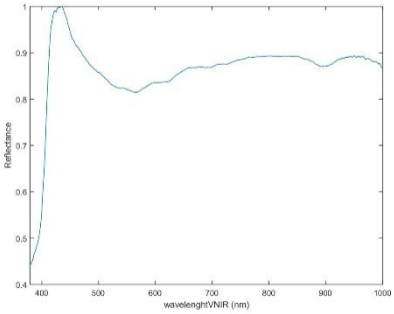

(k)

Figure A22. (a) Obsidian in frontal position. (b) Obsidian in reverse position. (c) Obsidian thickness. (d) Spectral signature calibrated and normalized (Frontal-SWIR-Ref. 99%). (e) Spectral signature calibrated and normalized (Reverse-SWIR-Ref. 99%). (f) Spectral signature calibrated and normalized (Frontal-SWIR-Ref. 10%). (g) Spectral signature calibrated and normalized (Reverse-SWIR-Ref. 10%). (h) Spectral signature calibrated and normalized (Frontal-SWIR-Ref. 50%). (i) Spectral signature calibrated and normalized (Reverse-SWIR-Ref. 50%). (j) Spectral signature calibrated and normalized (Frontal-VNIR-Ref.99%). (k) Spectral signature calibrated and normalized (Reverse-VNIR-Ref.99%).

Table A23. Information about the S23 obsidian.

Original label	Virtual label	Sigla	Group	Weight (g)	Measurement (cm) (Width/Large/Thickness)	Deposit	Municipality	Island
HOG-38-1575-69	S23	1567-1591	-		1.7/1.9/0.5	Horgazales	Aldea de San Nicolás	Gran Canaria

(a)

(b)

(c)

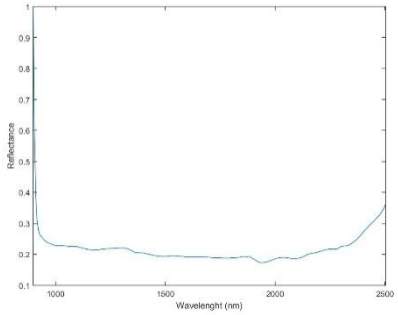

(d)

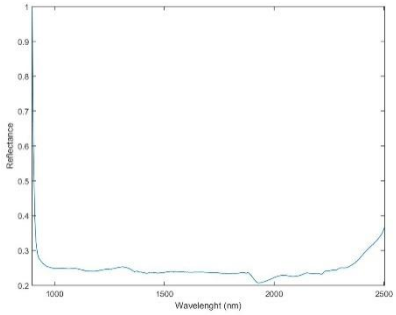

(e)

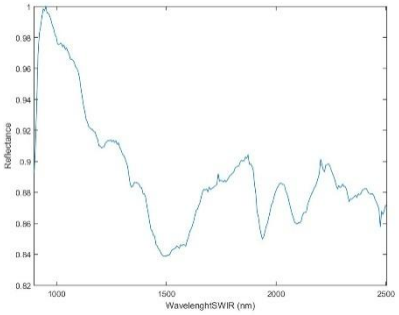

(f)

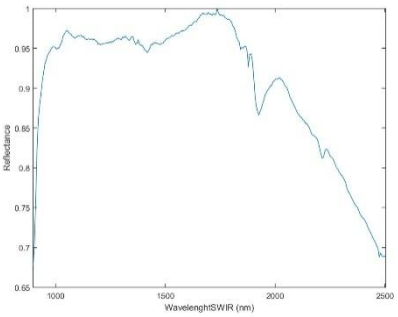

(g)

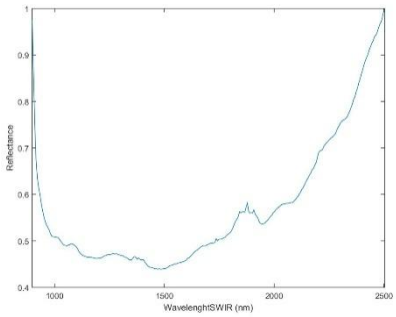

(h)

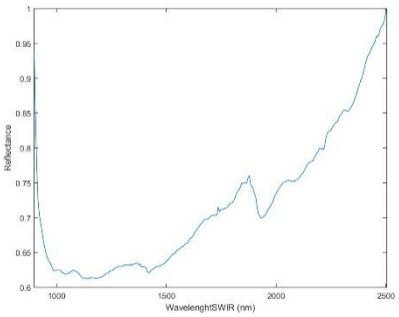

(i)

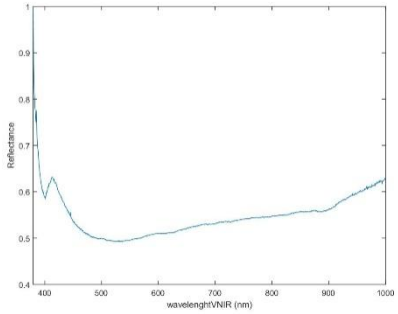

(j)

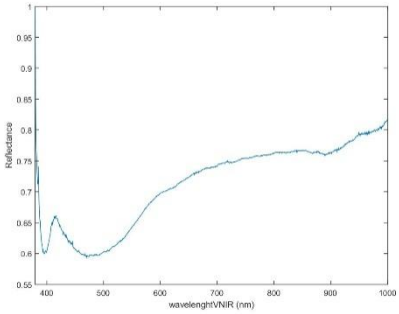

(k)

Figure A23. (a) Obsidian in frontal position. (b) Obsidian in reverse position. (c) Obsidian thickness. (d) Spectral signature calibrated and normalized (Frontal-SWIR-Ref. 99%). (e) Spectral signature calibrated and normalized (Reverse-SWIR-Ref. 99%). (f) Spectral signature calibrated and normalized (Frontal-SWIR-Ref. 10%). (g) Spectral signature calibrated and normalized (Reverse-SWIR-Ref. 10%). (h) Spectral signature calibrated and normalized (Frontal-SWIR-Ref. 50%). (i) Spectral signature calibrated and normalized (Reverse-SWIR-Ref. 50%). (j) Spectral signature calibrated and normalized (Frontal-VNIR-Ref.99%). (k) Spectral signature calibrated and normalized (Reverse-VNIR-Ref.99%).

Table A24. Information about the S24 obsidian.

Original label	Virtual label	Sigla	Group	Weight (g)	Measurement (cm) (Width/Large/Thickness)	Deposit	Municipality	Island
ANT-157	S24	204	OTHERS		1.3/1.5/0.5	San Antón	Firgas	Gran Canaria

(a)

(b)

(c)

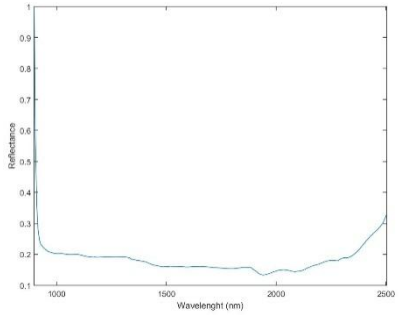

(d)

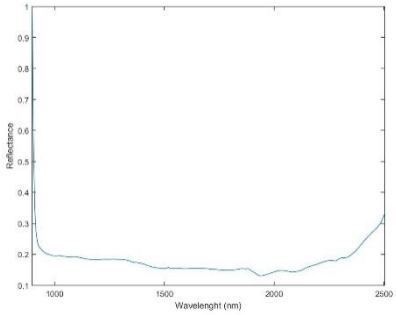

(e)

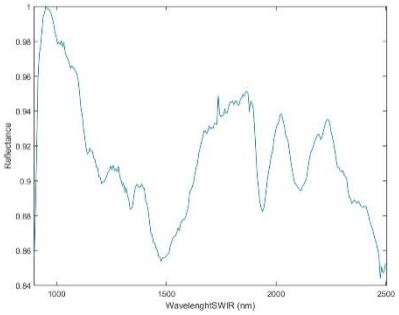

(f)

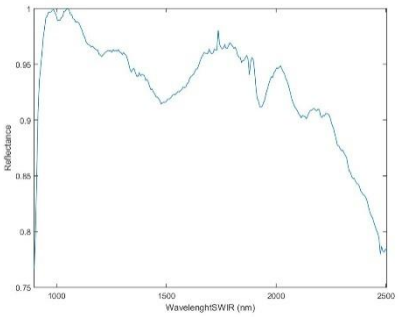

(g)

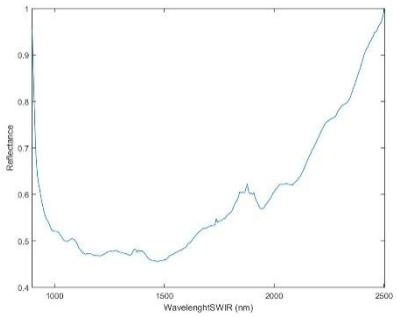

(h)

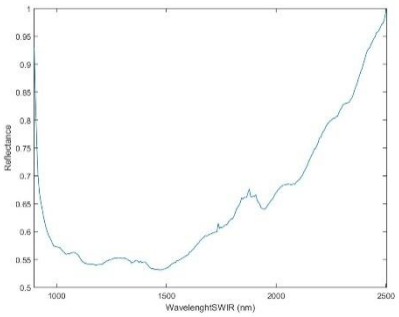

(i)

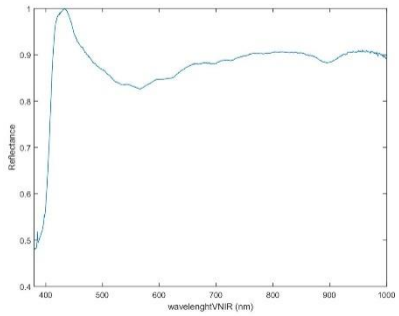

(j)

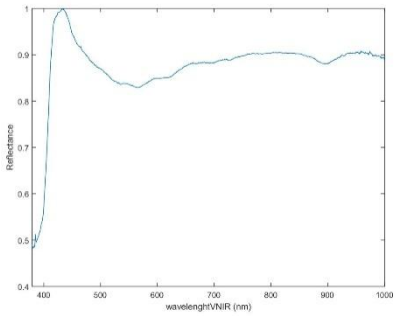

(k)

Figure A24. (a) Obsidian in frontal position. (b) Obsidian in reverse position. (c) Obsidian thickness. (d) Spectral signature calibrated and normalized (Frontal-SWIR-Ref. 99%). (e) Spectral signature calibrated and normalized (Reverse-SWIR-Ref. 99%). (f) Spectral signature calibrated and normalized (Frontal-SWIR-Ref. 10%). (g) Spectral signature calibrated and normalized (Reverse-SWIR-Ref. 10%). (h) Spectral signature calibrated and normalized (Frontal-SWIR-Ref. 50%). (i) Spectral signature calibrated and normalized (Reverse-SWIR-Ref. 50%). (j) Spectral signature calibrated and normalized (Frontal-VNIR-Ref.99%). (k) Spectral signature calibrated and normalized (Reverse-VNIR-Ref.99%).

Table A25. Information about the S25 obsidian.

Original label	Virtual label	Sigla	Group	Weight (g)	Measurement (cm) (Width/Large/Thickness)	Deposit	Municipality	Island
ANT-158	S25	207	HOG		1.35/1.8/0.15	San Antón	Firgas	Gran Canaria

(a)

(b)

(c)

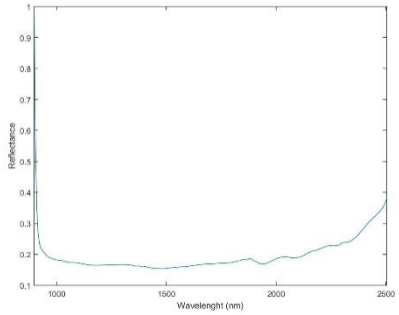

(d)

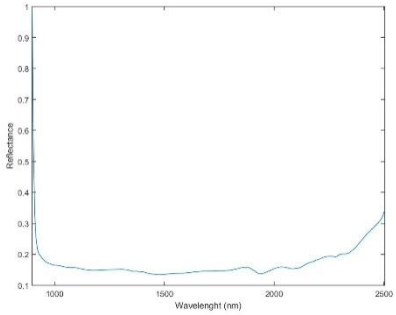

(e)

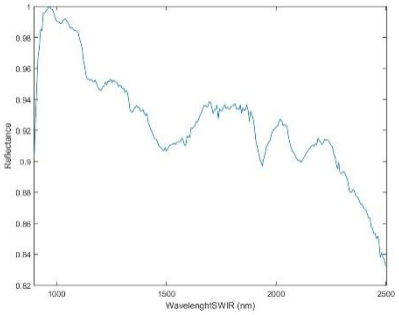

(f)

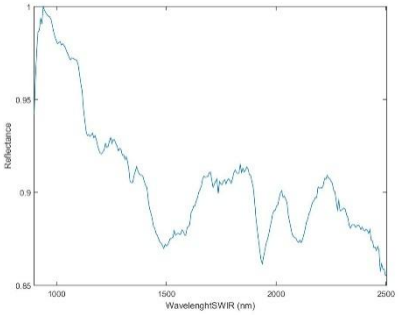

(g)

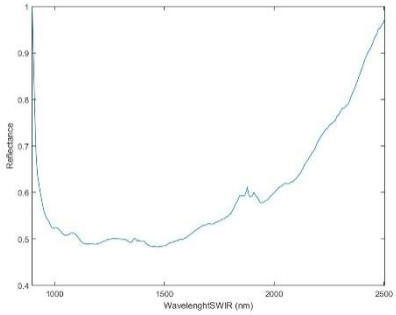

(h)

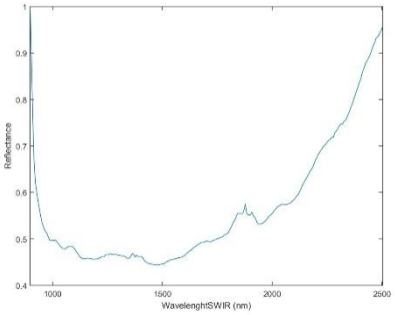

(i)

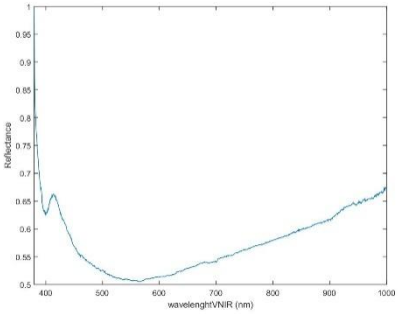

(j)

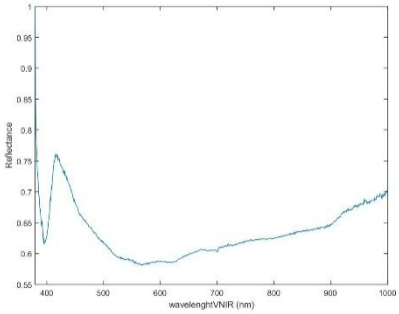

(k)

Figure A25. (a) Obsidian in frontal position. (b) Obsidian in reverse position. (c) Obsidian thickness. (d) Spectral signature calibrated and normalized (Frontal-SWIR-Ref. 99%). (e) Spectral signature calibrated and normalized (Reverse-SWIR-Ref. 99%). (f) Spectral signature calibrated and normalized (Frontal-SWIR-Ref. 10%). (g) Spectral signature calibrated and normalized (Reverse-SWIR-Ref. 10%). (h) Spectral signature calibrated and normalized (Frontal-SWIR-Ref. 50%). (i) Spectral signature calibrated and normalized (Reverse-SWIR-Ref. 50%). (j) Spectral signature calibrated and normalized (Frontal-VNIR-Ref.99%). (k) Spectral signature calibrated and normalized (Reverse-VNIR-Ref.99%).

Table A26. Information about the S26 obsidian.

Original label	Virtual label	Sigla	Group	Weight (g)	Measurement (cm) (Width/Large/Thickness)	Deposit	Municipality	Island
ANT-156	S26	187	-		0.9/2.15/0.5	San Antón	Firgas	Gran Canaria

(a)

(b)

(c)

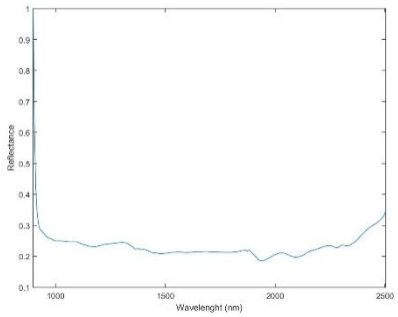

(d)

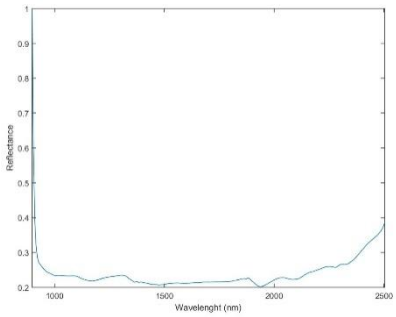

(e)

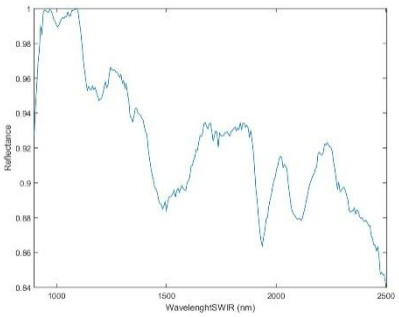

(f)

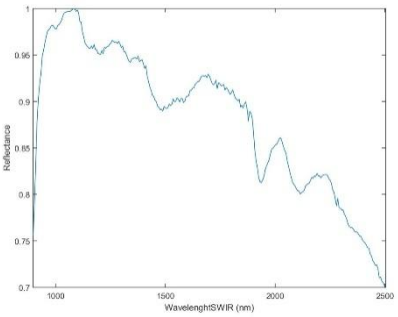

(g)

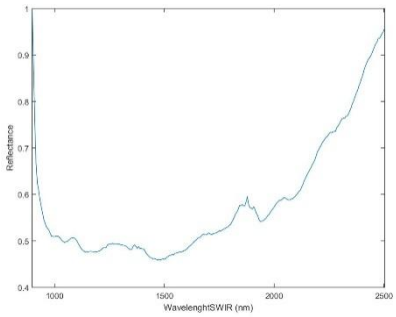

(h)

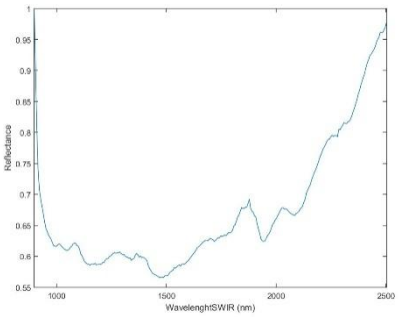

(i)

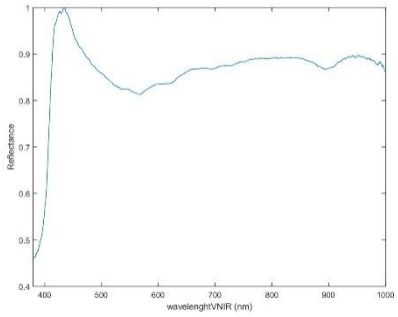

(j)

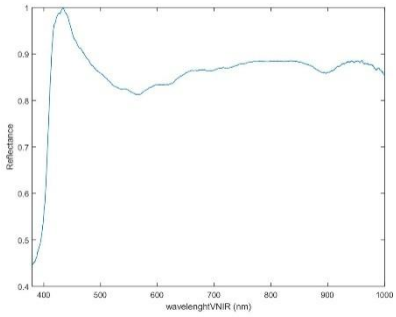

(k)

Figure A26. (a) Obsidian in frontal position. (b) Obsidian in reverse position. (c) Obsidian thickness. (d) Spectral signature calibrated and normalized (Frontal-SWIR-Ref. 99%). (e) Spectral signature calibrated and normalized (Reverse-SWIR-Ref. 99%). (f) Spectral signature calibrated and normalized (Frontal-SWIR-Ref. 10%). (g) Spectral signature calibrated and normalized (Reverse-SWIR-Ref. 10%). (h) Spectral signature calibrated and normalized (Frontal-SWIR-Ref. 50%). (i) Spectral signature calibrated and normalized (Reverse-SWIR-Ref. 50%). (j) Spectral signature calibrated and normalized (Frontal-VNIR-Ref.99%). (k) Spectral signature calibrated and normalized (Reverse-VNIR-Ref.99%).

Table A27. Information about the S27 obsidian.

Original label	Virtual label	Sigla	Group	Weight (g)	Measurement (cm) (Width/Large/Thickness)	Deposit	Municipality	Island
VAC-2-120-B	S27	-	HOG		2.6/3/0.8	Las vacas	Agüimes	Gran Canaria

(a)

(b)

(c)

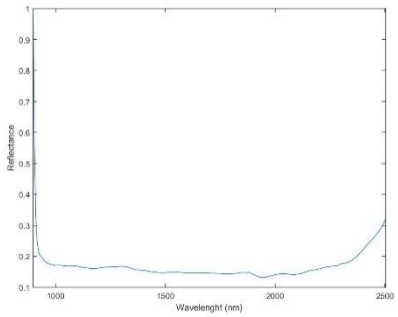

(d)

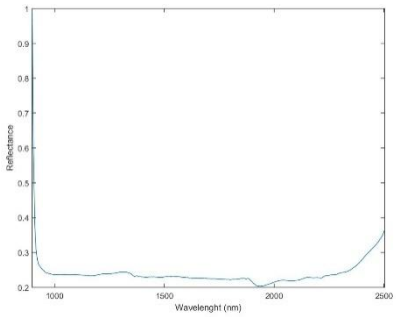

(e)

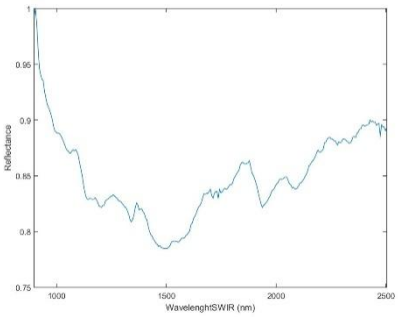

(f)

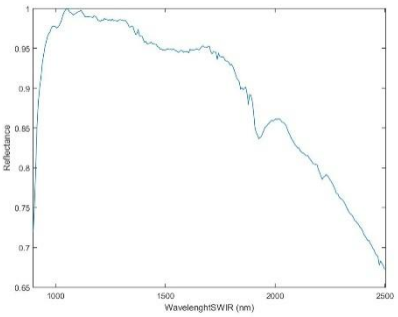

(g)

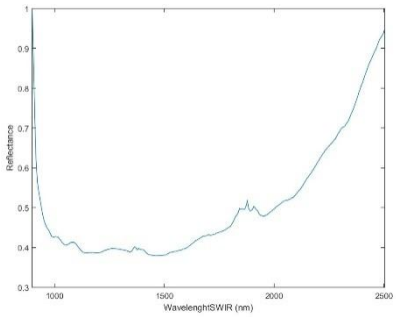

(h)

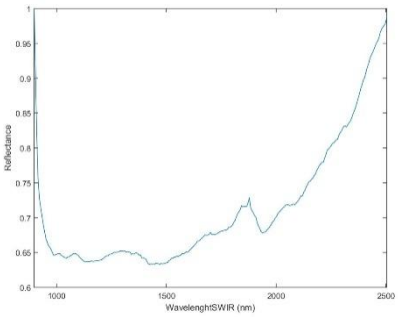

(i)

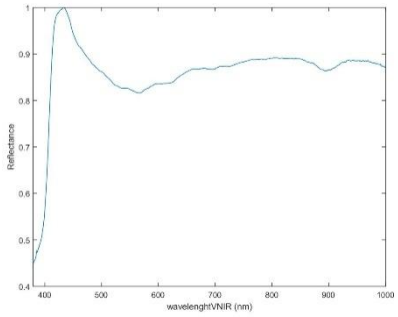

(j)

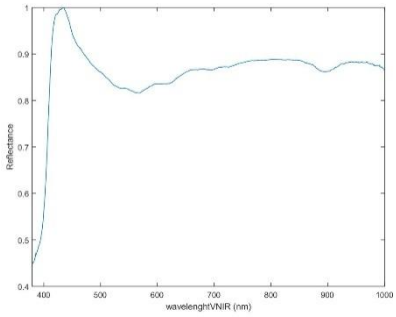

(k)

Figure A27. (a) Obsidian in frontal position. (b) Obsidian in reverse position. (c) Obsidian thickness. (d) Spectral signature calibrated and normalized (Frontal-SWIR-Ref. 99%). (e) Spectral signature calibrated and normalized (Reverse-SWIR-Ref. 99%). (f) Spectral signature calibrated and normalized (Frontal-SWIR-Ref. 10%). (g) Spectral signature calibrated and normalized (Reverse-SWIR-Ref. 10%). (h) Spectral signature calibrated and normalized (Frontal-SWIR-Ref. 50%). (i) Spectral signature calibrated and normalized (Reverse-SWIR-Ref. 50%). (j) Spectral signature calibrated and normalized (Frontal-VNIR-Ref.99%). (k) Spectral signature calibrated and normalized (Reverse-VNIR-Ref.99%).

Table A28. Information about the S28 obsidian.

Original label	Virtual label	Sigla	Group	Weight (g)	Measurement (cm) (Width/Large/Thickness)	Deposit	Municipality	Island
VAC-2-120-C	S28	-	HOG		1.35/2.2/0.6	Las vacas	Agüimes	Gran Canaria

(a)

(b)

(c)

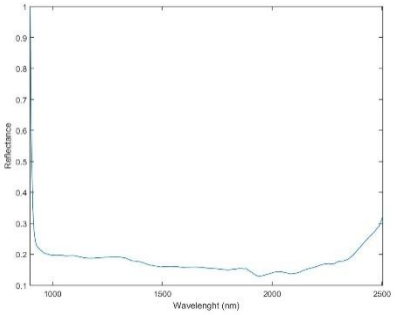

(d)

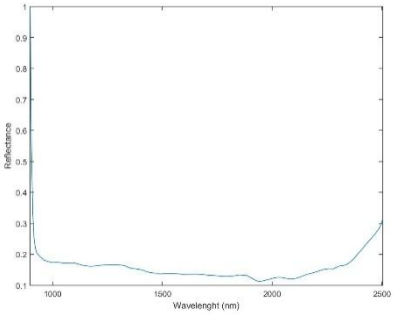

(e)

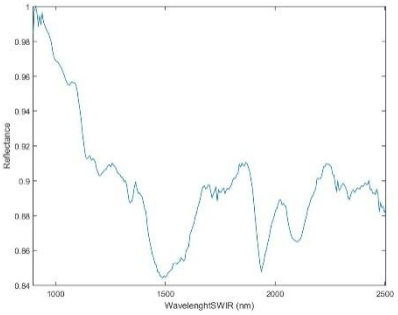

(f)

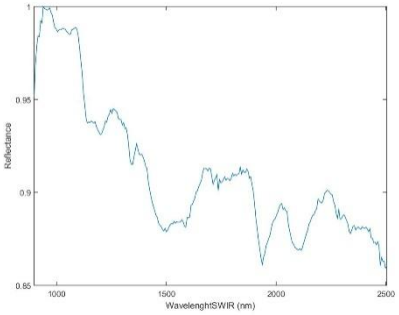

(g)

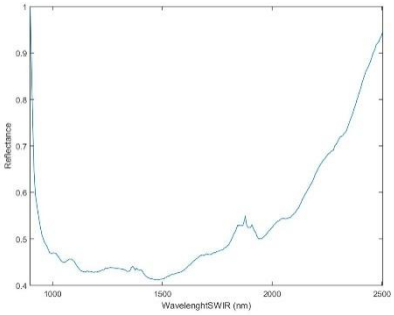

(h)

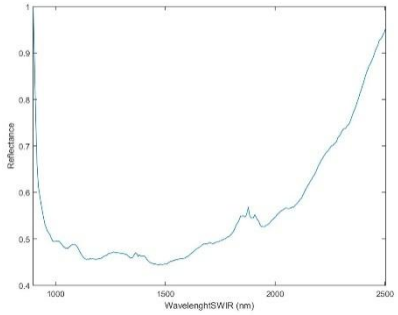

(i)

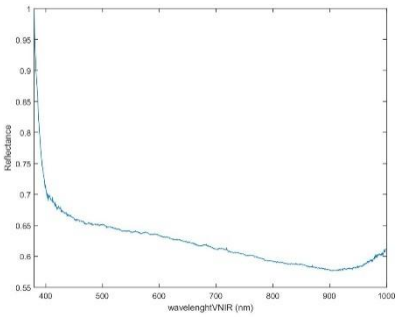

(j)

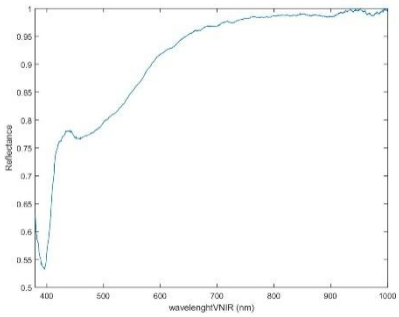

(k)

Figure A28. (a) Obsidian in frontal position. (b) Obsidian in reverse position. (c) Obsidian thickness. (d) Spectral signature calibrated and normalized (Frontal-SWIR-Ref. 99%). (e) Spectral signature calibrated and normalized (Reverse-SWIR-Ref. 99%). (f) Spectral signature calibrated and normalized (Frontal-SWIR-Ref. 10%). (g) Spectral signature calibrated and normalized (Reverse-SWIR-Ref. 10%). (h) Spectral signature calibrated and normalized (Frontal-SWIR-Ref. 50%). (i) Spectral signature calibrated and normalized (Reverse-SWIR-Ref. 50%). (j) Spectral signature calibrated and normalized (Frontal-VNIR-Ref.99%). (k) Spectral signature calibrated and normalized (Reverse-VNIR-Ref.99%).

Table A29. Information about the S29 obsidian.

Original label	Virtual label	Sigla	Group	Weight (g)	Measurement (cm) (Width/Large/Thickness)	Deposit	Municipality	Island
VAC-2-120-A	S29	-	HOG		2.2/3.4/1.1	Las vacas	Agüimes	Gran Canaria

(a)

(b)

(c)

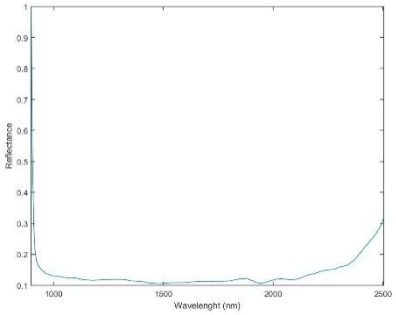

(d)

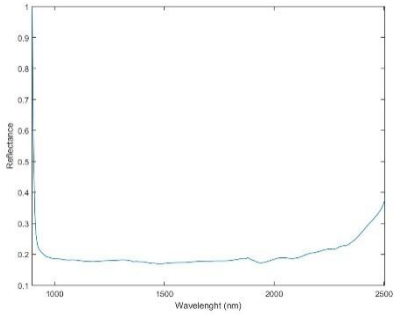

(e)

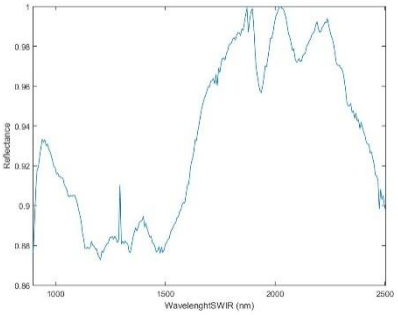

(f)

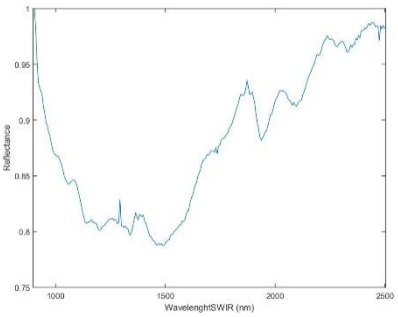

(g)

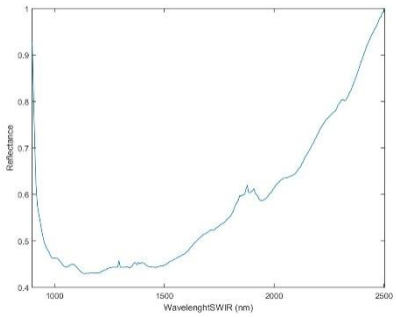

(h)

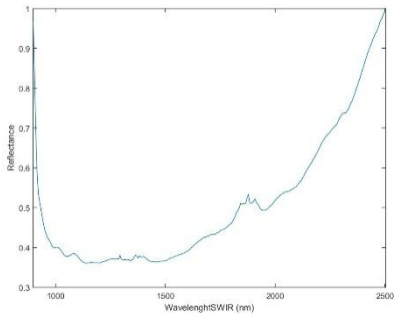

(i)

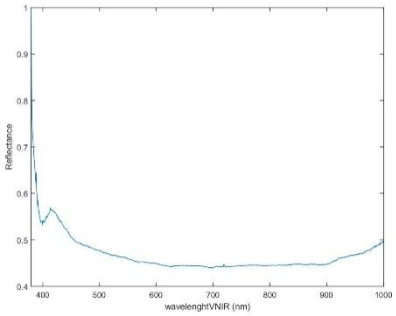

(j)

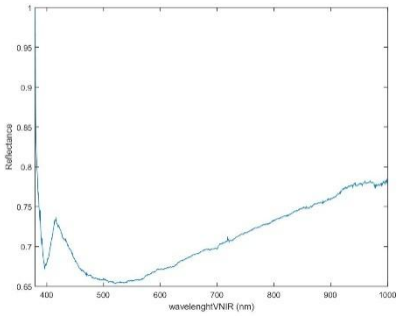

(k)

Figure A29. (a) Obsidian in frontal position. (b) Obsidian in reverse position. (c) Obsidian thickness. (d) Spectral signature calibrated and normalized (Frontal-SWIR-Ref. 99%). (e) Spectral signature calibrated and normalized (Reverse-SWIR-Ref. 99%). (f) Spectral signature calibrated and normalized (Frontal-SWIR-Ref. 10%). (g) Spectral signature calibrated and normalized (Reverse-SWIR-Ref. 10%). (h) Spectral signature calibrated and normalized (Frontal-SWIR-Ref. 50%). (i) Spectral signature calibrated and normalized (Reverse-SWIR-Ref. 50%). (j) Spectral signature calibrated and normalized (Frontal-VNIR-Ref.99%). (k) Spectral signature calibrated and normalized (Reverse-VNIR-Ref.99%).

Table A30. Information about the S30 obsidian.

Original label	Virtual label	Sigla	Group	Weight (g)	Measurement (cm) (Width/Large/Thickness)	Deposit	Municipality	Island
VAC-1-119	S30	-	HOG		4.5/4.8/2.25	Las vacas	Agüimes	Gran Canaria

(a)

(b)

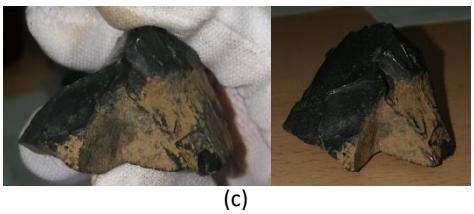

(c)

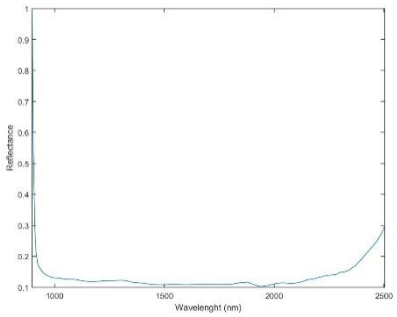

(d)

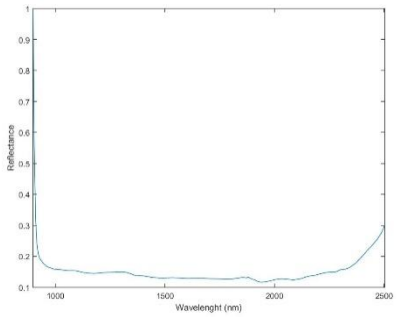

(e)

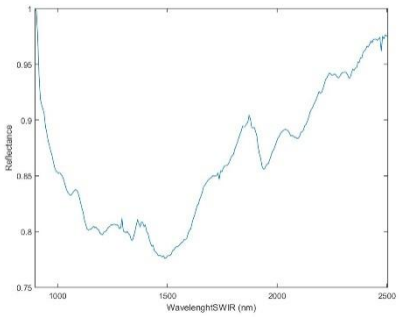

(f)

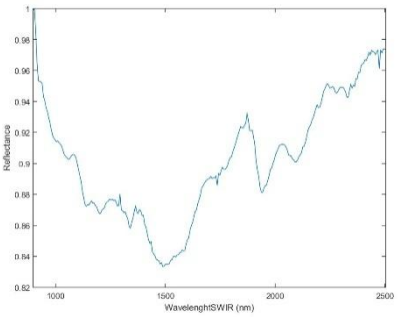

(g)

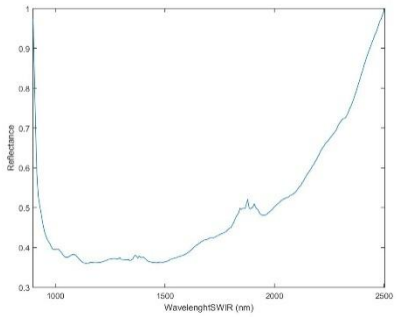

(h)

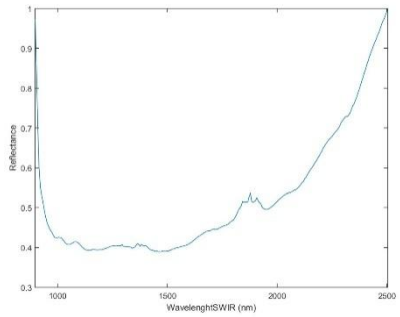

(i)

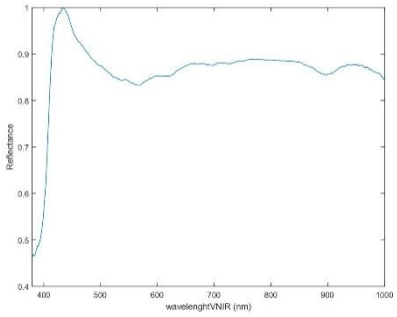

(j)

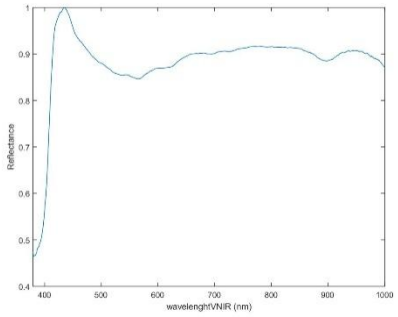

(k)

Figure A30. (a) Obsidian in frontal position. (b) Obsidian in reverse position. (c) Obsidian thickness. (d) Spectral signature calibrated and normalized (Frontal-SWIR-Ref. 99%). (e) Spectral signature calibrated and normalized (Reverse-SWIR-Ref. 99%). (f) Spectral signature calibrated and normalized (Frontal-SWIR-Ref. 10%). (g) Spectral signature calibrated and normalized (Reverse-SWIR-Ref. 10%). (h) Spectral signature calibrated and normalized (Frontal-SWIR-Ref. 50%). (i) Spectral signature calibrated and normalized (Reverse-SWIR-Ref. 50%). (j) Spectral signature calibrated and normalized (Frontal-VNIR-Ref.99%). (k) Spectral signature calibrated and normalized (Reverse-VNIR-Ref.99%).

Table A31. Information about the S31 obsidian.

Original label	Virtual label	Sigla	Group	Weight (g)	Measurement (cm) (Width/Large/Thickness)	Deposit	Municipality	Island
CNB-151	S31	839-1	HOG		0.8/1.1/0.4	El Cenobio de Valerón	Santa María de Guía	Gran Canaria

(a)

(b)

(c)

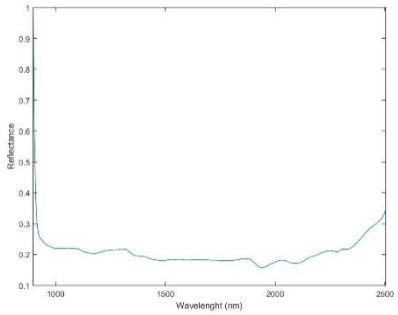

(d)

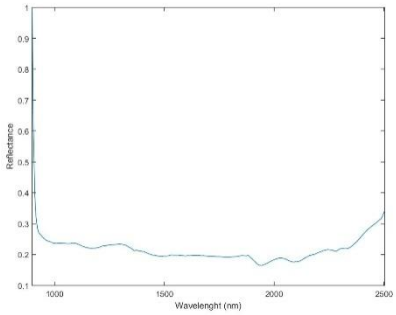

(e)

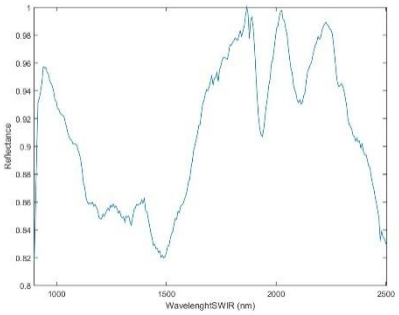

(f)

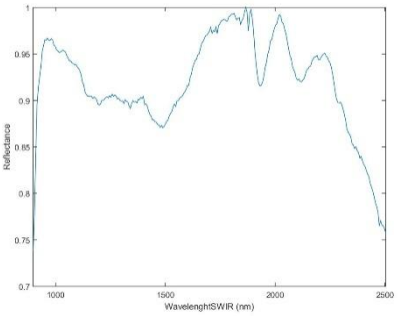

(g)

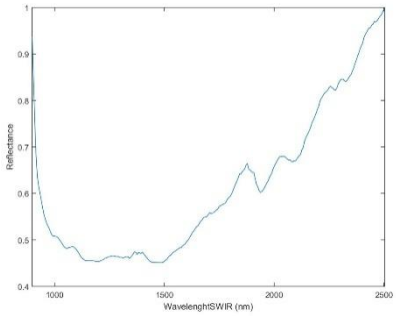

(h)

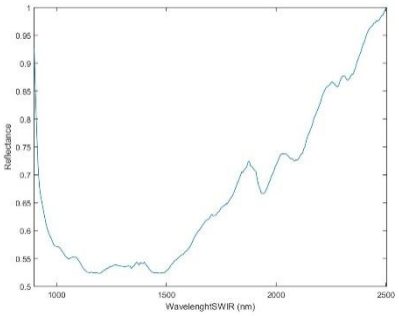

(i)

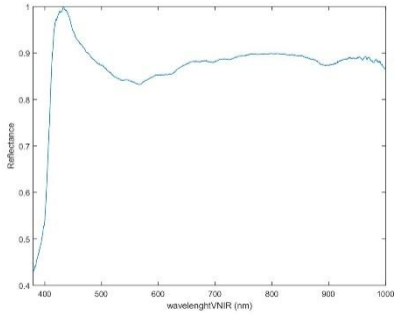

(j)

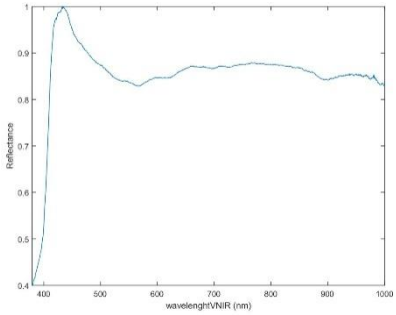

(k)

Figure A31. (a) Obsidian in frontal position. (b) Obsidian in reverse position. (c) Obsidian thickness. (d) Spectral signature calibrated and normalized (Frontal-SWIR-Ref. 99%). (e) Spectral signature calibrated and normalized (Reverse-SWIR-Ref. 99%). (f) Spectral signature calibrated and normalized (Frontal-SWIR-Ref. 10%). (g) Spectral signature calibrated and normalized (Reverse-SWIR-Ref. 10%). (h) Spectral signature calibrated and normalized (Frontal-SWIR-Ref. 50%). (i) Spectral signature calibrated and normalized (Reverse-SWIR-Ref. 50%). (j) Spectral signature calibrated and normalized (Frontal-VNIR-Ref.99%). (k) Spectral signature calibrated and normalized (Reverse-VNIR-Ref.99%).

Table A32.Information about the S32 obsidian.

Original label	Virtual label	Sigla	Group	Weight (g)	Measurement (cm) (Width/Large/Thickness)	Deposit	Municipality	Island
CNB-153	S32	844-2	HOG		1/1.35/0.35	El Cenobio de Valerón	Santa María de Guía	Gran Canaria

(a)

(b)

(c)

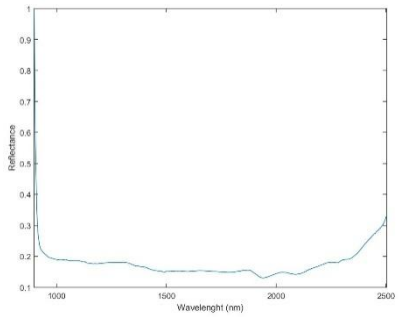

(d)

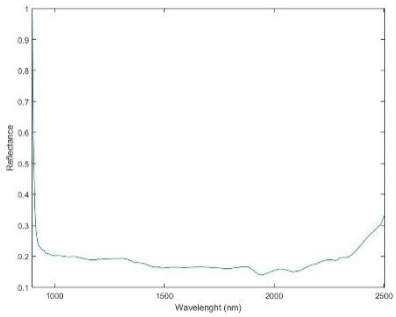

(e)

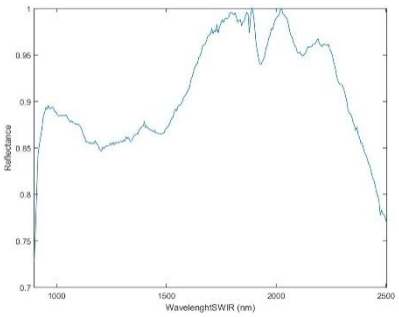

(f)

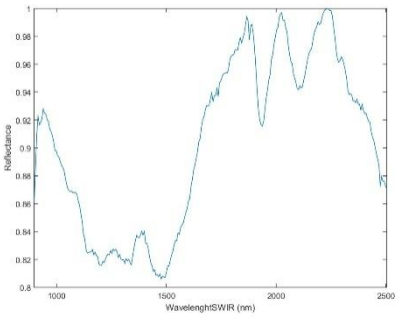

(g)

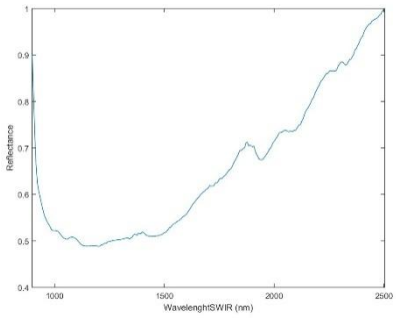

(h)

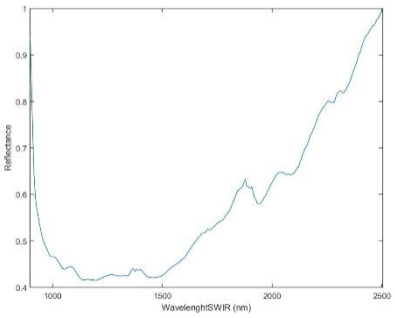

(i)

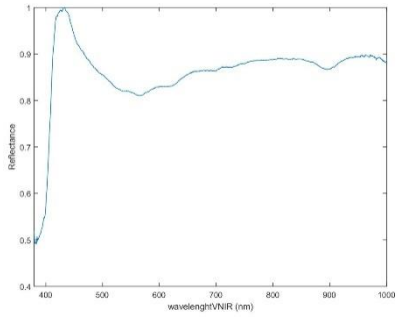

(j)

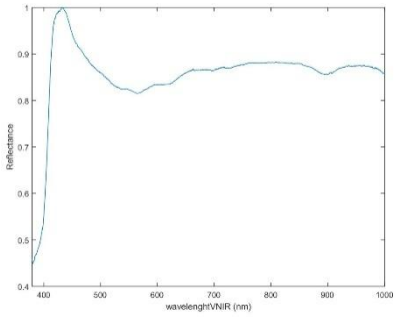

(k)

Figure A32. (a) Obsidian in frontal position. (b) Obsidian in reverse position. (c) Obsidian thickness. (d) Spectral signature calibrated and normalized (Frontal-SWIR-Ref. 99%). (e) Spectral signature calibrated and normalized (Reverse-SWIR-Ref. 99%). (f) Spectral signature calibrated and normalized (Frontal-SWIR-Ref. 10%). (g) Spectral signature calibrated and normalized (Reverse-SWIR-Ref. 10%). (h) Spectral signature calibrated and normalized (Frontal-SWIR-Ref. 50%). (i) Spectral signature calibrated and normalized (Reverse-SWIR-Ref. 50%). (j) Spectral signature calibrated and normalized (Frontal-VNIR-Ref.99%). (k) Spectral signature calibrated and normalized (Reverse-VNIR-Ref.99%).

Table A33. Information about the S33 obsidian.

Original label	Virtual label	Sigla	Group	Weight (g)	Measurement (cm) (Width/Large/Thickness)	Deposit	Municipality	Island
CNB-149-B	S33	820-2	N3		0.8/1.45/0.3	El Cenobio de Valerón	Santa María de Guía	Gran Canaria

(a)

(b)

(c)

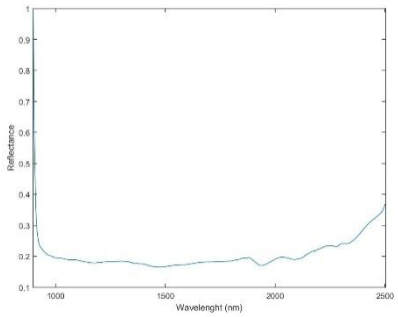

(d)

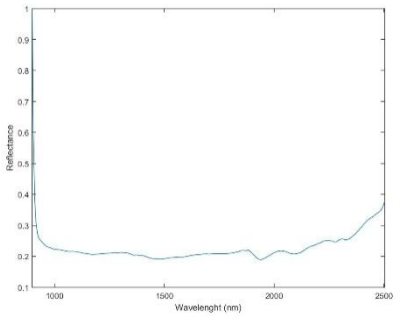

(e)

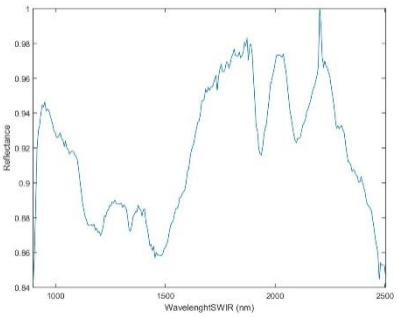

(f)

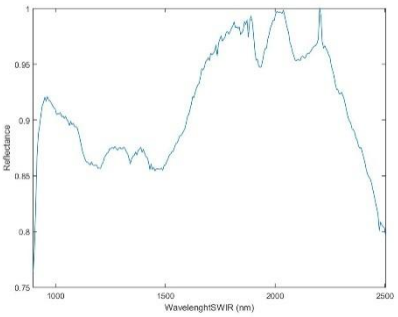

(g)

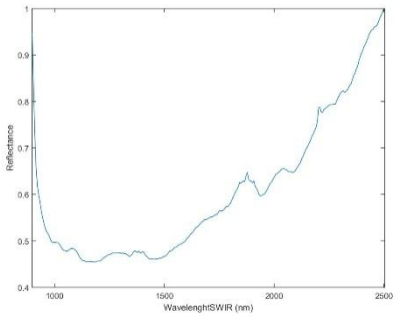

(h)

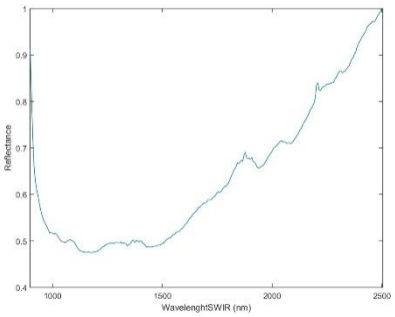

(i)

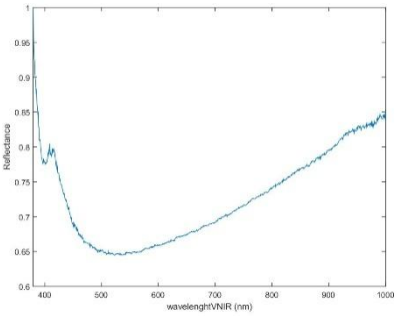

(j)

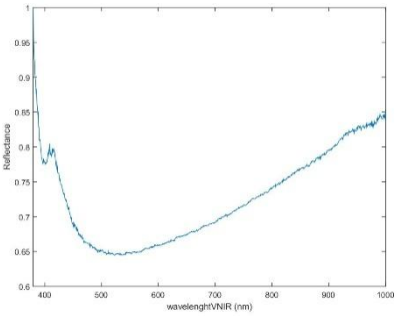

(k)

Figure A33. (a) Obsidian in frontal position. (b) Obsidian in reverse position. (c) Obsidian thickness. (d) Spectral signature calibrated and normalized (Frontal-SWIR-Ref. 99%). (e) Spectral signature calibrated and normalized (Reverse-SWIR-Ref. 99%). (f) Spectral signature calibrated and normalized (Frontal-SWIR-Ref. 10%). (g) Spectral signature calibrated and normalized (Reverse-SWIR-Ref. 10%). (h) Spectral signature calibrated and normalized (Frontal-SWIR-Ref. 50%). (i) Spectral signature calibrated and normalized (Reverse-SWIR-Ref. 50%). (j) Spectral signature calibrated and normalized (Frontal-VNIR-Ref.99%). (k) Spectral signature calibrated and normalized (Reverse-VNIR-Ref.99%).

Table A34. Information about the S34 obsidian.

Original label	Virtual label	Sigla	Group	Weight (g)	Measurement (cm) (Width/Large/Thickness)	Deposit	Municipality	Island
CNB-149-A	S34	820-3	HOG		0.9/1.4/0.4	El Cenobio de Valerón	Santa María de Guía	Gran Canaria

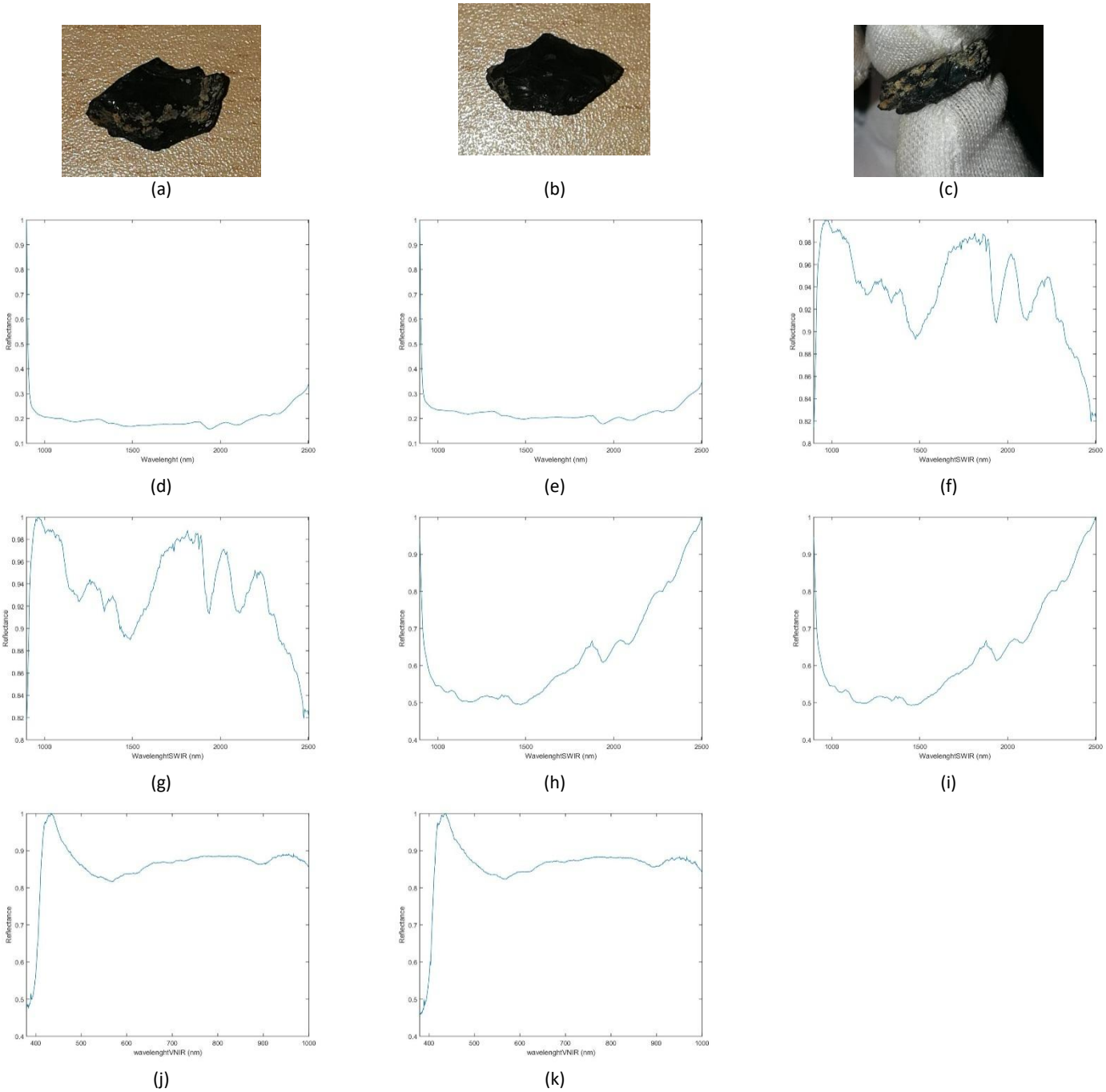

Figure A34. (a) Obsidian in frontal position. (b) Obsidian in reverse position. (c) Obsidian thickness. (d) Spectral signature calibrated and normalized (Frontal-SWIR-Ref. 99%). (e) Spectral signature calibrated and normalized (Reverse-SWIR-Ref. 99%). (f) Spectral signature calibrated and normalized (Frontal-SWIR-Ref. 10%). (g) Spectral signature calibrated and normalized (Reverse-SWIR-Ref. 10%). (h) Spectral signature calibrated and normalized (Frontal-SWIR-Ref. 50%). (i) Spectral signature calibrated and normalized (Reverse-SWIR-Ref. 50%). (j) Spectral signature calibrated and normalized (Frontal-VNIR-Ref.99%). (k) Spectral signature calibrated and normalized (Reverse-VNIR-Ref.99%).

Table A35. Information about the S39 and S40 obsidians.

Original label	Virtual label	Sigla	Group	Weight (g)	Measurement (cm) (Width/Large/Thickness)	Deposit	Municipality	Island
NO ETIQUETADA	S39	820-1	HOG		GRANDE: 0,9/ 1/ 0,2		Santa María de Guía	Gran Canaria
	S40				PEQUEÑA: 0,4/ 0,6/ 0,1			

(a)

(b)

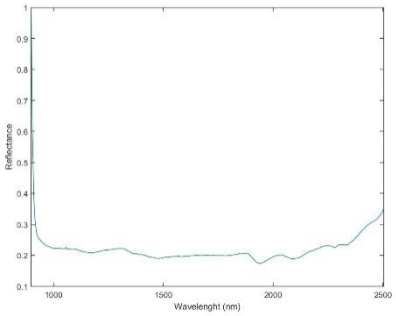

(c)

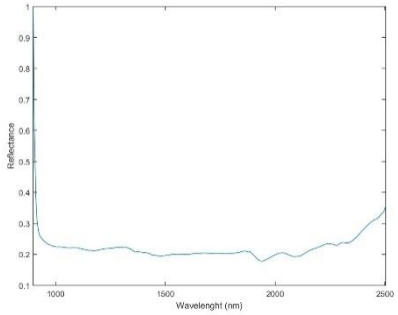

(d)

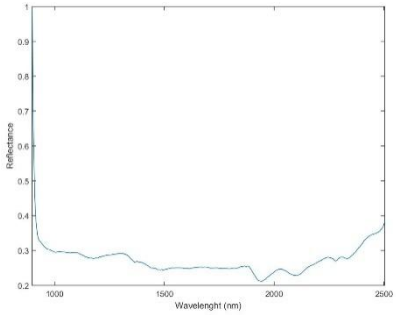

(e)

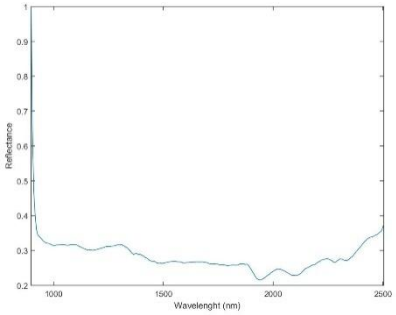

(f)

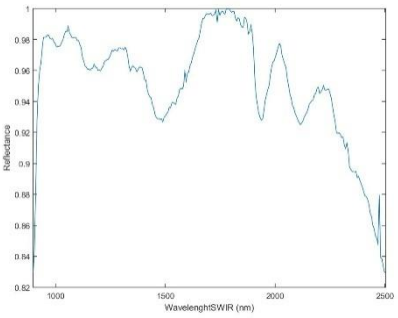

(g)

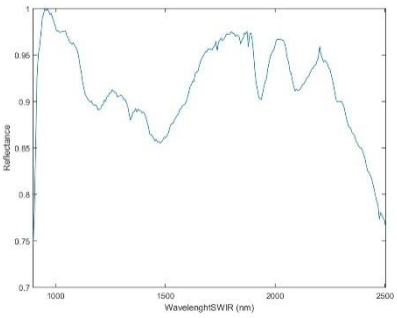

(h)

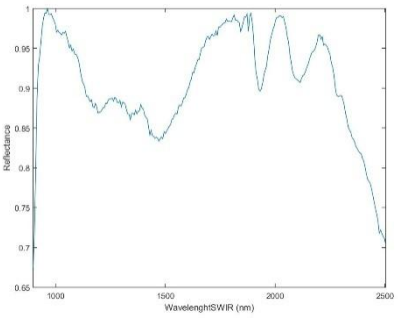

(i)

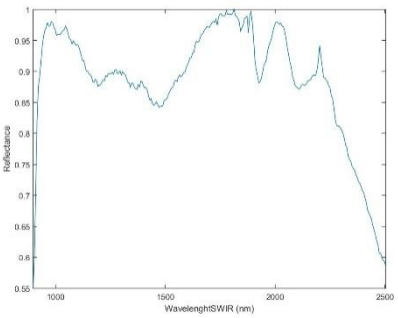

(j)

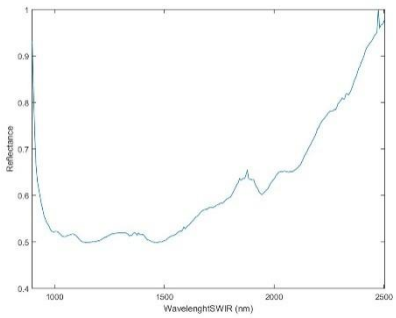

(k)

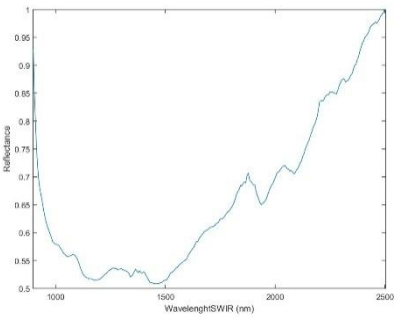

(l)

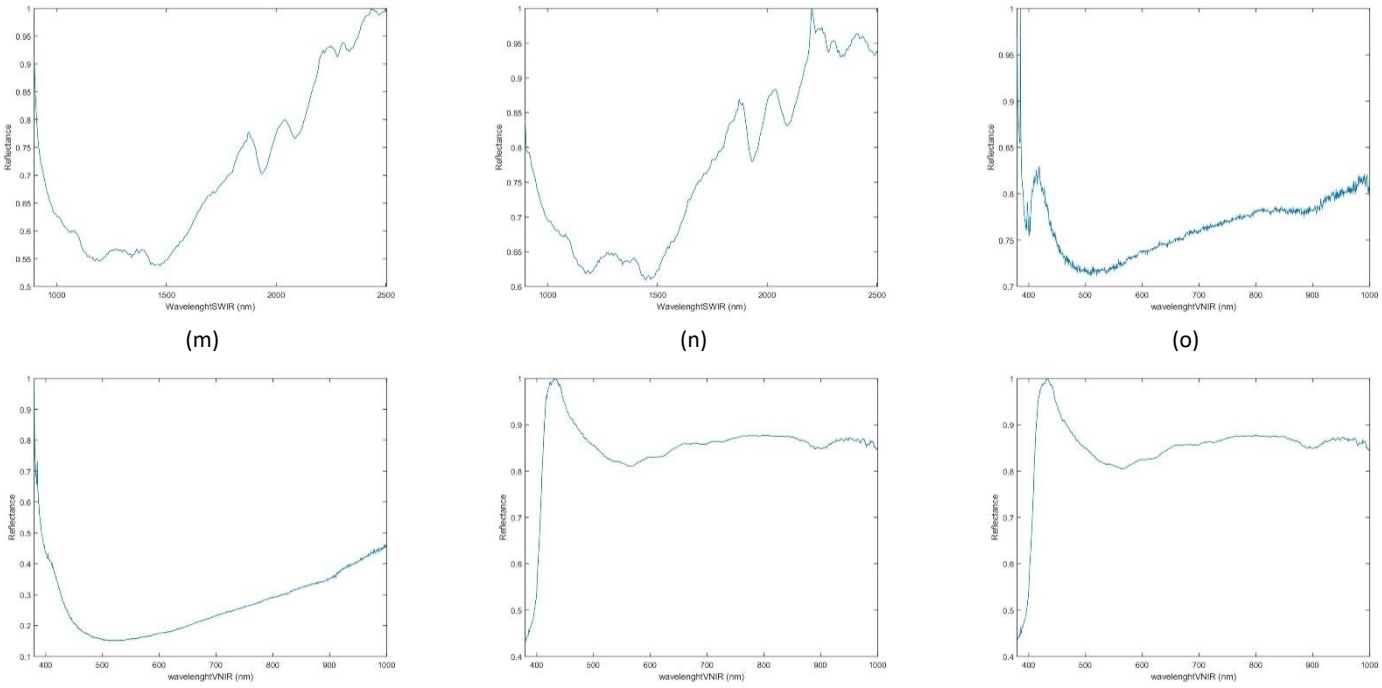

(m) (n) (o)

(p) (q) (r)

Figure A35. (a) Obsidian in frontal position. (b) Obsidian in reverse position. (c) Spectral signature calibrated and normalized (Frontal-S39-SWIR-Ref. 99%). (d) Spectral signature calibrated and normalized (Reverse-S39-SWIR-Ref. 99%). (e) Spectral signature calibrated and normalized (Frontal-S40-SWIR-Ref. 99%). (f) Spectral signature calibrated and normalized (Reverse-S40-SWIR-Ref. 99%). (g) Spectral signature calibrated and normalized (Frontal-S39-SWIR-Ref. 10%). (h) Spectral signature calibrated and normalized (Reverse-S39-SWIR-Ref. 10%). (i) Spectral signature calibrated and normalized (Frontal-S40-SWIR-Ref. 10%). (j) Spectral signature calibrated and normalized (Reverse-S40-SWIR-Ref. 10%). (k) Spectral signature calibrated and normalized (Frontal-S39-SWIR-Ref. 50%). (l) Spectral signature calibrated and normalized (Reverse-S39-SWIR-Ref. 50%). (m) Spectral signature calibrated and normalized (Frontal-S40-SWIR-Ref. 50%). (n) Spectral signature calibrated and normalized (Reverse-S40-SWIR-Ref. 50%). (o) Spectral signature calibrated and normalized (Frontal-S39-VNIR-Ref. 99%). (p) Spectral signature calibrated and normalized (Reverse-S39-VNIR-Ref. 99%). (q) Spectral signature calibrated and normalized (Frontal-S40-VNIR-Ref. 99%). (r) Spectral signature calibrated and normalized (Reverse-S40-VNIR-Ref. 99%).

Table A36. Information about the S35 obsidian.

Original label	Virtual label	Sigla	Group	Weight (g)	Measurement (cm) (Width/Large/Thickness)	Deposit	Municipality	Island
CNB-147-A	S35	811-1	HOG		1.1/1.2/0.4	El Cenobio de Valerón	Santa María de Guía	Gran Canaria

(a)

(b)

(c)

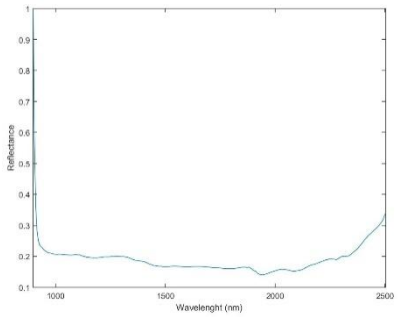

(d)

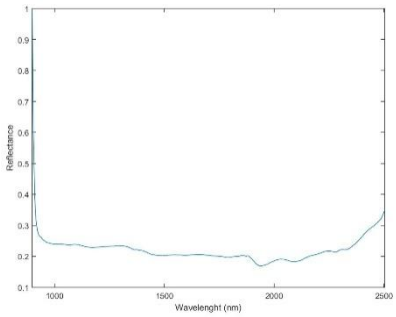

(e)

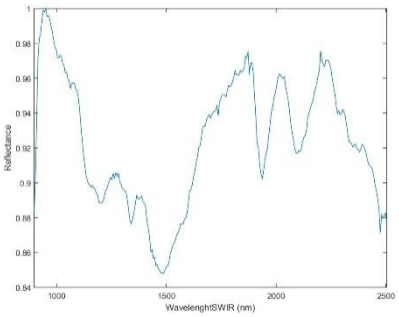

(f)

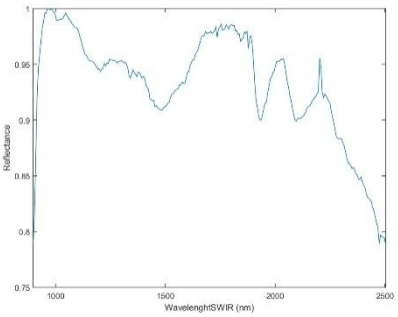

(g)

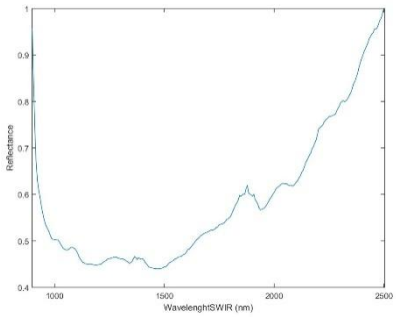

(h)

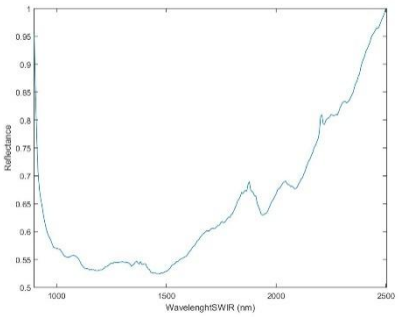

(i)

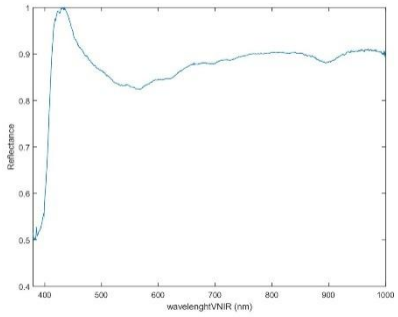

(j)

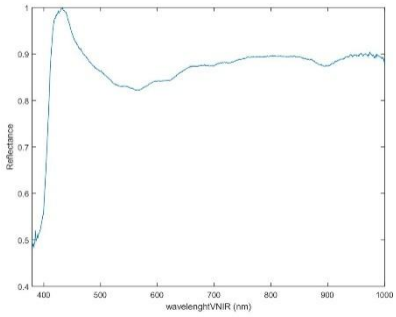

(k)

Figure A36. (a) Obsidian in frontal position. (b) Obsidian in reverse position. (c) Obsidian thickness. (d) Spectral signature calibrated and normalized (Frontal-SWIR-Ref. 99%). (e) Spectral signature calibrated and normalized (Reverse-SWIR-Ref. 99%). (f) Spectral signature calibrated and normalized (Frontal-SWIR-Ref. 10%). (g) Spectral signature calibrated and normalized (Reverse-SWIR-Ref. 10%). (h) Spectral signature calibrated and normalized (Frontal-SWIR-Ref. 50%). (i) Spectral signature calibrated and normalized (Reverse-SWIR-Ref. 50%). (j) Spectral signature calibrated and normalized (Frontal-VNIR-Ref.99%). (k) Spectral signature calibrated and normalized (Reverse-VNIR-Ref.99%).

Table A37. Information about the S36 obsidian.

Original label	Virtual label	Sigla	Group	Weight (g)	Measurement (cm) (Width/Large/Thickness)	Deposit	Municipality	Island
CNB-147-B	S36	811-3	HOG		0.6/1.2/0.3	El Cenobio de Valerón	Santa María de Guía	Gran Canaria

(a)

(b)

(c)

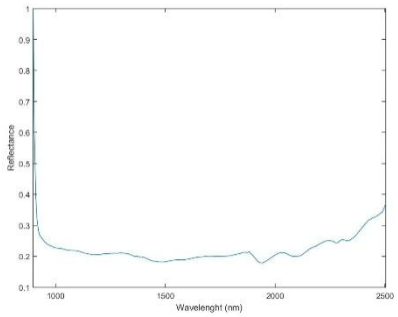

(d)

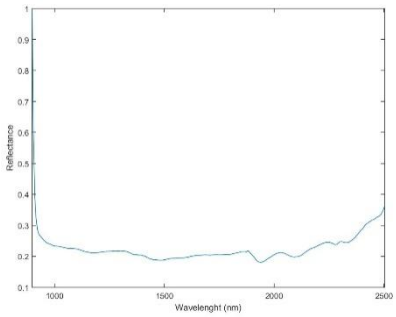

(e)

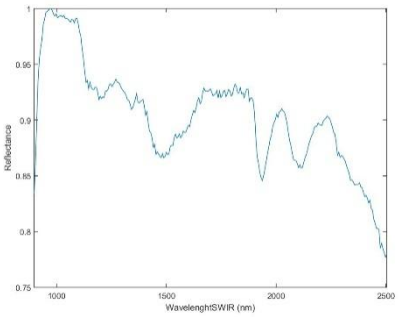

(f)

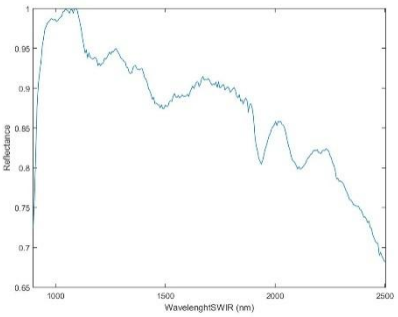

(g)

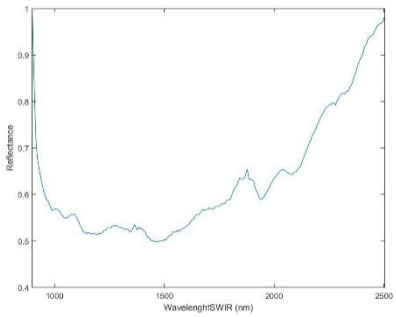

(h)

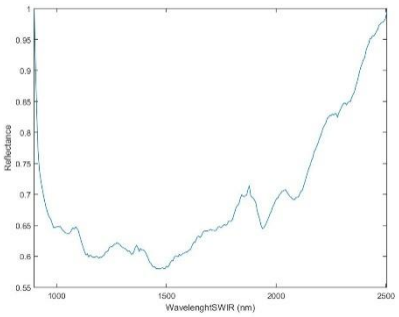

(i)

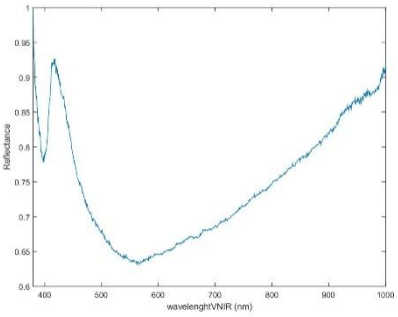

(j)

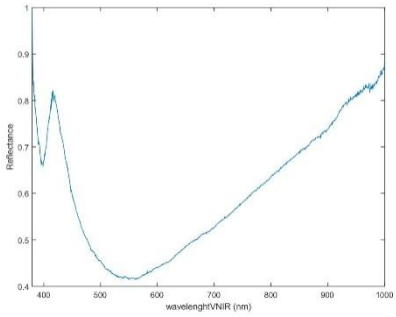

(k)

Figure A37. (a) Obsidian in frontal position. (b) Obsidian in reverse position. (c) Obsidian thickness. (d) Spectral signature calibrated and normalized (Frontal-SWIR-Ref. 99%). (e) Spectral signature calibrated and normalized (Reverse-SWIR-Ref. 99%). (f) Spectral signature calibrated and normalized (Frontal-SWIR-Ref. 10%). (g) Spectral signature calibrated and normalized (Reverse-SWIR-Ref. 10%). (h) Spectral signature calibrated and normalized (Frontal-SWIR-Ref. 50%). (i) Spectral signature calibrated and normalized (Reverse-SWIR-Ref. 50%). (j) Spectral signature calibrated and normalized (Frontal-VNIR-Ref.99%). (k) Spectral signature calibrated and normalized (Reverse-VNIR-Ref.99%).

Table A38. Information about the S41 obsidian.

Original label	Virtual label	Sigla	Group	Weight (g)	Measurement (cm) (Width/Large/Thickness)	Deposit	Municipality	Island
NO ETIQUETADA	S41	811-4	-		0.35/1.2/0.1		Santa María de Guía	Gran Canaria

(a)

(b)

(c)

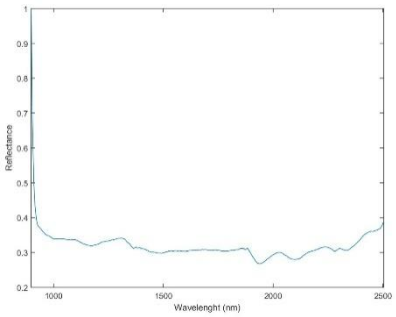

(d)

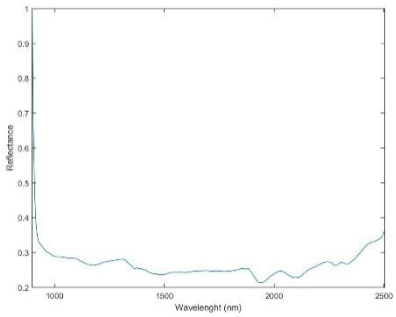

(e)

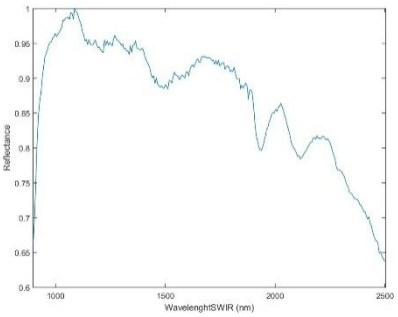

(f)

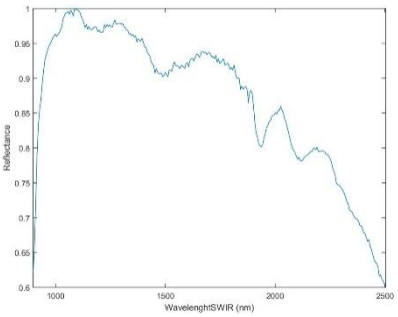

(g)

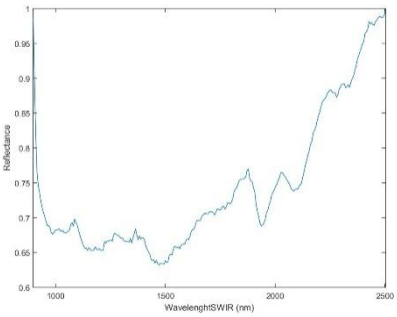

(h)

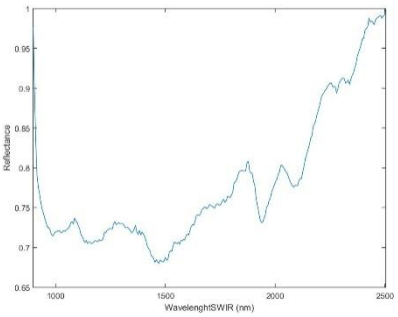

(i)

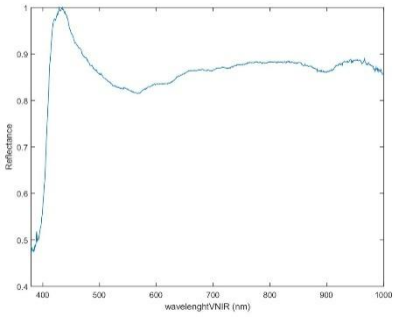

(j)

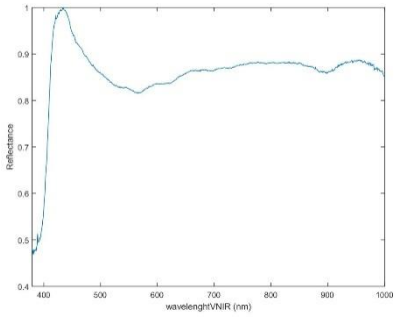

(k)

Figure A38. (a) Obsidian in frontal position. (b) Obsidian in reverse position. (c) Obsidian thickness. (d) Spectral signature calibrated and normalized (Frontal-SWIR-Ref. 99%). (e) Spectral signature calibrated and normalized (Reverse-SWIR-Ref. 99%). (f) Spectral signature calibrated and normalized (Frontal-SWIR-Ref. 10%). (g) Spectral signature calibrated and normalized (Reverse-SWIR-Ref. 10%). (h) Spectral signature calibrated and normalized (Frontal-SWIR-Ref. 50%). (i) Spectral signature calibrated and normalized (Reverse-SWIR-Ref. 50%). (j) Spectral signature calibrated and normalized (Frontal-VNIR-Ref.99%). (k) Spectral signature calibrated and normalized (Reverse-VNIR-Ref.99%).

Table A39. Information about the S42 obsidian.

Original label	Virtual label	Sigla	Group	Weight (g)	Measurement (cm) (Width/Large/Thickness)	Deposit	Municipality	Island
NO ETIQUETADA	S42	811-2	-		0.6/1.2/0.4		Santa María de Guía	Gran Canaria

(a)

(b)

(c)

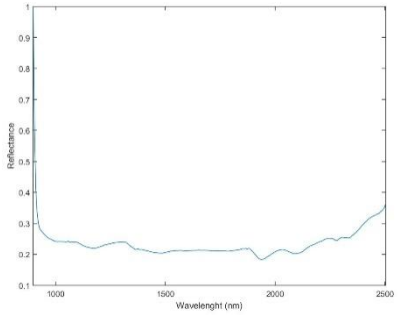

(d)

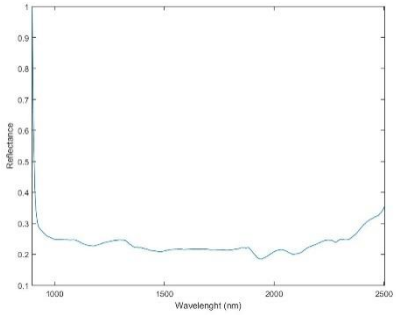

(e)

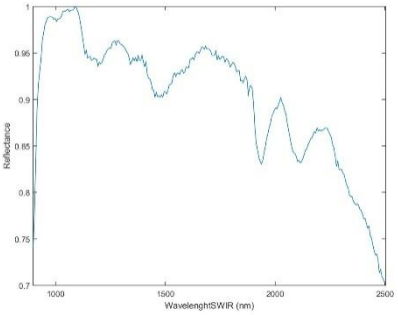

(f)

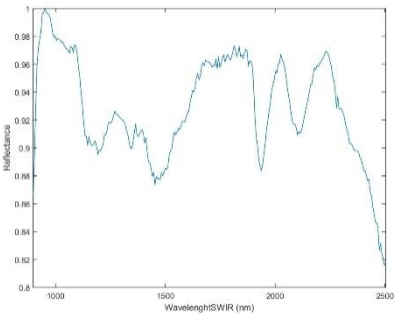

(g)

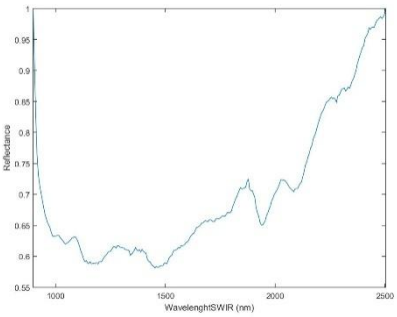

(h)

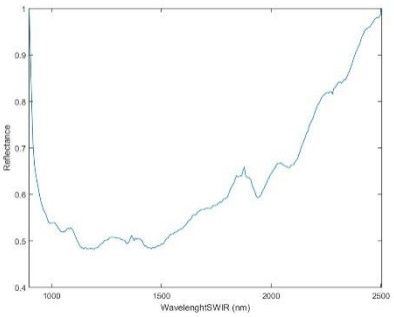

(i)

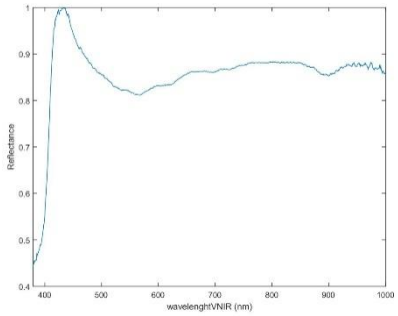

(j)

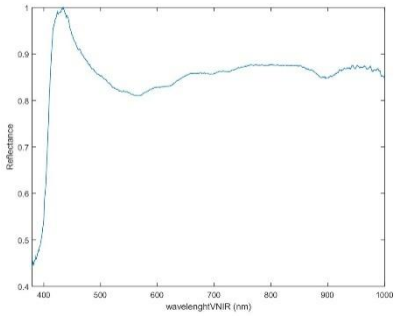

(k)

Figure A39. (a) Obsidian in frontal position. (b) Obsidian in reverse position. (c) Obsidian thickness. (d) Spectral signature calibrated and normalized (Frontal-SWIR-Ref. 99%). (e) Spectral signature calibrated and normalized (Reverse-SWIR-Ref. 99%). (f) Spectral signature calibrated and normalized (Frontal-SWIR-Ref. 10%). (g) Spectral signature calibrated and normalized (Reverse-SWIR-Ref. 10%). (h) Spectral signature calibrated and normalized (Frontal-SWIR-Ref. 50%). (i) Spectral signature calibrated and normalized (Reverse-SWIR-Ref. 50%). (j) Spectral signature calibrated and normalized (Frontal-VNIR-Ref.99%). (k) Spectral signature calibrated and normalized (Reverse-VNIR-Ref.99%).

Table A40. Information about the S37 obsidian.

Original label	Virtual label	Sigla	Group	Weight (g)	Measurement (cm) (Width/Large/Thickness)	Deposit	Municipality	Island
CNB-152	S37	843	HOG		0.8/1.8/0.3	El Cenobio de Valerón	Santa María de Guía	Gran Canaria

(a)

(b)

(c)

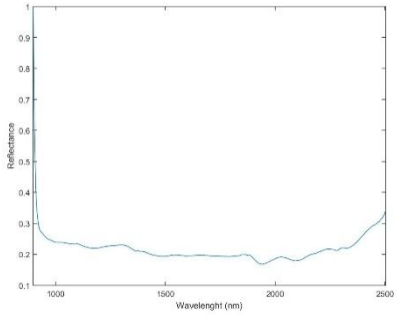

(d)

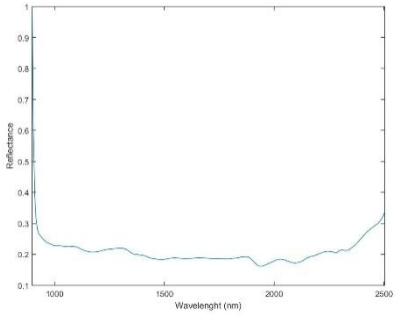

(e)

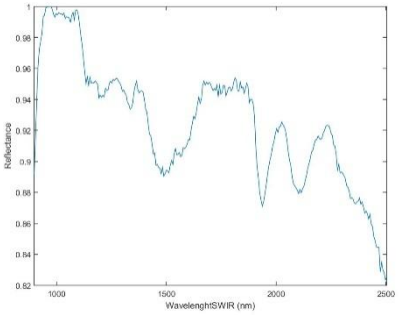

(f)

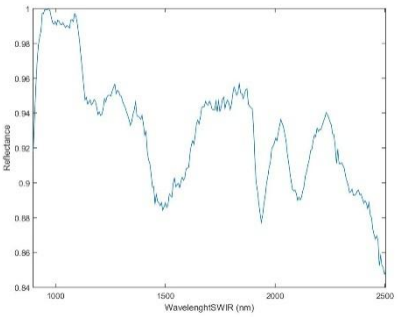

(g)

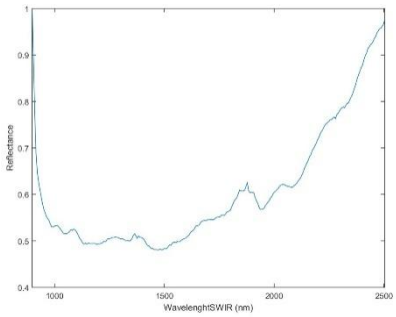

(h)

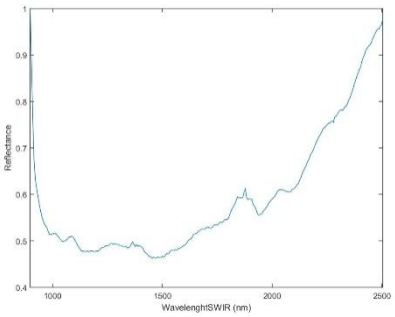

(i)

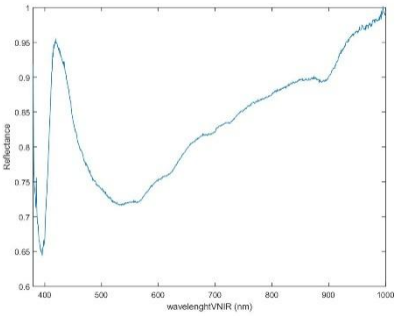

(j)

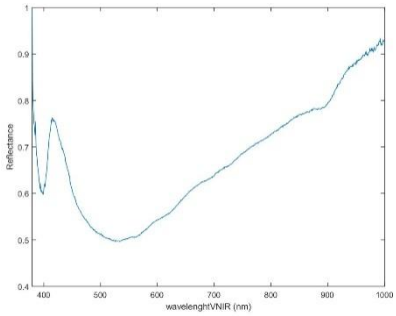

(k)

Figure A40. (a) Obsidian in frontal position. (b) Obsidian in reverse position. (c) Obsidian thickness. (d) Spectral signature calibrated and normalized (Frontal-SWIR-Ref. 99%). (e) Spectral signature calibrated and normalized (Reverse-SWIR-Ref. 99%). (f) Spectral signature calibrated and normalized (Frontal-SWIR-Ref. 10%). (g) Spectral signature calibrated and normalized (Reverse-SWIR-Ref. 10%). (h) Spectral signature calibrated and normalized (Frontal-SWIR-Ref. 50%). (i) Spectral signature calibrated and normalized (Reverse-SWIR-Ref. 50%). (j) Spectral signature calibrated and normalized (Frontal-VNIR-Ref.99%). (k) Spectral signature calibrated and normalized (Reverse-VNIR-Ref.99%).

Table A41. Information about the S38 obsidian.

Original label	Virtual label	Sigla	Group	Weight (g)	Measurement (cm) (Width/Large/Thickness)	Deposit	Municipality	Island
CNB-155	S38	857	HOG		0.6/1.35/0.15	El Cenobio de Valerón	Santa María de Guía	Gran Canaria

(a)

(b)

(c)

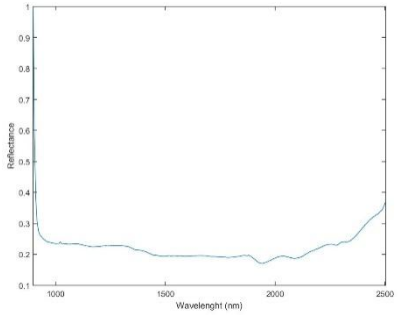

(d)

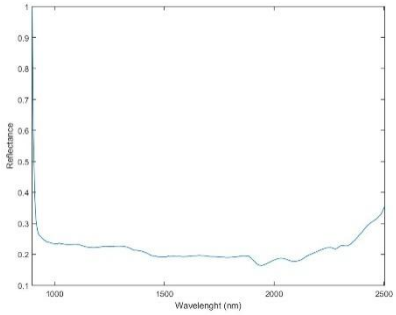

(e)

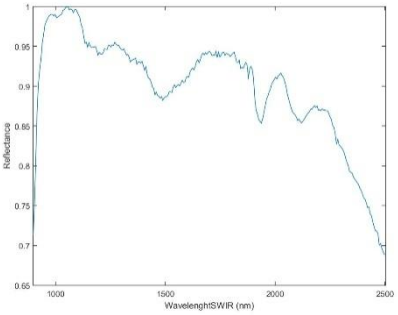

(f)

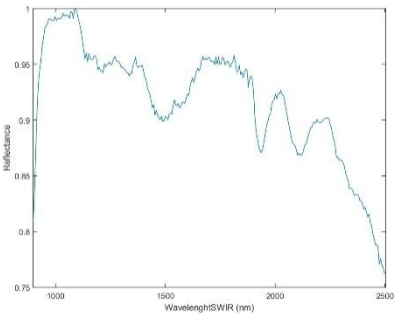

(g)

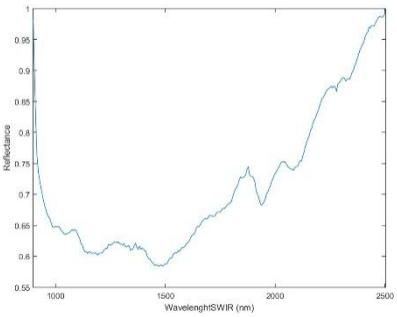

(h)

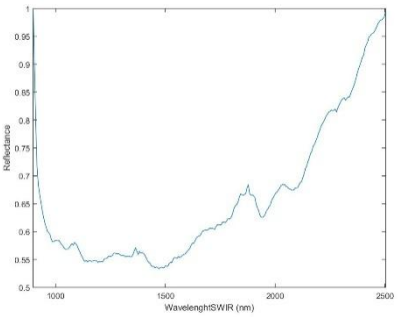

(i)

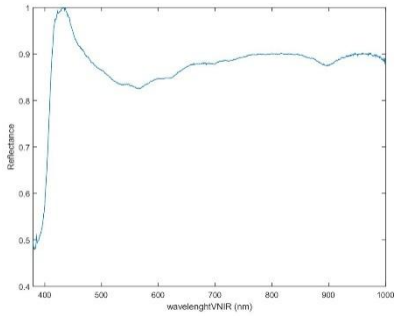

(j)

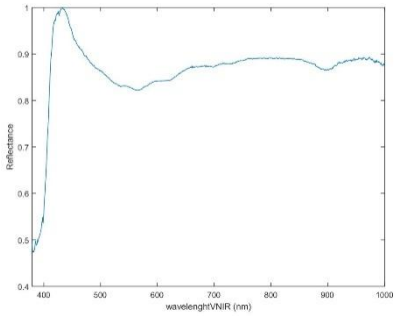

(k)

Figure A41. (a) Obsidian in frontal position. (b) Obsidian in reverse position. (c) Obsidian thickness. (d) Spectral signature calibrated and normalized (Frontal-SWIR-Ref. 99%). (e) Spectral signature calibrated and normalized (Reverse-SWIR-Ref. 99%). (f) Spectral signature calibrated and normalized (Frontal-SWIR-Ref. 10%). (g) Spectral signature calibrated and normalized (Reverse-SWIR-Ref. 10%). (h) Spectral signature calibrated and normalized (Frontal-SWIR-Ref. 50%). (i) Spectral signature calibrated and normalized (Reverse-SWIR-Ref. 50%). (j) Spectral signature calibrated and normalized (Frontal-VNIR-Ref.99%). (k) Spectral signature calibrated and normalized (Reverse-VNIR-Ref.99%).

Table A42. Information about the S43 obsidian.

Original label	Virtual label	Sigla	Group	Weight (g)	Measurement (cm) (Width/Large/Thickness)	Deposit	Municipality	Island
DUM-77	S43	36	N1		0.9/1.3/0.4	Dunas de Maspalomas	San Bartolomé de Tirajana	Gran Canaria

(a)

(b)

(c)

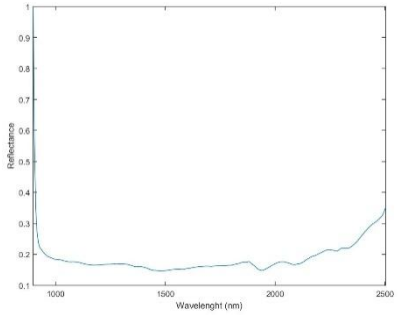

(d)

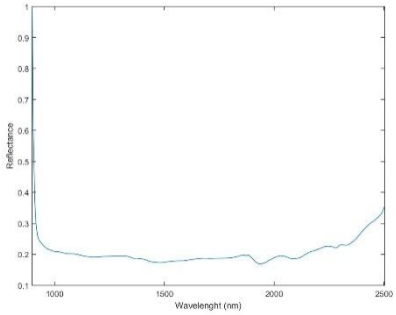

(e)

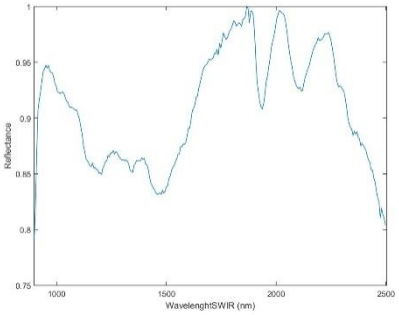

(f)

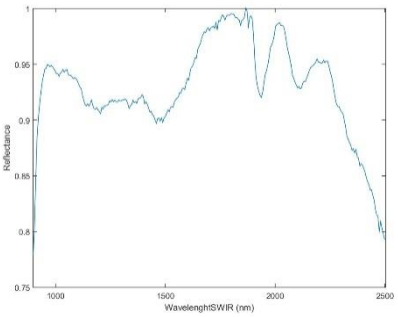

(g)

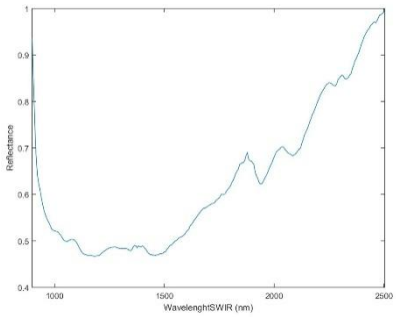

(h)

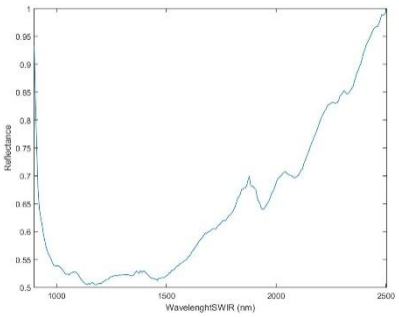

(i)

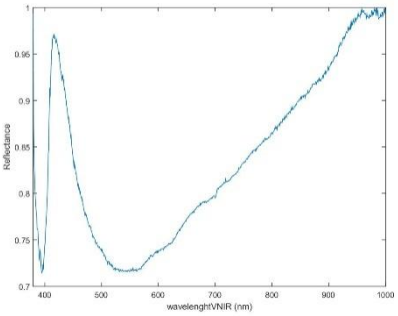

(j)

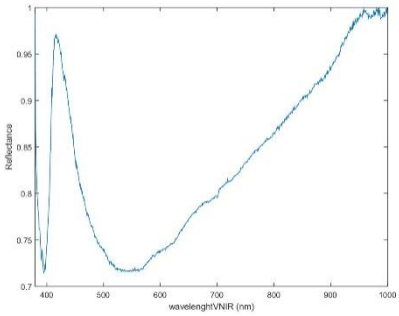

(k)

Figure A42. (a) Obsidian in frontal position. (b) Obsidian in reverse position. (c) Obsidian thickness. (d) Spectral signature calibrated and normalized (Frontal-SWIR-Ref. 99%). (e) Spectral signature calibrated and normalized (Reverse-SWIR-Ref. 99%). (f) Spectral signature calibrated and normalized (Frontal-SWIR-Ref. 10%). (g) Spectral signature calibrated and normalized (Reverse-SWIR-Ref. 10%). (h) Spectral signature calibrated and normalized (Frontal-SWIR-Ref. 50%). (i) Spectral signature calibrated and normalized (Reverse-SWIR-Ref. 50%). (j) Spectral signature calibrated and normalized (Frontal-VNIR-Ref.99%). (k) Spectral signature calibrated and normalized (Reverse-VNIR-Ref.99%).

Table A43. Information about the S44 obsidian.

Original label	Virtual label	Sigla	Group	Weight (g)	Measurement (cm) (Width/Large/Thickness)	Deposit	Municipality	Island
DUM-78	S44	573(3)	HOG		1/1.1/0.4	Dunas de Maspalomas	San Bartolomé de Tirajana	Gran Canaria

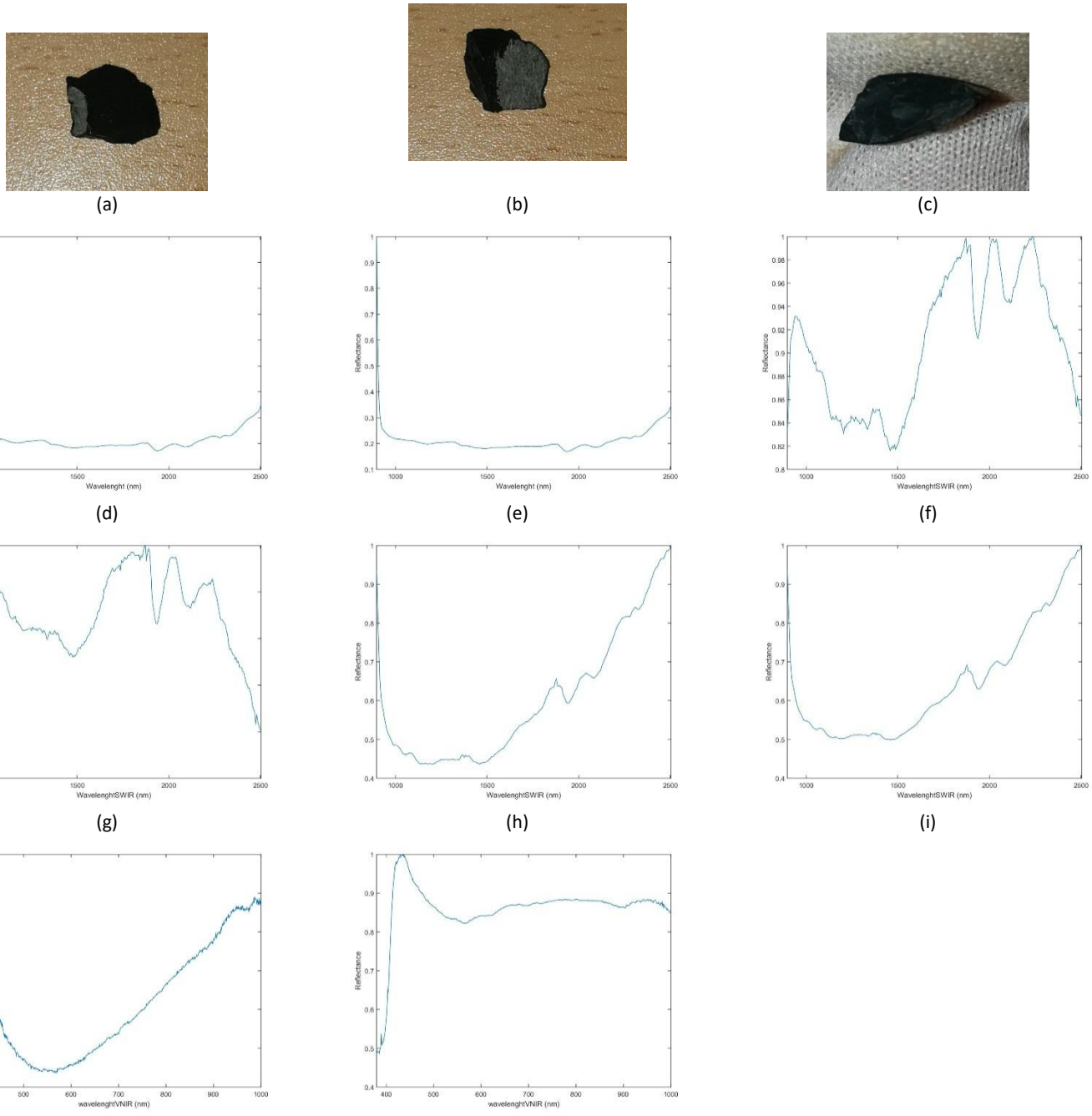

Figure A43. (a) Obsidian in frontal position. (b) Obsidian in reverse position. (c) Obsidian thickness. (d) Spectral signature calibrated and normalized (Frontal-SWIR-Ref. 99%). (e) Spectral signature calibrated and normalized (Reverse-SWIR-Ref. 99%). (f) Spectral signature calibrated and normalized (Frontal-SWIR-Ref. 10%). (g) Spectral signature calibrated and normalized (Reverse-SWIR-Ref. 10%). (h) Spectral signature calibrated and normalized (Frontal-SWIR-Ref. 50%). (i) Spectral signature calibrated and normalized (Reverse-SWIR-Ref. 50%). (j) Spectral signature calibrated and normalized (Frontal-VNIR-Ref.99%). (k) Spectral signature calibrated and normalized (Reverse-VNIR-Ref.99%).

Table A44. Information about the S45 obsidian.

Original label	Virtual label	Sigla	Group	Weight (g)	Measurement (cm) (Width/Large/Thickness)	Deposit	Municipality	Island
DUM-79	S45	683(1)	OTHERS		0.9/1.5/0.4	Dunas de Maspalomas	San Bartolomé de Tirajana	Gran Canaria

(a)

(b)

(c)

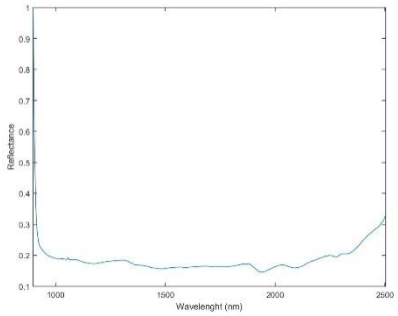

(d)

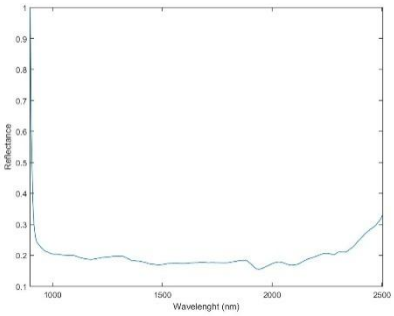

(e)

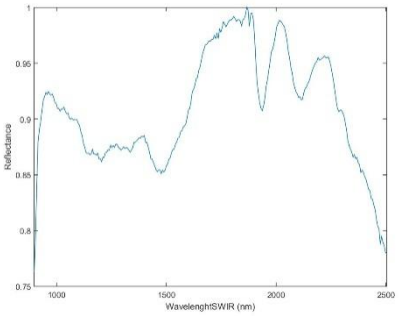

(f)

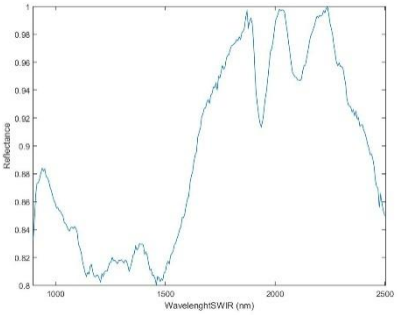

(g)

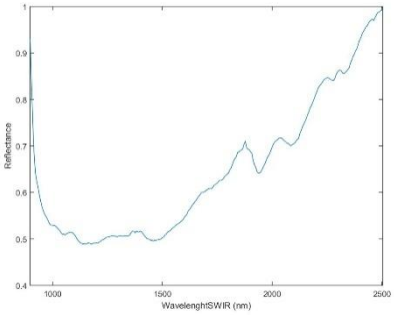

(h)

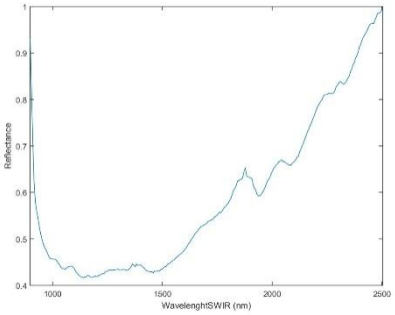

(i)

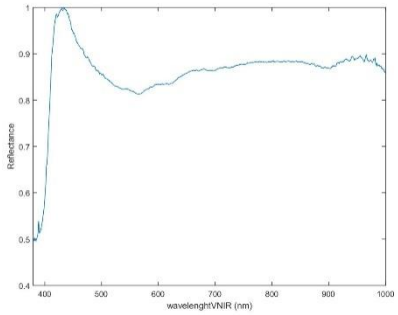

(j)

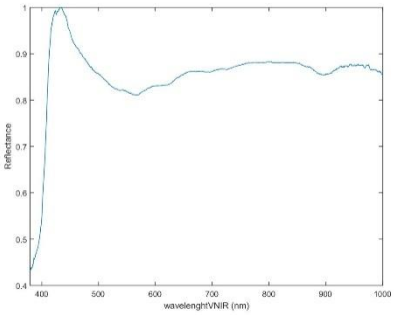

(k)

Figure A44. (a) Obsidian in frontal position. (b) Obsidian in reverse position. (c) Obsidian thickness. (d) Spectral signature calibrated and normalized (Frontal-SWIR-Ref. 99%). (e) Spectral signature calibrated and normalized (Reverse-SWIR-Ref. 99%). (f) Spectral signature calibrated and normalized (Frontal-SWIR-Ref. 10%). (g) Spectral signature calibrated and normalized (Reverse-SWIR-Ref. 10%). (h) Spectral signature calibrated and normalized (Frontal-SWIR-Ref. 50%). (i) Spectral signature calibrated and normalized (Reverse-SWIR-Ref. 50%). (j) Spectral signature calibrated and normalized (Frontal-VNIR-Ref.99%). (k) Spectral signature calibrated and normalized (Reverse-VNIR-Ref.99%).

Table A45. Information about the S46 obsidian.

Original label	Virtual label	Sigla	Group	Weight (g)	Measurement (cm) (Width/Large/Thickness)	Deposit	Municipality	Island
DUM-80	S46	355(1)	HOG		1/1.15/0.3	Dunas de Maspalomas	San Bartolomé de Tirajana	Gran Canaria

(a)

(b)

(c)

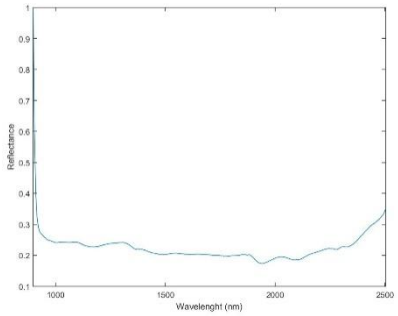

(d)

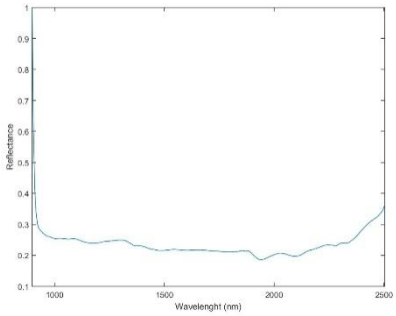

(e)

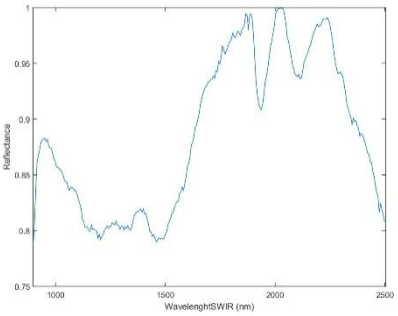

(f)

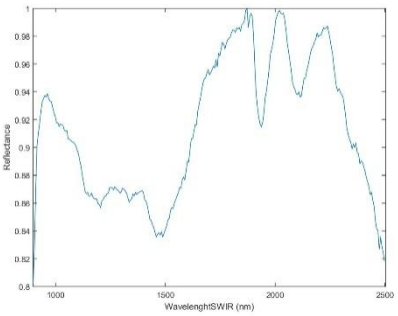

(g)

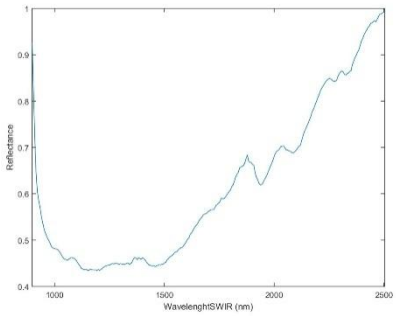

(h)

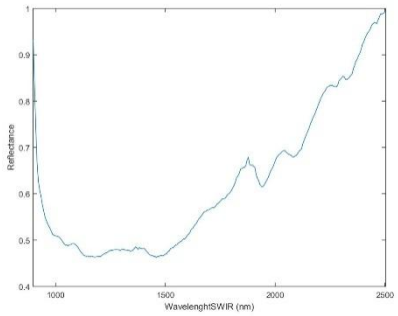

(i)

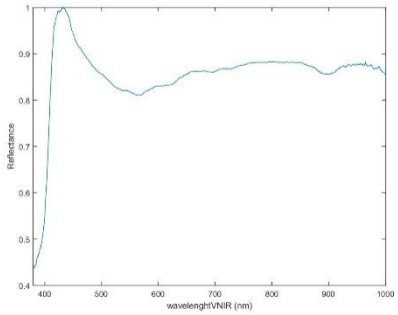

(j)

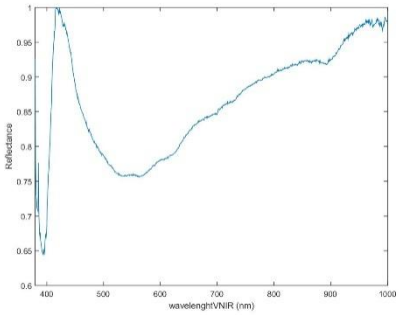

(k)

Figure A45. (a) Obsidian in frontal position. (b) Obsidian in reverse position. (c) Obsidian thickness. (d) Spectral signature calibrated and normalized (Frontal-SWIR-Ref. 99%). (e) Spectral signature calibrated and normalized (Reverse-SWIR-Ref. 99%). (f) Spectral signature calibrated and normalized (Frontal-SWIR-Ref. 10%). (g) Spectral signature calibrated and normalized (Reverse-SWIR-Ref. 10%). (h) Spectral signature calibrated and normalized (Frontal-SWIR-Ref. 50%). (i) Spectral signature calibrated and normalized (Reverse-SWIR-Ref. 50%). (j) Spectral signature calibrated and normalized (Frontal-VNIR-Ref.99%). (k) Spectral signature calibrated and normalized (Reverse-VNIR-Ref.99%).

Table A46. Information about the S47 obsidian.

Original label	Virtual label	Sigla	Group	Weight (g)	Measurement (cm) (Width/Large/Thickness)	Deposit	Municipality	Island
DUM-81	S47	336(1)	N3		1/1.1/0.15	Dunas de Maspalomas	San Bartolomé de Tirajana	Gran Canaria

(a)

(b)

(c)

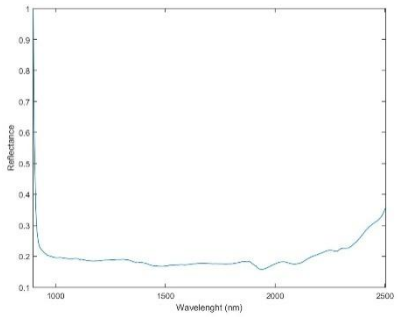

(d)

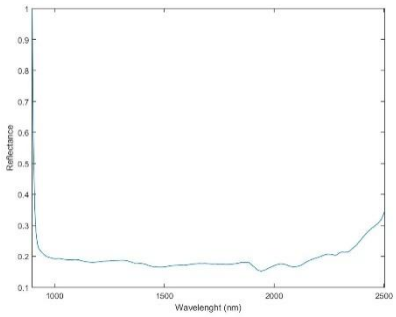

(e)

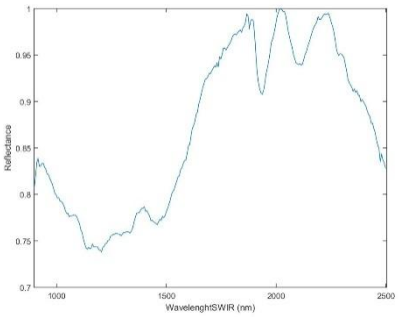

(f)

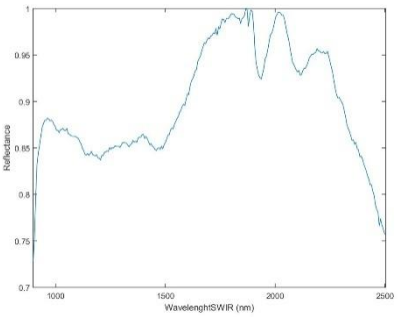

(g)

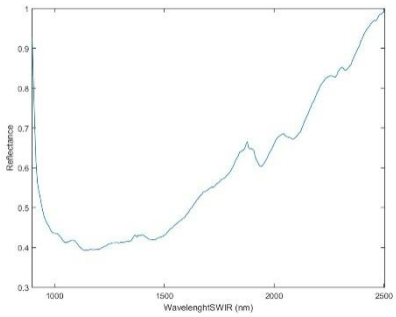

(h)

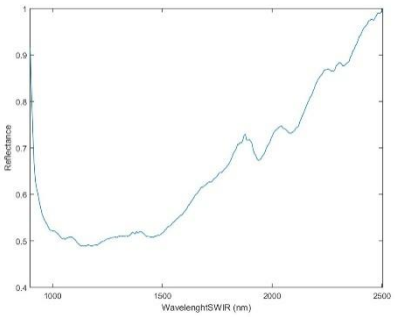

(i)

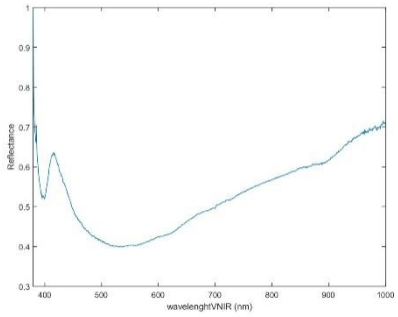

(j)

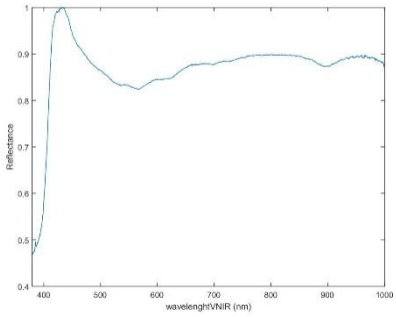

(k)

Figure A46. (a) Obsidian in frontal position. (b) Obsidian in reverse position. (c) Obsidian thickness. (d) Spectral signature calibrated and normalized (Frontal-SWIR-Ref. 99%). (e) Spectral signature calibrated and normalized (Reverse-SWIR-Ref. 99%). (f) Spectral signature calibrated and normalized (Frontal-SWIR-Ref. 10%). (g) Spectral signature calibrated and normalized (Reverse-SWIR-Ref. 10%). (h) Spectral signature calibrated and normalized (Frontal-SWIR-Ref. 50%). (i) Spectral signature calibrated and normalized (Reverse-SWIR-Ref. 50%). (j) Spectral signature calibrated and normalized (Frontal-VNIR-Ref.99%). (k) Spectral signature calibrated and normalized (Reverse-VNIR-Ref.99%).

Table A47. Information about the S48 obsidian.

Original label	Virtual label	Sigla	Group	Weight (g)	Measurement (cm) (Width/Large/Thickness)	Deposit	Municipality	Island
DUM-82	S48	370	HOG		1/1.7/0.25	Dunas de Maspalomas	San Bartolomé de Tirajana	Gran Canaria

(a)

(b)

(c)

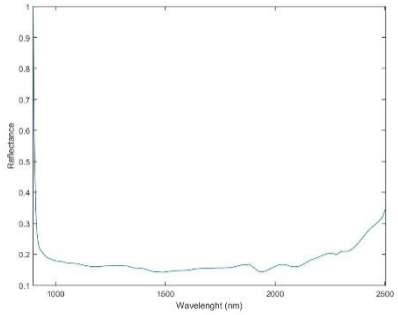

(d)

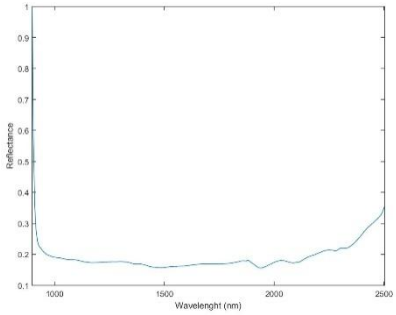

(e)

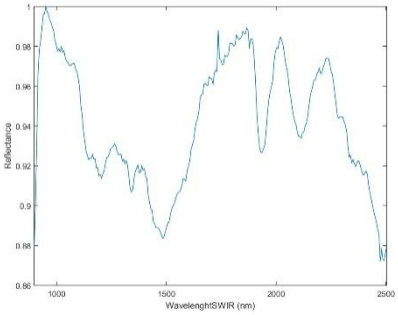

(f)

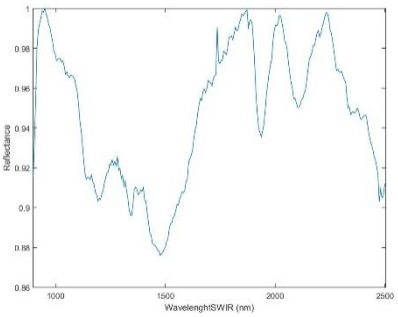

(g)

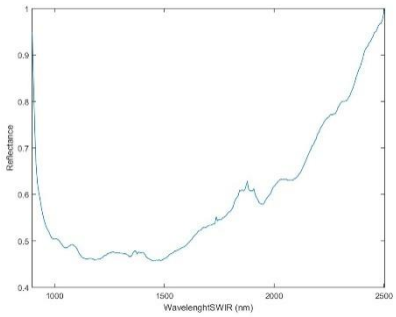

(h)

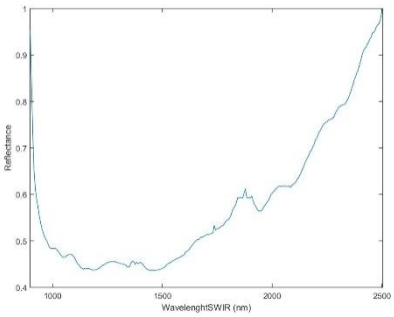

(i)

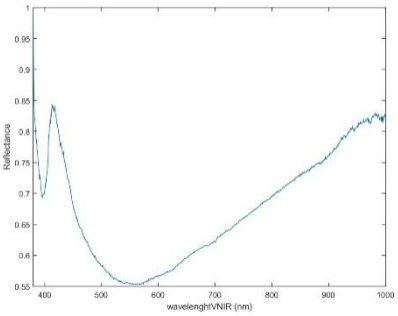

(j)

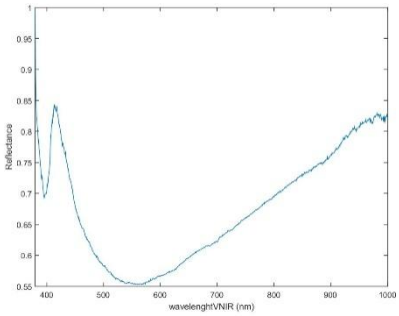

(k)

Figure A47. (a) Obsidian in frontal position. (b) Obsidian in reverse position. (c) Obsidian thickness. (d) Spectral signature calibrated and normalized (Frontal-SWIR-Ref. 99%). (e) Spectral signature calibrated and normalized (Reverse-SWIR-Ref. 99%). (f) Spectral signature calibrated and normalized (Frontal-SWIR-Ref. 10%). (g) Spectral signature calibrated and normalized (Reverse-SWIR-Ref. 10%). (h) Spectral signature calibrated and normalized (Frontal-SWIR-Ref. 50%). (i) Spectral signature calibrated and normalized (Reverse-SWIR-Ref. 50%). (j) Spectral signature calibrated and normalized (Frontal-VNIR-Ref.99%). (k) Spectral signature calibrated and normalized (Reverse-VNIR-Ref.99%).

Table A48. Information about the S49 obsidian.

Original label	Virtual label	Sigla	Group	Weight (g)	Measurement (cm) (Width/Large/Thickness)	Deposit	Municipality	Island
DUM-83	S49	261	HOG		1.1/1.7/0.7	Dunas de Maspalomas	San Bartolomé de Tirajana	Gran Canaria

(a)

(b)

(c)

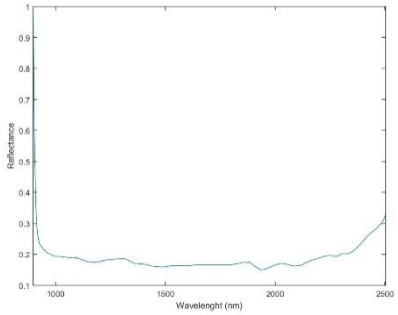

(d)

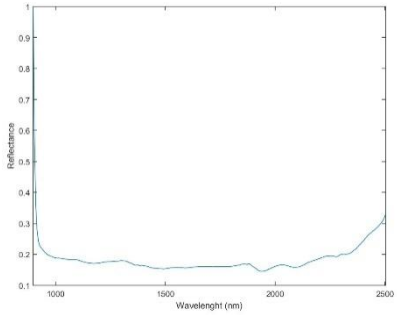

(e)

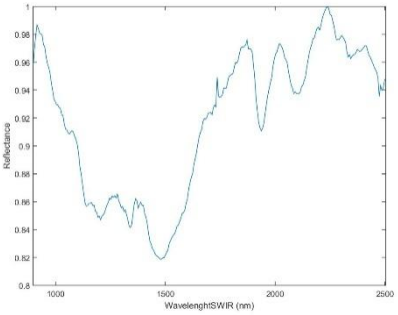

(f)

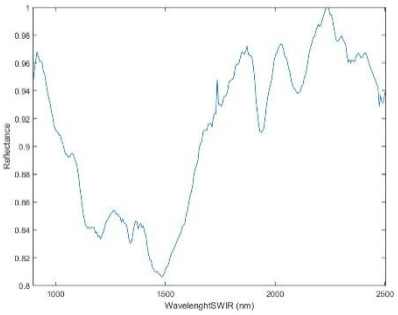

(g)

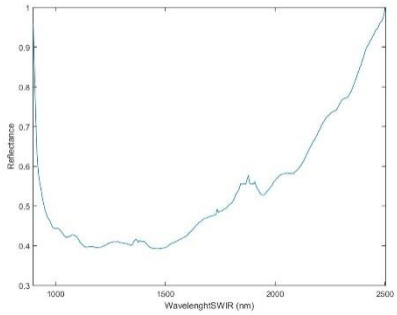

(h)

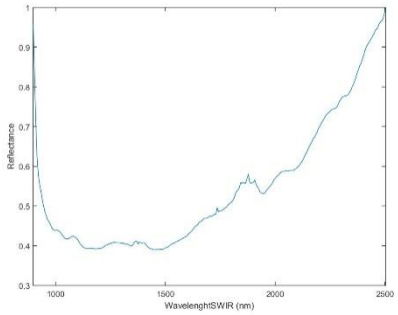

(i)

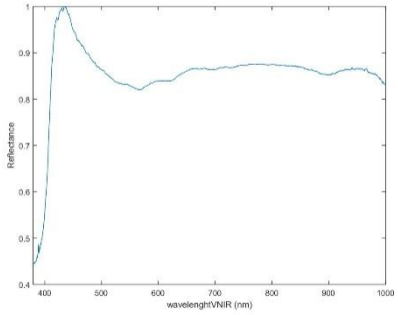

(j)

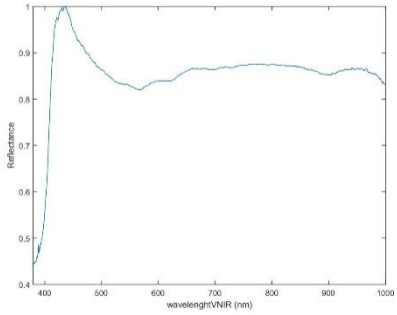

(k)

Figure A48. (a) Obsidian in frontal position. (b) Obsidian in reverse position. (c) Obsidian thickness. (d) Spectral signature calibrated and normalized (Frontal-SWIR-Ref. 99%). (e) Spectral signature calibrated and normalized (Reverse-SWIR-Ref. 99%). (f) Spectral signature calibrated and normalized (Frontal-SWIR-Ref. 10%). (g) Spectral signature calibrated and normalized (Reverse-SWIR-Ref. 10%). (h) Spectral signature calibrated and normalized (Frontal-SWIR-Ref. 50%). (i) Spectral signature calibrated and normalized (Reverse-SWIR-Ref. 50%). (j) Spectral signature calibrated and normalized (Frontal-VNIR-Ref.99%). (k) Spectral signature calibrated and normalized (Reverse-VNIR-Ref.99%).

Table A49. Information about the S50 obsidian.

Original label	Virtual label	Sigla	Group	Weight (g)	Measurement (cm) (Width/Large/Thickness)	Deposit	Municipality	Island
DUM-85	S50	310(7)	HOG		1.1/1.5/0.3	Dunas de Maspalomas	San Bartolomé de Tirajana	Gran Canaria

(a)

(b)

(c)

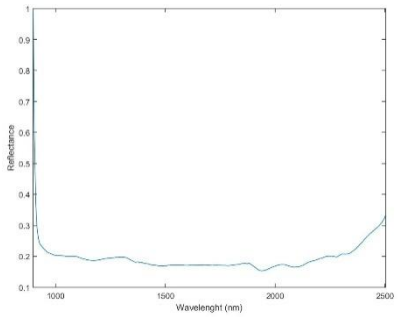

(d)

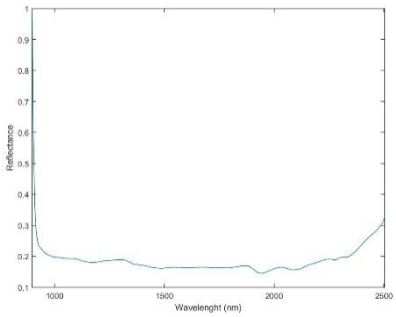

(e)

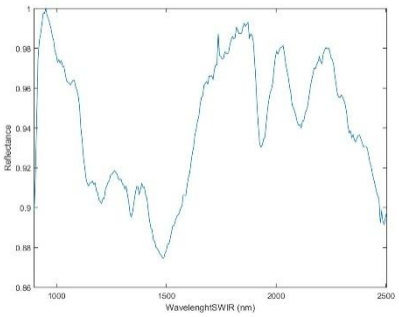

(f)

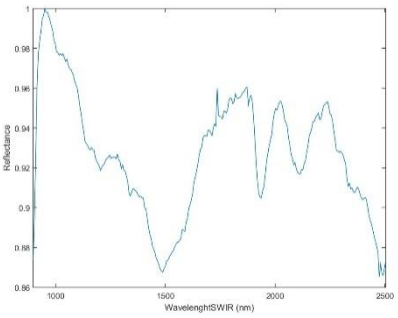

(g)

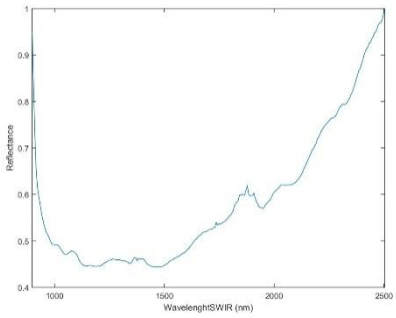

(h)

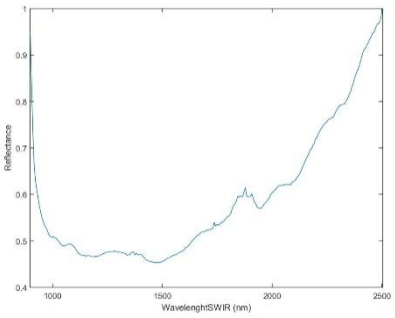

(i)

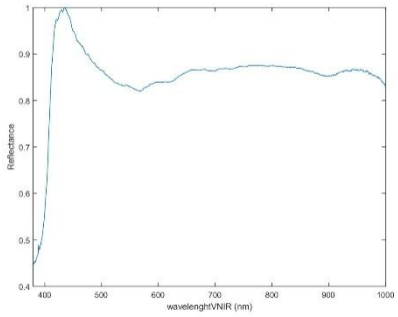

(j)

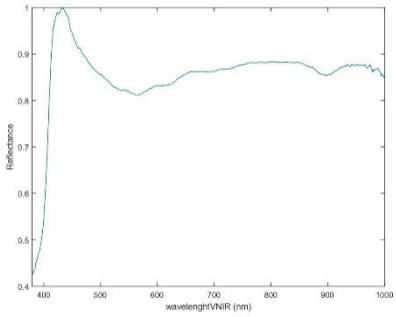

(k)

Figure A49. (a) Obsidian in frontal position. (b) Obsidian in reverse position. (c) Obsidian thickness. (d) Spectral signature calibrated and normalized (Frontal-SWIR-Ref. 99%). (e) Spectral signature calibrated and normalized (Reverse-SWIR-Ref. 99%). (f) Spectral signature calibrated and normalized (Frontal-SWIR-Ref. 10%). (g) Spectral signature calibrated and normalized (Reverse-SWIR-Ref. 10%). (h) Spectral signature calibrated and normalized (Frontal-SWIR-Ref. 50%). (i) Spectral signature calibrated and normalized (Reverse-SWIR-Ref. 50%). (j) Spectral signature calibrated and normalized (Frontal-VNIR-Ref.99%). (k) Spectral signature calibrated and normalized (Reverse-VNIR-Ref.99%).

Table A50. Information about the S51 obsidian.

Original label	Virtual label	Sigla	Group	Weight (g)	Measurement (cm) (Width/Large/Thickness)	Deposit	Municipality	Island
DUM-88-1	S51	428(1)	HOG		0.85/1.4/0.35	Dunas de Maspalomas	San Bartolomé de Tirajana	Gran Canaria

(a)

(b)

(c)

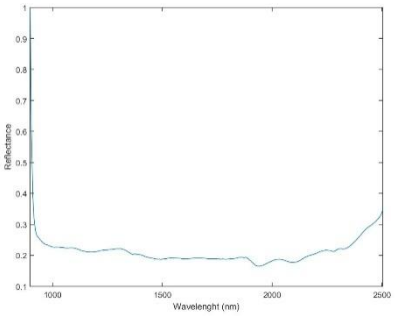

(d)

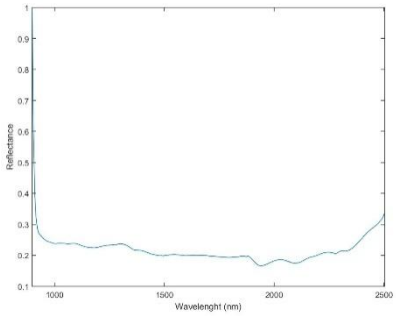

(e)

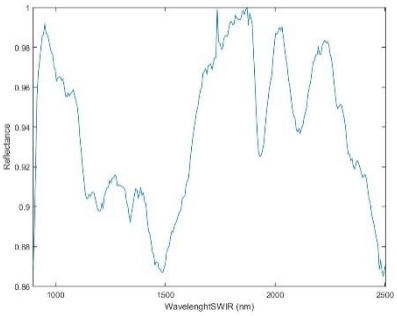

(f)

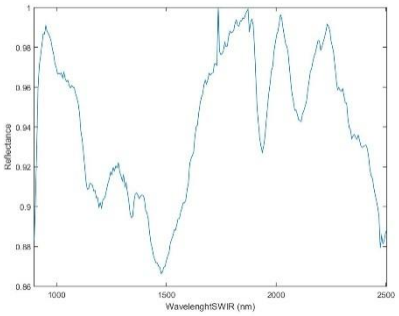

(g)

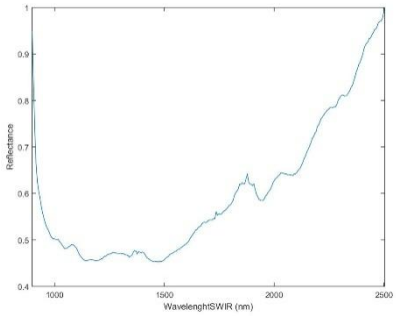

(h)

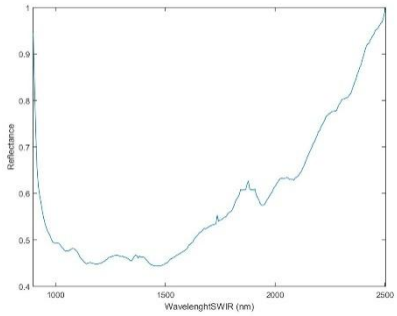

(i)

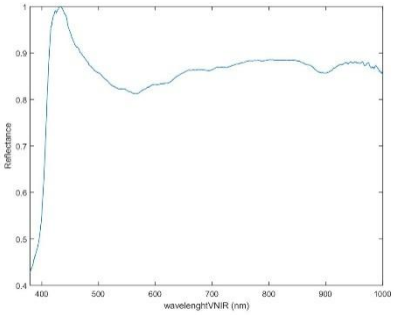

(j)

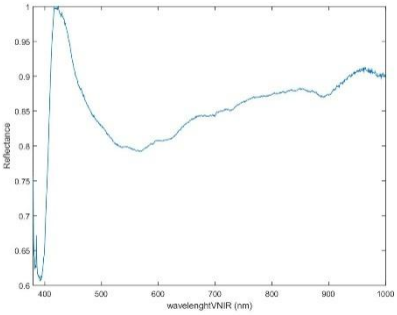

(k)

Figure A50. (a) Obsidian in frontal position. (b) Obsidian in reverse position. (c) Obsidian thickness. (d) Spectral signature calibrated and normalized (Frontal-SWIR-Ref. 99%). (e) Spectral signature calibrated and normalized (Reverse-SWIR-Ref. 99%). (f) Spectral signature calibrated and normalized (Frontal-SWIR-Ref. 10%). (g) Spectral signature calibrated and normalized (Reverse-SWIR-Ref. 10%). (h) Spectral signature calibrated and normalized (Frontal-SWIR-Ref. 50%). (i) Spectral signature calibrated and normalized (Reverse-SWIR-Ref. 50%). (j) Spectral signature calibrated and normalized (Frontal-VNIR-Ref.99%). (k) Spectral signature calibrated and normalized (Reverse-VNIR-Ref.99%).

Table A51. Information about the S52 obsidian.

Original label	Virtual label	Sigla	Group	Weight (g)	Measurement (cm) (Width/Large/Thickness)	Deposit	Municipality	Island
DUM-88-2	S52	428(2)	OTHERS		0.8/1.4/0.6	Dunas de Maspalomas	San Bartolomé de Tirajana	Gran Canaria

(a)

(b)

(c)

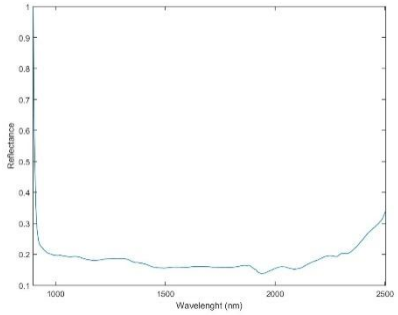

(d)

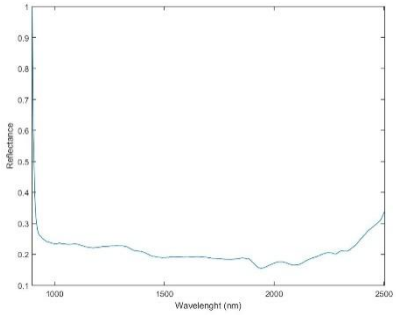

(e)

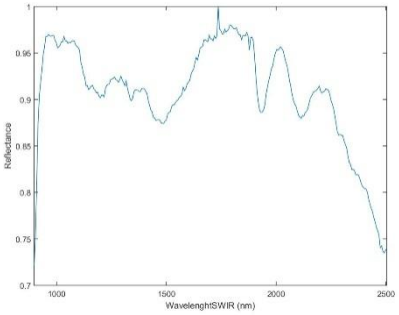

(f)

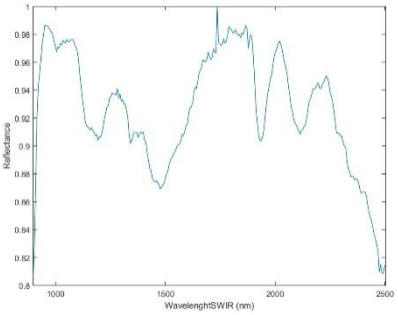

(g)

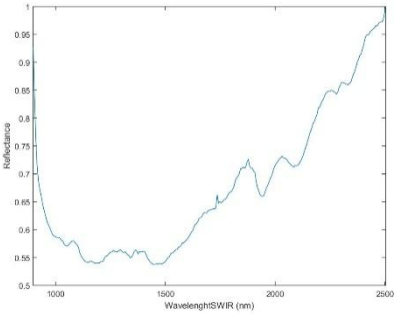

(h)

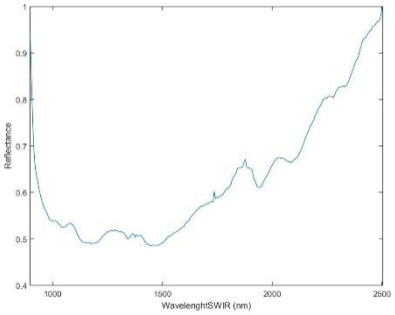

(i)

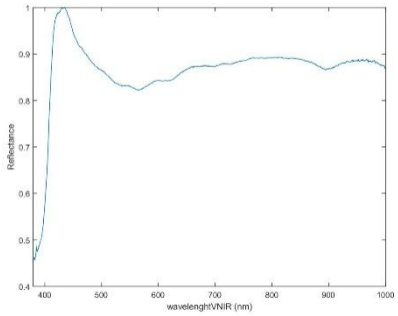

(j)

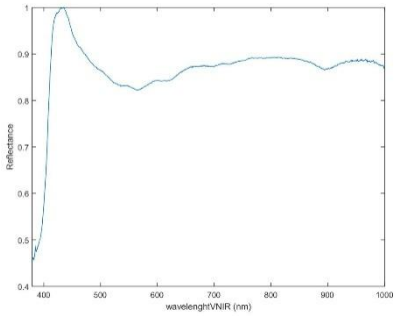

(k)

Figure A51. (a) Obsidian in frontal position. (b) Obsidian in reverse position. (c) Obsidian thickness. (d) Spectral signature calibrated and normalized (Frontal-SWIR-Ref. 99%). (e) Spectral signature calibrated and normalized (Reverse-SWIR-Ref. 99%). (f) Spectral signature calibrated and normalized (Frontal-SWIR-Ref. 10%). (g) Spectral signature calibrated and normalized (Reverse-SWIR-Ref. 10%). (h) Spectral signature calibrated and normalized (Frontal-SWIR-Ref. 50%). (i) Spectral signature calibrated and normalized (Reverse-SWIR-Ref. 50%). (j) Spectral signature calibrated and normalized (Frontal-VNIR-Ref.99%). (k) Spectral signature calibrated and normalized (Reverse-VNIR-Ref.99%).

Table A52. Information about the S53 obsidian.

Original label	Virtual label	Sigla	Group	Weight (g)	Measurement (cm) (Width/Large/Thickness)	Deposit	Municipality	Island
DUM-89	S53	306(6)	N1		1/1.6/0.35	Dunas de Maspalomas	San Bartolomé de Tirajana	Gran Canaria

(a)

(b)

(c)

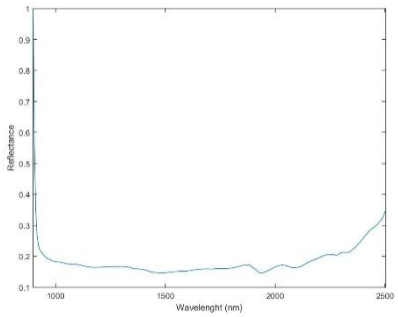

(d)

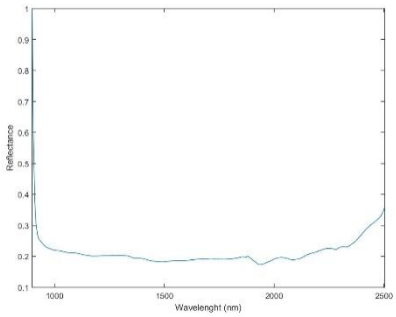

(e)

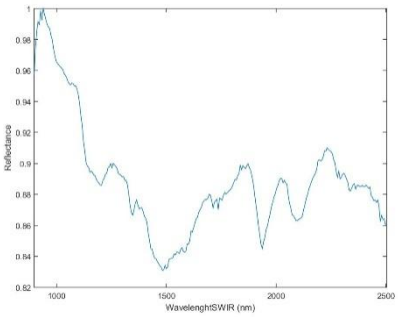

(f)

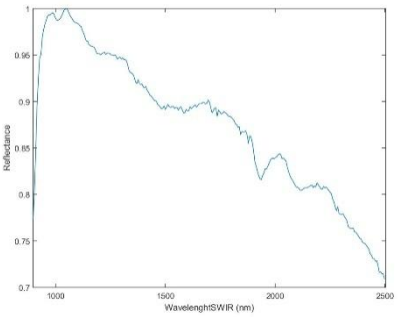

(g)

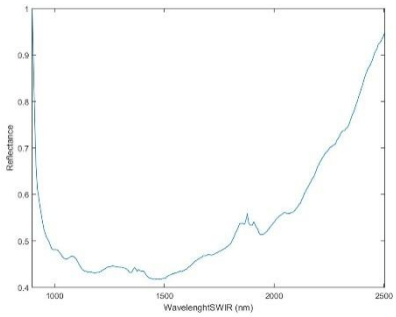

(h)

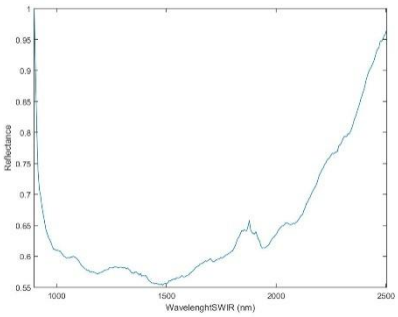

(i)

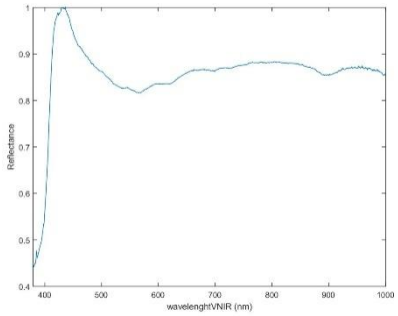

(j)

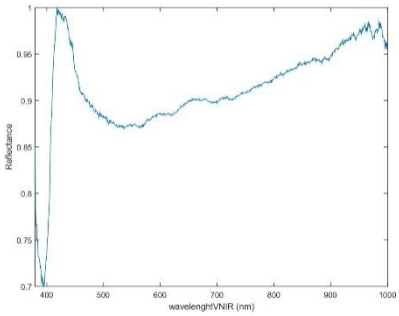

(k)

Figure A52. (a) Obsidian in frontal position. (b) Obsidian in reverse position. (c) Obsidian thickness. (d) Spectral signature calibrated and normalized (Frontal-SWIR-Ref. 99%). (e) Spectral signature calibrated and normalized (Reverse-SWIR-Ref. 99%). (f) Spectral signature calibrated and normalized (Frontal-SWIR-Ref. 10%). (g) Spectral signature calibrated and normalized (Reverse-SWIR-Ref. 10%). (h) Spectral signature calibrated and normalized (Frontal-SWIR-Ref. 50%). (i) Spectral signature calibrated and normalized (Reverse-SWIR-Ref. 50%). (j) Spectral signature calibrated and normalized (Frontal-VNIR-Ref.99%). (k) Spectral signature calibrated and normalized (Reverse-VNIR-Ref.99%).

Table A53. Information about the S54 obsidian.

Original label	Virtual label	Sigla	Group	Weight (g)	Measurement (cm) (Width/Large/Thickness)	Deposit	Municipality	Island
DUM-90	S54	391	HOG		1.1/2.1/0.6	Dunas de Maspalomas	San Bartolomé de Tirajana	Gran Canaria

(a)

(b)

(c)

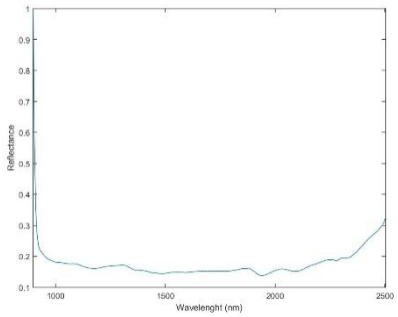

(d)

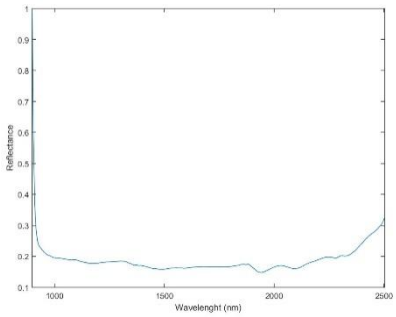

(e)

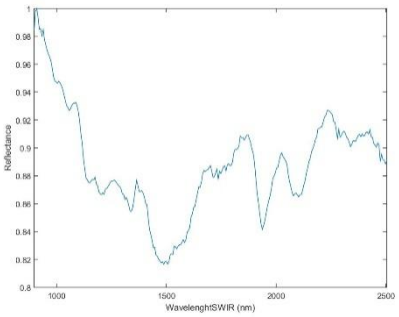

(f)

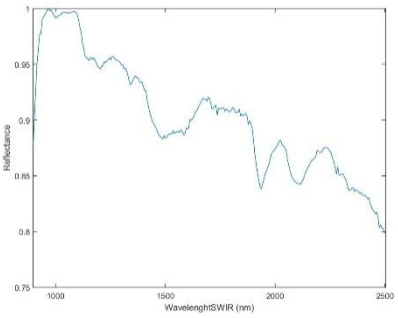

(g)

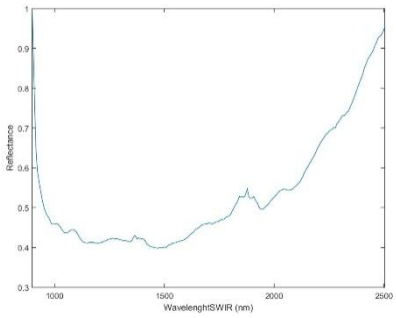

(h)

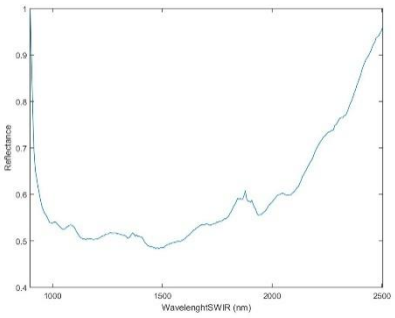

(i)

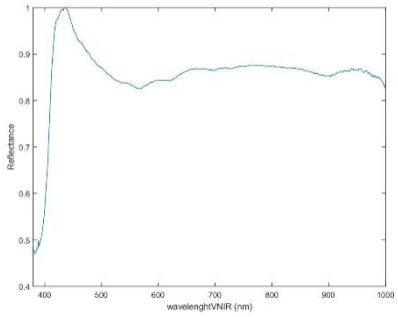

(j)

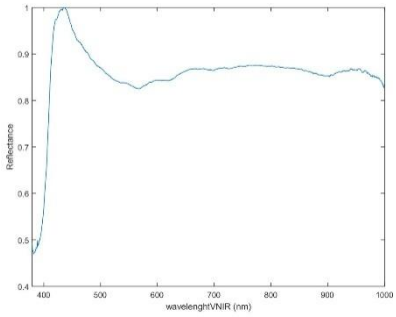

(k)

Figure A53. (a) Obsidian in frontal position. (b) Obsidian in reverse position. (c) Obsidian thickness. (d) Spectral signature calibrated and normalized (Frontal-SWIR-Ref. 99%). (e) Spectral signature calibrated and normalized (Reverse-SWIR-Ref. 99%). (f) Spectral signature calibrated and normalized (Frontal-SWIR-Ref. 10%). (g) Spectral signature calibrated and normalized (Reverse-SWIR-Ref. 10%). (h) Spectral signature calibrated and normalized (Frontal-SWIR-Ref. 50%). (i) Spectral signature calibrated and normalized (Reverse-SWIR-Ref. 50%). (j) Spectral signature calibrated and normalized (Frontal-VNIR-Ref.99%). (k) Spectral signature calibrated and normalized (Reverse-VNIR-Ref.99%).

Table A54. Information about the S55 obsidian.

Original label	Virtual label	Sigla	Group	Weight (g)	Measurement (cm) (Width/Large/Thickness)	Deposit	Municipality	Island
DUM-91	S55	308(1)	HOG		0.85/1.2/0.2	Dunas de Maspalomas	San Bartolomé de Tirajana	Gran Canaria

(a)

(b)

(c)

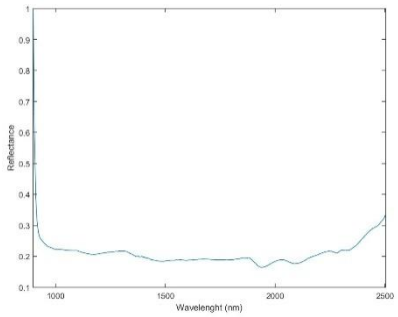

(d)

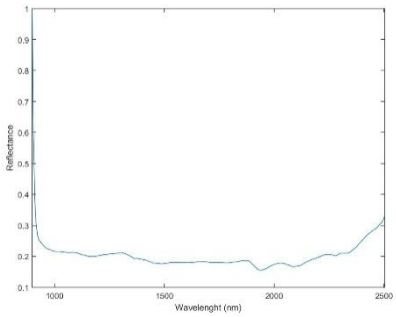

(e)

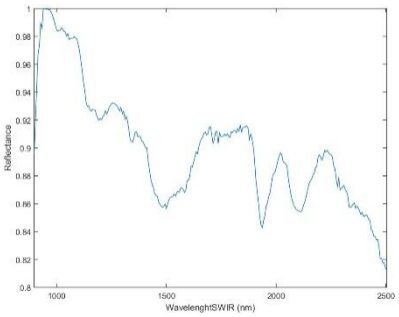

(f)

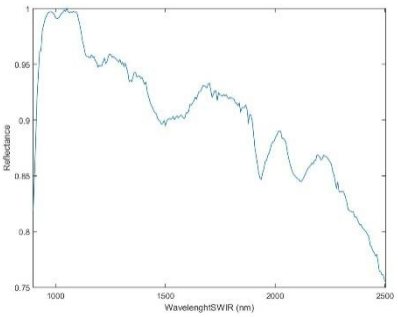

(g)

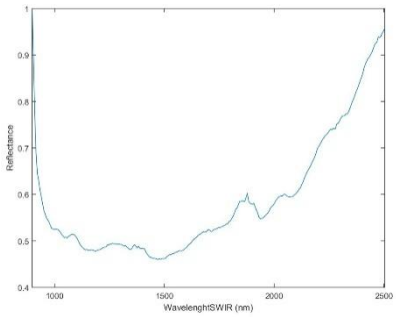

(h)

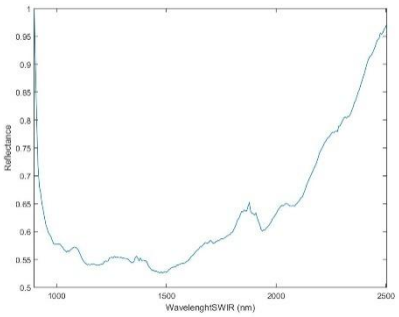

(i)

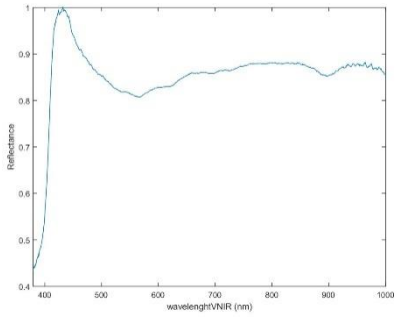

(j)

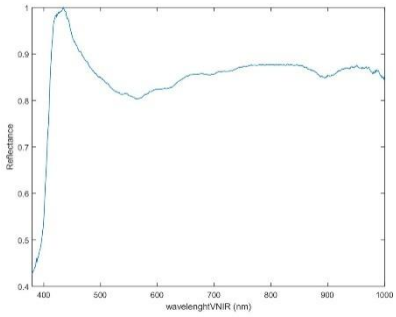

(k)

Figure A54. (a) Obsidian in frontal position. (b) Obsidian in reverse position. (c) Obsidian thickness. (d) Spectral signature calibrated and normalized (Frontal-SWIR-Ref. 99%). (e) Spectral signature calibrated and normalized (Reverse-SWIR-Ref. 99%). (f) Spectral signature calibrated and normalized (Frontal-SWIR-Ref. 10%). (g) Spectral signature calibrated and normalized (Reverse-SWIR-Ref. 10%). (h) Spectral signature calibrated and normalized (Frontal-SWIR-Ref. 50%). (i) Spectral signature calibrated and normalized (Reverse-SWIR-Ref. 50%). (j) Spectral signature calibrated and normalized (Frontal-VNIR-Ref.99%). (k) Spectral signature calibrated and normalized (Reverse-VNIR-Ref.99%).

Table A55. Information about the S56 obsidian.

Original label	Virtual label	Sigla	Group	Weight (g)	Measurement (cm) (Width/Large/Thickness)	Deposit	Municipality	Island
DUM-92	S56	321	N3		0.9/1/0.5	Dunas de Maspalomas	San Bartolomé de Tirajana	Gran Canaria

(a)

(b)

(c)

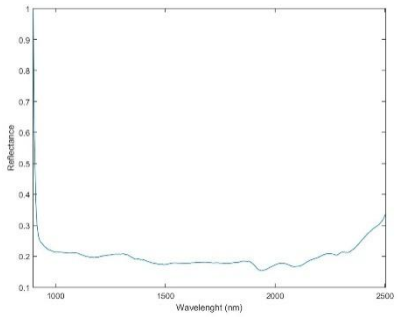

(d)

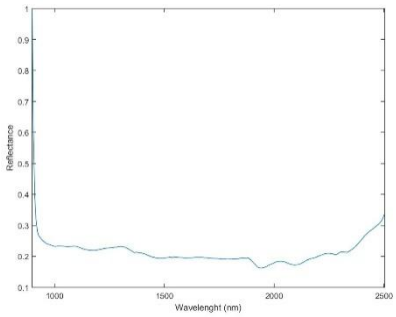

(e)

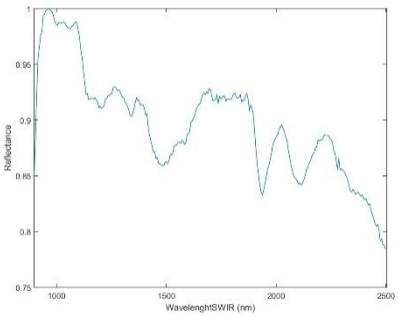

(f)

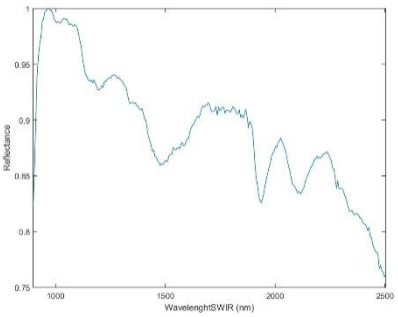

(g)

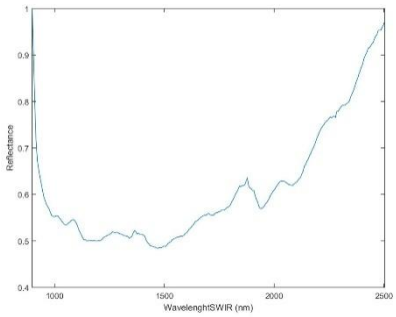

(h)

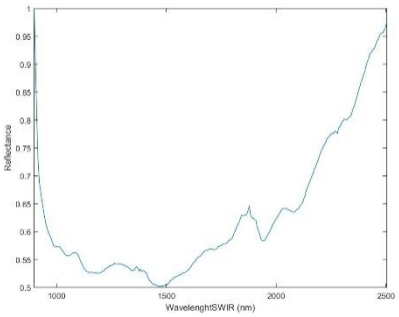

(i)

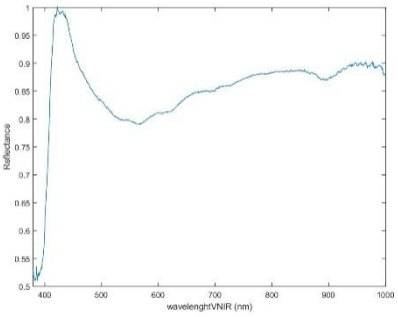

(j)

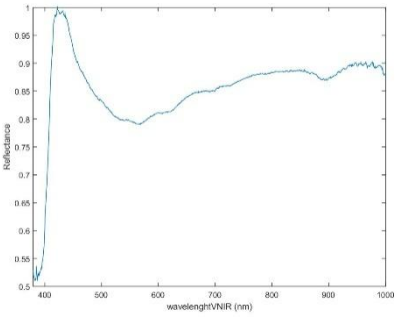

(k)

Figure A55. (a) Obsidian in frontal position. (b) Obsidian in reverse position. (c) Obsidian thickness. (d) Spectral signature calibrated and normalized (Frontal-SWIR-Ref. 99%). (e) Spectral signature calibrated and normalized (Reverse-SWIR-Ref. 99%). (f) Spectral signature calibrated and normalized (Frontal-SWIR-Ref. 10%). (g) Spectral signature calibrated and normalized (Reverse-SWIR-Ref. 10%). (h) Spectral signature calibrated and normalized (Frontal-SWIR-Ref. 50%). (i) Spectral signature calibrated and normalized (Reverse-SWIR-Ref. 50%). (j) Spectral signature calibrated and normalized (Frontal-VNIR-Ref.99%). (k) Spectral signature calibrated and normalized (Reverse-VNIR-Ref.99%).

Table A56. Information about the S57 obsidian.

Original label	Virtual label	Sigla	Group	Weight (g)	Measurement (cm) (Width/Large/Thickness)	Deposit	Municipality	Island
DUM-93	S57	329	OTHERS		0.6/2.8/0.15	Dunas de Maspalomas	San Bartolomé de Tirajana	Gran Canaria

(a)

(b)

(c)

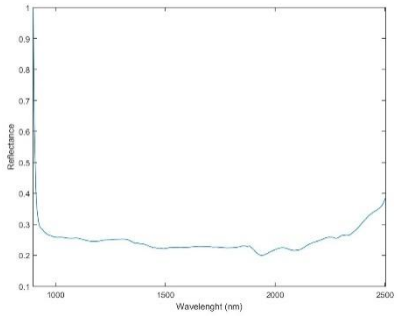

(d)

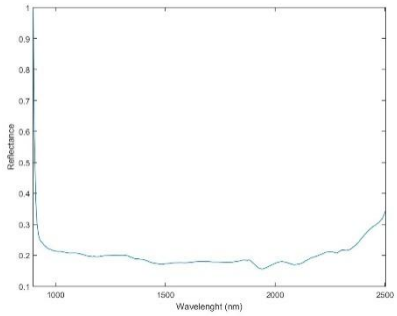

(e)

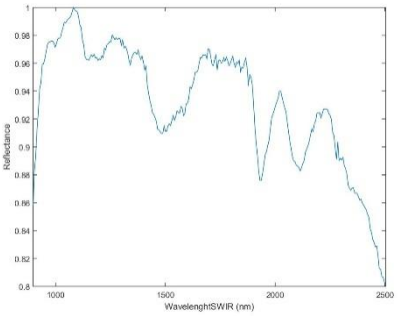

(f)

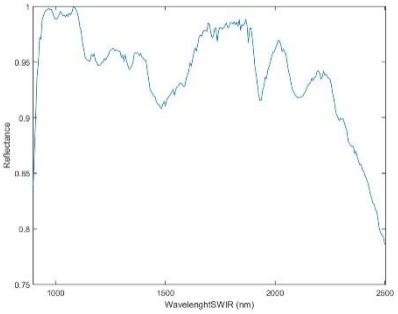

(g)

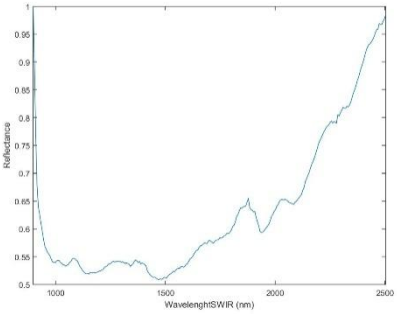

(h)

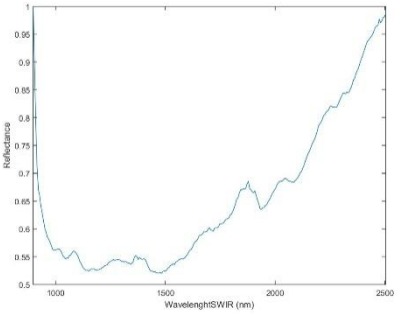

(i)

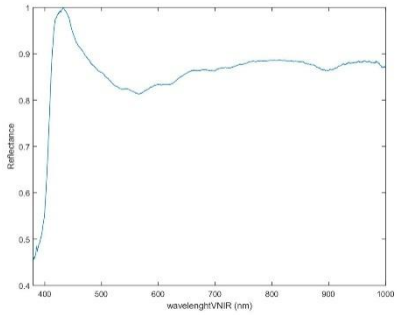

(j)

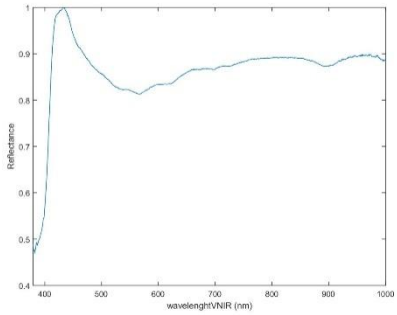

(k)

Figure A56. (a) Obsidian in frontal position. (b) Obsidian in reverse position. (c) Obsidian thickness. (d) Spectral signature calibrated and normalized (Frontal-SWIR-Ref. 99%). (e) Spectral signature calibrated and normalized (Reverse-SWIR-Ref. 99%). (f) Spectral signature calibrated and normalized (Frontal-SWIR-Ref. 10%). (g) Spectral signature calibrated and normalized (Reverse-SWIR-Ref. 10%). (h) Spectral signature calibrated and normalized (Frontal-SWIR-Ref. 50%). (i) Spectral signature calibrated and normalized (Reverse-SWIR-Ref. 50%). (j) Spectral signature calibrated and normalized (Frontal-VNIR-Ref.99%). (k) Spectral signature calibrated and normalized (Reverse-VNIR-Ref.99%).

Table A57. Information about the S58 obsidian.

Original label	Virtual label	Sigla	Group	Weight (g)	Measurement (cm) (Width/Large/Thickness)	Deposit	Municipality	Island
CHA-33	S58	2486	TAB		1/1.5/0.5	Chasogo	Guía de Isora	Tenerife

(a)

(b)

(c)

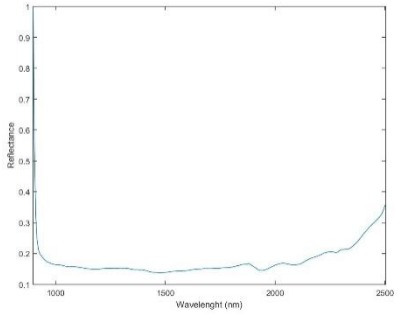

(d)

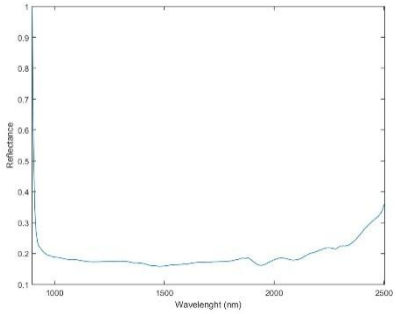

(e)

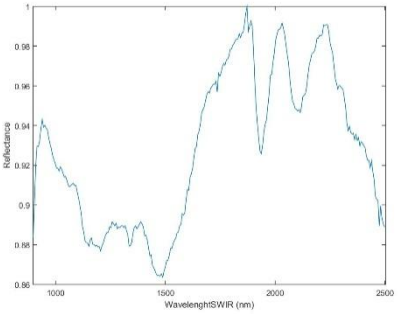

(f)

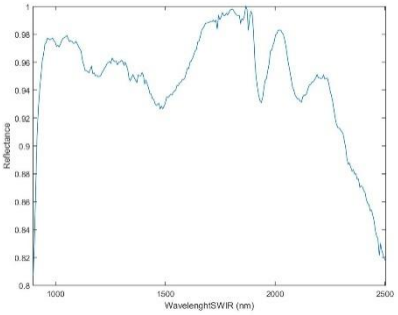

(g)

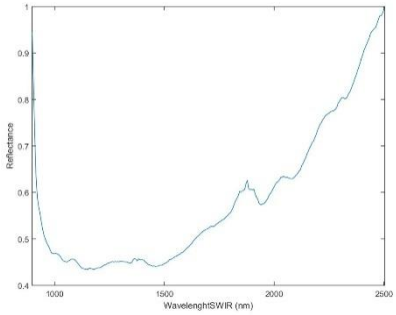

(h)

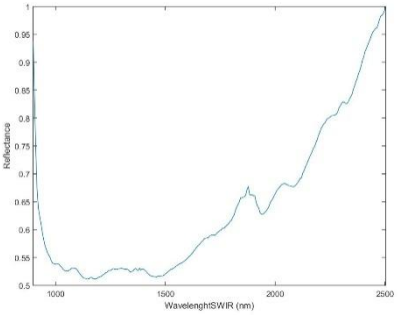

(i)

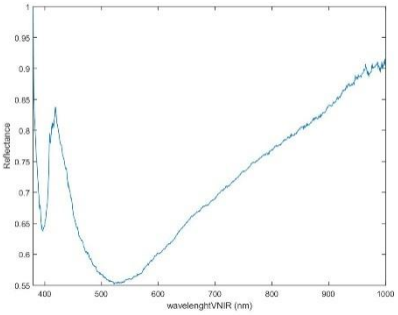

(j)

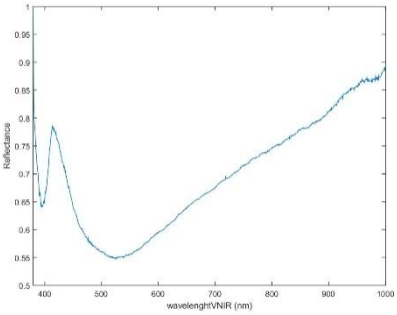

(k)

Figure A57. (a) Obsidian in frontal position. (b) Obsidian in reverse position. (c) Obsidian thickness. (d) Spectral signature calibrated and normalized (Frontal-SWIR-Ref. 99%). (e) Spectral signature calibrated and normalized (Reverse-SWIR-Ref. 99%). (f) Spectral signature calibrated and normalized (Frontal-SWIR-Ref. 10%). (g) Spectral signature calibrated and normalized (Reverse-SWIR-Ref. 10%). (h) Spectral signature calibrated and normalized (Frontal-SWIR-Ref. 50%). (i) Spectral signature calibrated and normalized (Reverse-SWIR-Ref. 50%). (j) Spectral signature calibrated and normalized (Frontal-VNIR-Ref.99%). (k) Spectral signature calibrated and normalized (Reverse-VNIR-Ref.99%).

Table A58. Information about the S59 obsidian.

Original label	Virtual label	Sigla	Group	Weight (g)	Measurement (cm) (Width/Large/Thickness)	Deposit	Municipality	Island
CHA-28	S59	968	TAB		1.2/2.8/0.5	Chasogo	Guía de Isora	Tenerife

(a)

(b)

(c)

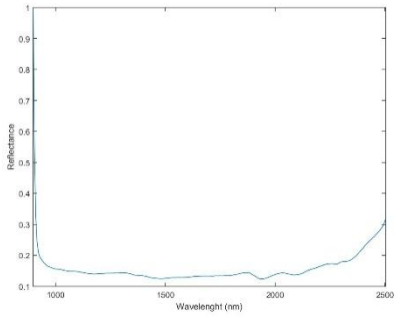

(d)

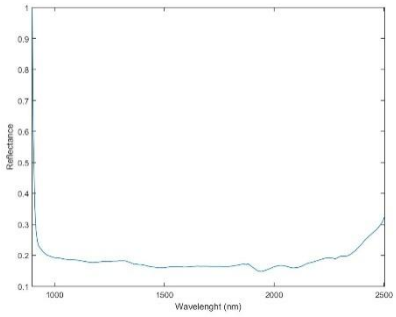

(e)

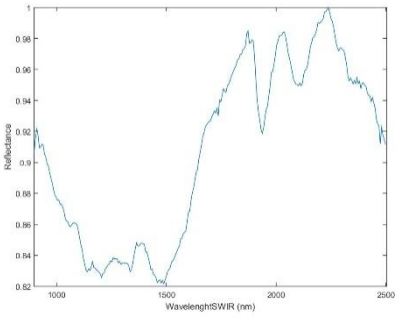

(f)

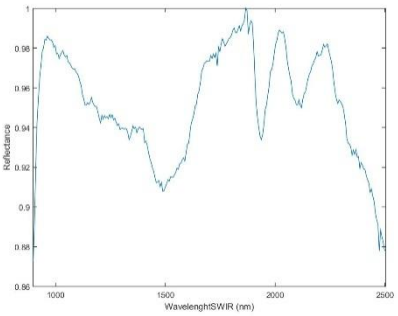

(g)

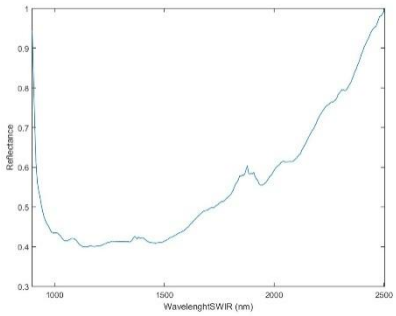

(h)

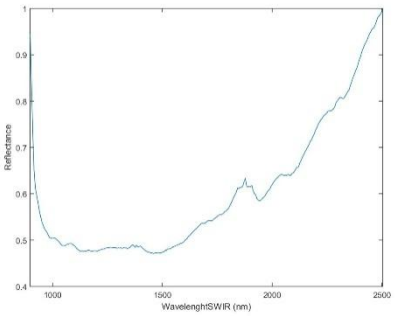

(i)

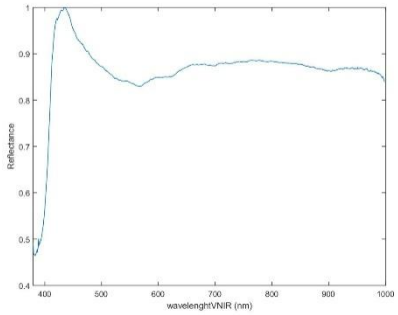

(j)

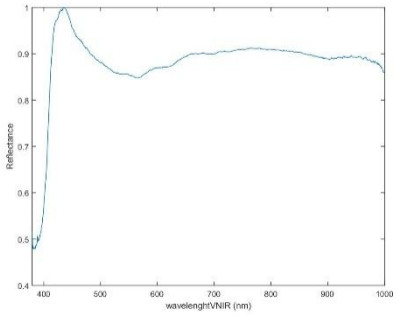

(k)

Figure A58. (a) Obsidian in frontal position. (b) Obsidian in reverse position. (c) Obsidian thickness. (d) Spectral signature calibrated and normalized (Frontal-SWIR-Ref. 99%). (e) Spectral signature calibrated and normalized (Reverse-SWIR-Ref. 99%). (f) Spectral signature calibrated and normalized (Frontal-SWIR-Ref. 10%). (g) Spectral signature calibrated and normalized (Reverse-SWIR-Ref. 10%). (h) Spectral signature calibrated and normalized (Frontal-SWIR-Ref. 50%). (i) Spectral signature calibrated and normalized (Reverse-SWIR-Ref. 50%). (j) Spectral signature calibrated and normalized (Frontal-VNIR-Ref.99%). (k) Spectral signature calibrated and normalized (Reverse-VNIR-Ref.99%).

Table A59. Information about the S60 obsidian.

Original label	Virtual label	Sigla	Group	Weight (g)	Measurement (cm) (Width/Large/Thickness)	Deposit	Municipality	Island
CHA-36	S60	2979	TAB		1.6/1.6/0.3	Chasogo	Guía de Isora	Tenerife

(a)

(b)

(c)

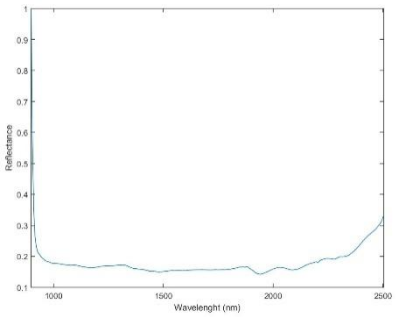

(d)

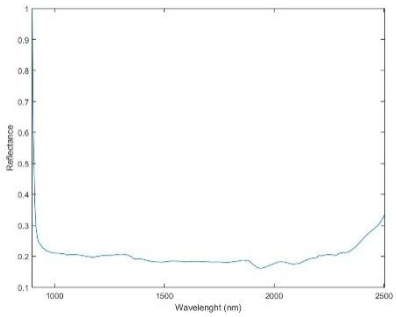

(e)

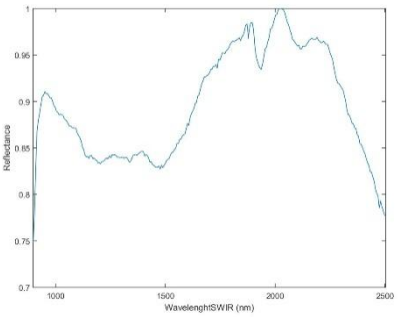

(f)

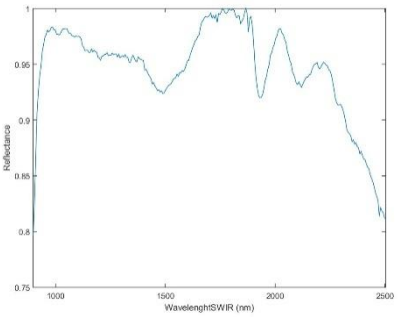

(g)

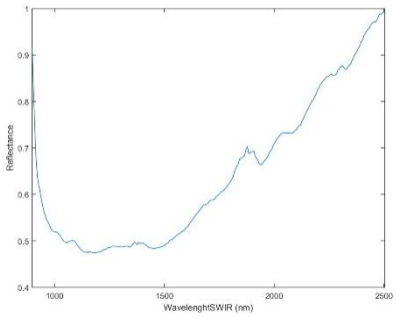

(h)

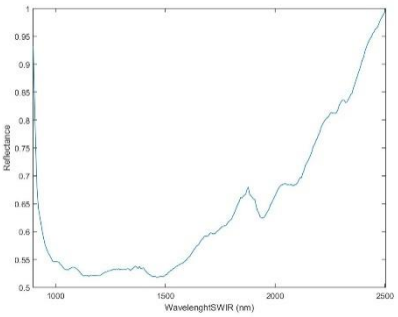

(i)

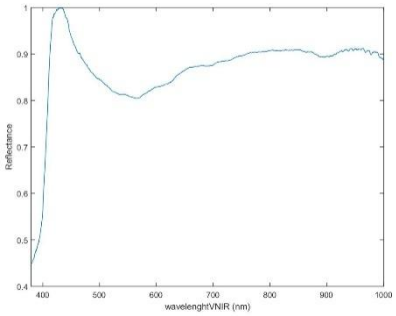

(j)

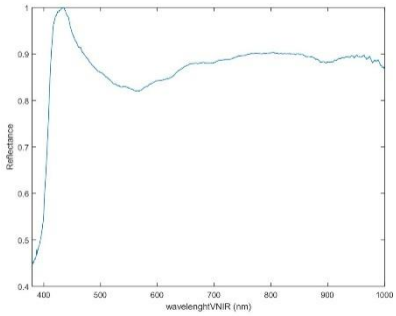

(k)

Figure A59. (a) Obsidian in frontal position. (b) Obsidian in reverse position. (c) Obsidian thickness. (d) Spectral signature calibrated and normalized (Frontal-SWIR-Ref. 99%). (e) Spectral signature calibrated and normalized (Reverse-SWIR-Ref. 99%). (f) Spectral signature calibrated and normalized (Frontal-SWIR-Ref. 10%). (g) Spectral signature calibrated and normalized (Reverse-SWIR-Ref. 10%). (h) Spectral signature calibrated and normalized (Frontal-SWIR-Ref. 50%). (i) Spectral signature calibrated and normalized (Reverse-SWIR-Ref. 50%). (j) Spectral signature calibrated and normalized (Frontal-VNIR-Ref.99%). (k) Spectral signature calibrated and normalized (Reverse-VNIR-Ref.99%).

Table A60. Information about the S61 obsidian.

Original label	Virtual label	Sigla	Group	Weight (g)	Measurement (cm) (Width/Large/Thickness)	Deposit	Municipality	Island
CHA-39	S61	2229	TAB		1.6/1.6/0.2	Chasogo	Guía de Isora	Tenerife

(a)

(b)

(c)

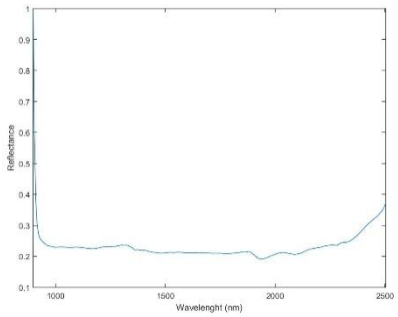

(d)

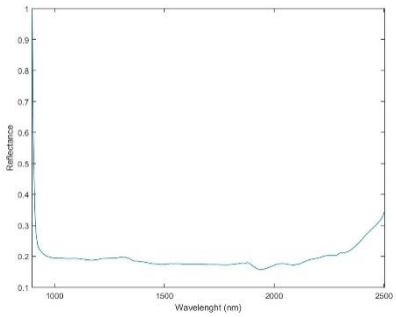

(e)

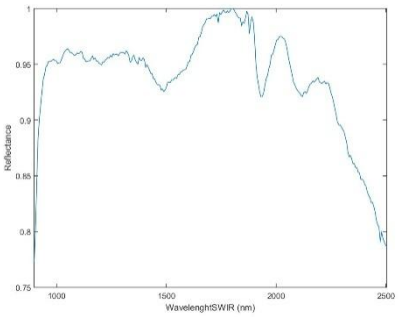

(f)

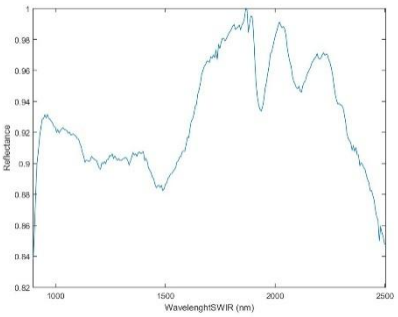

(g)

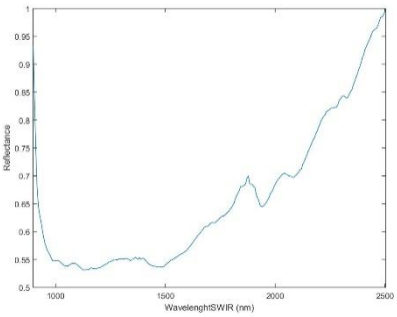

(h)

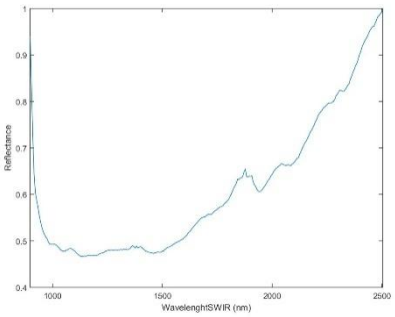

(i)

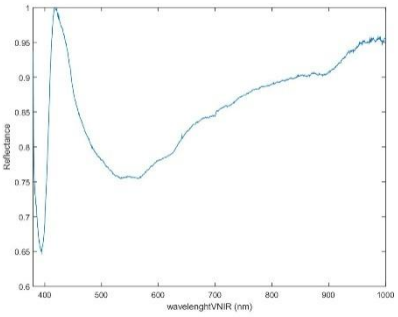

(j)

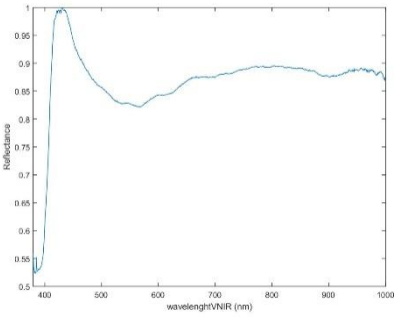

(k)

Figure A60. (a) Obsidian in frontal position. (b) Obsidian in reverse position. (c) Obsidian thickness. (d) Spectral signature calibrated and normalized (Frontal-SWIR-Ref. 99%). (e) Spectral signature calibrated and normalized (Reverse-SWIR-Ref. 99%). (f) Spectral signature calibrated and normalized (Frontal-SWIR-Ref. 10%). (g) Spectral signature calibrated and normalized (Reverse-SWIR-Ref. 10%). (h) Spectral signature calibrated and normalized (Frontal-SWIR-Ref. 50%). (i) Spectral signature calibrated and normalized (Reverse-SWIR-Ref. 50%). (j) Spectral signature calibrated and normalized (Frontal-VNIR-Ref.99%). (k) Spectral signature calibrated and normalized (Reverse-VNIR-Ref.99%).

Table A61. Information about the S62 obsidian.

Original label	Virtual label	Sigla	Group	Weight (g)	Measurement (cm) (Width/Large/Thickness)	Deposit	Municipality	Island
CHA-31	S62	2461	TAB		1/1.7/0.4	Chasogo	Guía de Isora	Tenerife

(a)

(b)

(c)

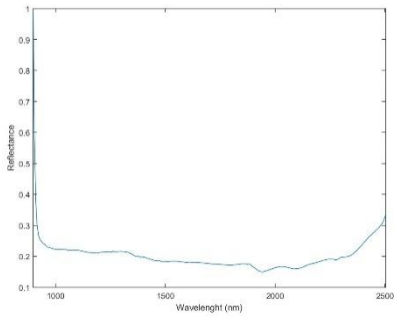

(d)

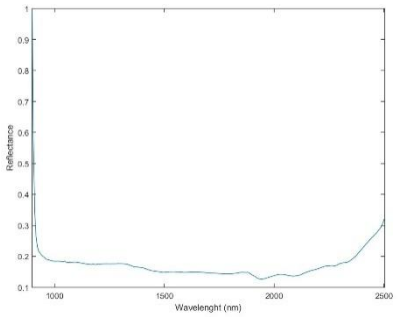

(e)

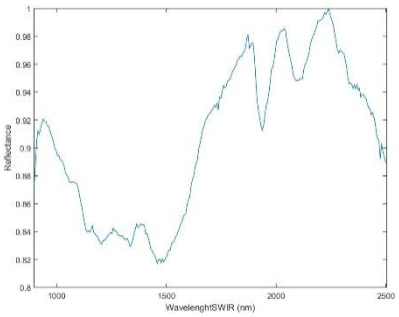

(f)

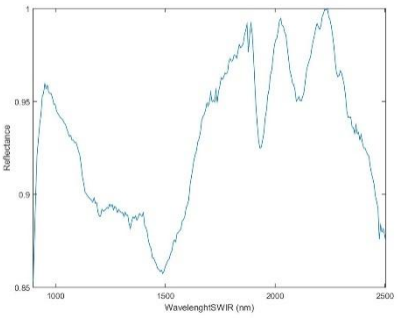

(g)

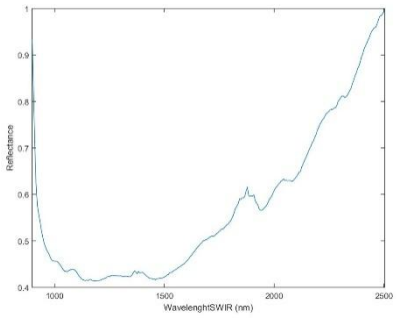

(h)

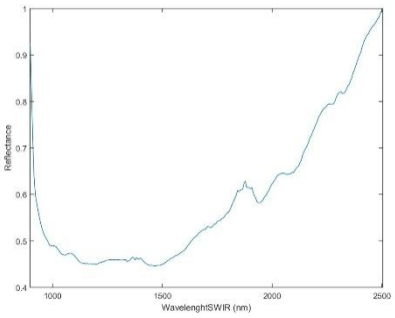

(i)

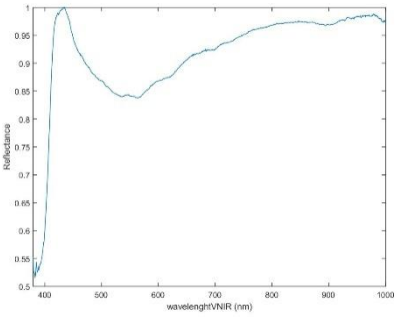

(j)

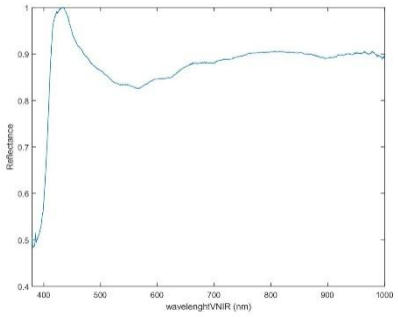

(k)

Figure A61. (a) Obsidian in frontal position. (b) Obsidian in reverse position. (c) Obsidian thickness. (d) Spectral signature calibrated and normalized (Frontal-SWIR-Ref. 99%). (e) Spectral signature calibrated and normalized (Reverse-SWIR-Ref. 99%). (f) Spectral signature calibrated and normalized (Frontal-SWIR-Ref. 10%). (g) Spectral signature calibrated and normalized (Reverse-SWIR-Ref. 10%). (h) Spectral signature calibrated and normalized (Frontal-SWIR-Ref. 50%). (i) Spectral signature calibrated and normalized (Reverse-SWIR-Ref. 50%). (j) Spectral signature calibrated and normalized (Frontal-VNIR-Ref.99%). (k) Spectral signature calibrated and normalized (Reverse-VNIR-Ref.99%).

Table A62. Information about the S63 obsidian.

Original label	Virtual label	Sigla	Group	Weight (g)	Measurement (cm) (Width/Large/Thickness)	Deposit	Municipality	Island
CHA-27	S63	565	TAB		1.4/1.5/0.6	Chasogo	Guía de Isora	Tenerife

(a)

(b)

(c)

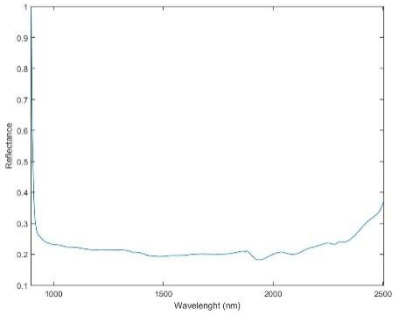

(d)

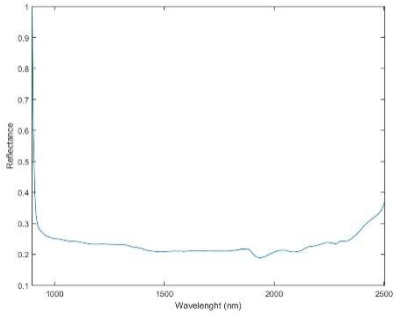

(e)

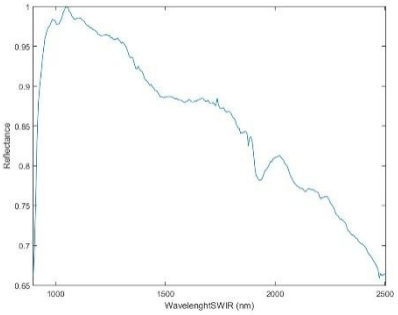

(f)

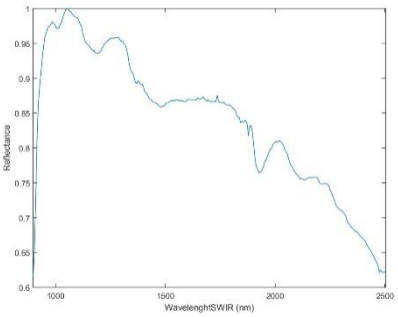

(g)

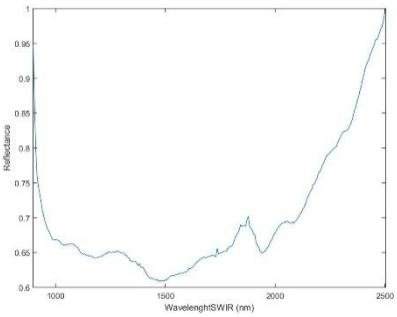

(h)

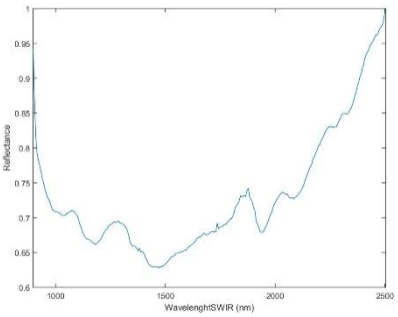

(i)

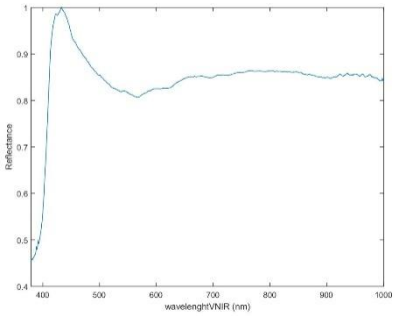

(j)

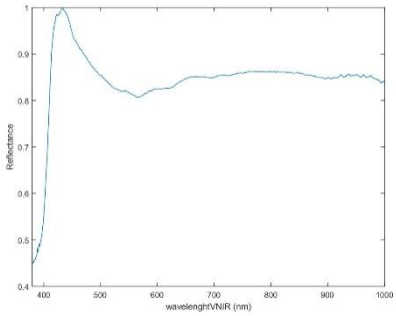

(k)

Figure A62. (a) Obsidian in frontal position. (b) Obsidian in reverse position. (c) Obsidian thickness. (d) Spectral signature calibrated and normalized (Frontal-SWIR-Ref. 99%). (e) Spectral signature calibrated and normalized (Reverse-SWIR-Ref. 99%). (f) Spectral signature calibrated and normalized (Frontal-SWIR-Ref. 10%). (g) Spectral signature calibrated and normalized (Reverse-SWIR-Ref. 10%). (h) Spectral signature calibrated and normalized (Frontal-SWIR-Ref. 50%). (i) Spectral signature calibrated and normalized (Reverse-SWIR-Ref. 50%). (j) Spectral signature calibrated and normalized (Frontal-VNIR-Ref.99%). (k) Spectral signature calibrated and normalized (Reverse-VNIR-Ref.99%).

Table A63. Information about the S64 obsidian.

Original label	Virtual label	Sigla	Group	Weight (g)	Measurement (cm) (Width/Large/Thickness)	Deposit	Municipality	Island
CHA-30	S64	885	TAB		0.6/1.6/0.15	Chasogo	Guía de Isora	Tenerife

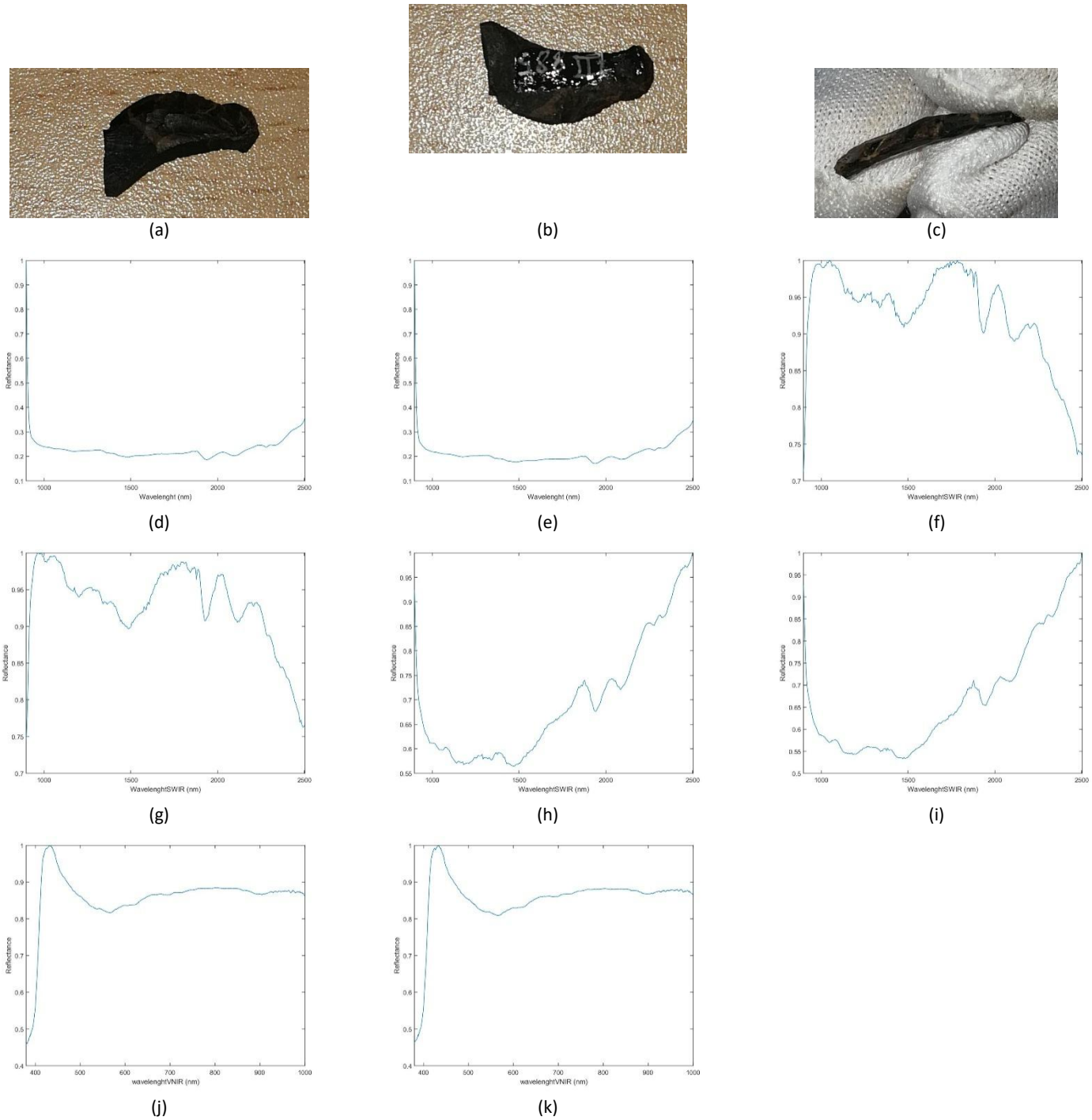

Figure A63. (a) Obsidian in frontal position. (b) Obsidian in reverse position. (c) Obsidian thickness. (d) Spectral signature calibrated and normalized (Frontal-SWIR-Ref. 99%). (e) Spectral signature calibrated and normalized (Reverse-SWIR-Ref. 99%). (f) Spectral signature calibrated and normalized (Frontal-SWIR-Ref. 10%). (g) Spectral signature calibrated and normalized (Reverse-SWIR-Ref. 10%). (h) Spectral signature calibrated and normalized (Frontal-SWIR-Ref. 50%). (i) Spectral signature calibrated and normalized (Reverse-SWIR-Ref. 50%). (j) Spectral signature calibrated and normalized (Frontal-VNIR-Ref.99%). (k) Spectral signature calibrated and normalized (Reverse-VNIR-Ref.99%).

Table A64. Information about the S65 and S66 obsidians.

Original label	Virtual label	Sigla	Group	Weight (g)	Measurement (cm) (Width/Large/Thickness)	Deposit	Municipality	Island
CHA-35	S65	4584	TAB		1.8/2/.07	Chasogo	Guía de Isora	Tenerife
	S66				0.8/1.2/0.15			

(a)

(b)

(c)

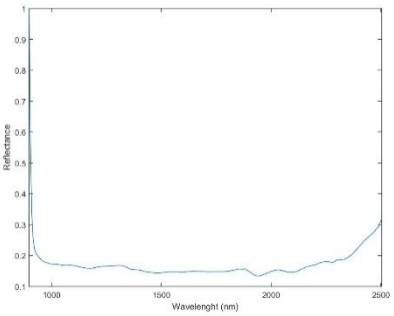

(d)

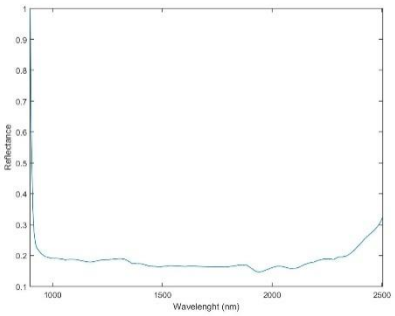

(e)

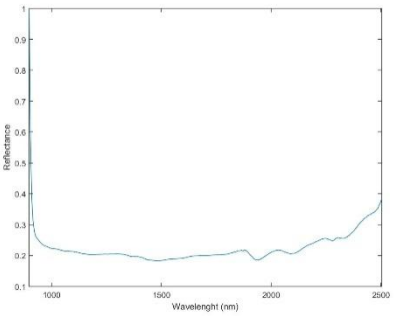

(f)

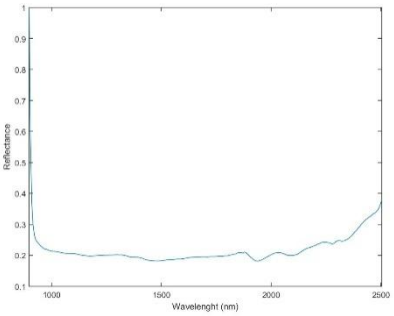

(g)

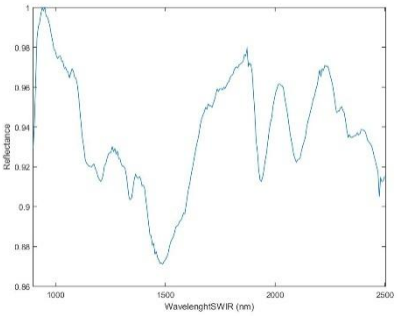

(h)

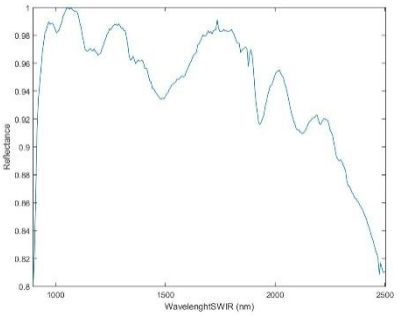

(i)

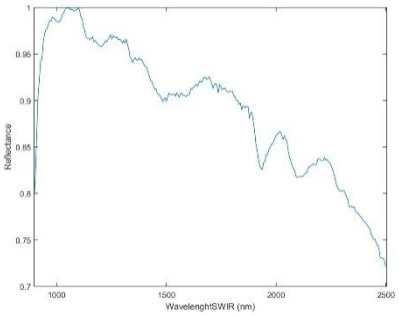

(j)

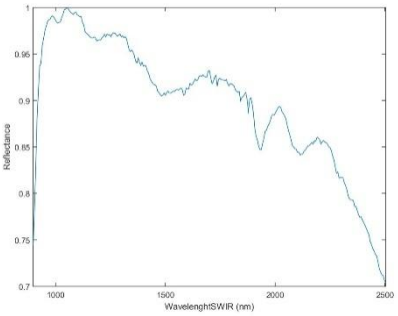

(k)

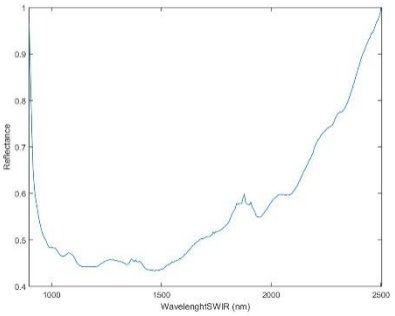

(l)

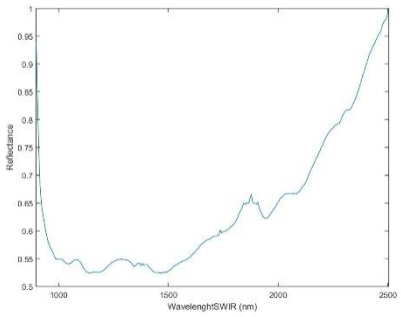

(m)

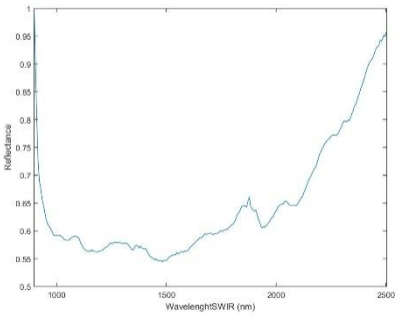

(n)

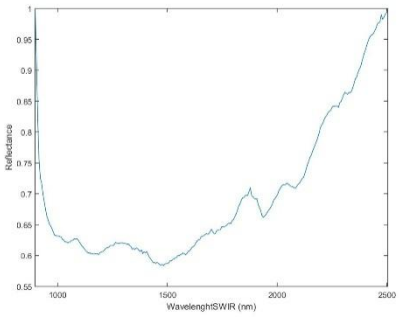

(o)

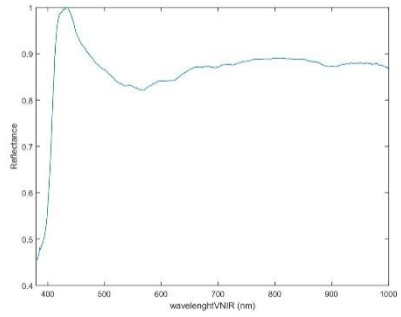

(p)

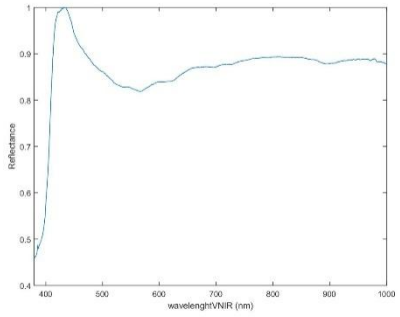

(q)

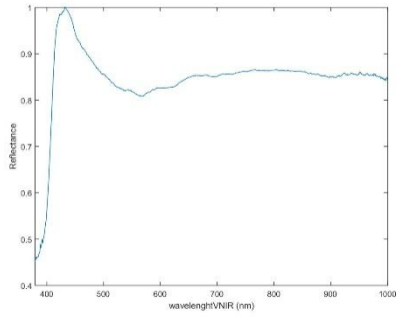

(r)

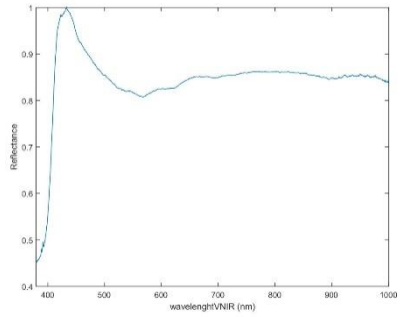

(s)

Figure A64. (a) Obsidian in frontal position. (b) Obsidian in reverse position. (c) Obsidian thickness (d) Spectral signature calibrated and normalized (Frontal-S65-SWIR-Ref. 99%). (e) Spectral signature calibrated and normalized (Reverse-S65-SWIR-Ref. 99%). (f) Spectral signature calibrated and normalized (Frontal-S66-SWIR-Ref. 99%). (g) Spectral signature calibrated and normalized (Reverse-S66-SWIR-Ref. 99%). (h) Spectral signature calibrated and normalized (Frontal-S65-SWIR-Ref. 10%). (i) Spectral signature calibrated and normalized (Reverse-S65-SWIR-Ref. 10%). (j) Spectral signature calibrated and normalized (Frontal-S66-SWIR-Ref. 10%). (k) Spectral signature calibrated and normalized (Reverse-S66-SWIR-Ref. 10%). (l) Spectral signature calibrated and normalized (Frontal-S65-SWIR-Ref. 50%). (m) Spectral signature calibrated and normalized (Reverse-S65-SWIR-Ref. 50%). (n) Spectral signature calibrated and normalized (Frontal-S66-SWIR-Ref. 50%). (o) Spectral signature calibrated and normalized (Reverse-S66-SWIR-Ref. 50%). (p) Spectral signature calibrated and normalized (Frontal-S65-VNIR-Ref. 99%). (q) Spectral signature calibrated and normalized (Reverse-S65-VNIR-Ref. 99%). (r) Spectral signature calibrated and normalized (Frontal-S66-VNIR-Ref. 99%). (s) Spectral signature calibrated and normalized (Reverse-S66-VNIR-Ref. 99%).

Table A65. Information about the S69 obsidian.

Original label	Virtual label	Sigla	Group	Weight (g)	Measurement (cm) (Width/Large/Thickness)	Deposit	Municipality	Island
TAB-1(1)	S69	-	TAB		5.5/6.3/4.4	La Guancha	La Tabona	Tenerife

(a)

(b)

(c)

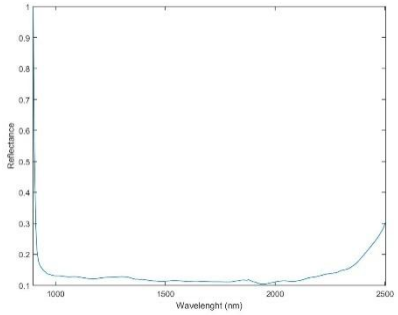

(d)

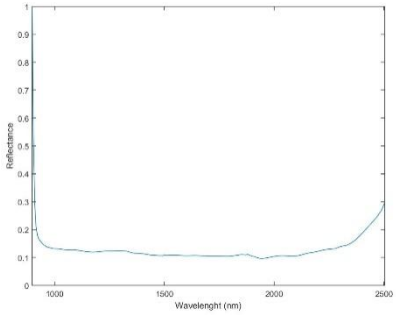

(e)

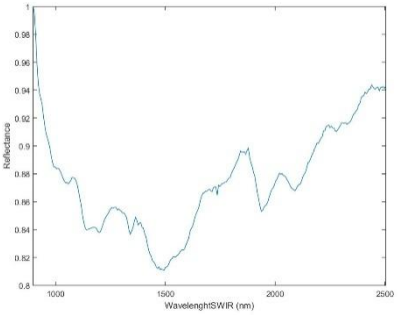

(f)

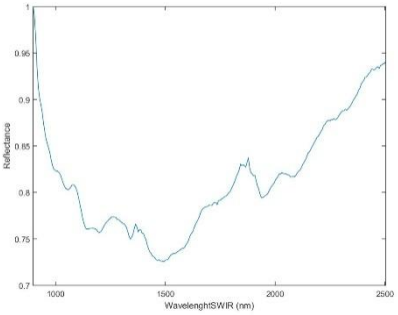

(g)

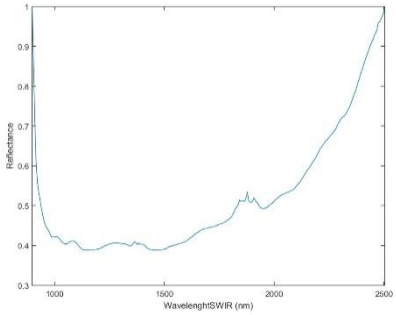

(h)

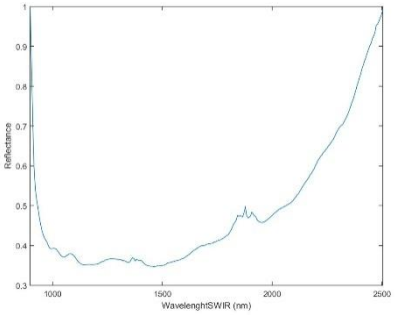

(i)

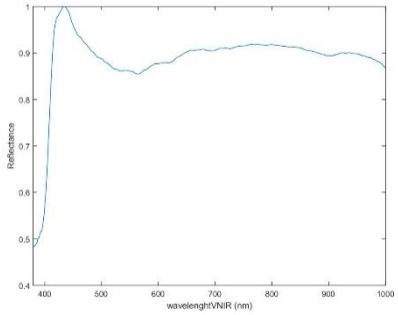

(j)

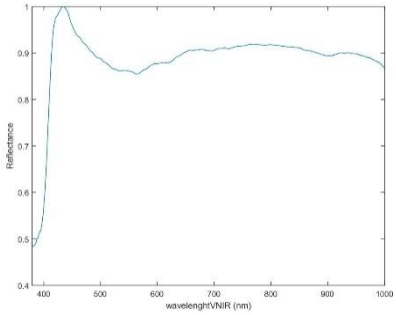

(k)

Figure A65. (a) Obsidian in frontal position. (b) Obsidian in reverse position. (c) Obsidian thickness. (d) Spectral signature calibrated and normalized (Frontal-SWIR-Ref. 99%). (e) Spectral signature calibrated and normalized (Reverse-SWIR-Ref. 99%). (f) Spectral signature calibrated and normalized (Frontal-SWIR-Ref. 10%). (g) Spectral signature calibrated and normalized (Reverse-SWIR-Ref. 10%). (h) Spectral signature calibrated and normalized (Frontal-SWIR-Ref. 50%). (i) Spectral signature calibrated and normalized (Reverse-SWIR-Ref. 50%). (j) Spectral signature calibrated and normalized (Frontal-VNIR-Ref.99%). (k) Spectral signature calibrated and normalized (Reverse-VNIR-Ref.99%).

Table A66. Information about the S68 obsidian.

Original label	Virtual label	Sigla	Group	Weight (g)	Measurement (cm) (Width/Large/Thickness)	Deposit	Municipality	Island
TAB-1(2)	S68	-	TAB		2.2/3/0.4	La Guancha	La Tabona	Tenerife

(a)

(b)

(c)

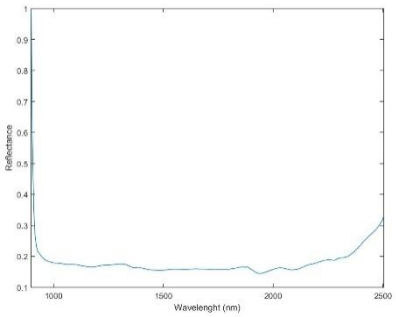

(d)

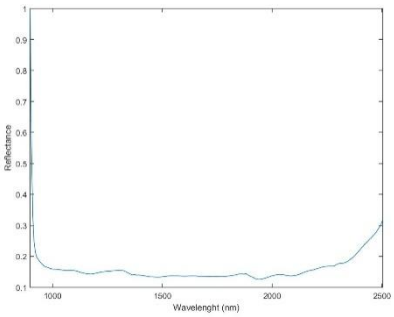

(e)

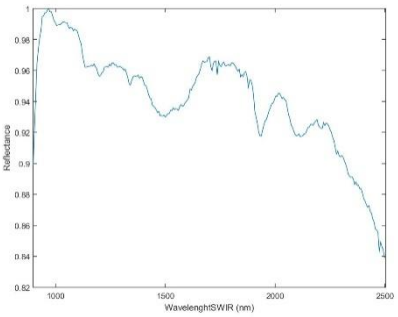

(f)

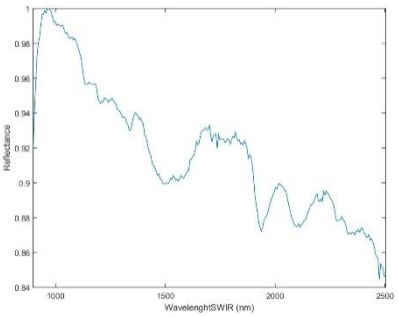

(g)

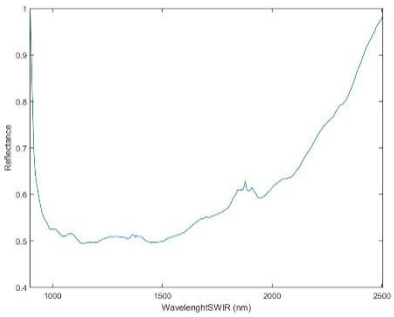

(h)

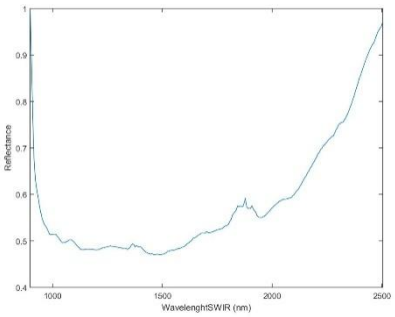

(i)

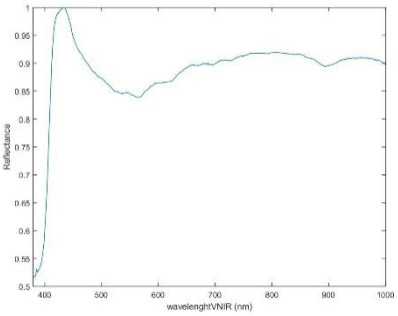

(j)

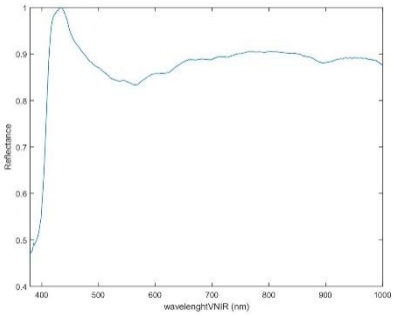

(k)

Figure A66. (a) Obsidian in frontal position. (b) Obsidian in reverse position. (c) Obsidian thickness. (d) Spectral signature calibrated and normalized (Frontal-SWIR-Ref. 99%). (e) Spectral signature calibrated and normalized (Reverse-SWIR-Ref. 99%). (f) Spectral signature calibrated and normalized (Frontal-SWIR-Ref. 10%). (g) Spectral signature calibrated and normalized (Reverse-SWIR-Ref. 10%). (h) Spectral signature calibrated and normalized (Frontal-SWIR-Ref. 50%). (i) Spectral signature calibrated and normalized (Reverse-SWIR-Ref. 50%). (j) Spectral signature calibrated and normalized (Frontal-VNIR-Ref.99%). (k) Spectral signature calibrated and normalized (Reverse-VNIR-Ref.99%).

Table A67. Information about the S67 obsidian.

Original label	Virtual label	Sigla	Group	Weight (g)	Measurement (cm) (Width/Large/Thickness)	Deposit	Municipality	Island
TAB-1(3)	S67	-	TAB		1.3/3.7/0.5	La Guancha	La Tabona	Tenerife

(a)

(b)

(c)

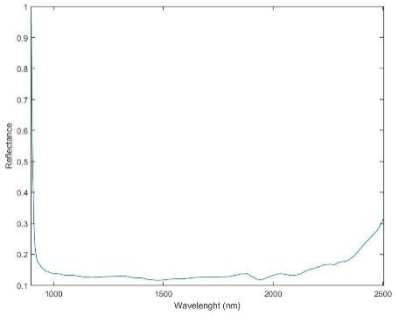

(d)

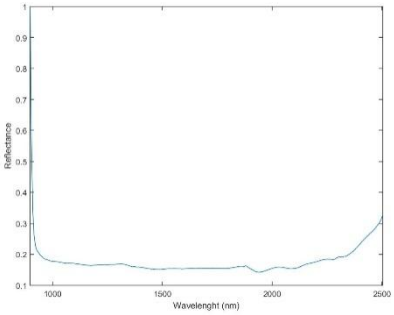

(e)

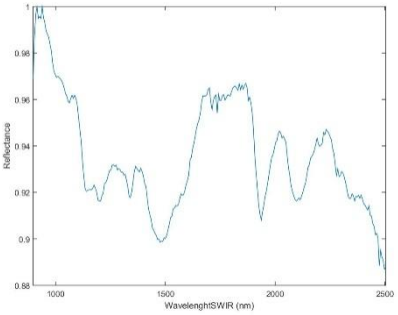

(f)

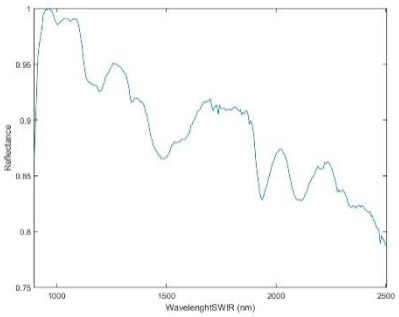

(g)

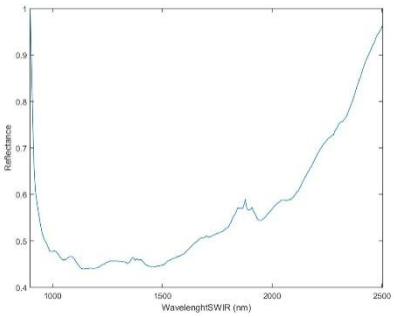

(h)

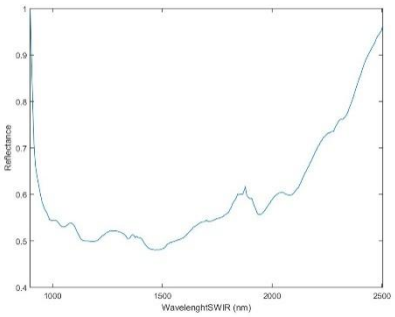

(i)

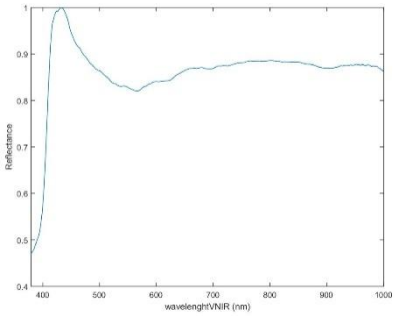

(j)

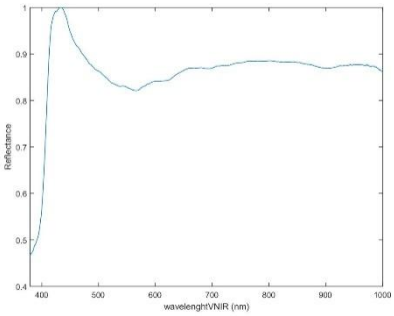

(k)

Figure A67. (a) Obsidian in frontal position. (b) Obsidian in reverse position. (c) Obsidian thickness. (d) Spectral signature calibrated and normalized (Frontal-SWIR-Ref. 99%). (e) Spectral signature calibrated and normalized (Reverse-SWIR-Ref. 99%). (f) Spectral signature calibrated and normalized (Frontal-SWIR-Ref. 10%). (g) Spectral signature calibrated and normalized (Reverse-SWIR-Ref. 10%). (h) Spectral signature calibrated and normalized (Frontal-SWIR-Ref. 50%). (i) Spectral signature calibrated and normalized (Reverse-SWIR-Ref. 50%). (j) Spectral signature calibrated and normalized (Frontal-VNIR-Ref.99%). (k) Spectral signature calibrated and normalized (Reverse-VNIR-Ref.99%).

ANEXX II

The all classification results

This Annex II presents the results of classification process in each phase.

1. Phase 1: classification results to choose the best white reference and the best classifier to continue in the next phase.

1.1 SVM with linear kernel (LIBSVM).

Table B1. Results obtained in the experiment 1 without to optimize the parameters in SVM classifier with linear kernel and LIBSVM library.

Obsidian Position	Level	Accuracy Ref 10%	Simulation time (h)	Accuracy Ref 50%	Simulation time (h)	Accuracy Ref 99%	Simulation time (h)
Frontal	Island	90.97%	0.20	89.69%	0.22	65.50%	0.51
	Municipality	63.19%	0.49	54.66%	0.49	33.41%	0.78
	Deposit	63.48%	0.51	54.64%	0.41	33.44%	0.94
Reverse	Island	89.21%	0.16	88.11%	0.16	69.25%	0.42
	Municipality	66.53%	0.31	58.28%	0.33	33.29%	0.71
	Deposit	65.62%	0.32	57.35%	0.43	33.23%	0.79
Frontal + Reverse	Island	90.21%	0.65	89.05%	0.66	66.93%	1.70
	Municipality	67.35%	1.33	58.71%	1.43	33.21%	2.99
	Deposit	67.78%	1.31	57.87%	1.49	33.46%	3.54

Table B2. Results obtained in the experiment 2 without to optimize the parameters in SVM classifier with linear kernel and LIBSVM library.

Obsidian Position	Obsidian sample	Accuracy (%)			Simulation Time (h)		
		Island	Municipality	Deposit	Island	Municipality	Deposit
Frontal + Reverse	1	75.69	39.45	37.61	0.35	0.69	0.74
Frontal + Reverse	2	73.33	47.22	35.56	0.35	0.69	0.68
Frontal + Reverse	3	76.51	40.94	32.89	0.35	0.69	0.68
Frontal + Reverse	4	72.73	45.45	35.54	0.34	0.70	0.69
Frontal + Reverse	5	70.14	29,17	26.39	0.34	0.69	0.68
Frontal + Reverse	6	69.75	20.99	22.22	0.34	0.70	0.68
Frontal + Reverse	7	68.98	32.12	31.02	0.34	0.69	0.68
Frontal + Reverse	8	71.30	48.15	47.22	0.34	0.69	0.68
Frontal + Reverse	9	67.35	36.05	36.73	0.34	0.69	0.68
Frontal + Reverse	10	70.18	33.33	37.72	0.34	0.69	0.69
Frontal + Reverse	11	78.53	36.20	33.13	0.34	0.69	0.69
Frontal + Reverse	12	78.83	49.64	46.72	0.35	0.69	0.68
Frontal + Reverse	13	80.95	47.06	47.06	0.35	0.69	0.68
Frontal + Reverse	14	83.18	40.84	39.94	0.34	0.69	0.68
Frontal + Reverse	15	73.50	50.43	47.01	0.35	0.70	0.69
Frontal + Reverse	16	75.00	44.85	42.28	0.34	0.69	0.68
Frontal + Reverse	17	73.10	10.15	34.52	0.34	0.69	0.68
Frontal + Reverse	18	83.19	0	12.15	0.34	0.67	0.67
Frontal + Reverse	19	89.49	0	13.23	0.34	0.66	0.66
Frontal + Reverse	20	75.76	3.37	0	0.34	0.66	0.66
Frontal + Reverse	21	54.79	1.18	0	0.34	0.67	0.66
Frontal + Reverse	22	66.02	1.41	0	0.34	0.67	0.66
Frontal + Reverse	23	39.34	2.90	0	0.34	0.68	0.67
Frontal + Reverse	24	55.04	0	0	0.34	0.68	0.68
Frontal + Reverse	25	71.97	0	0	0.34	0.68	0.68
Frontal + Reverse	26	72.80	0	0	0.33	0.69	0.68

Frontal + Reverse	27	70.03	15.40	14.67	0.34	0.64	0.64
Frontal + Reverse	28	79.80	23.27	18.98	0.33	0.68	0.67
Frontal + Reverse	29	84.31	12.04	12.44	0.30	0.64	0.63
Frontal + Reverse	30	80.63	63.81	67.12	0.35	0.58	0.58
Frontal + Reverse	31	63.70	0	0	0.35	0.69	0.68
Frontal + Reverse	32	71.43	0	0	0.34	0.69	0.68
Frontal + Reverse	33	65.92	0	0	0.34	0.69	0.68
Frontal + Reverse	34	55.17	0	0	0.34	0.69	0.68
Frontal + Reverse	35	49.73	0	0	0.34	0.69	0.68
Frontal + Reverse	36	57.43	0	0	0.34	0.69	0.69
Frontal + Reverse	37	67.76	0	0	0.34	0.69	0.68
Frontal + Reverse	38	54.08	0	0	0.35	0.69	0.69
Frontal + Reverse	39	45.97	0	0	0.38	0.69	0.68
Frontal + Reverse	40	28.57	0	0	0.35	0.70	0.69
Frontal + Reverse	41	44.12	0	0	0.35	0.70	0.69
Frontal + Reverse	42	59.34	0	0	0.34	0.70	0.69
Frontal + Reverse	43	60.63	0.90	0.90	0.35	0.69	0.68
Frontal + Reverse	44	61.31	1.79	1.79	0.35	0.69	0.68
Frontal + Reverse	45	68.32	0	0	0.35	0.69	0.68
Frontal + Reverse	46	64.12	1.18	1.76	0.34	0.69	0.68
Frontal + Reverse	47	69.15	0	0	0.34	0.69	0.68
Frontal + Reverse	48	44.24	18.22	18.22	0.34	0.69	0.68
Frontal + Reverse	49	56.47	14.83	14.83	0.40	0.69	0.68
Frontal + Reverse	50	42.97	15.23	15.23	0.34	0.69	0.68
Frontal + Reverse	51	46.19	20.00	20.00	0.34	0.69	0.69
Frontal + Reverse	52	41.29	14.84	14.84	0.34	0.69	0.68
Frontal + Reverse	53	39.51	3.70	3.70	0.33	0.69	0.67
Frontal + Reverse	54	63.31	3.25	3.25	0.34	0.68	0.67

Frontal + Reverse	55	51.92	8.33	8.33	0.34	0.69	0.68
Frontal + Reverse	56	55.56	6.67	6.67	0.35	0.69	0.68
Frontal + Reverse	57	63.28	1.69	1.69	0.32	0.69	0.68
Frontal + Reverse	58	39.09	37.82	36.80	0.31	0.68	0.67
Frontal + Reverse	59	23.28	24.69	24.69	0.32	0.67	0.67
Frontal + Reverse	60	31.62	31.91	31.05	0.32	0.68	0.67
Frontal + Reverse	61	33.50	35.24	34.74	0.32	0.74	0.67
Frontal + Reverse	62	21.76	23.53	21.47	0.34	0.68	0.67
Frontal + Reverse	63	99.59	97.51	97.51	0.34	0.69	0.68
Frontal + Reverse	64	67.86	74.40	74.40	0.34	0.69	0.68
Frontal + Reverse	65	79.08	41.84	41.42	0.34	0.67	0.66
Frontal + Reverse	66	54.46	55.36	55.36	0.34	0.69	0.68
Frontal + Reverse	67	37.48	15.05	15.05	0.32	0.67	0.66
Frontal + Reverse	68	55.10	13.52	13.52	0.31	0.65	0.64
Frontal + Reverse	69	84.04	77.19	77.19	0.27	0.62	0.61
Frontal + Reverse	Mean (%)	62.33	20.49	20.38			
Frontal + Reverse	STD (%)	16.63	22.87	22.26			
Frontal + Reverse	Total Time				23.45	47.12	46.56

1.2 SVM with linear kernel (LIBLINEAR).

Table B3. Results obtained in the experiment 1 without to optimize the parameters in SVM classifier with linear kernel and LIBLINEAR library.

Obsidian Position	Level	Accuracy Ref 10%	Simulation time (h)	Accuracy Ref 50%	Simulation time (h)	Accuracy Ref 99%	Simulation time (h)
Frontal	Island	77.97%	0.26	66.13%	0.25	66.00%	0.03
	Municipality	55.71%	1.62	51.53%	0.41	43.90%	0.27
	Deposit	56.62%	1.70	52.00%	0.45	43.56%	0.30
Reverse	Island	80.43%	0.25	75.58%	0.25	67.52%	0.03
	Municipality	59.01%	1.50	50.58%	0.39	42.56%	0.26
	Deposit	58.34%	1.72	51.00%	0.43	43.16%	0.30
Frontal + Reverse	Island	79.16%	0.56	68.28%	0.25	69.21%	0.06
	Municipality	56.84%	3.00	50.74%	0.80	41.60%	0.56
	Deposit	56.59%	3.27	50.52%	0.86	41.88%	0.65

1.3 Random Forest.

Table B4. Results obtained in the experiment 1 without to optimize the parameters in Random Forest classifier.

Obsidian Position	Level	Accuracy Ref 10%	Simulation time (h)	Accuracy Ref 50%	Simulation time (h)	Accuracy Ref 99%	Simulation time (h)
Frontal	Island	91.24%	0.08	91.01%	0.11	84.02%	0.13
	Municipality	67.70%	0.21	67.21%	0.22	50.28%	0.24
	Deposit	67.43%	0.19	67.34%	0.17	50.08%	0.26
Reverse	Island	90.21%	0.08	90.20%	0.07	82.36%	0.13
	Municipality	69.15%	0.16	68.94%	0.15	48.75%	0.24
	Deposit	68.66%	0.17	68.71%	0.15	48.43%	0.24
Frontal + Reverse	Island	90.80%	0.16	90.58%	0.16	82.92%	0.31
	Municipality	67.82%	0.35	67.72;%	0.34	48.34%	0.54
	Deposit	67.61%	0.36	67.43%	0.34	48.00%	0.54

Table B5. Results obtained in the experiment 2 without to optimize the parameters in Random Forest classifier.

Obsidian Position	Obsidian sample	Accuracy (%)			Simulation Time (h)		
		Island	Municipality	Deposit	Island	Municipality	Deposit
Frontal + Reverse	1	100	61.01	61.47	0.08	0.16	0.17
Frontal + Reverse	2	97.22	56.67	60.00	0.08	0.16	0.16
Frontal + Reverse	3	100	55.70	56.38	0.08	0.15	0.16
Frontal + Reverse	4	100	74.38	71.90	0.08	0.16	0.16
Frontal + Reverse	5	100	69.44	77.08	0.08	0.15	0.16
Frontal + Reverse	6	100	39.51	48.77	0.08	0.15	0.16
Frontal + Reverse	7	98.18	38.32	42.34	0.08	0.15	0.16
Frontal + Reverse	8	100	31.48	30.56	0.08	0.15	0.16
Frontal + Reverse	9	100	57.14	61.90	0.08	0.15	0.16
Frontal + Reverse	10	99.12	51.75	50.00	0.08	0.15	0.16
Frontal + Reverse	11	100	75.46	74.85	0.08	0.15	0.16
Frontal + Reverse	12	99.27	67.15	79.56	0.08	0.16	0.16
Frontal + Reverse	13	100	56.30	57.42	0.08	0.16	0.16
Frontal + Reverse	14	100	46.25	49.25	0.08	0.15	0.16
Frontal + Reverse	15	100	64.96	71.79	0.08	0.15	0.16
Frontal + Reverse	16	100	37.50	41.91	0.08	0.15	0.16
Frontal + Reverse	17	97.97	42.64	33.50	0.08	0.15	0.15
Frontal + Reverse	18	99.67	30.12	23.79	0.08	0.15	0.15
Frontal + Reverse	19	98.52	19.65	15.08	0.08	0.15	0.15
Frontal + Reverse	20	98.72	21.99	21.67	0.08	0.15	0.15
Frontal + Reverse	21	98.82	26.05	17.14	0.08	0.15	0.15
Frontal + Reverse	22	98.24	24.12	20.42	0.08	0.15	0.16
Frontal + Reverse	23	97.93	31.06	27.33	0.07	0.15	0.16
Frontal + Reverse	24	98.45	0.39	1.94	0.07	0.15	0.16
Frontal + Reverse	25	98.84	2.02	1.45	0.07	0.15	0.16
Frontal + Reverse	26	100	0.84	0.84	0.08	0.15	0.15

Frontal + Reverse	27	99.54	19.25	20.16	0.08	0.15	0.15
Frontal + Reverse	28	99.18	33.47	37.55	0.08	0.15	0.15
Frontal + Reverse	29	95.88	39.46	41.05	0.08	0.14	0.15
Frontal + Reverse	30	84.25	31.67	32.51	0.07	0.13	0.13
Frontal + Reverse	31	99.32	6.85	8.22	0.08	0.15	0.16
Frontal + Reverse	32	99.52	5.71	6.19	0.07	0.15	0.16
Frontal + Reverse	33	91.62	8.38	6.70	0.07	0.15	0.16
Frontal + Reverse	34	89.66	7.47	3.45	0.08	0.15	0.16
Frontal + Reverse	35	83.96	6.95	3.21	0.08	0.15	0.16
Frontal + Reverse	36	100	29.70	11.88	0.08	0.15	0.16
Frontal + Reverse	37	97.27	11.48	3.28	0.08	0.15	0.16
Frontal + Reverse	38	100	14.29	7.14	0.08	0.15	0.16
Frontal + Reverse	39	80.65	8.87	0	0.08	0.15	0.16
Frontal + Reverse	40	100	4.76	0	0.08	0.16	0.16
Frontal + Reverse	41	100	16.18	0	0.08	0.16	0.16
Frontal + Reverse	42	100	20.88	0	0.08	0.16	0.16
Frontal + Reverse	43	84.62	17.65	16.74	0.08	0.15	0.16
Frontal + Reverse	44	83.93	20.83	21.43	0.08	0.15	0.16
Frontal + Reverse	45	90.10	30.20	33.17	0.07	0.16	0.16
Frontal + Reverse	46	89.41	24.12	21.76	0.07	0.15	0.16
Frontal + Reverse	47	93.53	25.37	24.38	0.08	0.15	0.16
Frontal + Reverse	48	67.66	50.93	52.79	0.08	0.15	0.16
Frontal + Reverse	49	75.39	53.00	54.57	0.08	0.15	0.16
Frontal + Reverse	50	67.19	44.53	44.14	0.08	0.15	0.16
Frontal + Reverse	51	75.71	58.10	57.14	0.08	0.16	0.17
Frontal + Reverse	52	83.23	52.26	58.06	0.08	0.16	0.17
Frontal + Reverse	53	68.31	28.40	27.16	0.08	0.16	0.17
Frontal + Reverse	54	71.89	43.20	46.45	0.08	0.15	0.17

Frontal + Reverse	55	79.49	33.97	37.18	0.08	0.18	0.17
Frontal + Reverse	56	72.59	31.11	34.81	0.08	0.19	0.16
Frontal + Reverse	57	81.92	27.68	29.94	0.08	0.20	0.16
Frontal + Reverse	58	20.81	35.03	31.47	0.08	0.20	0.16
Frontal + Reverse	59	17.81	27.34	28.04	0.08	0.19	0.16
Frontal + Reverse	60	11.97	23.08	27.07	0.08	0.20	0.16
Frontal + Reverse	61	19.11	32.51	33.50	0.08	0.20	0.16
Frontal + Reverse	62	6.18	17.06	20.59	0.07	0.20	0.16
Frontal + Reverse	63	65.15	5.81	5.39	0.07	0.20	0.16
Frontal + Reverse	64	28.57	11.90	11.90	0.07	0.20	0.16
Frontal + Reverse	65	76.57	5.65	3.77	0.07	0.20	0.16
Frontal + Reverse	66	33.04	13.39	14.29	0.07	0.18	0.16
Frontal + Reverse	67	71.47	66.93	66.80	0,07	0.20	0.16
Frontal + Reverse	68	62.54	53.61	54.30	0.07	0.17	0.16
Frontal + Reverse	69	91.83	18.42	18.33	0.06	0.15	0.14
Frontal + Reverse	Mean (%)	83.94	31.87	31.23			
Frontal + Reverse	STD (%)	24.47	20.08	22.68			
Frontal + Reverse	Total Time				5.22	11.15	10.92

1.4 SVM RBF.

Table B6. Results obtained in the experiment 1 without to optimize the parameters in SVM RBF classifier and LIBSVM library.

Obsidian Position	Level	Accuracy Ref 10%	Simulation time (h)	Accuracy Ref 50%	Simulation time (h)	Accuracy Ref 99%	Simulation time (h)
Frontal	Island	83.72%	0.26	82.89%	0.30	65.49%	0.45
	Municipality	43.51%	0.45	34.24%	0.46	29.79%	0.73
	Deposit	43.62%	0.46	34.29%	0.48	29.83%	0.72
Reverse	Island	82.71%	0.22	78.30%	0.25	66.80%	0.39
	Municipality	43.98%	0.38	36.86%	0.40	29.78%	0.68
	Deposit	43.04%	0.38	36.78%	0.52	29.87%	0.68
Frontal + Reverse	Island	84.80%	1.00	83.17%	1.07	66.13%	1.65
	Municipality	46.09%	1.70	38.33%	2.21	29.78%	3.03
	Deposit	46.24%	1.70	38.62%	1.81	29.90%	3.00

Table B7. Results obtained in the experiment 2 without to optimize the parameters in SVM RBF classifier and LIBSVM library.

Obsidian Position	Obsidian sample	Accuracy (%)			Simulation Time (h)		
		Island	Municipality	Deposit	Island	Municipality	Deposit
Frontal + Reverse	1	100	33.94	31.19	0.55	0.91	0.90
Frontal + Reverse	2	97.22	41.11	40.00	0.51	0.91	0.91
Frontal + Reverse	3	100	41.61	45.64	0.50	0.91	0.91
Frontal + Reverse	4	100	46.28	44.63	0.50	0.91	0.91
Frontal + Reverse	5	100	44.44	45.83	0.50	0.91	0.91
Frontal + Reverse	6	99.38	25.93	29.63	0.50	0.90	0.91
Frontal + Reverse	7	97.45	29.20	29.93	0.50	0.90	0.90
Frontal + Reverse	8	100	25.00	26.39	0.50	0.91	0.90
Frontal + Reverse	9	100	32.65	36.73	0.50	0.91	0.91
Frontal + Reverse	10	100	40.35	45.61	0.50	0.91	0.91
Frontal + Reverse	11	100	23.93	23.93	0.49	0.90	0.90
Frontal + Reverse	12	100	31.39	31.39	0.50	0.90	0.90
Frontal + Reverse	13	99.44	19.33	19.61	0.49	0.90	0.90
Frontal + Reverse	14	100	19.22	19.22	0.50	0.90	0.90
Frontal + Reverse	15	100	39.32	39.32	0.50	0.91	0.91
Frontal + Reverse	16	100	30.51	31.99	0.50	0.90	0.90
Frontal + Reverse	17	100	1.02	0	0.50	0.91	0.91
Frontal + Reverse	18	100	0.17	0	0.49	0.88	0.88
Frontal + Reverse	19	100	0	0	0.49	0.87	0.87
Frontal + Reverse	20	93.10	1.12	0	0.49	0.88	0.88
Frontal + Reverse	21	98.32	0	0	0.49	0.88	0.88
Frontal + Reverse	22	89.96	1.94	0.18	0.50	0.89	0.89
Frontal + Reverse	23	87.99	1.66	0	0.49	0.89	0.89
Frontal + Reverse	24	96.12	0	0	0.54	0.90	0.90
Frontal + Reverse	25	93.93	0	0	0.49	0.90	0.90

Frontal + Reverse	26	100	0	0	0.50	0.90	0.90
Frontal + Reverse	27	99.27	23.01	25.76	0.48	0.86	0.86
Frontal + Reverse	28	98.78	60.20	63.27	0.50	0.89	0.89
Frontal + Reverse	29	97.54	52.46	53.49	0.48	0.85	0.85
Frontal + Reverse	30	83.78	0	3.02	0.42	0.75	0.75
Frontal + Reverse	31	97.95	0	0	0.50	0.91	0.91
Frontal + Reverse	32	98.10	0	0	0.50	0.91	0.91
Frontal + Reverse	33	94.97	0	0	0.50	0.91	0.91
Frontal + Reverse	34	89.08	0	0	0.50	0.91	0.91
Frontal + Reverse	35	87.17	0	0	0.50	0.91	0.91
Frontal + Reverse	36	100	0	0	0.50	0.91	0.91
Frontal + Reverse	37	99.45	0	0	0.50	0.91	0.91
Frontal + Reverse	38	98.98	0	0	0.50	0.91	0.91
Frontal + Reverse	39	98.39	0	0	0.50	0.91	0.91
Frontal + Reverse	40	100	0	0	0.50	0.92	0.92
Frontal + Reverse	41	100	0	0	0.50	0.91	0.91
Frontal + Reverse	42	100	0	0	0.50	0.91	0.91
Frontal + Reverse	43	89.59	0.90	0.90	0.50	0.90	0.90
Frontal + Reverse	44	97.02	0.60	0.60	0.50	0.91	0.91
Frontal + Reverse	45	99.50	1.49	1.49	0.50	0.90	0.90
Frontal + Reverse	46	99.41	0	0	0.50	0.91	0.91
Frontal + Reverse	47	98.01	0.50	0.50	0.50	0.90	0.90
Frontal + Reverse	48	80.30	2.60	3.35	0.51	0.90	0.90
Frontal + Reverse	49	82.65	3.47	3.47	0.50	0.90	0.90
Frontal + Reverse	50	86.72	3.91	3.91	0.49	0.90	0.90
Frontal + Reverse	51	89.52	6.19	6.19	0.50	0.90	0.90
Frontal + Reverse	52	96.13	4.52	4.52	0.49	0.91	0.91

Frontal + Reverse	53	85.19	1.23	1.23	0.50	0.90	0.90
Frontal + Reverse	54	92.90	0.89	0.89	0.50	0.90	0.90
Frontal + Reverse	55	96.15	1.92	1.92	0.50	0.91	0.91
Frontal + Reverse	56	96.30	6.67	6.67	0.50	0.91	0.91
Frontal + Reverse	57	100	2.26	2.26	0.50	0.91	0.91
Frontal + Reverse	58	26.14	0	0	0.50	0.89	0.89
Frontal + Reverse	59	14.46	0	0	0.48	0.88	0.88
Frontal + Reverse	60	5.13	1.14	1.14	0.47	0.90	0.90
Frontal + Reverse	61	9.93	0	0	0.48	0.89	0.89
Frontal + Reverse	62	5.88	0	0	0.47	0.89	0.89
Frontal + Reverse	63	41.49	0	0	0.49	0.90	0.90
Frontal + Reverse	64	7.74	0	0	0.49	0.91	0.91
Frontal + Reverse	65	46.65	0	0	0.48	0.88	0.88
Frontal + Reverse	66	8.93	0	0	0.50	0.91	0.91
Frontal + Reverse	67	17.77	43.58	43.84	0.46	0.87	0.87
Frontal + Reverse	68	25.43	34.36	34.71	0.46	0.86	0.86
Frontal + Reverse	69	0	0	0	0.24	0.67	0.67
Frontal + Reverse	Mean (%)	82.54	11.33	11.66			
Frontal + Reverse	STD (%)	31.03	16.98	17.56			
Frontal + Reverse	Total Time				33.88	61.65	61.52

2. Phase 2. Experiment 1 classification results to choose the best pre-processing.

Table B8. Results obtained in experiment 1 to choose the best pre-processing.

Pre-processing Type	Accuracy (%) ± STD			Simulation Time (h)		
	Island	Municipality	Deposit	Island	Municipality	Deposit
P0	90.80% ± 0.0045	67.82% ± 0.0080	67.61% ± 0.0100	0.16	0.35	0.36
P1	84.13% ± 0.0066	60.08% ± 0.0100	59.82% ± 0.0068	0.30	0.46	0.47
P2	83.81% ± 0.0064	57.81% ± 0.0110	57.50% ± 0.0045	0.29	0.47	0.48

3. Phase 3. Experiment 1 classification results to optimize the parameters in each classifier.

3.1 SVM with linear kernel.

Table B9. Results obtained in the experiment 1 to optimize the parameters in SVM classifier with linear kernel and LIBSVM library.

Cost Value [log(C)]	Iteration 1 Accuracy			Iteration 2 Accuracy (%)			Iteration 3 Accuracy (%)		
	Island	Mun	Dep	Isl	Mun	Dep	Isl	Mun	Dep
-10	0,6106	0,2948	0,2895	0,6146	0,2888	0,2865	0,6301	0,3023	0,2928
-8	0,6413	0,3215	0,3208	0,6373	0,3195	0,3165	0,6581	0,3314	0,3195
-6	0,6719	0,3673	0,3752	0,6637	0,3736	0,3673	0,6795	0,3805	0,3726
-4	0,7372	0,4550	0,4590	0,7296	0,4629	0,4484	0,7333	0,4718	0,4583
-2	0,7824	0,4840	0,5071	0,7774	0,4965	0,4965	0,7873	0,5104	0,5074
0	0,7923	0,5371	0,5572	0,7864	0,5384	0,5569	0,7966	0,5565	0,5612
2	0,8012	0,5790	0,5862	0,7933	0,5783	0,6014	0,8012	0,6044	0,5938
4	0,8121	0,6083	0,6179	0,7995	0,6050	0,6248	0,8061	0,6294	0,6261
6	0,8180	0,6353	0,6522	0,8098	0,6294	0,6479	0,8121	0,6538	0,6499
8	0,8223	0,6591	0,6683	0,8197	0,6591	0,6802	0,8160	0,6713	0,6670
10	0,8236	0,6568	0,6835	0,8239	0,6693	0,6894	0,8246	0,6723	0,6677
12	0,7732	0,6578	0,6637	0,7709	0,6581	0,6921	0,8022	0,6663	0,6789
14	0,6363	0,6396	0,6403	0,5378	0,6386	0,6726	0,5170	0,6238	0,6663
16	0,5114	0,6050	0,6215	0,5605	0,5997	0,6353	0,6073	0,5964	0,6281
18	0,5410	0,5638	0,5529	0,5875	0,5691	0,5816	0,5875	0,5635	0,6017
20	0,5414	0,5625	0,5582	0,5852	0,5450	0,5711	0,5265	0,5556	0,5694

Cost Value [log(C)]	Iteration 4 Accuracy (%)			Iteration 5 Accuracy (%)			Iteration 6 Accuracy (%)		
	Isl	Mun	Dep	Isl	Mun	Dep	Isl	Mun	Dep
-10	0,6192	0,2994	0,3000	0,6169	0,2756	0,2878	0,6133	0,3040	0,2872
-8	0,6413	0,3264	0,3258	0,6439	0,3109	0,3264	0,6393	0,3333	0,3178
-6	0,6733	0,3699	0,3785	0,6640	0,3492	0,3693	0,6673	0,3920	0,3581
-4	0,7376	0,4629	0,4583	0,7237	0,4510	0,4573	0,7277	0,4728	0,4590
-2	0,7840	0,4876	0,5061	0,7669	0,4804	0,4972	0,7801	0,5087	0,5002
0	0,7966	0,5381	0,5549	0,7870	0,5295	0,5493	0,7920	0,5539	0,5483
2	0,8025	0,5816	0,5915	0,7896	0,5727	0,5981	0,8048	0,5961	0,5885
4	0,8124	0,6093	0,6202	0,7939	0,6004	0,6169	0,8101	0,6251	0,6156
6	0,8157	0,6330	0,6449	0,7989	0,6274	0,6442	0,8098	0,6512	0,6373
8	0,8193	0,6574	0,6700	0,8032	0,6472	0,6637	0,8088	0,6624	0,6630
10	0,8223	0,6693	0,6838	0,8051	0,6555	0,6832	0,8127	0,6673	0,6703
12	0,6960	0,6667	0,6841	0,8009	0,6482	0,6772	0,7870	0,6710	0,6637
14	0,7590	0,6472	0,6653	0,5879	0,6001	0,6522	0,5321	0,6409	0,6433
16	0,5687	0,5809	0,5895	0,5941	0,5826	0,6261	0,5272	0,5859	0,6011
18	0,5005	0,5974	0,5720	0,5562	0,5500	0,6053	0,5331	0,5730	0,5790
20	0,5796	0,5615	0,5800	0,6617	0,5391	0,5849	0,5351	0,5427	0,5556

Cost Value [log(C)]	Iteration 7 Accuracy (%)			Iteration 8 Accuracy (%)			Iteration 9 Accuracy (%)		
	Isl	Mun	Dep	Isl	Mun	Dep	Isl	Mun	Dep
-10	0,6179	0,2984	0,2875	0,6106	0,2924	0,2852	0,6159	0,3030	0,2944
-8	0,6386	0,3241	0,3083	0,6337	0,3211	0,3126	0,6413	0,3386	0,3132
-6	0,6686	0,3782	0,3577	0,6627	0,3680	0,3548	0,6726	0,3841	0,3647
-4	0,7244	0,4543	0,4474	0,7247	0,4570	0,4543	0,7263	0,4675	0,4553
-2	0,7824	0,4893	0,4893	0,7788	0,4975	0,5038	0,7745	0,5091	0,5087
0	0,7949	0,5394	0,5434	0,7910	0,5486	0,5427	0,7913	0,5506	0,5608
2	0,7989	0,5856	0,5813	0,8002	0,5902	0,5829	0,7985	0,5912	0,5997
4	0,8078	0,6169	0,6152	0,8088	0,6294	0,6152	0,8048	0,6225	0,6215
6	0,8081	0,6314	0,6426	0,8190	0,6525	0,6396	0,8170	0,6429	0,6535
8	0,8081	0,6538	0,6723	0,8223	0,6752	0,6601	0,8134	0,6650	0,6762
10	0,8164	0,6624	0,6855	0,8256	0,6663	0,6752	0,8187	0,6611	0,6864
12	0,7629	0,6551	0,6802	0,7669	0,6802	0,6706	0,7712	0,6611	0,6864
14	0,6357	0,6195	0,6700	0,6733	0,6462	0,6330	0,6067	0,6439	0,6634
16	0,5180	0,5793	0,6281	0,5480	0,6053	0,6238	0,6380	0,6189	0,6400
18	0,5579	0,5668	0,5704	0,6914	0,5443	0,5997	0,5305	0,5694	0,6192
20	0,5968	0,5529	0,5730	0,5536	0,5546	0,5661	0,6884	0,5107	0,5711

Cost Value [log(C)]	Iteration 10 Accuracy (%)		
	Isl	Mun	Dep
-10	0,6189	0,3053	0,3056
-8	0,6429	0,3241	0,3258
-6	0,6739	0,3838	0,3703
-4	0,7339	0,4632	0,4474
-2	0,7880	0,5012	0,4870
0	0,8002	0,5496	0,5364
2	0,8131	0,5931	0,5813
4	0,8180	0,6185	0,6060
6	0,8216	0,6370	0,6433
8	0,8223	0,6594	0,6644
10	0,8253	0,6614	0,6759
12	0,8223	0,6663	0,6805
14	0,6218	0,6218	0,6466
16	0,5552	0,6235	0,6294
18	0,5496	0,5575	0,6133
20	0,5526	0,5295	0,5654

3.2 Random Forest

Table B10. Results obtained in the experiment 1 to optimize the parameters in Random Forest classifier.

Number of trees	Iteration 1 Accuracy (%)			Iteration 2 Accuracy (%)			Iteration 3 Accuracy (%)		
	Dep	Mun	Isl	Dep	Mun	Isl	Dep	Mun	Isl
10	0,5572	0,5582	0,8272	0,5491	0,5580	0,8283	0,5514	0,5547	0,8243
30	0,5842	0,5905	0,8480	0,5844	0,5893	0,8444	0,5827	0,5880	0,8411
50	0,6057	0,6020	0,8470	0,6035	0,6032	0,8487	0,5962	0,5929	0,8342
70	0,6142	0,6172	0,8539	0,6045	0,5999	0,8520	0,6028	0,6045	0,8425
90	0,6123	0,6093	0,8506	0,6081	0,6071	0,8497	0,5962	0,6012	0,8454
110	0,6169	0,6100	0,8490	0,6065	0,6078	0,8556	0,6051	0,6012	0,8411
130	0,6175	0,6123	0,8546	0,6157	0,6134	0,8540	0,6028	0,6002	0,8425
150	0,6149	0,6103	0,8526	0,6107	0,6134	0,8533	0,6065	0,5959	0,8421
170	0,6179	0,6113	0,8533	0,6190	0,6170	0,8514	0,6140	0,6012	0,8448
190	0,6149	0,6126	0,8553	0,6134	0,6187	0,8570	0,6098	0,6042	0,8431
210	0,6179	0,6159	0,8562	0,6163	0,6160	0,8583	0,6134	0,6035	0,8382
230	0,6179	0,6067	0,8533	0,6154	0,6131	0,8573	0,6111	0,6048	0,8441
250	0,6192	0,6093	0,8533	0,6180	0,6088	0,8537	0,6081	0,5969	0,8434
270	0,6159	0,6106	0,8599	0,6220	0,6183	0,8550	0,6107	0,6042	0,8434
290	0,6189	0,6192	0,8533	0,6131	0,6150	0,8553	0,6081	0,6032	0,8441
310	0,6195	0,6159	0,8579	0,6190	0,6127	0,8530	0,6101	0,6061	0,8438
330	0,6189	0,6142	0,8562	0,6226	0,6117	0,8560	0,6114	0,6055	0,8415
350	0,6159	0,6149	0,8546	0,6147	0,6131	0,8586	0,6081	0,6068	0,8484
370	0,6235	0,6179	0,8553	0,6127	0,6147	0,8563	0,6084	0,6032	0,8454
390	0,6185	0,6205	0,8546	0,6127	0,6140	0,8576	0,6154	0,6045	0,8444
410	0,6185	0,6162	0,8556	0,6160	0,6140	0,8570	0,6088	0,6055	0,8441
430	0,6241	0,6222	0,8576	0,6154	0,6154	0,8612	0,6111	0,6002	0,8431
450	0,6248	0,6205	0,8536	0,6190	0,6147	0,8556	0,6124	0,6065	0,8444
470	0,6175	0,6123	0,8566	0,6160	0,6216	0,8556	0,6088	0,6051	0,8451
490	0,6215	0,6225	0,8556	0,6187	0,6124	0,8553	0,6124	0,6042	0,8457
500	0,6172	0,6182	0,8543	0,6210	0,6147	0,8579	0,6117	0,6088	0,8438

Number of trees	Iteration 4 Accuracy (%)			Iteration 5 Accuracy (%)			Iteration 6 Accuracy (%)		
	Dep	Mun	Isl	Dep	Mun	Isl	Dep	Mun	Isl
10	0,5461	0,5485	0,8481	0,5527	0,5485	0,8214	0,5493	0,5664	0,8246
30	0,5834	0,5903	0,8461	0,5870	0,5821	0,8309	0,5724	0,6040	0,8404
50	0,5900	0,6005	0,8504	0,6009	0,5979	0,8355	0,5859	0,6073	0,8404
70	0,5953	0,6022	0,8523	0,5985	0,6074	0,8392	0,5902	0,6126	0,8464
90	0,5969	0,6068	0,8546	0,5953	0,6101	0,8388	0,5968	0,6169	0,8408
110	0,5966	0,6098	0,8523	0,6022	0,6114	0,8362	0,5935	0,6113	0,8391
130	0,5982	0,6104	0,8566	0,5966	0,6061	0,8375	0,6004	0,6228	0,8447
150	0,5966	0,6107	0,8527	0,5966	0,6051	0,8398	0,6024	0,6169	0,8447
170	0,6045	0,6002	0,8553	0,6002	0,6065	0,8355	0,5997	0,6202	0,8408
190	0,6081	0,6032	0,8540	0,6022	0,6104	0,8401	0,5971	0,6179	0,8408
210	0,6088	0,6051	0,8537	0,6009	0,6117	0,8401	0,6027	0,6274	0,8457
230	0,5982	0,6061	0,8546	0,6022	0,6137	0,8385	0,6007	0,6245	0,8480
250	0,6071	0,6094	0,8573	0,6074	0,6117	0,8385	0,5984	0,6215	0,8464
270	0,6068	0,6078	0,8540	0,6032	0,6163	0,8431	0,6007	0,6248	0,8408
290	0,6055	0,6071	0,8530	0,6061	0,6140	0,8408	0,6040	0,6268	0,8417
310	0,6111	0,6121	0,8533	0,6055	0,6150	0,8411	0,5974	0,6225	0,8450
330	0,6035	0,6078	0,8550	0,6012	0,6127	0,8375	0,6044	0,6255	0,8434
350	0,6028	0,6104	0,8566	0,6065	0,6065	0,8378	0,5994	0,6251	0,8431
370	0,6074	0,6081	0,8570	0,6015	0,6131	0,8408	0,6014	0,6278	0,8450
390	0,6045	0,6107	0,8553	0,6111	0,6173	0,8395	0,5984	0,6231	0,8454
410	0,6098	0,6121	0,8563	0,6035	0,6173	0,8418	0,6070	0,6294	0,8427
430	0,6084	0,6088	0,8556	0,6051	0,6173	0,8418	0,6053	0,6205	0,8437
450	0,6048	0,6071	0,8527	0,6035	0,6147	0,8401	0,5991	0,6225	0,8434
470	0,6055	0,6104	0,8537	0,6045	0,6154	0,8411	0,6047	0,6251	0,8417
490	0,6131	0,6051	0,8556	0,6012	0,6187	0,8421	0,6050	0,6222	0,8467
500	0,6091	0,6107	0,8537	0,6042	0,6183	0,8408	0,6067	0,6264	0,8464

Number of trees	Iteration 7 Accuracy (%)			Iteration 8 Accuracy (%)			Iteration 9 Accuracy (%)		
	Dep	Mun	Isl	Dep	Mun	Isl	Dep	Mun	Isl
10	0,5539	0,5529	0,8206	0,5443	0,5648	0,8154	0,5964	0,5470	0,8154
30	0,5902	0,5948	0,8368	0,5829	0,6004	0,8404	0,6100	0,5941	0,8404
50	0,5948	0,6106	0,8381	0,5951	0,6212	0,8384	0,6100	0,5922	0,8384
70	0,6076	0,6090	0,8411	0,5964	0,6189	0,8457	0,6080	0,6014	0,8457
90	0,6096	0,6146	0,8437	0,5968	0,6215	0,8470	0,6159	0,6020	0,8470
110	0,6037	0,6245	0,8398	0,6014	0,6238	0,8513	0,6166	0,5987	0,8513
130	0,6060	0,6067	0,8450	0,5941	0,6288	0,8480	0,6175	0,6113	0,8480
150	0,6133	0,6126	0,8414	0,6011	0,6245	0,8480	0,6241	0,6073	0,8480
170	0,6086	0,6222	0,8424	0,5974	0,6208	0,8487	0,6215	0,6109	0,8487
190	0,6034	0,6175	0,8457	0,6017	0,6284	0,8503	0,6205	0,6076	0,8503
210	0,6100	0,6198	0,8444	0,6014	0,6238	0,8450	0,6215	0,6123	0,8450
230	0,6076	0,6212	0,8440	0,6057	0,6231	0,8447	0,6235	0,6080	0,8447
250	0,6136	0,6231	0,8467	0,6037	0,6231	0,8500	0,6271	0,6100	0,8500
270	0,6126	0,6212	0,8411	0,6020	0,6248	0,8460	0,6159	0,6073	0,8460
290	0,6116	0,6212	0,8483	0,6063	0,6268	0,8470	0,6215	0,6106	0,8470
310	0,6076	0,6235	0,8487	0,6044	0,6245	0,8470	0,6235	0,6142	0,8470
330	0,6119	0,6261	0,8480	0,6011	0,6291	0,8483	0,6185	0,6090	0,8483
350	0,6103	0,6189	0,8447	0,6020	0,6238	0,8483	0,6222	0,6090	0,8483
370	0,6100	0,6189	0,8483	0,6073	0,6324	0,8490	0,6258	0,6159	0,8490
390	0,6189	0,6189	0,8440	0,6057	0,6271	0,8480	0,6274	0,6113	0,8480
410	0,6090	0,6281	0,8483	0,5964	0,6284	0,8470	0,6245	0,6100	0,8470
430	0,6149	0,6195	0,8464	0,6011	0,6255	0,8470	0,6241	0,6080	0,8470
450	0,6113	0,6241	0,8473	0,6034	0,6281	0,8497	0,6175	0,6080	0,8497
470	0,6133	0,6175	0,8467	0,6057	0,6291	0,8497	0,6301	0,6156	0,8497
490	0,6109	0,6238	0,8447	0,6047	0,6251	0,8473	0,6264	0,6100	0,8473
500	0,6093	0,6205	0,8467	0,6004	0,6288	0,8510	0,6241	0,6142	0,8510

Number of trees	Iteration 10 Accuracy (%)		
	Dep	Mun	Isl
10	0,5556	0,5493	0,8154
30	0,5862	0,5945	0,8404
50	0,5948	0,6083	0,8384
70	0,6116	0,6103	0,8457
90	0,6070	0,6113	0,8470
110	0,6106	0,6142	0,8513
130	0,6113	0,6156	0,8480
150	0,6090	0,6129	0,8480
170	0,6044	0,6152	0,8487
190	0,6129	0,6179	0,8503
210	0,6090	0,6218	0,8450
230	0,6116	0,6149	0,8447
250	0,6067	0,6198	0,8500
270	0,6133	0,6212	0,8460
290	0,6119	0,6225	0,8470
310	0,6073	0,6212	0,8470
330	0,6060	0,6245	0,8483
350	0,6050	0,6182	0,8483
370	0,6086	0,6241	0,8490
390	0,6136	0,6218	0,8480
410	0,6109	0,6248	0,8470
430	0,6126	0,6192	0,8470
450	0,6116	0,6192	0,8497
470	0,6109	0,6182	0,8497
490	0,6156	0,6192	0,8473
500	0,6096	0,6225	0,8510

3.3 SVM RBF

Table B11. Results obtained in the experiment 1 to optimize the parameters in SVM RBF classifier and LIBSVM library at island level.

ISLAND LEVEL	Iteration 1							Iteration 2						
Accuracy island(%)	Gamma Value [log(g)]							Gamma Value [log(g)]						
Cost Value [log(C)]	-10	-5	0	5	10	15	20	-10	-5	0	5	10	15	20
-10	0,6024	0,6024	0,6024	0,6024	0,6024	0,6024	0,6024	0,6030	0,6030	0,6030	0,6030	0,6030	0,6030	0,6030
-5	0,6024	0,6667	0,7570	0,6301	0,6024	0,6024	0,6024	0,6030	0,6680	0,7474	0,6340	0,6030	0,6030	0,6030
0	0,6314	0,7867	0,8404	0,7544	0,6024	0,6024	0,6024	0,6320	0,7857	0,8351	0,7573	0,6030	0,6030	0,6030
5	0,7649	0,8477	0,8619	0,7676	0,6024	0,6024	0,6024	0,7613	0,8427	0,8668	0,7685	0,6030	0,6030	0,6030
10	0,8216	0,8783	0,8632	0,7676	0,6024	0,6024	0,6024	0,8197	0,8754	0,8632	0,7685	0,6030	0,6030	0,6030
15	0,8483	0,8978	0,8595	0,7676	0,6024	0,6024	0,6024	0,8493	0,8938	0,8576	0,7685	0,6030	0,6030	0,6030
20	0,8477	0,8839	0,8595	0,7676	0,6024	0,6024	0,6024	0,8510	0,8708	0,8576	0,7685	0,6030	0,6030	0,6030

Island	Iteration 3							Iteration 4						
Accuracy island(%)	Gamma Value [log(g)]							Gamma Value [log(g)]						
Cost Value [log(C)]	-10	-5	0	5	10	15	20	-10	-5	0	5	10	15	20
-10	0,5935	0,5935	0,5935	0,5935	0,5935	0,5935	0,5935	0,6053	0,6053	0,6053	0,6053	0,6053	0,6053	0,6053
-5	0,5935	0,6591	0,7422	0,6268	0,5935	0,5935	0,5935	0,6053	0,6769	0,7547	0,6373	0,6053	0,6053	0,6053
0	0,6304	0,7844	0,8424	0,7517	0,5935	0,5935	0,5935	0,6416	0,7920	0,8493	0,7639	0,6053	0,6053	0,6053
5	0,7573	0,8460	0,8714	0,7679	0,5935	0,5935	0,5935	0,7791	0,8520	0,8681	0,7755	0,6053	0,6053	0,6053
10	0,8164	0,8780	0,8632	0,7679	0,5935	0,5935	0,5935	0,8262	0,8826	0,8612	0,7755	0,6053	0,6053	0,6053
15	0,8530	0,8975	0,8619	0,7679	0,5935	0,5935	0,5935	0,8599	0,9014	0,8592	0,7755	0,6053	0,6053	0,6053
20	0,8480	0,8843	0,8619	0,7679	0,5935	0,5935	0,5935	0,8635	0,8869	0,8592	0,7755	0,6053	0,6053	0,6053

Island	Iteration 5							Iteration 6						
Accuracy island(%)	Gamma Value [log(g)]							Gamma Value [log(g)]						
Cost Value [log(C)]	-10	-5	0	5	10	15	20	-10	-5	0	5	10	15	20
-10	0,6017	0,6017	0,6017	0,6017	0,6017	0,6017	0,6017	0,6149	0,6149	0,6149	0,6149	0,6149	0,6149	0,6149
-5	0,6017	0,6663	0,7484	0,6334	0,6017	0,6017	0,6017	0,6149	0,6749	0,7521	0,6442	0,6149	0,6149	0,6149
0	0,6311	0,7850	0,8470	0,7603	0,6017	0,6017	0,6017	0,6452	0,7943	0,8444	0,7755	0,6149	0,6149	0,6149
5	0,7471	0,8424	0,8645	0,7679	0,6017	0,6017	0,6017	0,7633	0,8464	0,8698	0,7857	0,6152	0,6149	0,6149
10	0,8147	0,8770	0,8642	0,7679	0,6017	0,6017	0,6017	0,8220	0,8731	0,8668	0,7857	0,6152	0,6149	0,6149
15	0,8473	0,8932	0,8595	0,7679	0,6017	0,6017	0,6017	0,8473	0,8902	0,8638	0,7857	0,6152	0,6149	0,6149
20	0,8467	0,8579	0,8595	0,7679	0,6017	0,6017	0,6017	0,8338	0,8806	0,8638	0,7857	0,6152	0,6149	0,6149

Island	Iteration 7							Iteration 8						
Accuracy island(%)	**Gamma Value [log(g)]**							**Gamma Value [log(g)]**						
Cost Value [log(C)]	**-10**	**-5**	**0**	**5**	**10**	**15**	**20**	**-10**	**-5**	**0**	**5**	**10**	**15**	**20**
-10	0,6067	0,6067	0,6067	0,6067	0,6067	0,6067	0,6067	0,5865	0,5865	0,5865	0,5865	0,5865	0,5865	0,5865
-5	0,6067	0,6762	0,7474	0,6311	0,6067	0,6067	0,6067	0,5865	0,6578	0,7339	0,6149	0,5865	0,5865	0,5865
0	0,6377	0,7791	0,8361	0,7498	0,6067	0,6067	0,6067	0,6179	0,7748	0,8206	0,7392	0,5865	0,5865	0,5865
5	0,7610	0,8391	0,8592	0,7613	0,6067	0,6067	0,6067	0,7501	0,8262	0,8493	0,7557	0,5865	0,5865	0,5865
10	0,8183	0,8767	0,8562	0,7613	0,6067	0,6067	0,6067	0,8084	0,8579	0,8576	0,7557	0,5865	0,5865	0,5865
15	0,8497	0,8978	0,8523	0,7613	0,6067	0,6067	0,6067	0,8404	0,8853	0,8592	0,7557	0,5865	0,5865	0,5865
20	0,8576	0,8721	0,8523	0,7613	0,6067	0,6067	0,6067	0,8335	0,8721	0,8592	0,7557	0,5865	0,5865	0,5865

Island	Iteration 9							Iteration 10						
Accuracy island(%)	**Gamma Value [log(g)]**							**Gamma Value [log(g)]**						
Cost Value [log(C)]	**-10**	**-5**	**0**	**5**	**10**	**15**	**20**	**-10**	**-5**	**0**	**5**	**10**	**15**	**20**
-10	0,6017	0,6017	0,6017	0,6017	0,6017	0,6017	0,6017	0,6126	0,6126	0,6126	0,6126	0,6126	0,6126	0,6126
-5	0,6017	0,6719	0,7263	0,6297	0,6017	0,6017	0,6017	0,6126	0,6802	0,7369	0,6393	0,6126	0,6126	0,6126
0	0,6377	0,7771	0,8338	0,7405	0,6017	0,6017	0,6017	0,6502	0,7857	0,8332	0,7514	0,6126	0,6126	0,6126
5	0,7583	0,8384	0,8622	0,7514	0,6017	0,6017	0,6017	0,7732	0,8414	0,8619	0,7600	0,6126	0,6126	0,6126
10	0,8094	0,8717	0,8625	0,7514	0,6017	0,6017	0,6017	0,8239	0,8783	0,8625	0,7600	0,6126	0,6126	0,6126
15	0,8477	0,8988	0,8589	0,7514	0,6017	0,6017	0,6017	0,8513	0,8945	0,8576	0,7600	0,6126	0,6126	0,6126
20	0,8361	0,8727	0,8589	0,7514	0,6017	0,6017	0,6017	0,8566	0,8760	0,8576	0,7600	0,6126	0,6126	0,6126

Table B12. Results obtained in the experiment 1 to optimize the parameters in SVM RBF classifier and LIBSVM library at municipality level.

MUNICIALITY LEVEL	Iteration 1							Iteration 2						
Accuracy (%)	**Gamma Value [log(g)]**							**Gamma Value [log(g)]**						
Cost Value [log(C)]	**-10**	**-5**	**0**	**5**	**10**	**15**	**20**	**-10**	**-5**	**0**	**5**	**10**	**15**	**20**
-10	0,3079	0,3079	0,3079	0,3079	0,3079	0,3079	0,3079	0,2901	0,2901	0,2901	0,2901	0,2901	0,2901	0,2901
-5	0,3079	0,3485	0,4042	0,3330	0,3079	0,3079	0,3079	0,2901	0,3284	0,3811	0,3126	0,2901	0,2901	0,2901
0	0,3290	0,4814	0,5780	0,4566	0,3079	0,3079	0,3079	0,3162	0,4731	0,5826	0,4369	0,2901	0,2901	0,2901
5	0,4909	0,6307	0,6973	0,4850	0,3079	0,3079	0,3079	0,4672	0,6159	0,6901	0,4603	0,2901	0,2901	0,2901
10	0,6162	0,7557	0,7036	0,4850	0,3079	0,3079	0,3079	0,5987	0,7425	0,6930	0,4603	0,2901	0,2901	0,2901
15	0,7112	0,7870	0,7033	0,4850	0,3079	0,3079	0,3079	0,6977	0,7854	0,6924	0,4603	0,2901	0,2901	0,2901
20	0,7590	0,7715	0,7033	0,4850	0,3079	0,3079	0,3079	0,7481	0,7781	0,6924	0,4603	0,2901	0,2901	0,2901

MUNICIALITY LEVEL Accuracy (%)	Iteration 3 Gamma Value [log(g)]							Iteration 4 Gamma Value [log(g)]						
Cost Value [log(C)]	**-10**	**-5**	**0**	**5**	**10**	**15**	**20**	**-10**	**-5**	**0**	**5**	**10**	**15**	**20**
-10	0,2928	0,2928	0,2928	0,2928	0,2928	0,2928	0,2928	0,2971	0,2971	0,2971	0,2971	0,2971	0,2971	0,2971
-5	0,2928	0,3366	0,3900	0,3205	0,2928	0,2928	0,2928	0,2971	0,3436	0,3904	0,3201	0,2971	0,2971	0,2971
0	0,3254	0,4860	0,5849	0,4524	0,2928	0,2928	0,2928	0,3277	0,4787	0,5885	0,4517	0,2971	0,2971	0,2971
5	0,4751	0,6317	0,6897	0,4810	0,2928	0,2928	0,2928	0,4725	0,6320	0,6808	0,4665	0,2971	0,2971	0,2971
10	0,6096	0,7577	0,7023	0,4810	0,2928	0,2928	0,2928	0,5978	0,7478	0,6897	0,4665	0,2971	0,2971	0,2971
15	0,7122	0,7976	0,7016	0,4810	0,2928	0,2928	0,2928	0,7066	0,7893	0,6864	0,4665	0,2971	0,2971	0,2971
20	0,7705	0,7880	0,7016	0,4810	0,2928	0,2928	0,2928	0,7580	0,7801	0,6864	0,4665	0,2971	0,2971	0,2971

MUNICIALITY LEVEL Accuracy (%)	Iteration 5 Gamma Value [log(g)]							Iteration 6 Gamma Value [log(g)]						
Cost Value [log(C)]	**-10**	**-5**	**0**	**5**	**10**	**15**	**20**	**-10**	**-5**	**0**	**5**	**10**	**15**	**20**
-10	0,2990	0,2990	0,2990	0,2990	0,2990	0,2990	0,2990	0,2944	0,2944	0,2944	0,2944	0,2944	0,2944	0,2944
-5	0,2990	0,3360	0,3884	0,3231	0,2990	0,2990	0,2990	0,2944	0,3340	0,3844	0,3175	0,2944	0,2944	0,2944
0	0,3238	0,4847	0,5806	0,4586	0,2990	0,2990	0,2990	0,3208	0,4906	0,5852	0,4481	0,2944	0,2944	0,2944
5	0,4725	0,6363	0,6970	0,4824	0,2990	0,2990	0,2990	0,4771	0,6205	0,6825	0,4672	0,2948	0,2944	0,2944
10	0,6126	0,7570	0,7085	0,4824	0,2990	0,2990	0,2990	0,6050	0,7438	0,6868	0,4672	0,2948	0,2944	0,2944
15	0,7161	0,7890	0,7062	0,4824	0,2990	0,2990	0,2990	0,7076	0,7850	0,6845	0,4672	0,2948	0,2944	0,2944
20	0,7616	0,7873	0,7062	0,4824	0,2990	0,2990	0,2990	0,7662	0,7742	0,6845	0,4672	0,2948	0,2944	0,2944

MUNICIALITY LEVEL Accuracy (%)	Iteration 7 Gamma Value [log(g)]							Iteration 8 Gamma Value [log(g)]						
Cost Value [log(C)]	**-10**	**-5**	**0**	**5**	**10**	**15**	**20**	**-10**	**-5**	**0**	**5**	**10**	**15**	**20**
-10	0,3056	0,3056	0,3056	0,3056	0,3056	0,3056	0,3056	0,2994	0,2994	0,2994	0,2994	0,2994	0,2994	0,2994
-5	0,3056	0,3469	0,3956	0,3307	0,3056	0,3056	0,3056	0,2994	0,3406	0,4003	0,3290	0,2994	0,2994	0,2994
0	0,3366	0,4913	0,5842	0,4629	0,3056	0,3056	0,3056	0,3261	0,4837	0,5743	0,4593	0,2994	0,2994	0,2994
5	0,4801	0,6383	0,6835	0,4847	0,3056	0,3056	0,3056	0,4728	0,6225	0,6832	0,4804	0,2994	0,2994	0,2994
10	0,6100	0,7501	0,7043	0,4847	0,3056	0,3056	0,3056	0,6011	0,7382	0,6937	0,4804	0,2994	0,2994	0,2994
15	0,7181	0,7949	0,7033	0,4847	0,3056	0,3056	0,3056	0,7062	0,7864	0,6924	0,4804	0,2994	0,2994	0,2994
20	0,7610	0,7903	0,7033	0,4847	0,3056	0,3056	0,3056	0,7471	0,7738	0,6924	0,4804	0,2994	0,2994	0,2994

MUNICIALITY LEVEL Accuracy (%)	Iteration 9 Gamma Value [log(g)]							Iteration 10 Gamma Value [log(g)]						
Cost Value [log(C)]	**-10**	**-5**	**0**	**5**	**10**	**15**	**20**	**-10**	**-5**	**0**	**5**	**10**	**15**	**20**
-10	0,3010	0,3010	0,3010	0,3010	0,3010	0,3010	0,3010	0,2888	0,2888	0,2888	0,2888	0,2888	0,2888	0,2888
-5	0,3010	0,3383	0,3940	0,3234	0,3010	0,3010	0,3010	0,2888	0,3271	0,3795	0,3155	0,2888	0,2888	0,2888
0	0,3244	0,4847	0,5902	0,4510	0,3010	0,3010	0,3010	0,3126	0,4662	0,5595	0,4372	0,2888	0,2888	0,2888
5	0,4669	0,6324	0,6940	0,4758	0,3010	0,3010	0,3010	0,4590	0,6076	0,6766	0,4576	0,2888	0,2888	0,2888
10	0,6050	0,7560	0,7099	0,4758	0,3010	0,3010	0,3010	0,5879	0,7300	0,6835	0,4576	0,2888	0,2888	0,2888
15	0,7174	0,8005	0,7118	0,4758	0,3010	0,3010	0,3010	0,6848	0,7850	0,6828	0,4576	0,2888	0,2888	0,2888
20	0,7659	0,7864	0,7118	0,4758	0,3010	0,3010	0,3010	0,7402	0,7679	0,6828	0,4576	0,2888	0,2888	0,2888

Table B13. Results obtained in the experiment 1 to optimize the parameters in SVM RBF classifier and LIBSVM library at deposit level.

DEPOSIT LEVEL Accuracy (%)	Iteration 1 Gamma Value [log(g)]							Iteration 2 Gamma Value [log(g)]						
Cost Value [log(C)]	**-10**	**-5**	**0**	**5**	**10**	**15**	**20**	**-10**	**-5**	**0**	**5**	**10**	**15**	**20**
-10	0,2915	0,2915	0,2915	0,2915	0,2915	0,2915	0,2915	0,2878	0,2878	0,2878	0,2878	0,2878	0,2878	0,2878
-5	0,2915	0,3267	0,3874	0,3185	0,2915	0,2915	0,2915	0,2878	0,3271	0,3818	0,3149	0,2878	0,2878	0,2878
0	0,3248	0,4725	0,5773	0,4418	0,2915	0,2915	0,2915	0,3228	0,4804	0,5783	0,4474	0,2878	0,2878	0,2878
5	0,4626	0,6261	0,6785	0,4606	0,2915	0,2915	0,2915	0,4791	0,6291	0,6891	0,4695	0,2878	0,2878	0,2878
10	0,5948	0,7573	0,6868	0,4606	0,2915	0,2915	0,2915	0,6116	0,7620	0,6967	0,4695	0,2878	0,2878	0,2878
15	0,7095	0,7982	0,6878	0,4606	0,2915	0,2915	0,2915	0,7244	0,7969	0,6963	0,4695	0,2878	0,2878	0,2878
20	0,7656	0,7877	0,6878	0,4606	0,2915	0,2915	0,2915	0,7791	0,7781	0,6963	0,4695	0,2878	0,2878	0,2878

DEPOSIT LEVEL Accuracy (%)	Iteration 3 Gamma Value [log(g)]							Iteration 4 Gamma Value [log(g)]						
Cost Value [log(C)]	**-10**	**-5**	**0**	**5**	**10**	**15**	**20**	**-10**	**-5**	**0**	**5**	**10**	**15**	**20**
-10	0,2855	0,2855	0,2855	0,2855	0,2855	0,2855	0,2855	0,2931	0,2931	0,2931	0,2931	0,2931	0,2931	0,2931
-5	0,2855	0,3221	0,3834	0,3149	0,2855	0,2855	0,2855	0,2931	0,3333	0,3821	0,3195	0,2931	0,2931	0,2931
0	0,3139	0,4725	0,5701	0,4411	0,2855	0,2855	0,2855	0,3175	0,4669	0,5770	0,4461	0,2931	0,2931	0,2931
5	0,4655	0,6067	0,6700	0,4672	0,2855	0,2855	0,2855	0,4619	0,6274	0,6789	0,4682	0,2931	0,2931	0,2931
10	0,5813	0,7445	0,6894	0,4672	0,2855	0,2855	0,2855	0,6096	0,7534	0,6917	0,4682	0,2931	0,2931	0,2931
15	0,6967	0,7877	0,6878	0,4672	0,2855	0,2855	0,2855	0,7214	0,7992	0,6907	0,4682	0,2931	0,2931	0,2931
20	0,7735	0,7798	0,6878	0,4672	0,2855	0,2855	0,2855	0,7735	0,7847	0,6907	0,4682	0,2931	0,2931	0,2931

DEPOSIT LEVEL Accuracy (%)	Iteration 5 Gamma Value [log(g)]							Iteration 6 Gamma Value [log(g)]						
Cost Value [log(C)]	**-10**	**-5**	**0**	**5**	**10**	**15**	**20**	**-10**	**-5**	**0**	**5**	**10**	**15**	**20**
-10	0,2862	0,2862	0,2862	0,2862	0,2862	0,2862	0,2862	0,2901	0,2901	0,2901	0,2901	0,2901	0,2901	0,2901
-5	0,2862	0,3271	0,3881	0,3188	0,2862	0,2862	0,2862	0,2901	0,3300	0,3821	0,3208	0,2901	0,2901	0,2901
0	0,3155	0,4692	0,5694	0,4415	0,2862	0,2862	0,2862	0,3218	0,4791	0,5806	0,4464	0,2901	0,2901	0,2901
5	0,4682	0,6175	0,6828	0,4649	0,2865	0,2862	0,2862	0,4810	0,6363	0,6881	0,4692	0,2901	0,2901	0,2901
10	0,5938	0,7405	0,6934	0,4649	0,2865	0,2862	0,2862	0,6083	0,7613	0,6977	0,4692	0,2901	0,2901	0,2901
15	0,7089	0,7946	0,6927	0,4649	0,2865	0,2862	0,2862	0,7138	0,7946	0,6973	0,4692	0,2901	0,2901	0,2901
20	0,7725	0,7778	0,6927	0,4649	0,2865	0,2862	0,2862	0,7672	0,7929	0,6973	0,4692	0,2901	0,2901	0,2901

DEPOSIT LEVEL Accuracy (%)	Iteration 7 Gamma Value [log(g)]							Iteration 8 Gamma Value [log(g)]						
Cost Value [log(C)]	**-10**	**-5**	**0**	**5**	**10**	**15**	**20**	**-10**	**-5**	**0**	**5**	**10**	**15**	**20**
-10	0,2964	0,2964	0,2964	0,2964	0,2964	0,2964	0,2964	0,2901	0,2901	0,2901	0,2901	0,2901	0,2901	0,2901
-5	0,2964	0,3389	0,4059	0,3274	0,2964	0,2964	0,2964	0,2901	0,3261	0,3858	0,3215	0,2901	0,2901	0,2901
0	0,3277	0,5077	0,5856	0,4566	0,2964	0,2964	0,2964	0,3201	0,4774	0,5717	0,4385	0,2901	0,2901	0,2901
5	0,4870	0,6433	0,6861	0,4807	0,2964	0,2964	0,2964	0,4675	0,6238	0,6845	0,4616	0,2901	0,2901	0,2901
10	0,6228	0,7573	0,6937	0,4807	0,2964	0,2964	0,2964	0,6057	0,7534	0,6930	0,4616	0,2901	0,2901	0,2901
15	0,7191	0,8042	0,6934	0,4807	0,2964	0,2964	0,2964	0,7092	0,7910	0,6924	0,4616	0,2901	0,2901	0,2901
20	0,7755	0,7900	0,6934	0,4807	0,2964	0,2964	0,2964	0,7735	0,7751	0,6924	0,4616	0,2901	0,2901	0,2901

DEPOSIT LEVEL Accuracy (%)	Iteration 9 Gamma Value [log(g)]							Iteration 10 Gamma Value [log(g)]						
Cost Value [log(C)]	**-10**	**-5**	**0**	**5**	**10**	**15**	**20**	**-10**	**-5**	**0**	**5**	**10**	**15**	**20**
-10	0,2895	0,2895	0,2895	0,2895	0,2895	0,2895	0,2895	0,2786	0,2786	0,2786	0,2786	0,2786	0,2786	0,2786
-5	0,2895	0,3277	0,3891	0,3155	0,2895	0,2895	0,2895	0,2786	0,3162	0,3716	0,3073	0,2786	0,2786	0,2786
0	0,3205	0,4886	0,5800	0,4408	0,2895	0,2895	0,2895	0,3089	0,4649	0,5852	0,4484	0,2786	0,2786	0,2786
5	0,4692	0,6264	0,6845	0,4646	0,2895	0,2895	0,2895	0,4702	0,6222	0,6769	0,4659	0,2789	0,2786	0,2786
10	0,6007	0,7507	0,6901	0,4646	0,2895	0,2895	0,2895	0,5908	0,7438	0,6769	0,4659	0,2789	0,2786	0,2786
15	0,7132	0,7903	0,6891	0,4646	0,2895	0,2895	0,2895	0,7079	0,7916	0,6766	0,4659	0,2789	0,2786	0,2786
20	0,7580	0,7847	0,6891	0,4646	0,2895	0,2895	0,2895	0,7573	0,7807	0,6766	0,4659	0,2789	0,2786	0,2786

4. Phase 4: classification results in experiment 2 with the optimums parameters in each classifier.

Table B14. Results obtained in the experiment 2 with the optimums parameters in SVM classifier with linear kernel and LIBSVM library.

Obsidian sample	Accuracy			Simulation Time (h)		
	Island	Municipality	Deposit	Island	Municipality	Deposit
1	0,9954	0,5505	0,5596	6,83	0,45	0,44
2	0,9778	0,6500	0,6222	6,89	0,44	0,44
3	0,9933	0,6510	0,6443	7,14	0,45	0,44
4	1,0000	0,7438	0,8017	7,47	0,45	0,44
5	1,0000	0,5972	0,5903	7,61	0,45	0,44
6	0,9630	0,6420	0,6667	7,53	0,45	0,44
7	0,8358	0,4562	0,4526	7,36	0,44	0,43
8	0,8194	0,6574	0,6991	7,41	0,44	0,44
9	0,9932	0,7483	0,8095	7,59	0,45	0,44
10	0,9386	0,7982	0,8860	7,61	0,45	0,45
11	1,0000	0,9141	0,9018	7,46	0,45	0,44
12	0,9781	0,8613	0,8540	7,13	0,45	0,44
13	0,8039	0,6695	0,6723	6,84	0,44	0,43
14	0,8498	0,7207	0,7207	6,79	0,44	0,44
15	0,9829	0,8889	0,8803	6,92	0,45	0,44
16	1,0000	0,0331	0,0368	6,93	0,43	0,43
17	0,9594	0,1421	0,1523	6,98	0,44	0,44
18	0,9750	0,2895	0,3428	6,69	0,44	0,43
19	0,9740	0,1533	0,2101	6,57	0,42	0,43
20	0,9695	0,1990	0,2584	6,71	0,44	0,43
21	0,8000	0,3025	0,2992	6,72	0,44	0,43
22	0,9173	0,4049	0,4243	6,77	0,44	0,43
23	0,9607	0,5652	0,6335	6,89	0,45	0,44
24	0,9574	0,0000	0,0000	7,07	0,44	0,43
25	0,9451	0,0202	0,0202	6,93	0,44	0,43
26	0,8870	0,0167	0,0209	6,95	0,45	0,43
27	0,6444	0,0504	0,0669	6,12	0,40	0,39
28	0,9306	0,0796	0,0837	6,67	0,42	0,41
29	0,9358	0,4596	0,4192	6,27	0,41	0,41
30	0,8123	0,3137	0,3140	5,06	0,38	0,40
31	0,9932	0,0342	0,0411	7,14	0,45	0,46
32	0,9952	0,0429	0,0476	7,06	0,45	0,43
33	0,8883	0,1229	0,0950	7,06	0,45	0,46
34	0,8621	0,1954	0,0920	7,06	0,45	0,44
35	0,9198	0,1016	0,0856	7,04	0,45	0,43
36	0,9802	0,5941	0,4158	7,14	0,45	0,44
37	0,9563	0,3005	0,1530	7,17	0,45	0,44
38	0,9898	0,5918	0,4694	7,11	0,45	0,44
39	0,5726	0,1048	0,0000	6,91	0,45	0,43
40	1,0000	0,5714	0,0000	7,06	0,45	0,45
41	0,8824	0,8235	0,0147	7,17	0,45	0,47
42	1,0000	0,4505	0,0879	7,12	0,45	0,46
43	0,9683	0,3439	0,3846	7,09	0,44	0,45
44	0,9821	0,2024	0,2143	7,09	0,45	0,44
45	0,9455	0,2921	0,2475	7,14	0,45	0,43
46	0,9882	0,3941	0,3647	7,13	0,47	0,44
47	0,9453	0,3333	0,3184	7,06	0,45	0,44
48	0,9851	0,5985	0,5204	7,31	0,45	0,44
49	0,9306	0,5426	0,5394	7,08	0,45	0,43
50	0,9297	0,3281	0,3242	6,96	0,46	0,43
51	0,9619	0,6143	0,6524	7,06	0,45	0,44
52	0,9613	0,6968	0,7226	7,00	0,45	0,43

53	0,9630	0,1728	0,1646	7,02	0,44	0,43
54	0,9467	0,2396	0,2663	7,07	0,45	0,43
55	0,9744	0,4231	0,4295	7,32	0,45	0,44
56	0,8963	0,3926	0,3926	7,03	0,46	0,44
57	0,9661	0,7571	0,7514	7,20	0,46	0,44
58	0,0279	0,3756	0,3553	6,79	0,45	0,43
59	0,0776	0,3668	0,3598	6,52	0,44	0,43
60	0,1368	0,4046	0,3590	6,45	0,45	0,44
61	0,0943	0,2779	0,3027	6,59	0,45	0,45
62	0,0147	0,1206	0,1118	6,70	0,44	0,44
63	0,0415	0,0498	0,0041	6,74	0,45	0,43
64	0,0298	0,0476	0,0476	6,94	0,45	0,44
65	0,2469	0,0962	0,0732	6,68	0,43	0,42
66	0,0982	0,0000	0,0000	7,10	0,45	0,43
67	0,3411	0,5292	0,5305	6,43	0,43	0,42
68	0,3574	0,3872	0,3711	6,33	0,41	0,40
69	0,1099	0,1330	0,1316	2,72	0,34	0,34

Table B15. Results obtained in the experiment 2 with the optimums parameters in Random Forest classifier.

Obsidian sample	Accuracy (%)			Simulation Time (h)		
	Island	Municipality	Deposit	Island	Municipality	Deposit
1	0,9495	0,1835	0,2110	0,15	0,37	0,34
2	0,9556	0,2167	0,2389	0,15	0,36	0,38
3	0,9530	0,2215	0,2416	0,15	0,36	0,35
4	0,9835	0,2893	0,3388	0,15	0,36	0,79
5	0,9792	0,2222	0,2361	0,15	0,38	0,42
6	0,9630	0,2284	0,2531	0,15	0,44	0,89
7	0,9562	0,1898	0,2007	0,15	0,47	0,71
8	0,8565	0,1204	0,1250	0,15	0,39	0,35
9	0,9864	0,4490	0,4694	0,15	0,45	0,41
10	0,9474	0,3684	0,4298	0,15	0,47	0,37
11	0,9141	0,3252	0,3620	0,15	0,39	0,37
12	0,9416	0,3796	0,4088	0,15	0,38	0,37
13	0,9692	0,3641	0,3697	0,15	0,45	0,36
14	0,9309	0,3483	0,3514	0,14	0,46	0,36
15	0,9744	0,5128	0,5470	0,15	0,45	0,37
16	0,9816	0,0735	0,0846	0,15	0,41	0,37
17	0,8020	0,1066	0,0457	0,15	0,51	0,37
18	0,8785	0,1547	0,0765	0,14	0,40	0,36
19	0,8418	0,0717	0,0309	0,14	0,39	0,36
20	0,9583	0,1332	0,1043	0,14	0,38	0,35
21	0,7765	0,1412	0,0874	0,14	0,50	0,36
22	0,8944	0,1496	0,1268	0,14	0,47	0,36
23	0,9420	0,3830	0,2008	0,15	0,39	0,36
24	0,9574	0,0000	0,0000	0,14	0,38	0,36
25	0,9682	0,0029	0,0000	0,15	0,38	0,37
26	0,8243	0,0000	0,0000	0,14	0,35	0,37
27	0,8680	0,0816	0,0962	0,14	0,35	0,35
28	0,8694	0,1837	0,2204	0,14	0,37	0,36
29	0,9358	0,4319	0,4342	0,14	0,35	0,34
30	0,7383	0,2557	0,2788	0,13	0,32	0,32
31	0,9863	0,0411	0,0548	0,15	0,37	0,35
32	0,9857	0,0619	0,0619	0,15	0,40	0,37
33	0,8715	0,0615	0,0112	0,15	0,42	0,38
34	0,8736	0,0230	0,0115	0,15	0,39	0,41
35	0,8984	0,0481	0,0160	0,15	0,37	0,37
36	0,9604	0,1386	0,0594	0,15	0,38	0,36
37	0,9344	0,0546	0,0164	0,15	0,37	0,36
38	0,9388	0,2347	0,0510	0,15	0,39	0,35
39	0,8710	0,0565	0,0000	0,15	0,63	0,44
40	1,0000	0,2857	0,0000	0,15	0,40	0,38
41	1,0000	0,2794	0,0000	0,15	0,41	0,43
42	0,6374	0,1758	0,0000	0,15	0,37	0,39
43	0,9095	0,1041	0,1131	0,15	0,42	0,37
44	0,9226	0,1429	0,1548	0,15	0,38	0,41
45	0,8713	0,2475	0,2426	0,15	0,38	0,39
46	0,9529	0,2706	0,2294	0,15	0,60	0,38
47	0,9154	0,1692	0,1493	0,15	0,36	0,41
48	0,9851	0,2305	0,2342	0,15	0,40	0,35
49	0,8927	0,3186	0,3533	0,15	0,35	0,37
50	0,8789	0,2617	0,2773	0,15	0,35	0,42
51	0,7762	0,4190	0,4286	0,15	0,49	0,38
52	0,8065	0,3419	0,3548	0,15	0,39	0,42
53	0,9588	0,0412	0,0453	0,15	0,50	0,37
54	0,9201	0,1243	0,1124	0,15	0,42	0,36
55	0,9359	0,1923	0,1731	0,15	0,39	0,39
56	0,7259	0,1704	0,1407	0,15	0,40	0,38
57	0,8870	0,2429	0,2655	0,15	0,37	0,47

58	0,1015	0,1904	0,2157	0,14	0,37	0,36
59	0,1534	0,1605	0,1887	0,14	0,35	0,39
60	0,1595	0,2308	0,2621	0,14	0,37	0,54
61	0,1638	0,2233	0,2481	0,14	0,51	0,35
62	0,0441	0,1765	0,2088	0,14	0,39	0,39
63	0,0913	0,0373	0,0415	0,15	0,38	0,36
64	0,0655	0,0833	0,0893	0,15	0,37	0,37
65	0,2636	0,0879	0,1067	0,14	0,36	0,39
66	0,0893	0,0804	0,0893	0,15	0,37	0,39
67	0,5875	0,7497	0,7613	0,15	0,36	0,37
68	0,1787	0,3047	0,3173	0,14	0,36	0,41
69	0,1862	0,1439	0,1566	0,11	0,30	0,31

Table B16. Results obtained in the experiment 2 with the optimums parameters in SVM RBF classifier and LIBSVM library.

Obsidian sample	Accuracy (%)			Simulation Time (h)		
	Island	Municipality	Deposit	Island	Municipality	Deposit
1	0,9404	0,6560	0,6697	4,90	0,25	0,20
2	0,9500	0,7278	0,7000	4,83	0,25	0,20
3	0,9195	0,7181	0,6644	4,84	0,25	0,20
4	1,0000	0,8512	0,7851	4,94	0,25	0,20
5	0,9167	0,5972	0,5972	5,20	0,25	0,20
6	0,9383	0,6728	0,5988	5,89	0,25	0,20
7	0,8723	0,5584	0,5949	5,33	0,25	0,20
8	0,8380	0,4491	0,4630	5,16	0,25	0,20
9	0,9932	0,7279	0,7075	4,87	0,25	0,21
10	0,9386	0,8070	0,7368	4,83	0,25	0,21
11	0,9816	0,8160	0,7914	5,34	0,25	0,20
12	0,9781	0,7883	0,7810	5,07	0,25	0,20
13	0,9216	0,6639	0,6527	4,82	0,24	0,20
14	0,8529	0,5826	0,5916	4,83	0,24	0,20
15	0,9402	0,8632	0,8547	4,95	0,25	0,21
16	0,8860	0,0735	0,0735	4,86	0,24	0,20
17	0,6294	0,1624	0,1472	4,68	0,24	0,20
18	0,8869	0,3278	0,2679	4,68	0,23	0,20
19	0,7923	0,1854	0,2287	4,48	0,22	0,20
20	0,9213	0,2247	0,3740	4,66	0,24	0,20
21	0,6689	0,3311	0,2958	4,58	0,23	0,20
22	0,8486	0,4049	0,4120	4,72	0,23	0,20
23	0,9027	0,5342	0,4224	4,76	0,24	0,20
24	0,8527	0,0000	0,0000	4,92	0,25	0,20
25	0,9162	0,0607	0,0549	4,73	0,24	0,20
26	0,8117	0,0335	0,0418	5,22	0,25	0,20
27	0,7507	0,1036	0,1091	4,42	0,21	0,17
28	0,8837	0,1286	0,1408	4,70	0,22	0,19
29	0,8843	0,4010	0,4113	4,89	0,21	0,17
30	0,6317	0,2889	0,3221	3,39	0,19	0,15
31	0,8288	0,2671	0,2671	4,85	0,25	0,20
32	0,9333	0,2667	0,2429	4,77	0,25	0,20
33	0,8324	0,1229	0,0838	4,87	0,25	0,20
34	0,7874	0,2069	0,1667	4,79	0,25	0,20
35	0,8930	0,1711	0,1658	4,77	0,25	0,21
36	0,9208	0,4950	0,3465	4,83	0,25	0,21
37	0,9235	0,2951	0,1858	4,80	0,25	0,20
38	0,9388	0,5510	0,3776	4,85	0,25	0,20
39	0,6774	0,1290	0,0081	4,83	0,25	0,21
40	0,9524	0,8571	0,0476	5,06	0,25	0,21
41	0,9265	0,6912	0,0588	4,85	0,25	0,20
42	0,7912	0,7143	0,0330	4,80	0,25	0,21
43	0,8959	0,2896	0,2896	4,81	0,25	0,20
44	0,7738	0,2321	0,2440	4,83	0,24	0,20
45	0,8168	0,3663	0,3515	4,70	0,25	0,20
46	0,8824	0,5000	0,4647	4,78	0,25	0,20
47	0,8109	0,2736	0,2687	4,76	0,25	0,20
48	0,9814	0,4312	0,3717	4,87	0,25	0,20
49	0,8991	0,6782	0,6845	4,78	0,25	0,20
50	0,8984	0,3633	0,3906	4,80	0,24	0,20
51	0,8238	0,7429	0,7333	4,78	0,25	0,20
52	0,8839	0,7871	0,7935	4,79	0,25	0,20
53	0,8189	0,1893	0,1934	5,08	0,25	0,20
54	0,9142	0,2840	0,2781	4,83	0,24	0,20
55	0,9551	0,3205	0,3333	4,81	0,25	0,20
56	0,7704	0,2148	0,2222	4,83	0,25	0,20

57	0,8701	0,5819	0,5537	4,82	0,25	0,20
58	0,2157	0,2437	0,2487	4,39	0,23	0,19
59	0,2698	0,4127	0,4109	4,23	0,24	0,19
60	0,3048	0,3134	0,3276	4,48	0,24	0,20
61	0,2283	0,2084	0,2134	4,43	0,24	0,19
62	0,0735	0,1353	0,1324	4,14	0,24	0,19
63	0,2946	0,2780	0,1784	4,64	0,25	0,20
64	0,1429	0,0774	0,1369	4,54	0,24	0,20
65	0,3431	0,0649	0,0628	4,36	0,22	0,18
66	0,1786	0,0000	0,0000	4,61	0,24	0,20
67	0,6239	0,6329	0,6265	4,39	0,24	0,20
68	0,4089	0,2738	0,2623	4,14	0,23	0,19
69	0,2737	0,0974	0,1028	2,73	0,21	0,17